TRANSCRIPTOME CHANGES AND THE ROLE OF RNA HELICASES IN *Ustilago maydis* DURING TELIOSPORE DORMANCY AND GERMINATION

A dissertation submitted to the Committee on Graduate Studies

in partial fulfillment of the requirements

for the degree of

Doctor of Philosophy

in the faculty of Arts and Science

TRENT UNIVERSITY

Peterborough, Ontario, Canada

Environmental and Life Sciences Ph.D. Graduate Program

September 2025

ABSTRACT

Transcriptome Changes and the Role of RNA Helicases in *Ustilago maydis* During Teliospore Dormancy and Germination

Amanda Marie Seto

Crop losses due to pathogens, pests, and weeds account for 20–40% of global production, with fungal pathogens responsible for the most significant yield reductions and economic impact. The diseases caused by fungi spread through dormant spores, which protect its genetic material under adverse conditions. Dormancy is maintained until favorable germination conditions are met. Despite their importance in the fungal lifecycle, the molecular transitions from dormancy to germination remain poorly understood. The research presented uses the basidiomycete *Ustilago maydis*, the causal agent of Common Smut of Corn, to investigate fungal spore dormancy and germination. It aims to 1) identify the molecular transitions and stages of teliospore germination and 2) the roles of RNA helicases during teliospore germination. RNA-seq and respiration analyses were used to propose teliospore germination stages and a microdissection technique was developed for studying these stages. Transcriptomic analysis identified patterns of gene transcript level changes during germination, with GO term enrichment identifying genes involved in cell morphogenesis, metabolism, and RNA metabolism. Several RNA helicases were identified with potential roles during dormancy and germination. Previous work in the Saville Laboratory proposed that mRNAs are stored as dsRNA in dormant teliospores. I hypothesized that RNA helicases function to make these mRNAs available for translation upon germination. Forty-six RNA helicases were identified in *U. maydis*, and 28 RNA

helicases were proposed to have roles in growth, pathogenesis, stress response, and teliospore dormancy and germination. The RNA helicases *udbp3* and *uded1* were selected for functional analysis by creating mutant strains. The results suggest that *udbp3* negatively regulates osmotic stress response, potentially modulating stress-responsive genes during dormancy. The altered *uded1* expression in mutant strains leads to slow and polarized growth and dsRNA formation. This suggests *uded1* represses translation by stabilizing sense/antisense transcripts in dormant spores and then reactivates translation during germination. These findings increase our understanding of the molecular events during teliospore germination and offer insights into factors contributing to disease progression in fungal plant pathogens.

Keywords: genome annotation, microdissection, patterns of gene expression, RNA-seq, RNA helicases, stages of teliospore germination, stress response, teliospore dormancy and germination, teliospore respiration, *udbp3*, *uded1*, *Ustilago maydis*

PREFACE

This dissertation is presented in manuscript format and is based on four chapters. Chapter 2 was published in the *Canadian Journal of Plant Pathology*. Chapter 3 was published in the *Journal of Visualized Experiments*. Chapter 4 was published in *IMA Fungus*. Chapter 5 was published in the *International Journal of Molecular Sciences*.

The format for each chapter may vary slightly, where the format, reference, and citation style for each journal the chapter was published in was used. Co-authors and their contributions are listed in the preface of each chapter. Permissions from copyright holders for published chapters are found in Appendix I.

Chapters 2 and 4 have supplementary materials that contain large datasets and can be downloaded as separate PDF files.

ACKNOWLEDGEMENTS

Sometimes when I come across a thesis, I like to read the acknowledgments section. I don't know about you, but I always find myself wondering who the person is beyond just a name on the title page. It is the only time you get a glimpse of the person beneath the pages of research. I can relate to their struggles, sacrifices, and successes. I understand their gratitude for the people who supported them through their journey. It gives me hope that even when things get tough, I will make it through to the other side. If you are reading this, I would like to acknowledge and thank you. Yes, you! Thank you for taking the time to read this. Even if you are just skimming through the pages looking for something specific, I am grateful for the time you are taking to read what I consider my research baby. Now, let me introduce you to all the amazing people who accompanied me on this incredible journey because, without them, I would not be where I am today.

"The success of your journey and your destination all depend on who's driving."
Bruce Springsteen, Born to Run (2016)

This journey would not have been possible without a chance meeting that the late Dr. Tom Phillips made possible. I had graduated with my undergraduate degree and had been working for a couple of years before I decided to pursue my Master of Science. Commander Tom, as he was often called, was a family friend and my dad's former colleague. He heard that I wanted to pursue an M.Sc. but was having a difficult time finding a suitable supervisor. He suggested a meeting with someone he thought I might be interested in doing my M.Sc. with. It was through Tom that I met Dr. Barry Saville. I will forever be grateful to Tom for introducing me to Barry. Commander Tom, wherever you

are, thank you. It was you who gave me the map and told me to drive. I will raise a Guinness in your honour.

"All of science is nothing more than the refinement of everyday thinking."
Albert Einstein, Physics and Reality (1936)

That brings me to one of the navigators on this ship, my supervisor Dr. Barry Saville. Barry, we have been through a lot over the years. You saw something in me after our initial meeting with Commander Tom. We embarked on our first journey together when I wanted to get my M.Sc. What a successful trip that was! But I had another destination in mind, and you supported my decision to pursue what I would say has been the hardest journey so far. My Ph.D. journey. This adventure has not been for the faint of heart, and it took a lot of time, sacrifice, determination, patience, and acceptance that things will not always go my way. Through every turn and detour, you were always there. You encouraged and challenged me to look at things from a different angle. You allowed me the freedom and time to explore the various rabbit holes I would find myself in, but you would also nudge me when it was time to move on and get back on the road. You have seen me at my very best and worst. During the low points, and there were many (both personally and academically), you never stopped being there for me. Your humour, positivity, and passion for science bring out the best in your students. I am grateful for the funding you provided and the opportunities you encouraged me to take in sharing my work with the fungal and phytopathological communities. I would not be the scientist I am today if it were not for your guidance on this journey. Thank you for taking a chance and believing in me. This fulfilling adventure has been all the more meaningful because you joined and stayed with me. What an adventure it has been.

Many thanks to my supervisory committee, Dr. Craig Brunetti and Dr. Janet Yee. You both offered valuable insight, direction, and suggestions during my research. Thank you for your support and kindness. You helped shape me into the researcher I am today. When it felt like there was just too much to do and so little time, you both kept us on track and reminded me of the destination this ship was heading towards.

"If you can meet with Triumph and Disaster
And treat those two imposters just the same"
Rudyard Kipling, If— (1910)

I have seen so many faces come and go in the Saville Laboratory. Some of you were with us for a short time, and others for a long time. There have been so many people that I will try not to forget anyone! From the OG Saville Laboratory group when I first joined the lab: Dr. Michael Donaldson, Dr. Erin Morrison, Dr. Colleen Doyle, and Dr. Kitty Cheung; to the next generation: Kayla Marsh, Dr. Lauren Todd, Kristi Campbell, Ibraheem Alimi, Emilee Storfie, Victoria Kennedy, Monique Lariviere, and Emma Kaszecki; and finally to all of the undergraduate, placement, and summer students that I had the privilege of working with (there were so many of you!). Wow, it has been a ride. Each of you had an impact on me as a researcher, scientist, mentor, and teacher. You encouraged and challenged me to be the best that I could be. Thank you for helping me celebrate my triumphs when things finally started working, for listening to my frustrations when I questioned my ability to clone *E. coli*, for offering suggestions on how to make my presentations better, for crying with me when things broke in the lab, for laughing with me when things got crazy, for sending me pandas to cheer me up, for reminding me to eat, for making sure I refuelled on caffeine, and for listening to my ramblings of the ghost children

in the hallways of the DNA Building after work hours. Thank you for being my sound board and offering suggestions that would improve my experiments. To those of you who were with me during my low points. Thank you for checking in on me, ensuring that I was okay, and offering your support. I have always been a firm believer that the key to surviving graduate school after securing a great supervisor is having great lab mates. I have been honoured to have had so many amazing lab mates over the years. You have all made this journey memorable for me.

"There is a way out of every box, a solution to every puzzle;
it's just a matter of finding it."
Captain Jean-Luc Picard, Star Trek: The Next Generation, S7, E8, Attached (1993)

My time at Trent University has been such a positive experience. I would like to thank several individuals in the School of Graduate Studies, the Environmental and Life Sciences Program, the Departments of Forensic Science and Biology, and Science Facilities. I am grateful to Linda Cardwell in ENLS for her guidance and encouragement when I applied for the Ph.D. program. Your positive energy and enthusiasm are infectious. Thank you for always looking out for the students! To Mary-Lynn Scriver in the ENLS office and Jane Rennie in the School of Graduate Studies. Thank you for your administrative support. I have been fortunate to provide teaching assistance to both the Forensic Science and Biology departments at Trent University. Thank you to Lesley Hewett, Adrian Borlestean, and Smolly Coulson for guiding and supporting the teaching assistants. Each of you helped shape me into a more effective teacher and attentive listener. Thank you to Angela Sikma and Chris Williams in Science Facilities for keeping our labs safe for everyone, for being just a phone call away whenever the autoclave broke down

(and it broke down constantly), and for the random conversations in the hallways. Thank you to Dr. Paul Frost and your lab for the use and technical assistance of your microrespirometer. To Dr. Aaron Shafer — many thanks to you and your lab for the use of your ABI QuantStudio 3 Real-Time PCR system.

"I believe that family is worth more than money or gold."
Savage Garden, Affirmation (1999)

I would not be who I am today without the love and support of my family and friends. To my friends, thank you for checking in on me and supporting me during the chaos my life has been during this journey. To my family, words cannot express how grateful I am to have had you all in my corner, cheering and supporting me through this long and difficult journey. A special thank you to my parents, George and Karen Seto. Dad and Mom, words cannot express how grateful I am for your love and support during my Ph.D. journey. You were both my pillars of strength throughout this sometimes chaotic adventure. As a young girl, you both taught me to reach for my dreams, to never give up, and to fight for what I believe in. You encouraged me to keep moving forward whenever I encountered an obstacle. Thank you for listening to my rants and raves about experiments that were not working, for putting up with my long work hours, for offering a different perspective on how to deal with adversity, and for your advice on life in general. Mom, I know that the past couple of years have not been easy. You are one of the strongest people I know. I don't think I have the words to express how much you mean to me. Thank you for encouraging me to keep going and to finish this journey when I wanted to quit. You never stopped being my cheerleader and I am thankful for all that you've done for me. To my sister and her family — Sonia, Omid, Keon, Nirvan, and Tahdig — thank you for

always being in my corner and supporting me on this journey. Sonia, I never thought that we would get the chance to collaborate on something in our professional lives. Thank you for lending your artistic skills to create a figure for one of my manuscripts, and for listening to me and lifting me up when I started to doubt myself. Keon, my little dance partner, thank you for just being a little ray of sunshine. Your smiles warmed my heart and were just what I needed whenever I was down and needed a pick-me-up. I look forward to our next dance! Nirvan, little baby boy, you are only a week old as I write this. Even though we are so far away and have yet to meet in person, I want to let you know that your auntie already loves you, and I look forward to all the adventures we will have together. To my grandparents — Edward and Louise Seto and George and Margery Wong — thank you for your love and support. You taught me the importance of family and taking care of one another. Even though you did not fully understand my research or why I kept going back to school, you still checked in on how I was doing. I miss you all deeply, and I hope that wherever you are, you are proud of me. I finally did it! To my uncles and aunts on both the Seto and Wong sides — Howie, Karen, Ivan, Rose, Gord, and Doug — thank you for checking in on me. Your love and support have meant the world to me. To my in-laws-to-be, Arthur and Mary-Jane Branch, thank you for your constant support and encouragement. It has meant the world to me during this challenging adventure. To my brother-in-law-to-be and his family — Tim, Christina, and Isla — thank you for your support and love throughout the years. I appreciated it.

"Breathe, just breathe
Take the world off your shoulder
Put it on me
Breathe, just breathe
Let the life that you live be all that you need."
Ryan Star, Breathe (2009)

To my heart, best friend, and partner in life, Richard Branch — how can I possibly summarize all you've meant to me throughout this adventure? I do not know if I can, but I will try. Thank you for your endless support and words of encouragement throughout the years. You understood, better than anyone, the struggle and self-doubt I encountered every step of the way. Through it all, you celebrated both the small and big wins and supported me during the challenging times. You encouraged and challenged me to be the best I could be. Thank you for listening to me talk about my research, tolerating the random and sometimes long work hours, and providing feedback on my presentations, figure layouts, and written work. You're probably better at explaining my research in layman's terms than I am! I think I even managed to avoid having teliospore germination time courses with time points in the middle of the night this time! I cannot express how grateful I am to have had you remind me of the importance of getting enough sleep, eating better, taking time to recharge, and your patience as I got myself to the finish line long after you had finished your Ph.D. journey. I am thankful for your belief in me when I did not believe in myself, your humour and ability to make me laugh, providing me with an endless supply of peanut- and nut-free chocolates, and random hugs when I did not know I needed one. You have been my greatest supporter throughout this adventure, and I feel incredibly lucky to have had you by my side every step of the way. Thank you for your unconditional love throughout this journey and for continuing to love me even on my bad days.

DEDICATION

In loving memory of George Seto

Dad, you never stopped believing in me and encouraging me to be all I could be.

You taught me not to sweat the small stuff because it's all just small stuff; to work smarter, not harder; to never give up; to always reach for my dreams; and that the only easy day was yesterday.

In the moments when I didn't think I had it in me to keep going, you always reminded me that I am capable of anything.

You are in my thoughts every single day. I deeply miss our talks, the warmth of your smile, your unique sense of humour, your unwavering strength, and your devotion to your family. You helped shape me into the person I am today.

I'm forever grateful for your teachings, love, and never-ending support. This is for you.

I miss and love you, Dad.

I'll see you in my dreams.

♥ *Panda*

TABLE OF CONTENTS

ABSTRACT ii
PREFACE iv
ACKNOWLEDGEMENTS v
DEDICATION xii
LIST OF TABLES xvi
LIST OF FIGURES xviii
LIST OF ABBREVIATIONS AND SYMBOLS xxi
Chapter 1 General Introduction 1
Agriculture and Global Food Security 1
Impact of Crop Loss and Plant Disease 3
Fungal Spore Dormancy and Germination 4
Ustilago maydis 9
Research Objectives 10
References 14
Chapter 2 Exploring mechanisms of gene expression control during *Ustilago maydis* teliospore germination 21
Abstract 21
Introduction 23
Materials and Methods 25
Results 29
Discussion 34
Acknowledgements 43
Disclosure Statement 43
Tables and Figures 44
Supplementary Materials 59
References 63
Chapter 3 Investigating Teliospore Germination Using Microrespiration Analysis and Microdissection 68
Summary 68
Abstract 68
Introduction 70

Protocol 71
3.1 Corn Cob Infection 71
3.2 Teliospore Harvesting 71
3.3 Teliospore Viability and Germination Test 73
3.4 Induction of Germination for Respiration Monitoring 74
3.5 Obtaining Oxygen Consumption Rate (OCR) Measurements 75
3.6 Data Analysis 75
3.7 Induction of Teliospore Germination to Isolate Teliospores at Distinct Stages of Germination 76
3.8 Preparation of Petri Dish and Micromanipulator 76
3.9 Isolation of Stage-specific Germinating Teliospores 77
3.10 Recovery of Collection Droplet 77
Representative Results 77
Discussion 79
Disclosures 84
Acknowledgements 84
Tables and Figures 85
References 88
Chapter 4 Annotation and functional predictions of RNA helicases in *Ustilago maydis* . 91
Abstract 91
Introduction 92
Characteristics of SF1 and SF2 RNA helicase superfamilies 94
Identification of *Ustilago maydis* RNA helicases 98
Functions of RNA helicases and their potential roles in *Ustilago maydis* 101
Conclusions 132
Acknowledgements 132
Additional Information 132
Tables and Figures 134
Supplementary Materials 165
References 175
Chapter 5 Characterization of RNA Helicase Genes in *Ustilago maydis* Reveals Links to Stress Response and Teliospore Dormancy 197
Abstract 197

Introduction 199
Results 202
Discussion 211
Materials and Methods 220
Tables and Figures 234
Supplementary Materials 245
References 260
Chapter 6 General Discussion 267
Introduction 267
Gene Expression Control during Teliospore Germination 268
Microrespiration Analysis and Microdissection of Germinating Teliospores 271
Annotation and Functional Predictions of RNA Helicases in *Ustilago maydis* 273
Characterization of *udbp3* and *uded1* in *Ustilago maydis* Reveals Links to Stress Response and Teliospore Dormancy 274
Future Directions 276
General Conclusions 285
References 289
Appendix I Permission from Copyright Holders 295
Chapter 2: Exploring mechanisms of gene expression control during *Ustilago maydis* teliospore germination 295
Chapter 3: Investigating Teliospore Germination Using Microrespiration Analysis and Microdissection 296
Chapter 4: Annotation and functional predictions of RNA helicases in *Ustilago maydis* 297
Chapter 5: Characterization of RNA Helicase Genes in *Ustilago maydis* Reveals Links to Stress Response and Teliospore Dormancy 298

LIST OF TABLES

Table 2.1. Transcript level fold changes were calculated for T00 relative to 518/521/Dikaryon, T00 relative to T09, and T09 relative to T18 using the normalized expression values. 44

Table 2.2. Summary of the number of transcripts characterized by Cufflinks Cuffcompare. 45

Table 2.3. Summary of transcript characterizations for each pattern of transcript level change. 46

Table 2.4. Gene ontology statistical overrepresentation test results performed using the PANTHER Classification System. 48

Table S2.1. Identification of gene transcript patterns during teliospore germination. 59

Table S2.2. Reference gene list for GO enrichment analysis. 60

Table S2.3. Sequences of SYBR Green RT-qPCR primers used in this study. 61

Table S2.4. PANTHER statistical overrepresentation test results. 62

Table 3.1. Number of germinating teliospores successfully isolated for each germination stage in a standard isolation experiment. 85

Table 4.1. RNA helicases in *U. maydis* and their orthologs in *S. cerevisiae*, *C. elegans*, *D. melanogaster*, *M. musculus*, and *H. sapiens*. 134

Table 4.2. *Ustilago maydis* RNA helicase gene transcript levels during *in planta* pathogenesis. 137

Table 4.3. Functions of RNA helicases during RNA transcription. 140

Table 4.4. Functions of RNA helicases during pre-mRNA splicing. 142

Table 4.5. Functions of RNA helicases during RNA export. 147

Table 4.6. Functions of RNA helicases during ribosome biogenesis. 148

Table 4.7. Functions of RNA helicases that are involved in translation. 153

Table 4.8. RNA helicases that are involved in RNA degradation. 156

Table 4.9. RNA helicases that are involved in mitochondrial RNA processing. 157

Table S4.1. Results of predicted functional protein partners for each RNA helicase identified in *Ustilago maydis*. 165

Table 5.1. The *Ustilago maydis* strains used in this study. 234

Table S5.1. Plasmids used in this study. 245

Table S5.2. Primers used in this study. 246

LIST OF FIGURES

Figure 2.1. Representative transcript level change for each pattern in the 518/521/Dikaryon, T00, T09, and T18 RNA-seq libraries. 54

Figure 2.2. Transcript levels of genes, determined by RT-qPCR, selected from patterns 12 to 18 in the dikaryon (518 × 521) and germinating *U. maydis* teliospores at T04/T06 and T08/T12 relative to T00. 55

Figure 2.3. Stages of teliospore germination. 56

Figure 2.4. Molecular and physiological transitions during teliospore germination. 57

Figure 3.1. Time course of oxygen consumption during teliospore germination. 86

Figure 3.2. Stages of teliospore germination. 86

Figure 3.3. Microdissection to isolate distinct morphological stages of germinating teliospores. 87

Figure 4.1. Helicase superfamilies and characteristics of SF1 and SF2 RNA helicases 158

Figure 4.2. Maximum likelihood phylogenetic tree of SF1 RNA helicases. 160

Figure 4.3. Maximum likelihood phylogenetic tree of SF2 DEAD-box RNA helicases. 161

Figure 4.4. Maximum likelihood phylogenetic tree of SF2 DEAH/RHA RNA helicases. 162

Figure 4.5. Maximum likelihood phylogenetic tree of SF2 Ski2-like RNA helicases... 163

Figure 4.6. Maximum likelihood phylogenetic tree of RNA helicases with unknown function. 164

Figure S4.1. The original maximum likelihood phylogenetic tree of SF1 Upf1-like RNA helicases. 166

Figure S4.2. The original maximum likelihood phylogenetic tree of SF2 DEADbox RNA helicases. 171

Figure S4.3. The original maximum likelihood phylogenetic tree of SF2 DEAH RNA helicases. 173

Figure S4.4. The original maximum likelihood phylogenetic tree of SF2 Ski2-like RNA helicases. 174

Figure 5.1. Protein sequence alignment and maximum likelihood phylogenetic tree for Udbp3 and its orthologs. 235

Figure 5.2. Uded1 protein sequence alignment and maximum likelihood phylogenetic tree. 237

Figure 5.3. The effects of osmotic stress on Δ*udbp3* mutants. 238

Figure 5.4. Growth of *uded1* mutants in permissive and repressive growth conditions. 239

Figure 5.5. The effects of sorbitol addition to solid medium on the growth of *uded1* mutants. 240

Figure 5.6. Mating assay of *uded1* mutants. 241

Figure 5.7. The *uded1* transcript is upregulated in the deletion strains when grown in permissive conditions..... 241

Figure 5.8. RT-PCR detection of the *ssm1* and *as-ssm1* transcripts in crg1:*uded1* mutants where *as-ssm1* is expressed from an autonomously replicating vector. 242

Figure 5.9. The *uded1* transcript is upregulated in the crg1:*uded1* mutants grown in permissive conditions..... 243

Figure 5.10. S1 nuclease protection assay of *ssm1* and *as-ssm1* interactions. 244

Figure S5.1. Forced dikaryon formation of *udbp3* deletion mutants. 249

Figure S5.2. *udbp3* mutant pathogenesis assay in maize. 250

Figure S5.3. Teliospore germination test of *udbp3* deletion mutants..... 251

Figure S5.4. Growth of Δ*udbp3* at different temperatures. 252

Figure S5.5. *udbp3* deletion mutants tolerance to various stressors. 253

Figure S5.6. Growth of the *uded1* deletion strains in repressive and permissive growth conditions. 254

Figure S5.7. The effects of sorbitol addition to solid medium on the growth of *uded1* mutants. 255

Figure S5.8. Mating assay of *uded1* mutants. 256

Figure S5.9. Mating assay of *uded1* mutants comparing three days versus five days... 257

Figure S5.10. Pathogenesis assay of Δ*uded1* crg1:*uded1* mutant strains in maize seedlings. 258

Figure S5.11. RT-qPCR analysis of *uded1* transcript levels in the 518 crg1:*uded1* [pCM768] control samples grown in repressive (YEPS) and permissive (YEPA) conditions. 259

LIST OF ABBREVIATIONS AND SYMBOLS

%	percentage, a number or ratio that is expressed as a fraction of 100
Δ	gene deletion
× *g*	relative centrifugal force
µg	microgram
µL	microlitre
µm	micrometre
µmol	micromole
°	degree
°C	degrees Celsius
$2^{-\Delta\Delta CT}$	comparative C_T
ATP	adenosine triphosphate
ATPase	enzyme that hydrolyses ATP
BLASTp	basic local alignment search tool using a protein sequence
cAMP	cyclic adenosine monophosphate
Cas9	CRISPR-associated protein 9
cDNA	complementary DNA
cm	centimetre
CM	complete medium
CO_2	carbon dioxide
CoA	coenzyme A
CRISPR	clustered regularly interspaced short palindromic repeats
CT	cycle threshold
$CuSO_4$	copper sulfate
DAPI	4′,6-diamidino-2-phenylindole
DCMA	double complete medium
DEPC	diethyl pyrocarbonate/dicarbonate

dH_2O	deionized water
DI	disease index
DIC	differential interference contrast
DNA	deoxyribonucleic acid
DNase	deoxyribonuclease
dpi	days post-infection
dsRNA	double-stranded RNA
EST	expressed sequence tag
FDR	false discovery rate
Fuz^+	mycelial phenotype of crossed compatible strains
g/L	grams per litre
g	grams
GO	gene ontology
GTP	guanosine triphosphate
h	hour(s)
L	litre
M	molar
MAPK	mitogen-activated protein kinase
mg	milligrams
min	minute(s)
mm	millimetre
MM	minimal medium
mM	millimolar
MMS	methyl methanesulphonate
mL	millilitre
mRNA	messenger RNA
MUSCLE	multiple sequence comparison by log-expectation
NAD	nicotinamide adenine dinucleotide

NCBI	National Center for Biotechnology Information
ng	nanogram
nM	nanomolar
nmol	nanomoles
O_2	oxygen
OCR	oxygen consumption rate
OD_{600}	optical density at 600 nanometres
PANTHER	protein analysis through evolutionary relationships
PCR	polymerase chain reaction
PDA	potato dextrose agar
PDB	potato dextrose broth
PIG	post induction of germination
PPP	pentose phosphate pathway
RNA	ribonucleic acid
RNase	ribonucleases
RNA-seq	RNA sequencing
RNP	ribonucleoprotein
rpm	revolutions per minute
RQ	relative quantity
rRNA	ribosomal RNA
RT	room temperature
RT-PCR	reverse-transcriptase PCR
RT-qPCR	reverse-transcriptase quantitative PCR
s	second(s)
SF1	superfamily 1
SF2	superfamily 2
SGD	*Saccharomyces* genome database
STRING	search tool for recurring instances of neighbouring genes

TCA	tricarboxylic acid
tRNA	transfer RNA
U	units
USD	United States dollar
V-ATPase	vacuolar ATPase
w/v	weight per volume
wt	wild-type
YEPA	yeast extract, peptone, L-arabinose
YEPS	yeast extract, peptone, sucrose

CHAPTER 1

GENERAL INTRODUCTION

AGRICULTURE AND GLOBAL FOOD SECURITY

Agriculture was developed during the transition from a hunter-gatherer lifestyle to a farming lifestyle. During this time, populations began to create long-term settlements, increasing the demand for food supplies. Throughout history, agriculture and technological development have allowed societies worldwide to grow (Mazoyer & Roudart, 2006). The innovations in agriculture have contributed to increased production and enhancement of quality products (van der Veen, 2010). As the world population increases, the demand for food also increases and as a result, poses a challenge to food security (Tian et al., 2021). In 2022, approximately 9.2% of the world's population faced hunger and 42% of the people in the world were unable to afford or access a healthy diet (FAO et al., 2023). In 2018, the global population was estimated to increase to approximately 9.7 billion people by 2050. This upward trajectory of the world's population means an increase of at least 70% more food products are required to feed this population. As a result, food insecurity is a concern if changes in agriculture and food systems are not made (Cole et al., 2018).

"Food security is when all people, at all times, have physical and economic access to sufficient, safe and nutritious food that meets their dietary needs and food preferences for an active and healthy life" (FAO, 2008). Understanding food security requires the consideration of the links between 1) food availability, 2) food access, 3) food utilization, and 4) stability over time. These factors rely on each other, and stability is achieved when the first three factors are adequate over time (Nicholson et al., 2021). Food insecurity has major health effects on developing children. The major food insecurity and malnutrition

drivers are global conflicts, climate extremes, economic status, and increasing inequality. The pandemic, war in Ukraine, economic rebound, and increased food and energy prices have all contributed to food insecurity (FAO et al., 2023; Independent Group of Scientists appointed by the Secretary-General, 2023). Innovations in agriculture and the development of technologies to increase food availability and affordability are areas to focus on (FAO et al., 2023).

Agricultural innovations are geared towards increasing production and enhancing the quality of food products. Improving crop quality by introducing crops that are higher-yielding or more resistant to environmental conditions and crop diseases is an example of agricultural innovation (van der Veen, 2010). As the population rises and urbanization increases, there is a shift in diet. Typically, this shift in diet includes increased consumption of meat products. A more sustainable diet is required to protect current natural resources, the environment, and biodiversity. Protein sources from non-animal products require new agricultural innovations (Cole et al., 2018). Cereal grains can provide an alternative source of protein and are a major source of energy and carbohydrates (Poutanen et al., 2022). Cereal crops account for 53% of the available food in the world. The three major cereal crops, wheat, maize, and rice, account for approximately 90% of the world's production. Wheat and rice are the most widely consumed cereal crops, however, maize production is the highest among the three (Górska-Warsewicz et al., 2023). World cereal crop production in 2023 totaled 3.1 billion tonnes, marking a 2% (61 million tonne) rise from 2022, a development attributed primarily to enhanced maize output. The top five cereal crops produced were maize (1.2 billion tonnes), rice (800 million tonnes), wheat (799 million tonnes), barley (146 million tonnes), and sorghum (57 million tonnes). Maize had the

fastest growth since 2010 due to its use in foods, biofuels, and animal feeds (FAO, 2024). However, the forecast for the 2024/2025 world cereal crop market indicates slight decreases in cereal crop production (2.842 billion tonnes) and trade (484.2 million tonnes), and a 1% increase in crop utilization (2.867 billion tonnes). The decreased global production is largely due to a decline in maize production caused by adverse weather conditions and plant disease in parts of Europe, South Africa, and South America (FAO, 2025). The production, utilization, and trade of these important cereal crops indicate their economic importance on a global scale. However, crop loss and plant diseases, especially those caused by fungi, can hinder cereal crop production and thus decrease food security.

IMPACT OF CROP LOSS AND PLANT DISEASE

Crop loss caused by pathogens, pests, and weeds accounts for approximately 20–40% of global production (Savary et al., 2012). The Food and Agricultural Organization of the United Nations lists 168 crops that are important for human nutrition. Cereal crops are among the highest-producing crops globally and maize accounts for the majority of cereal crop production globally (FAO, 2023). Crop loss caused by plant diseases results in a global loss of approximately $220 billion USD (reviewed in Faraji Rad, 2023). Plant diseases are caused by fungi, bacteria, viruses, and nematodes where fungal pathogens are the most economically important causing the greatest crop loss (Faraji Rad, 2023; Khan & Sharma, 2020). Fungi pose a significant threat to global agriculture; hundreds of species have been identified as plant pathogens, causing farmers to lose an estimated 10–23% of their crops to fungal diseases each year (reviewed in Stukenbrock & Gurr, 2023). Increased awareness of fungal pathogens and research is required to mitigate the impact of fungal diseases.

Fungal plant pathogens successfully spread disease by producing large amounts of spores. The production of spores allows for their survival and dispersal in the environment. The mechanisms and vectors for dispersal differ among fungi, however, the primary function of spores is to protect the fungal genome during adverse environmental conditions and/or during dispersal via air, water, or animal (Money, 2016). Understanding the mechanisms involved in fungal spore development, dormancy, dispersal, and germination can aid in developing methods for combatting fungal plant diseases.

FUNGAL SPORE DORMANCY AND GERMINATION

Dormancy is observed in many living organisms and is defined as a period of rest or interrupted phenotypic development (Cochrane, 1974; Sussman & Douthit, 1973). It is an adaptation in response to fluctuating environmental conditions or reduced resources which can cause a period of stress for the organism. Transitioning to a dormant state enables an organism to survive these stressful conditions until favourable conditions are restored (Lubzens et al., 2010). Dormancy can differ in response and length for different organisms. For example, metazoans such as tardigrades, nematodes, and rotifers undergo an extreme form of dormancy called cryptobiosis in response to stressful environmental conditions. Cryptobiosis involves a dramatic metabolic reduction and may include desiccation, osmotic pressure adjustments, and reduced oxygen consumption (Clegg, 2001; Møbjerg & Neves, 2021). Plant seed dormancy is broadly characterized by reduced metabolic activity where dormancy is maintained inherently or is imposed. Inherently dormant seeds cannot germinate even when placed in favourable environmental conditions. These seeds often require external stimuli to break dormancy such as heat, scarification, and agents that decay

the seed coat. In contrast, seeds that are under imposed dormancy will germinate when placed in favourable conditions (Lamont & Pausas, 2023). Different forms of dormancy are also seen in mammals, birds, and insects. One common example is hibernation, a mammalian strategy to survive winter conditions. Mammals that undergo hibernation undergo metabolic changes before the start of hibernation. These metabolic changes include a shift towards producing more body lipids to increase mass and a decrease in body temperature, heart rate, and respiration (Storey, 2003). Despite the many forms of dormancy, one common thread is a reduction in metabolism and phenotypical growth can only resume when certain requirements are met.

Fungi may form specialized structures called spores when entering dormancy. These structures allow for the preservation of the organism and its genetic material. The formation of fungal spores differs among fungi but typically they are formed within sacs or fruiting bodies. Fungal spores are then released into the environment for dispersal. Asexual spores are genetically identical to their parental strain. In contrast, sexual spores are produced through the fusion of opposite mating types to produce spores containing a combination of their parental strains. Dispersed spores remain dormant until suitable conditions or requirements are met to allow for germination to occur (Money, 2016; Sephton-Clark & Voelz, 2018).

Several types of fungal dormancy have been described, however, there are two major types. Exogenous dormancy is a type of fungal dormancy that is often seen in asexual spores. It has also been referred to as enforced dormancy, environmental dormancy, or quiescence (Sussman & Douthit, 1973). Fungi undergo exogenous dormancy when in unfavourable environmental conditions, either chemical or physical. Germination can be

induced by removing unfavorable conditions and ensuring the presence of water and other essential nutrients (Cochrane, 1974; Feofilova et al., 2012; Sussman & Douthit, 1973). In contrast, endogenous or constitutive dormancy is often seen in sexual spores. This form of dormancy is maintained by either a permeability barrier, metabolic block, or the presence of a self-inhibitor. This type of dormancy is often imposed during the formation of the spore (Cochrane, 1974; Feofilova et al., 2012; Sussman & Douthit, 1973). Key characteristics are shared amongst fungi despite the different forms of dormancy. These include the formation of a specialized spore cell wall, and reduced water content, metabolism, and respiration (Sussman & Douthit, 1973).

Some fungal spores, such as constitutively dormant spores, may require a process that breaks dormancy before germination can occur. An example of this is called an after-ripening process. This process is described as an aging period before the spore can germinate and is often seen in overwintering spores. Typically, these spores require alternating cold and warm temperatures before germination can be induced. For example, in *Calvatia gigantea* basidiospores, germination rates were improved when there was a storage period in temperatures that ranged from −18 °C to 12 °C. Further improvements in germination rates were observed when the storage period was at least one year but less than 3 years (Bulmer & Beneke, 1962). Other fungi require an activation period before germination can occur. An example of an activation period is called heat activation where the spore is exposed to a specific temperature range to break dormancy. This is commonly seen with ascospores produced by *Neurospora* and *Talaromyces*. For example, dormancy in *Talaromyces macroporus* ascospores is broken when exposed to a temperature range of 80 °C to 90 °C and germination rates increased with extended heat activation treatment

times. Heat activation allows for the degradation of stored trehalose to glucose which is then released into the surrounding medium. Germination is initiated when the inner protoplast of the ascospore is ejected and is followed by the development of the germ tube (Dijksterhuis et al., 2002; Kikoku, 2003). Other requirements that fungal spores may require to break dormancy are specific growth temperatures, medium pH, and light exposure (Griffin, 1994).

Spore germination involves an irreversible transition that can be characterized physiologically, morphologically, and biochemically (Gottlieb, 1950; Sussman & Douthit, 1973). This transition may include increased metabolism and respiration, spore swelling and the development of a germ tube, utilization of stored reserves, and biosynthesis of proteins and nucleic acids (Gottlieb, 1950; Griffin, 1994; Sussman & Douthit, 1973).

Spore swelling is observed in spores of some fungal species after germination is initiated. This involves water uptake from the environment that increases the spore water content and diameter of the fungal spore (Griffin, 1994). Examples of spore swelling are seen in the conidia of the ascomycetes *Botrytis cinerea* and *Aspergillus niger*. The increased size of conidia signals the onset of germination. An increase in the number of cell organelles, such as mitochondria and endoplasmic reticulum in the cytoplasm is also observed (Hawker & Hendy, 1963; Tsukahara, 1968).

Dormant fungal spores have low respiration rates, and during germination, these rates will increase dramatically (Griffin, 1994). Early studies on *Ustilago maydis* teliospore germination demonstrated that teliospores had low oxygen consumption levels. Once germination was initiated, these levels began to increase before visible signs of germination were present (Caltrider & Gottlieb, 1963; Chapter 3). Dormant conidiospores of

Neurospora crassa have low respiration levels and contain stored enzymes required for the cytochrome-mediated electron transport pathway. Once germination is initiated these enzymes become active and restore the respiratory system so that respiration rates increase (Stade & Brambl, 1981).

During the early stages of germination, the spore will utilize its carbon stores to fuel the increase in cellular metabolism and morphological changes. One example is trehalose stored in the conidia of ascomycete fungi, such as *Neurospora crassa*, *Aspergillus nidulans*, and *Botrytis cinerea*. The trehalose content in conidia varies for each species but can range from 1.5% to 10% of the fresh weight (Doehlemann et al., 2006; Ruijter et al., 2003; Schmit & Brody, 1976). In *N. crassa* and *A. nidulans*, trehalose degradation began 30 minutes after germination initiation and before visible signs of germination (d'Enfert, 1997). The breakdown of trehalose produces glucose which may be used as a carbon source during the early stages of germination. The glucose can be utilized in the glycolysis pathway, increasing cell metabolism (Ruijter et al., 2003).

On a molecular level, after germination is induced, there is rapid synthesis of proteins and nucleic acids. Protein synthesis is first detected before the transcription of new mRNAs indicating that there are stored mRNAs in the fungal spore. In *Lasiodiplodia theobromae*, an early increase in protein synthesis is detected soon after the conidia are placed in the germination medium. This protein synthesis is independent from transcription but is dependent on pre-existing mRNA. As germination progresses, protein synthesis then becomes partially dependent on new transcription of RNAs (Brambl & Van Etten, 1970). A similar process is seen in *A. nidulans* where the translation machinery is activated to synthesize proteins using pre-existing mRNAs after germination is initiated. These proteins

are required for morphological changes and development of the germ tube (Osherov & May, 2000). This indicates that dormant fungal spores store mRNAs required for the initial stages of germination, such as cellular metabolism and development (Griffin, 1994).

Ustilago maydis

The fungal plant pathogen *Ustilago maydis* (DC. Corda) is a basidiomycete and the causal agent of the disease common smut of corn (Kämper et al., 2006). In 2012, a survey among international fungal pathologists was conducted to determine the top ten most economically or scientifically important fungal plant pathogens. *Ustilago maydis* was ranked among the top ten for its scientific importance as a model for studying fungal plant-pathogen interactions (Dean et al., 2012).

Several factors make *U. maydis* a model for studying fungal plant-pathogen interactions. The *U. maydis* genome has been sequenced and annotated (Brefort et al., 2009; Kämper et al., 2006). The sequenced genome has allowed researchers to develop improved methods for genetic manipulation such as creating gene deletion mutants through homologous recombination (Kämper, 2004) and more recently the CRISPR-Cas9 system for genome editing (Schuster et al., 2016; Zuo et al., 2020). The *U. maydis* life cycle allows for understanding and characterizing the effects molecular changes have on the growth and development of the fungus. The length of the sexual cycle in *U. maydis* is 21 days post-infection of seedlings. This allows researchers to study the effects of altered gene expression or deletion on *U. maydis* infection, virulence, and pathogenesis (Brefort et al., 2009; Kämper et al., 2006). *Ustilago maydis* is also readily cultured in a laboratory, making

it ideal to work with for biochemical and physiological investigations (Kämper et al., 2006).

Ustilago maydis is described as having a dimorphic lifestyle. The non-pathogenic form is a yeast-like haploid cell that divides by budding. The sexual phase is initiated when compatible haploid cells fuse to create the filamentous and pathogenic form called the dikaryon. The dikaryon proliferates and develops an appressorium that penetrates plant cells. Dikaryotic mycelia grow within and between plant cells where karyogamy and fragmentation occur (Brefort et al., 2009; Kahmann & Kämper, 2004; Kämper et al., 2006; Saville et al., 2012). The formation of a tumour and teliospores is initiated in infected plant tissue. The initiation of teliospore development signals the start of meiosis which pauses, at the pachytene checkpoint during prophase I, when teliospores mature and enter dormancy (Banuett & Herskowitz, 1996; Saville et al., 2012). The tumour will then crack open to release dormant teliospores into the environment for dispersal and disease spread. In optimal conditions, teliospores will germinate and resume meiosis. A promycelium emerges from the teliospore and, as meiosis is completed, haploid basidiospores are formed and bud off (Banuett & Herskowitz, 1996; Brefort et al., 2009; Ramberg & McLaughlin, 1980; Saville et al., 2012). The non-pathogenetic haploid and the pathogenetic dikaryon are the two forms of *U. maydis* that can be propagated *in vitro*, however, producing teliospores requires growth in the plant (Brefort et al., 2009).

RESEARCH OBJECTIVES

Fungal spores are responsible for protecting the fungus during adverse environmental conditions and through their dispersal they can spread disease. Despite their importance to

the fungal lifecycle, there has been limited research into the molecular transitions that occur during the switch from dormancy to germination. The objectives of this thesis are: 1) identify the stages and molecular transitions of teliospore germination, and 2) determine the involvement of RNA helicases during teliospore dormancy and germination. This dissertation is a compilation of four manuscripts, each representing an individual chapter, and a general discussion of the findings and directions for future work.

The first research objective was to identify stages of teliospore germination and molecular transitions which are addressed in Chapters 2 and 3. The stages of teliospore germination were defined (Chapters 2 and 3) based on the research of promycelium development from Ramberg and McLaughlin (1980) and teliospore germination observations in Caltrider and Gottlieb (1963). Previous research in the Saville Laboratory uncovered transcriptional waves during teliospore germination (Sacadura & Saville, 2003; Zahiri et al., 2005). The limitations of these studies were the number of transcripts analyzed and that asynchronously germinating teliospores were used. In Chapter 2, RNA-seq was used to detect transcript levels above the background of asynchronous germination. Patterns of mRNA transcript level changes were identified and GO enrichment analysis was used to determine which biological pathways were activated during teliospore germination initiation. Identifying subtle changes in mRNA transcript levels is challenging due to the asynchronous nature of teliospore germination. To address this challenge, Chapter 3 describes a protocol I developed to isolate stage-specific germinating teliospores using microdissection. This method could be used to obtain a homogenous sample of germinating teliospores for use in downstream applications such as RNA-seq. A new

method for measuring respiration during teliospore germination is also presented in Chapter 3.

The second research objective was to determine the role of RNA helicases during teliospore dormancy and germination. This objective was based on previous research by Donaldson and Saville (2013) and Ostrowski and Saville (2017). It was proposed that prior to dormancy, mRNA transcripts are processed in the form of double-stranded RNA (dsRNA) and/or as RNA-protein (RNP) complexes containing RNA binding proteins. Stabilization of mRNAs is crucial for preservation during teliospore dormancy. When germination is initiated, these mRNAs are made available for translation. RNA helicases are RNA-binding proteins that may bind and stabilize mRNAs during dormancy and unwind dsRNA for translation. The second research objective was first addressed by identifying all RNA helicases in *U. maydis* (Chapter 4). The RNA helicases in *U. maydis* had not been previously identified or annotated. I identified the RNA helicases using sequence similarities to previously characterized RNA helicases in other organisms such as *Saccharomyces cerevisiae* (Fairman-Williams et al., 2010) and *Homo sapiens* (Bourgeois et al., 2016) and performed reciprocal BLASTp searches to identify putative *U. maydis* orthologs. These RNA helicases were further classified by constructing maximum likelihood phylogenetic trees for each RNA helicase family. STRING analysis was performed to predict protein-protein interactions. I also utilized RNA-seq data from the Saville Laboratory and Lanver et al. (2018) to determine transcript profiles for all putative RNA helicases and propose possible roles during *U. maydis* growth, pathogenesis, and teliospore dormancy and germination. The list of *U. maydis* RNA helicases from Chapter 4 and the patterns of mRNA transcript level changes from Chapter 2 were used to identify

RNA helicases that were upregulated in the dormant teliospore and have decreased transcript levels during germination. I identified five RNA helicases with this pattern of expression and selected the orthologs to *S. cerevisiae DBP3* and *DED1* for characterization in *U. maydis* (Chapter 5). Characterization of *udbp3* was carried out by creating gene deletion strains in the sexually compatible haploid strains in *U. maydis*. Expression and deletion strains of *uded1* were created to determine the effects of altered expression had on *U. maydis* growth, pathogenesis, and dsRNA formation.

There are two major themes in the research presented in this thesis. The identification of key molecular and physiological transitions in teliospore germination is presented in Chapters 2 and 3. Building on this foundation, the role of RNA helicases in these processes was examined in Chapters 4 and 5. This was accomplished by identifying all RNA helicases encoded by *U. maydis* and then characterizing two of these helicases. This work provides insight into the broader functions of RNA helicases in plant pathogenic fungi. It uncovers their roles in relation to modulating gene expression during key molecular and physiological transitions and in response to environmental factors. This insight reveals that interfering with helicase function or the processes they are involved in could provide novel ways to interfere with the growth and development of fungal pathogens and provide new methods for disrupting fungal plant disease progression.

REFERENCES

Banuett, F., & Herskowitz, I. (1996). Discrete developmental stages during teliospore formation in the corn smut fungus, *Ustilago maydis*. *Development, 122*(10), 2965–2976.

Bourgeois, C. F., Mortreux, F., & Auboeuf, D. (2016). The multiple functions of RNA helicases as drivers and regulators of gene expression. *Nature Reviews Molecular Cell Biology, 17*(7), 426–438.

Brambl, R. M., & Van Etten, J. L. (1970). Protein synthesis during fungal spore germination: V. Evidence that the ungerminated conidiospores of *Botryodiplodia theobromae* contain messenger ribonucleic acid. *Archives of Biochemistry and Biophysics, 137*(2), 442–452.

Brefort, T., Doehlemann, G., Mendoza-Mendoza, A., Reissmann, S., Djamei, A., & Kahmann, R. (2009). *Ustilago maydis* as a pathogen. *Annual Review of Phytopathology, 47*, 423–445. https://doi.org/10.1146/annurev-phyto-080508-081923

Bulmer, G. S., & Beneke, E. S. (1962, 1962/01/01). Studies on *Calvatia gigantea*. II. Factors Affecting Basidiospore Germination. *Mycologia, 54*(1), 34–43. https://doi.org/10.1080/00275514.1962.12024976

Caltrider, P. G., & Gottlieb, D. (1963). Respiratory activity and enzymes for glucose catabolism in fungus spores. *Phytopathology, 53*(9), 1021–1030.

Clegg, J. S. (2001, 2001/04/01/). Cryptobiosis — a peculiar state of biological organization. *Comparative Biochemistry and Physiology Part B: Biochemistry and Molecular Biology, 128*(4), 613–624. https://doi.org/https://doi.org/10.1016/S1096-4959(01)00300-1

Cochrane, V. W. (1974). Dormancy in Spores of Fungi. *Transactions of the American Microscopical Society, 93*(4), 599–609. https://doi.org/10.2307/3225161

Cole, M. B., Augustin, M. A., Robertson, M. J., & Manners, J. M. (2018, 2018/08/06). The science of food security. *NPJ Science of Food, 2*(1), 14. https://doi.org/10.1038/s41538-018-0021-9

d'Enfert, C. (1997, 1997/04/01/). Fungal Spore Germination: Insights from the Molecular Genetics of *Aspergillus nidulans* and *Neurospora crassa*. *Fungal Genetics and Biology, 21*(2), 163–172. https://doi.org/https://doi.org/10.1006/fgbi.1997.0975

Dean, R., Van Kan, J. A., Pretorius, Z. A., Hammond-Kosack, K. E., Di Pietro, A., Spanu, P. D., Rudd, J. J., Dickman, M., Kahmann, R., Ellis, J., & Foster, G. D. (2012, May).

The Top 10 fungal pathogens in molecular plant pathology. *Molecular Plant Pathology, 13*(4), 414–430. https://doi.org/10.1111/j.1364-3703.2011.00783.x

Dijksterhuis, J., van Driel, K. G., Sanders, M. G., Molenaar, D., Houbraken, J. A., Samson, R. A., & Kets, E. P. (2002, 2002/07/01). Trehalose degradation and glucose efflux precede cell ejection during germination of heat-resistant ascospores of Talaromyces macrosporus. *Archives of Microbiology, 178*(1), 1–7. https://doi.org/10.1007/s00203-002-0410-x

Doehlemann, G., Berndt, P., & Hahn, M. (2006). Trehalose metabolism is important for heat stress tolerance and spore germination of *Botrytis cinerea*. *Microbiology, 152*(9), 2625–2634. https://doi.org/https://doi.org/10.1099/mic.0.29044-0

Donaldson, M. E., & Saville, B. J. (2013, Jul). *Ustilago maydis* natural antisense transcript expression alters mRNA stability and pathogenesis. *Molecular Microbiology, 89*(1), 29–51. https://doi.org/10.1111/mmi.12254

Fairman-Williams, M. E., Guenther, U.-P., & Jankowsky, E. (2010). SF1 and SF2 helicases: family matters. *Current Opinion in Structural Biology, 20*(3), 313–324.

FAO. (2008). An Introduction to the Basic Concepts of Food Security. In *Food Security Information for Action: Practical Guides*.

FAO. (2023). *Agricultural production statistics 2000–2022* (FAOSTAT Analytical Briefs, Issue 79). https://openknowledge.fao.org/items/43fde039-dc0f-484a-97ef-e2e335c0bf1a

FAO. (2024). *Agricultural production statistics 2010–2023* (FAOSTAT Analytical Briefs, Issue 96). https://openknowledge.fao.org/handle/20.500.14283/cd3755en

FAO. (2025). *Crop Prospects and Food Situation* (Triannual Global Report, Issue 1). https://doi.org/10.4060/cd4597en

FAO, IFAD, UNICEF, WFP, & WHO. (2023). *The State of Food Security and Nutrition in the World 2023. Urbanization, agrifood systems transformation and healthy diets across the rural–urban continuum.* Rome, FAO. https://doi.org/https://doi.org/10.4060/cc3017en

Faraji Rad, Z. (2023). Microneedle Technologies for Food and Crop Health: Recent Advances and Future Perspectives. *Advanced Engineering Materials, 25*(4), 2201194. https://doi.org/https://doi.org/10.1002/adem.202201194

Feofilova, E. P., Ivashechkin, A. A., Alekhin, A. I., & Sergeeva, Y. E. (2012, 2012/01/01). Fungal spores: Dormancy, germination, chemical composition, and role in biotechnology (review). *Applied Biochemistry and Microbiology, 48*(1), 1–11. https://doi.org/10.1134/S0003683812010048

Górska-Warsewicz, H., Rejman, K., Ganczewski, G., & Kwiatkowski, B. (2023). Chapter 18 - Economic importance of nutritional and healthy cereals and/or cereal products. In M. Rakszegi, M. Papageorgiou, & J. M. Rocha (Eds.), *Developing Sustainable and Health Promoting Cereals and Pseudocereals* (pp. 433–450). Academic Press. https://doi.org/https://doi.org/10.1016/B978-0-323-90566-4.00008-4

Gottlieb, D. (1950). The physiology of spore germination in fungi. *The Botanical Review, 16*(5), 229–257.

Griffin, D. H. (1994). Spore dormancy and germination. In *Fungal Physiology* (Vol. 2nd ed, pp. 375–398). John Wiley & Sons.

Hawker, L. E., & Hendy, R. J. (1963). An Electron-Microscope Study of Germination of Conidia of *Botrytis cinerea*. *Journal of General Microbiology, 33*(1), 43–46. https://doi.org/https://doi.org/10.1099/00221287-33-1-43

Independent Group of Scientists appointed by the Secretary-General. (2023). *Global Sustainable Development Report 2023: Times of crisis, times of change: Science for accelerating transformations to sustainable development*. https://sdgs.un.org/gsdr/gsdr2023

Kahmann, R., & Kämper, J. (2004). Ustilago maydis: how its biology relates to pathogenic development. *New Phytologist, 164*(1), 31–42. https://doi.org/https://doi.org/10.1111/j.1469-8137.2004.01156.x

Kämper, J. (2004, Feb). A PCR-based system for highly efficient generation of gene replacement mutants in *Ustilago maydis*. *Molecular Genetics and Genomics, 271*(1), 103–110. https://doi.org/10.1007/s00438-003-0962-8

Kämper, J., Kahmann, R., Bolker, M., Ma, L. J., Brefort, T., Saville, B. J., Banuett, F., Kronstad, J. W., Gold, S. E., Muller, O., Perlin, M. H., Wosten, H. A., de Vries, R., Ruiz-Herrera, J., Reynaga-Pena, C. G., Snetselaar, K., McCann, M., Perez-Martin, J., Feldbrugge, M., Basse, C. W., Steinberg, G., Ibeas, J. I., Holloman, W., Guzman, P., Farman, M., Stajich, J. E., Sentandreu, R., Gonzalez-Prieto, J. M., Kennell, J. C., Molina, L., Schirawski, J., Mendoza-Mendoza, A., Greilinger, D., Munch, K., Rossel, N., Scherer, M., Vranes, M., Ladendorf, O., Vincon, V., Fuchs, U., Sandrock, B., Meng, S., Ho, E. C., Cahill, M. J., Boyce, K. J., Klose, J., Klosterman, S. J., Deelstra, H. J., Ortiz-Castellanos, L., Li, W., Sanchez-Alonso, P., Schreier, P. H., Hauser-Hahn, I., Vaupel, M., Koopmann, E., Friedrich, G., Voss, H., Schluter, T., Margolis, J., Platt, D., Swimmer, C., Gnirke, A., Chen, F., Vysotskaia, V., Mannhaupt, G., Guldener, U., Munsterkotter, M., Haase, D., Oesterheld, M., Mewes, H. W., Mauceli, E. W., DeCaprio, D., Wade, C. M., Butler, J., Young, S., Jaffe, D. B., Calvo, S., Nusbaum, C., Galagan, J., & Birren, B. W. (2006, Nov 2). Insights from the genome of the biotrophic fungal plant pathogen *Ustilago maydis*. *Nature, 444*(7115), 97–101. https://doi.org/10.1038/nature05248

Khan, M. R., & Sharma, R. K. (2020, 2020/12/01). Fusarium-nematode wilt disease complexes, etiology and mechanism of development. *Indian Phytopathology, 73*(4), 615–628. https://doi.org/10.1007/s42360-020-00240-z

Kikoku, Y. (2003). Heat Activation Characteristics of Talaromyces Ascospores. *Journal of Food Science, 68*(7), 2331–2335. https://doi.org/https://doi.org/10.1111/j.1365-2621.2003.tb05768.x

Lamont, B. B., & Pausas, J. G. (2023). Seed dormancy revisited: Dormancy-release pathways and environmental interactions. *Functional Ecology, 37*(4), 1106–1125. https://doi.org/https://doi.org/10.1111/1365-2435.14269

Lanver, D., Müller, A. N., Happel, P., Schweizer, G., Haas, F. B., Franitza, M., Pellegrin, C., Reissmann, S., Altmüller, J., & Rensing, S. A. (2018). The biotrophic development of Ustilago maydis studied by RNA-seq analysis. *The Plant Cell, 30*(2), 300–323.

Lubzens, E., Cerda, J., & Clark, M. (2010). *Dormancy and resistance in harsh environments* (Vol. 21). Springer Science & Business Media. https://doi.org/https://doi.org/10.1007/978-3-642-12422-8

Mazoyer, M., & Roudart, L. (2006). *A history of world agriculture: from the neolithic age to the current crisis*. NYU Press.

Møbjerg, N., & Neves, R. C. (2021, 2021/04/01/). New insights into survival strategies of tardigrades. *Comparative Biochemistry and Physiology Part A: Molecular & Integrative Physiology, 254*, 110890. https://doi.org/https://doi.org/10.1016/j.cbpa.2020.110890

Money, N. P. (2016). Chapter 3 - Spore Production, Discharge, and Dispersal. In S. C. Watkinson, L. Boddy, & N. P. Money (Eds.), *The Fungi (Third Edition)* (pp. 67–97). Academic Press. https://doi.org/https://doi.org/10.1016/B978-0-12-382034-1.00003-7

Nicholson, C. F., Stephens, E. C., Kopainsky, B., Jones, A. D., Parsons, D., & Garrett, J. (2021, 2021/03/01/). Food security outcomes in agricultural systems models: Current status and recommended improvements. *Agricultural Systems, 188*, 103028. https://doi.org/https://doi.org/10.1016/j.agsy.2020.103028

Osherov, N., & May, G. (2000). Conidial Germination in *Aspergillus nidulans* Requires RAS Signaling and Protein Synthesis. *Genetics, 155*(2), 647–656. https://doi.org/10.1093/genetics/155.2.647

Ostrowski, L. A., & Saville, B. J. (2017, Mar). Natural antisense transcripts are linked to the modulation of mitochondrial function and teliospore dormancy in *Ustilago*

maydis. *Molecular Microbiology, 103*(5), 745–763. https://doi.org/10.1111/mmi.13587

Poutanen, K. S., Kårlund, A. O., Gómez-Gallego, C., Johansson, D. P., Scheers, N. M., Marklinder, I. M., Eriksen, A. K., Silventoinen, P. C., Nordlund, E., Sozer, N., Hanhineva, K. J., Kolehmainen, M., & Landberg, R. (2022). Grains – a major source of sustainable protein for health. *Nutrition Reviews, 80*(6), 1648–1663. https://doi.org/10.1093/nutrit/nuab084

Ramberg, J. E., & McLaughlin, D. J. (1980). Ultrastructural study of promycelial development and basidiospore initiation in *Ustilago maydis*. *Canadian Journal of Botany, 58*(14), 1548–1561.

Ruijter, G. J. G., Bax, M., Patel, H., Flitter, S. J., Vondervoort, P. J. I. v. d., Vries, R. P. d., vanKuyk, P. A., & Visser, J. (2003). Mannitol Is Required for Stress Tolerance in *Aspergillus niger* Conidiospores. *Eukaryotic Cell, 2*(4), 690–698. https://doi.org/doi:10.1128/ec.2.4.690-698.2003

Sacadura, N. T., & Saville, B. J. (2003). Gene expression and EST analyses of *Ustilago maydis* germinating teliospores. *Fungal Genetics and Biology, 40*(1), 47–64. https://doi.org/10.1016/s1087-1845(03)00078-1

Savary, S., Ficke, A., Aubertot, J.-N., & Hollier, C. (2012, 2012/12/01). Crop losses due to diseases and their implications for global food production losses and food security. *Food Security, 4*(4), 519–537. https://doi.org/10.1007/s12571-012-0200-5

Saville, B. J., Donaldson, M. E., & Doyle, C. E. (2012). Investigating host induced meiosis in a fungal plant pathogen. In S. Andrew (Ed.), *Meiosis - Molecular Mechanisms and Cytogenetic Diversity*. InTech. https://doi.org/10.5772/30032

Schmit, J. C., & Brody, S. (1976, 1976/03//). Biochemical genetics of *Neurospora crassa* conidial germination. *Bacteriological Reviews, 40*(1), 1–41. https://doi.org/10.1128/br.40.1.1-41.1976

Schuster, M., Schweizer, G., Reissmann, S., & Kahmann, R. (2016, 2016/04/01/). Genome editing in *Ustilago maydis* using the CRISPR–Cas system. *Fungal Genetics and Biology, 89*, 3–9. https://doi.org/https://doi.org/10.1016/j.fgb.2015.09.001

Sephton-Clark, P. C. S., & Voelz, K. (2018). Chapter Four - Spore Germination of Pathogenic Filamentous Fungi. In S. Sariaslani & G. M. Gadd (Eds.), *Advances in Applied Microbiology* (Vol. 102, pp. 117–157). Academic Press. https://doi.org/https://doi.org/10.1016/bs.aambs.2017.10.002

Stade, S., & Brambl, R. (1981). Mitochondrial biogenesis during fungal spore germination: respiration and cytochrome c oxidase in *Neurospora crassa*. *Journal of Bacteriology, 147*(3), 757–767. https://doi.org/doi:10.1128/jb.147.3.757–767.1981

Storey, K. B. (2003). Mammalian hibernation. Transcriptional and translational controls. *Advances in Experimental Medicine and Biology, 543*, 21–38.

Stukenbrock, E., & Gurr, S. (2023). Address the growing urgency of fungal disease in crops. *Nature, 617*(7959), 31–34.

Sussman, A. S., & Douthit, H. A. (1973). Dormancy in microbial spores. *Annual Review of Plant Physiology, 24*(1), 311–352. https://doi.org/10.1146/annurev.pp.24.060173.001523

Tian, Z., Wang, J.-W., Li, J., & Han, B. (2021). Designing future crops: challenges and strategies for sustainable agriculture. *The Plant Journal, 105*(5), 1165–1178. https://doi.org/https://doi.org/10.1111/tpj.15107

Tsukahara, T. (1968). Electron microscopy of swelling and germinating conidiospores of *Aspergillus niger*. *Sabouraudia, 6*(3), 185–191. https://doi.org/10.1080/00362176885190371

van der Veen, M. (2010, 2010/03/01). Agricultural innovation: invention and adoption or change and adaptation? *World Archaeology, 42*(1), 1–12. https://doi.org/10.1080/00438240903429649

Zahiri, A. R., Babu, M. R., & Saville, B. J. (2005, Jun). Differential gene expression during teliospore germination in *Ustilago maydis*. *Molecular Genetics and Genomics, 273*(5), 394–403. https://doi.org/10.1007/s00438-005-1142-9

Zuo, W., Depotter, J. R. L., & Doehlemann, G. (2020, 2020/03/01/). Cas9HF1 enhanced specificity in *Ustilago maydis*. *Fungal Biology, 124*(3), 228–234. https://doi.org/https://doi.org/10.1016/j.funbio.2020.02.006

CHAPTER 2

PREFACE

Title: Exploring mechanisms of gene expression control during *Ustilago maydis* teliospore germination

Authors: Amanda M. Seto, Michael E. Donaldson, and Barry J. Saville

Reference: Published in *Canadian Journal of Plant Pathology* (2025)
doi: https://doi.org/10.1080/07060661.2024.2413557
2024 Impact Factor: 1.5

Contributions: B.J.S. conceived, directed, and obtained funding for the research presented in this study. M.E.D. collected and isolated RNA for the RNA-seq submission and performed RNA-seq analysis. A.M.S. performed the preliminary teliospore germination trials, carried out the teliospore germination time course for RNA-seq, identified gene transcript level changes from RNA-seq analysis, isolated RNA from biological replicates of teliospore germination time courses, haploid cells, and dikaryon for RT-qPCR assessment, carried out the RT-qPCR assessment of gene transcript level changes, and conducted the gene ontology analysis. A.M.S. created Tables 2.1–2.4, S2.1–S2.4, and Figures 2.1–2.3. Sonia Seto of Sonia Seto Studios created Figure 2.4. A.M.S. drafted the manuscript. B.J.S. edited the initial draft and assembly of the manuscript. All authors edited the manuscript prior to submission.

CHAPTER 2

Exploring mechanisms of gene expression control during *Ustilago maydis* teliospore germination

Published in *Canadian Journal of Plant Pathology* (2025), **47**(1): 80–97

doi: https://doi.org/10.1080/07060661.2024.2413557

ABSTRACT

Fungal plant pathogens produce spores for survival and dispersion. Developing an understanding of the mechanisms involved in spore dormancy and germination will aid in mitigating the impact of diseases they cause. The thick-walled diploid teliospores of *Ustilago maydis* were used as a model for studying fungal spore dormancy and germination. These spores develop only in infected maize tissue and can remain dormant for long periods of time. Teliospores germinate under favourable conditions, resume meiosis, and produce basidiospores to initiate new rounds of infection. Previous research identified changing gene transcripts during teliospore germination, but analysis was hampered by asynchronous germination. The more comprehensive RNA-seq analysis of *U. maydis* teliospore germination presented here aimed to identify gene altered transcript levels detectable above the background of fluctuating changes resulting from asynchronous germination. The analyses identified 18 different patterns of gene transcript level changes. It also indicated that gene expression is controlled at the transcriptional and post-transcriptional levels. Gene ontology term enrichment analyses of these patterns revealed genes that are involved in cell morphogenesis, metabolism, and RNA metabolism.

Keywords: asynchronous teliospore germination; germination proteins; patterns of gene expression; predicting gene expression control; RNA-seq; stages of teliospore germination; *Ustilago maydis*

INTRODUCTION

Teliospores are a type of dormant resistant spore produced by economically devastating rust, bunt, and smut fungi (Piepenbring et al. 1998; Helfer 2014). They provide a means of dispersal and protection between cycles of growth and development within hosts and are integral to the completion of meiosis. As such, they contribute to disease spread and, through sexual reproduction, the creation and maintenance of virulence genotypes (Saville et al. 2012). However, fungal spores have received relatively little study and knowledge of molecular events associated with their germination are limited. Here we expand the investigation of teliospore germination and transcript level changes in the tractable smut fungus *Ustilago maydis* (DC) Corda. The goal was to identify gene functions and gene expression control mechanisms to fill a major knowledge gap in our understanding of teliospore germination.

Ustilago maydis infects maize causing common smut of corn. The disease is characterized by tumour formation on all aerial parts of the plant. Dormant diploid teliospores are produced in the tumours. Teliospores are released into the environment where they can germinate and initiate new rounds of infection (Kämper et al. 2006; reviewed in Brefort et al. 2009). Teliospore germination is concomitant with the completion of meiosis. The first visible indication of germination is the emergence of a promycelium through the ruptured three-layer cell wall of the teliospore (Ramberg and McLaughlin 1980). At this stage, the nucleus is in late prophase I of meiosis and it moves into the growing promycelium. Meiosis is completed as the promycelium extends and becomes a basidium from which basidiospores bud off (O'Donnell and McLaughlin 1984). An update of the stages of teliospore germination based on microscopic observations was

proposed by Ostrowski et al. (2018), which indicated that molecular changes occurred before visible signs of germination were apparent.

Events that occur prior to the visual signal of germination have been investigated. Early studies indicated that: 1) dormant teliospores have low levels of oxygen consumption; 2) dormant teliospores contained enzyme activities indicating that the glycolysis pathway for glucose catabolism was present, but that many pentose phosphate pathway (PPP) and tricarboxylic acid (TCA) cycle enzyme activities were undetectable; and 3) germination is initiated by the presence of select sugars (Gottlieb and Caltrider 1963; Caltrider and Gottlieb 1966). Tripathi and Gottlieb (1974) found that rRNAs, tRNAs, and mRNAs were synthesized at 2, 4, and 6 h post induction of germination (PIG) and that significant protein synthesis, detected by the presence of polyribosomes, occurred at 4–6 h PIG. However, Lin et al. (1971) detected a measurable increase in protein synthesis before mRNA transcription. This last finding is consistent with the Ostrowski et al. (2018) detection of respiration approximately 45 minutes PIG, which suggests dormant teliospores contain proteins and mRNAs that become available for translation by existing ribosomes after the signal for germination is received. Pre-formed mRNAs may be stored as double-stranded RNAs (dsRNAs) and/or bound to protein complexes in the form of ribonucleoproteins (RNPs) (reviewed in Griffin 1994; Donaldson and Saville 2013; Ostrowski and Saville 2017). Further insight regarding transcripts in dormant and germinating teliospores was gained by the analysis of expressed sequence tag (EST) libraries (Sacadura and Saville 2003; Ho et al. 2007) and cDNA microarray hybridization results (Zahiri et al. 2005). These studies revealed some of the molecular processes occurring during germination. Zahiri et al. (2005) further identified waves of transcription

during germination and the presence of gene expression control at the translational and transcriptional levels. A limitation of these studies is that they were not comprehensive and that germination events were not synchronous in the teliospore populations used.

The asynchronous germination of *U. maydis* teliospores is the greatest challenge to studying their germination. Teliospore formation and maturation are not synchronous even within a single tumour (Banuett and Herskowitz 1996) and earlier investigations used teliospores harvested from several tumours (Sacadura and Saville 2003; Zahiri et al. 2005). As such, the samples used for nucleic acid isolations contained teliospores at multiple stages of germination. This limited the ability to detect changes in transcript levels associated with specific stages. Here, we present data from our attempts to isolate more synchronously germinating populations of teliospores as well as a "brute force-" type approach attempting to identify gene transcript level changes above the background variation created by asynchronous germination using RNA-seq.

The RNA-seq data allowed us to identify patterns of gene transcript level changes, to identify the activity of significant biological processes through gene ontology (GO) enrichment analysis, to propose modes of expression control for specific genes, and to create a model for teliospore germination integrating these analyses with previous studies. This work provides a substantial increase in our knowledge of the transition from teliospore dormancy to germination which can inform studies directed toward disrupting the disease cycle of fungal pathogens.

MATERIALS AND METHODS

Ustilago maydis *strains, growth conditions, and teliospore cultivation*

Ustilago maydis haploid strains 521 (a1b1) and 518 (a2b2) were picked and cultured as described by Zahiri et al. (2005), and maize cob inoculations were carried out in a greenhouse setting utilizing modifications outlined in Donaldson et al. (2017). Teliospores were harvested from either all infected cobs, one infected cob, or from individual tumours following the teliospore harvesting method described by Ostrowski et al. (2018).

Preparation of the 518×521 forced dikaryon and teliospore germination time courses

The 518×521 forced dikaryon was prepared and spotted on potato dextrose agar (PDA) plates containing charcoal as described by Donaldson et al. (2017). Following 2 days of growth at room temperature, filamentous growth was confirmed through microscopy. Mycelial cells were harvested from plates with a sterile spatula and frozen with liquid nitrogen. Samples were stored at −80 °C prior to RNA isolation.

Teliospores isolated from entire cobs and individual tumours were germinated in YEPS Gold medium (10 g L^{-1} yeast extract, 20 g L^{-1} peptone, 20 g L^{-1} sucrose) supplemented with streptomycin sulphate (160 µg mL^{-1}) and incubated at 28 °C with shaking at 90 rpm. Samples were taken at regular intervals to assess the stages of germination present.

Samples for RNA-seq library creation and validation time courses consisted of teliospores germinating in potato dextrose broth (24 g L^{-1}) supplemented with streptomycin sulphate (160 µg mL^{-1}) and incubated at 28 °C with shaking at 90 rpm. For RNA-seq library creation, teliospores were sampled at 0 h, 9 h, and 18 h post-induction of germination (PIG). For RNA-seq validation, two additional biological replicate time courses were used. Samples were taken at 0 h, 4 h, and 8 h PIG for the first biological replicate time course and 0 h, 6 h, and 12 h PIG for the second biological replicate time

course. These time points were selected to replicate the percentage of germination observed for RNA-seq rather than use identical time points. Teliospore germination rates are variable between biological replicates and preliminary germination time courses were carried out with biological replicate samples of 518×521 teliospores to determine a time point where the germination percentages were similar to the RNA-seq germination time course.

For all teliospore germination time courses, germination was observed at 400× magnification using an Axio Scope.A1 compound microscope (Carl Zeiss RTMicroImaging) as described by Donaldson et al. (2013). The percentage of germination for each time point was quantified using a haemocytometer and the stages of germination present were identified based on the germination stages described in Ostrowski et al. (2018). For each time point, the germination medium was removed and teliospores were frozen with liquid nitrogen and stored at -80°C until RNA isolation.

RNA isolation, cDNA library preparation, and RNA-sequencing

RNA isolation and cDNA library preparation of germination time course samples for stranded RNA-sequencing were carried out as outlined in Donaldson et al. (2017). Briefly, the paired-end reads for each teliospore germination time point were aligned to the *U. maydis* genome, updated gene models were created using *de novo* and genome-guided transfrag assemblies, and differential gene expression was identified using CLC Genomics Workbench v9.0 (Donaldson et al. 2017). RNA-seq fastq files are available from the NCBI Sequence Read Archive database (accession number PRJNA371633).

Identification of gene transcript level change patterns during teliospore germination and gene ontology analysis

Significantly different gene transcript level changes in the T00 library relative to the

haploid and dikaryon libraries were identified (FDR = < 0.05 and p = < 0.001). Transcript-level fold changes were calculated for T00 relative to T09, T00 relative to T18, and T09 relative to T18 using the normalized expression values (Supplementary Table S2.1). The criteria listed in Table 2.1 were used to determine the patterns of transcript level changes during germination and the number of transcripts that fit the criteria are identified for each pattern.

Gene ontology (GO) term analysis was carried out for each pattern using the web-based PANTHER classification system (http://www.pantherdb.org/). The statistical overrepresentation test was used to determine which functional classes based on GO terms were statistically over and underrepresented in each pattern. The Fisher's exact test with FDR multiple test correction was used to determine statistical significance (FDR = <0.05 and p = <0.05) of the overrepresentation analysis results (Mi et al. 2019, 2021). Separate overrepresentation analyses were conducted for each pattern where the list of genes was used as the test list. The list of genes that were over and underrepresented in each pattern were determined relative to a reference list of genes. The reference list was derived from the 1,815 gene transcripts that were significantly different at T00 when compared to the haploid and dikaryon cell type libraries. This list contained 1,657 gene IDs once redundant gene IDs and non-coding RNAs were removed (Supplementary Table S2.2). The complete GO annotation datasets (version release 2021-11-16) for biological process, molecular function, and cellular component were used.

RT-qPCR assessment of transcript level changes

Reverse transcriptase quantitative PCR (RT-qPCR) using SYBR green was carried out using primers directed against the ORF of selected genes. Primers were designed using the

OligoArchitect Online tool (Sigma-Aldrich) for designing SYBR Green I primers (Supplementary Table S2.3). Following RNA isolation and DNase I treatment, first-strand cDNA synthesis was performed on 400 ng of total RNA using TaqMan Reverse Transcription Reagents (Applied Biosystems) primed with Oligo $d(T)_{16}$. The resulting cDNA was diluted fourfold (1:3) with DEPC-treated dH_2O. RT-qPCR was performed on the QuantStudio 3 Real-Time PCR system (Applied Biosystems) using the *Power* SYBR Green PCR Master Mix (Applied Biosystems). Each 20 µL RT-qPCR reaction contained 1× *Power* SYBR Green PCR Master Mix, 500 nM of each primer, and 2.0 µL cDNA. PCR cycling conditions were 50 °C for 2 min, 95 °C for 10 min followed by 40 cycles of 95 °C for 15 s and 60 °C for 1 min. The endogenous control was *UMAG_00175* which encodes for eukaryotic translation initiation factor 3 subunit F. *UMAG_00175* was previously established as a suitable housekeeping gene for RT-qPCR (Morrison et al. 2012; Seto 2013). All data were collected and analysed using the QuantStudio Design and Analysis Software version 1.4.3. The relative quantity (RQ) was calculated using the comparative CT ($2^{-\Delta\Delta CT}$) method (Livak and Schmittgen 2001) where *UMAG_00175* was set as the endogenous control and T00 as the reference sample.

RESULTS

RNA-seq library creation and transcript characterization

RNA-seq libraries were created from a teliospore germination time course to identify gene transcript level changes occurring above the background of asynchronous germination. The time points selected were 0 h (T00), 9 h (T09), and 18 h (T18) PIG. The germination stages present at each time point were as follows: at T00 there were 100% Stage I teliospores, at

T09 there were 100% Stage I teliospores, and at T18 there were 94.8% Stage I, 2.5% Stage II, and 2.7% Stages III–IV teliospores.

A total of 1,815 transcripts were identified as significantly different at T00 when compared to the haploid and dikaryon libraries. We divided these transcripts into two groups where 940 transcripts were downregulated at T00 and 875 transcripts were upregulated at T00. All gene transcripts were characterized by Cufflinks Cuffcompare (Table 2.2). Based on the Cufflinks Cuffcompare, among the 940 downregulated transcripts at T00, 13 are potential new alternatively spliced genes, 19 are natural antisense transcripts, and 5 are noncoding RNAs. In the list of 875 upregulated transcripts, there are 15 potential new alternatively spliced genes, 48 natural antisense transcripts, and 38 noncoding RNAs (Table2.2).

Patterns of gene transcript level change during teliospore germination

We identified 18 patterns of gene transcript level changes during teliospore germination. Patterns 1 through 9 are associated with the 940 downregulated transcripts at T00 (Fig. 2.1*A*) and patterns 10 through 18 are associated with the 875 upregulated transcripts at T00 (Fig. 2.1*B*). The number of transcripts and transcript characterizations that are associated with each pattern are listed in Table 2.3. Most gene transcripts are found in patterns 2, 5, 14, and 17.

RT-qPCR assessment of the patterns of gene transcript level change

RT-qPCR with SYBR green detection was used to independently assess the existence of the 18 patterns of gene transcript level changes (Fig. 2.1) identified through RNA-seq. We used two biological replicates of the teliospore germination time course and aimed to replicate the percentage of germination observed for RNA-seq. The first biological

replicate germination time course resulted in the following time points and stages of germination present: 0 h (T00) PIG (Stage I – 100%), 4 h (T04) PIG (Stage I – 99.8%, Stage II – 0.2%), 8 h (T08) PIG (Stage I – 98%, Stage II – 1.6%, Stage III – 0.4%). The second biological replicate germination time course resulted in using timepoints 0 h (T00), 6 h (T06), and 12 h (T12) PIG. Time points T00 and T06 consisted of Stage I (100%) germinating teliospores, and at T12 Stages I (93.9%), II (3.6%), and III (2.5%) were present.

One or two genes were selected from each of patterns 12 to 18 to assess transcript level change by RT-qPCR. Variation in transcript levels was detected with the two genes that were selected from pattern 12 in the biological replicates. The pattern of transcript level change for genes selected from pattern 13 differed from the RNA-seq data. The transcript level changes of the gene from pattern 15 were consistent with the RNA-seq data in the second biological replicate. However, the results showed that both biological replicates support patterns 14, 16, 17, and 18 with at least one of the genes selected (Fig. 2.2).

Gene ontology analysis during teliospore germination

Gene ontology (GO) analysis was performed for each pattern of gene transcript level change (patterns 1–18) to determine which biological processes were enriched. Patterns 2, 5, 7, and 14 resulted in a significant overrepresentation of GO terms (summarized in Table 2.4). The full list of genes for each GO term can be found in Supplementary Table S2.4.

The gene transcripts in pattern 2 are upregulated in the haploid and dikaryon cell types, downregulated at T00, increased at T09, and have less than a 2-fold change in transcript level from T09 to T18. Of the 385 gene transcripts, 374 are unique genes and GO

term enrichment analysis indicated a significant overrepresentation of genes associated with the cell cortex (GO:0005938), cytoskeleton (GO:0005856), endoplasmic reticulum (GO:0005783), membrane protein complex (GO:0098796), and cytoplasm (GO:0005737) (Table 2.4). In pattern 2, specific genes of note encode four previously characterized septins (*UMAG_10503*, *UMAG_10644*, *UMAG_03449*, and *UMAG_03599*) which are highly conserved GTP-binding proteins (Boyce et al. 2005; Banuett et al. 2008; Alvarez-Tabarés and Pérez-Martín 2010); enzymes involved in protein glycosylation and proteins ensuring proper protein folding (*UMAG_01018* and *UMAG_10287*); the vacuolar ATPase (V-ATPase) pump subunits (*UMAG_00508*, *UMAG_00630*, *UMAG_02064*, *UMAG_04167*, *UMAG_04345*, *UMAG_04716*, *UMAG_05503*, and *UMAG_10926*); the glycolytic pathway enzymes hexokinase (*UMAG_11945*), glyceraldehyde 3-phosphate dehydrogenase (GAPDH) (*UMAG_02491*), and phosphoglycerate mutase (*UMAG_05339*); the TCA cycle enzymes NAD^+-dependent isocitrate dehydrogenase subunit 1 (*UMAG_01329*), and succinyl-CoA synthetase β subunit (*UMAG_11353*); and a pentose phosphate pathway enzyme 6-phosphogluconate dehydrogenase (*UMAG_02577*).

The 310 gene transcripts in pattern 5 contained 301 unique genes. These transcripts are upregulated in the haploid and dikaryon cell types, downregulated at T00, and have less than a 2-fold change during germination. The GO analysis showed an overrepresentation of genes with the biological process GO categories transmembrane transport (GO:0055085) and small molecule metabolic process (GO:0044281) (Table 2.4). Genes of note in pattern 5 encode the mitochondrial ATP synthase subunits for the F_1 central stalk (*UMAG_01103*, *UMAG_10754*) and F_0 peripheral stalk (*UMAG_10548*, *UMAG_12050*, and *UMAG_02360*); the glycolytic pathway enzymes phosphofructokinase-2

(*UMAG_10293*); fructose-biphosphate aldolase (*UMAG_00674*), and enolase (*UMAG_03356*); the two subunits of pyruvate dehydrogenase, *UMAG_03854* and *UMAG_06105*), an enzyme that connects the glycolysis pathway to the TCA cycle (Harris et al. 2002); the TCA cycle enzymes citrate synthase (*UMAG_01627*), malate dehydrogenase (*UMAG_00403*), and a subunit of the mitochondrial NAD^+-dependent isocitrate dehydrogenase (*UMAG_01328*); the pentose phosphate pathway enzyme glucose-6-phosphate dehydrogenase (*UMAG_04930*); and the enzyme phosphoglucomutase (*UMAG_00486*), which connects the glycolytic pathway to gluconeogenesis to regulate glycogen and trehalose metabolism (Deveau et al. 2008).

The 28 unique gene transcripts in pattern 7 are downregulated at T00 in comparison to the haploid and dikaryon cell types. The transcript levels decrease during the early stages of germination which is followed by an increase in transcript levels at T18. The GO analysis resulted in a significant enrichment for genes with the GO term polysaccharide metabolic process (GO:0005976) (Table 2.4). Specific genes of interest encode the cell wall modifying enzymes xylanase, *xyn2* (*UMAG_03411*), an endoglucanase (*UMAG_04368*), and two chitinases *cts1* (*UMAG_10419*) and *cts2* (*UMAG_02758*).

Pattern 14 is the only pattern where genes are upregulated in the dormant teliospore and have significant GO term results during germination. The 403 transcripts included 373 unique genes and the transcript levels did not change during germination in this pattern. GO term enrichment analysis indicated an overrepresentation of genes involved in RNA metabolism, regulation, and cell metabolism. Specific genes of interest include those that encode subunits of RNA polymerase I, II, and III (*UMAG_01184*, *UMAG_01363*, *UMAG_05029*, *UMAG_03863*, *UMAG_04460*, *UMAG_04722*, *UMAG_10429*,

UMAG_10433, *UMAG_10512*, *UMAG_10858*, and *UMAG_10936*); RNA helicases and members of the Brix domain protein family (*UMAG_05200*, *UMAG_10095*, *UMAG_05214*, *UMAG_06129*, *UMAG_10410*, *UMAG_05180*, *UMAG_03844*, and *UMAG_00293*); components of the pre-mRNA splicing machinery (*UMAG_05608*, *UMAG_06130*, *UMAG_10902*, *UMAG_12244*, *UMAG_01323*, *UMAG_12130*, *UMAG_12224*, *UMAG_10381*, *UMAG_10312*, and *UMAG_11043*) and translation initiation and elongation machinery (*UMAG_02401*, *UMAG_01463*, *UMAG_06090*, *UMAG_05559*, *UMAG_10363*, *UMAG_03952*, *UMAG_06323*, *UMAG_05091*, and *UMAG_04152*); the glycolysis enzymes triose-phosphate isomerase (*UMAG_10627*), and a hexokinase (*UMAG_11945*), an acetate kinase (*UMAG_03413*), an ATP-citrate synthase (*UMAG_01005*), which converts TCA cycle derived citrate to acetyl-CoA and oxaloacetate to fuel the synthesis of fatty acids, the mevalonate pathway, and histone acetylation (Chypre et al. 2012); a subunit of the highly regulated α-ketoglutarate dehydrogenase (*UMAG_10533*), and the first and rate-limiting enzyme in the de novo purine biosynthesis pathway for nucleotide metabolism, amidophosphoribosyltransferase (*UMAG_06035*) (Moffatt and Ashihara 2002).

DISCUSSION

RNA-seq was used to identify genes with changing transcript levels during *U. maydis* teliospore germination. The goals were to identify gene functions and gain insight into the control of gene expression during teliospore germination. A challenge in this was the asynchronous germination of teliospores which was noted in other studies (Gottlieb and Caltrider 1963; Bainbridge 1971; Duran 1972; Zahiri et al. 2005). Transcriptional waves

were detected during teliospore germination using cDNA library creation with Sanger sequencing (Sacadura and Saville 2003) and microarray analyses (Zahiri et al. 2005). The limitation to these studies were the number of transcripts analysed. RNA-seq allowed an analysis of greater transcript numbers and the detection of gene transcript levels that were changing above the background caused by asynchronous germination. To limit the variability due to stage of germination in the presented work, RNA was isolated from teliospores primarily at the early stages of germination. The sequencing and analysis allowed for the prediction of 18 patterns of gene transcript level change.

RT-qPCR was used to assess the patterns of transcript level change. The variability we observed between replicate germination time courses highlights the limitations of time course-based germination assays. Each time point contained a mixture of teliospores at different stages of germination. Previous research showed this as well and noted that the transition between some germination stages occurs more rapidly than others (Caltrider and Gottlieb 1966; Ramberg and McLaughlin 1980; O'Donnell and McLaughlin 1984). Germination asynchrony may be attributed to the asynchronous maturation of teliospores observed by Banuett and Herskowitz (1996). The inherent variation in germination rates in a population of teliospores would be expected to yield inconsistent levels of gene transcripts across biological replicates. This is what we observed in the RT-qPCR results, however, five of the seven RNA-seq predicted patterns assessed were supported based on transcript level trends. This supports the concept of distinct gene expression patterns during teliospore germination.

Dormant *U. maydis* teliospores have low metabolic activity which is characterized by low respiration rate (Caltrider and Gottlieb 1963; Ostrowski et al. 2018). Therefore, in

the dormant state there is limited energy for gene expression. Consistent with this, meiosis is paused at the pachytene checkpoint in dormant teliospores. The pachytene checkpoint is a control point before the first meiotic division. In *Saccharomyces cerevisiae*, this is the last stage before a cell is committed to these meiotic divisions (Roeder and Bailis 2000). Teliospore germination signals the exit from the pachytene checkpoint, and meiosis resumes (Saville et al. 2012). The detection of patterns of transcript level change in the present study revealed that restarting metabolism and growth involves different modes of controlling the expression of sets of genes. This includes the activation of mRNAs stored in the teliospore (Griffin 1994; Donaldson and Saville 2013; Ostrowski and Saville 2017) and is related to the earlier detection of enzyme activities in the teliospore (Caltrider and Gottlieb 1963). These earlier studies indicated that, during their formation and entry into dormancy, the teliospores are prepared for germination. The RNA-seq data is consistent with this as it detected alternatively spliced genes not previously detected, natural antisense transcripts and non-coding RNAs which provides RNA evidence of post-transcriptional expression control that is required to activate stored mRNAs. The analyses also provided insight into associated biological functions via GO term enrichment analysis.

GO term enrichment analysis identified the overrepresentation of genes with certain biological functions in the transcript level change patterns 2, 5, 7, and 14. Identifying patterns of transcript level change allows us to suggest a basis of gene expression control. Transcription increases mRNA levels, translation and subsequent degradation decreases mRNA levels, and mRNAs may be stabilized in a way that inhibits translation and degradation (Mattick and Amaral 2022). To relate gene expression changes to the visual

events of teliospore germination there is a need to consider the seven stages of teliospore germination presented in Fig. 2.3.

Teliospore germination is stimulated by the presence of specific sugars (Caltrider and Gottlieb 1966) and respiration was detected 45 minutes PIG (Ostrowski et al. 2018). Early studies indicated that new translation occurred in the teliospore before new transcription (Lin et al. 1971) therefore the early events of germination are occurring in Stage I germinating teliospores, which are morphologically indistinguishable from dormant teliospores (Fig. 2.3). The patterns of transcript level change are consistent with this; pattern 7 shows transcript levels that are decreased in comparison to the dikaryon and haploid cells, which is followed by a further decrease early in germination and increase later in germination. This is consistent with stored mRNAs being translated, degraded, and replaced by new transcription. This suggests a need for the encoded proteins early in germination and as germination proceeds. A GO term overrepresented in pattern 7 was polysaccharide metabolic process (GO:0005976) with xylanase, endoglucanase, and chitinase genes being expressed. One of the earliest morphological changes of germination is the thinning of the internal teliospore walls in a specific location, preliminary to the teliospores rupturing. *Tilletia contraversa* teliospore cell walls are composed of polysaccharides such as chitin, hemicelluloses, and pectic substances (Graham 1960). If *U. maydis* teliospore cell walls are similar, then the pattern 7-identified endo-xylanases and -glucanases may function to degrade the middle and outer cell walls to aid in the promycelium emergence. *Ustilago maydis* chitinases are involved in degrading the remnant of chitin between mother and daughter cells to support cell separation during haploid growth (Langner et al. 2015), so a similar role in breaking down the teliospore cell wall is

possible. This cell wall degradation and the subsequent cell wall turnover are also required for promycelium eruption and extension (Stage II and later) which requires these enzymes. Therefore, having these genes activated early by translating stored mRNA and followed by increased transcription is consistent with observed germination events.

The indication that stored mRNAs are translated early in teliospore germination suggests that the teliospores are prepared for germination. The control mechanisms suggested by pattern 14 and the genes found therein are consistent with this suggestion. Pattern 14 has transcript levels that are elevated in the dormant teliospore relative to the dikaryon. These transcript levels remain elevated during germination, suggesting that there is increased transcription during teliospore formation, that the mRNAs are stabilized during dormancy, and are translated as germination begins. While this pattern of transcript levels could also indicate a requirement for the genes to be expressed in the dormant teliospore, the extremely low level of metabolism detected suggests that mRNAs are stored in preparation for germination. The pattern further suggests that the signal for germination also triggers transcription of these genes which leads to an elevated level of mRNAs which are translated and then degraded further indicating ongoing transcript turnover. Pattern 14 GO term enrichment analysis identified an overrepresentation of transcripts that are involved in RNA processing, ribonucleoprotein complex organization and assembly, rRNA processing, and ribosome biogenesis, all of which would be components of preparing mRNA for translation and then initiating translation. These are all molecular events that would be required to initiate and maintain gene expression during the teliospore germination which is consistent with the proposed control mechanism.

Among the genes found in pattern 14 were several RNA helicases. These enzymes function in all aspects of RNA metabolism and are capable of unwinding dsRNA, remodelling RNAs, displacing proteins, and assembling RNPs (Fairman-Williams et al. 2010; Jankowsky 2011; Linder and Fuller-Pace 2013). These events would be required early in germination to make stored mRNAs available for translation. The helicases could unwind mRNAs bound in tertiary structure or annealed to their complementary antisense RNAs, making them available for ribosome binding. Helicases also have the capacity to link these events to sugar sensing. The RNA helicase Dbp2, UMAG_10095 in *U. maydis*, has been noted in other fungi to be involved in ribosome biogenesis and cellular homeostasis. The yeast and mammalian orthologs, DDX5, were also shown to have a conserved role in glucose sensing and promoting glycolysis during growth (Beck et al. 2014; Xing et al. 2017). The presence of Dbp2 transcripts in pattern 14 indicates its encoded protein could be present in the teliospore and produced during germination. The presence of this protein would allow *U. maydis* to link the detection of glucose level shifts to RNA processing. Essentially this would mean that helicases link the control of gene expression directly to metabolic shifts, in this instance a change in cellular carbon status. This, in turn, indicates that the pattern of gene expression is intimately linked to metabolic shifts.

GO term enrichment analysis for pattern 14 also revealed other functions relevant to germination initiation and progression. These include events that may be involved in initiating germination like transporter activity and heterocyclic compound binding as well as several subunits of RNA polymerase I, II, and III. These events would be components of sensing the environment and transducing the signal to stimulate gene transcription.

There were also genes linked to various metabolic processes, which includes a pair of genes that encode triosephosphate isomerase (TPI1), an enzyme from the glycolysis pathway for which activity was detected in dormant teliospores (Caltrider and Gottlieb 1963). Our analysis identified two genes that encode for *U. maydis tpi1*. One is found in pattern 14, *UMAG_10627,* which is upregulated in the teliospore and the other in pattern 5, *UMAG_03299*, which is downregulated. The presence of enzymatic activity in the spore means that at least some of the genes with increased transcript levels also have proteins expressed in the teliospore. For example, TPI1 in *S. cerevisiae* and its product GAP were identified as components of a negative regulatory process that maintains dormancy in both yeast stationary cells and spores. Increased levels of GAP may increase the threshold for glucose requirements for the re-entry to mitotic growth (Liu et al. 2022). The increased transcript levels of the *UMAG_10627* and the presence of the enzyme in dormant teliospores (Caltrider and Gottlieb 1963) suggest that a similar negative regulatory process is present in *U. maydis* teliospores.

Transcript level change pattern 5 is the same as 14 except the transcript levels in the dormant teliospore are reduced relative to the dikaryon and haploid cells. The transcript levels remain at a constant level during germination. This suggests a steady state of mRNAs is maintained through transcription, translation, and subsequent degradation. In this pattern, GO term enrichment analysis indicated an overrepresentation of transmembrane transport, gene expression, and various metabolic processes separate from energy production as well as a major focus on processes related to mitochondrial function. Caltrider and Gottlieb (1963) and Ostrowski et al. (2018) noted an increase in respiration, which occurs as early as 45 minutes PIG and plateaus at germination Stage III. Increased

oxygen consumption is an indicator of mitochondrial activity and ensures ATP production to fuel many biological pathways (Walker and White 2017). Membrane-bound mitochondrial ATP synthases are responsible for converting ADP to ATP (Neupane et al. 2019). Genes that encode for the assembly of the central and peripheral stalk structures of mitochondrial ATP synthases were found in pattern 5. The central and peripheral stalks are the backbone of ATP synthases as they connect the F_0 to the F_1 domains (Duvezin-Caubet et al. 2006). The appearance of the ATP synthase genes in pattern 5 suggests that a steady state level of production (i.e., transcription, translation, and mRNA degradation during germination), is required to support the energetic requirements of teliospore germination and promycelium development.

Some of the genes identified in pattern 5 allow us to relate this data to early studies which indicated that all enzymes from the glycolytic pathway and some enzymes from both the TCA cycle and pentose phosphate pathway (PPP) (Caltrider and Gottlieb 1963) were present in Stage I teliospores. Notably, transcripts of key carbohydrate metabolism enzyme phosphoglucomutase, *UMAG_00486*, and the TCA enzyme malate dehydrogenase were found in pattern 5. The enzyme activity for both enzymes were detected at increased concentrations 6 h PIG (Caltrider and Gottlieb 1963). This suggested stored proteins are activated or mRNAs are translated for these genes, and this indicates that the genes are controlled at post-transcriptional, translational, and post-translational levels during Stage I of germination.

Transcripts that encode for the assembly of V-ATPases pumps, which are membrane-bound pumps found in fungal vacuoles, were found in pattern 2. The activity of V-ATPase pumps contributes to the acidification of organelles and cellular homeostasis,

as well as stress response, and they have a role in secretory vesicle transport for cell wall biogenesis (Bowman and Bowman 2010; Schachtschabel et al. 2012; Rane et al. 2013; Jia et al. 2018). The presence of these gene transcripts in pattern 2 indicates that transcription of these genes increased following germination induction, and an elevated steady state of transcription, translation, and degradation was reached. This is consistent with the need of V-ATPase pump activity to support promycelium development and elongation as the teliospore transitions from Stages I through VII. All four *U. maydis* septin genes also have transcripts in pattern 2. Alvarez-Tabarés and Pérez-Martín (2010) determined that septins are not required for teliospore germination however, the promycelium produced by septin minus strains was swollen suggesting that there are defects in the development of the cell wall and osmoregulation. Therefore, the septin and other pattern 2 genes are transcriptionally regulated during teliospore germination, and this transcription is likely initiated by a signal associated with the induction of teliospore germination.

The use of RNA-seq allowed us to identify 18 potential patterns of transcript level change, identified key GO terms, and specific genes associated with *U. maydis* teliospore germination that provided insight into the molecular and metabolic changes associated with teliospore germination. The asynchronous teliospore germination led to biological variation in replicate teliospore germination time courses, which influenced the certainty of determining the exact timing of transcript level changes. Given this limitation, we focused on four patterns of transcript level change that had significant GO term enrichment results and summarized those findings in Fig. 2.4. We note that these patterns of transcript level change happen early in the germination process and propose gene expression control mechanisms to explain the patterns. One mechanism involves stabilization of the mRNA

in dormant teliospores with translation during germination as well as increased transcription that maintains a steady state level of mRNA during germination. The added control of genes with this pattern of expression comes during teliospore formation when these genes are either upregulated or downregulated. They are upregulated during teliospore formation, and the transcripts are stored at an elevated level. These transcripts are translated upon germination when their transcription is also increased maintaining the high level of expression during germination. Another group of genes is upregulated during teliospore germination with increased transcription, translation, and degradation that achieves a high steady state level of the transcripts. Together these patterns of gene expression control indicate that some events are set during teliospore formation, primed for germination, and others are turned on when germination is induced. Identifying these genes will allow the methods of gene expression control to be investigated further and could provide targets for influencing teliospore germination thereby controlling disease spread.

ACKNOWLEDGEMENTS

We would like to acknowledge Sonia Seto Studios and thank Sonia Seto for the creation of Figure 2.4. We acknowledge funding for this project provided by the Natural Sciences and Engineering Research Council (NSERC) of Canada and the Ministry of Ontario Research and Innovation, Ontario Research Fund Research Excellence award (BJS).

DISCLOSURE STATEMENT

No potential conflict of interest was reported by the author(s).

TABLES AND FIGURES

Table 2.1. Transcript level fold changes were calculated for T00 relative to 518/521/Dikaryon, T00 relative to T09, and T09 relative to T18 using the normalized expression values. Each pattern of transcript level change had specific fold change criteria. The calculated fold changes are located in Supplementary Table S2.1.

Pattern ID	518/521/Dikaryon	T09 vs T00	T18 vs T09
1	≥ 2 fold	≥ 2 fold	≥ 2 fold
2	≥ 2 fold	≥ 2 fold	> -2 fold and < 2 fold
3	≥ 2 fold	≥ 2 fold	≥ -2 fold
4	≥ 2 fold	> -2 fold and < 2 fold	≥ 2 fold
5	≥ 2 fold	> -2 fold and < 2 fold	> -2 fold and < 2 fold
6	≥ 2 fold	> -2 fold and < 2 fold	≥ 2 fold
7	≥ 2 fold	≥ -2 fold	≥ 2 fold
8	≥ 2 fold	≥ -2 fold	> -2 fold and < 2 fold
9	≥ 2 fold	≥ -2 fold	≥ -2 fold
10	≤ -2 fold	≥ 2 fold	≥ 2 fold
11	≤ -2 fold	≥ 2 fold	> -2 fold and < 2 fold
12	≤ -2 fold	≥ 2 fold	≥ -2 fold
13	≤ -2 fold	> -2 fold and < 2 fold	≥ 2 fold
14	≤ -2 fold	> -2 fold and < 2 fold	> -2 fold and < 2 fold
15	≤ -2 fold	> -2 fold and < 2 fold	≥ 2 fold
16	≤ -2 fold	≥ -2 fold	≥ 2 fold
17	≤ -2 fold	≥ -2 fold	> -2 fold and < 2 fold
18	≤ -2 fold	≥ - 2 fold	≥ -2 fold

Table 2.2. Summary of the number of transcripts characterized by Cufflinks Cuffcompare. Transcripts are significantly different at T00 compared to the haploid and dikaryon libraries.

Description	Cuffcompare code	T00 Downregulated	T00 Upregulated
Open reading frame (ORF)		885	726
Single exon transfrag that overlaps a reference exon and is at least 10 bp of a reference intron, possible pre-mRNA fragment	e	9	29
At least one splice junction is shared with a reference transcript, indicating a potential novel isoform	j	13	15
Generic exonic overlap with a reference transcript	o	8	11
Possible polymerase run-on fragment which is within 2 kBases of a reference transcript	p	1	8
Intergenic transcript (noncoding RNA)	u	5	38
Exonic overlap with a reference on the opposite strand (antisense transcript)	x	19	48
Total transcripts		**940**	**875**

Table 2.3. Summary of transcript characterizations for each pattern of transcript level change.

Pattern ID	Transcript Characterization	Number of transcripts
1	ORF	71
	Possible pre-mRNA fragment	3
	Generic exonic overlap	2
2	ORF	370
	Possible pre-mRNA fragment	1
	Potential novel isoform	7
	Generic exonic overlap	3
	Noncoding RNA	2
	Antisense	2
3	ORF	6
	Possible polymerase run-on fragment	1
4	ORF	76
	Antisense	2
5	ORF	291
	Possible pre-mRNA fragment	4
	Potential novel isoform	1
	Generic exonic overlap	2
	Noncoding RNA	2
	Antisense	10
6	ORF	3
	Potential novel isoform	1
	Noncoding RNA	1
	Antisense	1
7	ORF	23
	Generic exonic overlap	1
	Antisense	4
8	ORF	41
	Possible pre-mRNA fragment	1
	Potential novel isoform	4
9	ORF	4
10	ORF	0
	Possible polymerase run-on fragment	2
	Noncoding RNA	1
	Antisense	1
11	ORF	19
	Possible pre-mRNA fragment	2
	Potential novel isoform	2
	Generic exonic overlap	1
	Possible polymerase run-on fragment	1
	Noncoding RNA	8
	Antisense	1
12	ORF	2

	Generic exonic overlap	1
	Noncoding RNA	1
	Antisense	1
13	ORF	2
	Noncoding RNA	1
	Antisense	2
14	ORF	355
	Possible pre-mRNA fragment	11
	Potential novel isoform	2
	Generic exonic overlap	5
	Possible polymerase run-on fragment	2
	Noncoding RNA	17
	Antisense	11
15	ORF	10
	Possible pre-mRNA fragment	3
	Generic exonic overlap	1
	Noncoding RNA	2
	Antisense	1
16	ORF	5
	Possible pre-mRNA fragment	1
	Potential novel isoform	1
17	ORF	312
	Possible pre-mRNA fragment	11
	Potential novel isoform	10
	Generic exonic overlap	2
	Possible polymerase run-on fragment	1
	Noncoding RNA	8
	Antisense	27
18	ORF	21
	Possible pre-mRNA fragment	1
	Generic exonic overlap	1
	Possible polymerase run-on fragment	1
	Antisense	4

Table 2.4. Gene ontology statistical overrepresentation test results performed using the PANTHER Classification System. Gene transcript level change patterns 2, 5, 7, and 14 resulted in significant (FDR = <0.05 and p = <0.05) over and underrepresentation of GO terms. The predicted number of genes is the calculated number of genes in the test list expected to contain the GO term based on the reference list. The actual number of genes is the number of genes that contain the GO term. The over or under denotes whether there is an over (+) or underrepresentation (−) of the GO term when the actual number of genes is compared to the predicted number of genes.

Pattern identification	GO Category	GO Term	FDR, p values	Predicted number of genes	Actual number of genes	Over or Under (+/−)
2	Biological process	nucleic acid metabolic process (GO:0090304)	1.90×10^{-2}, 1.35×10^{-5}	33.18	10	−
		RNA metabolic process (GO:0016070)	2.10×10^{-2}, 7.47×10^{-6}	27.09	6	−
	Molecular function	nucleic acid binding (GO:0003676)	2.86×10^{-2}, 2.36×10^{-5}	38.60	14	−
	Cellular component	cell cortex (GO:0005938)	6.03×10^{-2}, 8.08×10^{-4}	5.64	17	+
		cytoskeleton (GO:0005856)	6.07×10^{-2}, 9.15×10^{-4}	9.48	23	+
		endoplasmic reticulum (GO:0005783)	6.76×10^{-2}, 4.53×10^{-4}	16.25	34	+
		membrane protein complex (GO:0098796)	5.81×10^{-2}, 5.84×10^{-4}	17.15	35	+
		cytoplasm (GO:0005737)	1.38×10^{-2}, 6.96×10^{-5}	142.65	185	+
		nucleus (GO:0005634)	1.93×10^{-3}, 3.23×10^{-6}	56.20	24	−
		intracellular organelle lumen (GO:0070013)	5.52×10^{-2}, 9.24×10^{-4}	30.92	13	−
		membrane-enclosed lumen (GO:0031974)	5.02×10^{-2}, 9.24×10^{-4}	30.92	13	−
		organelle lumen (GO:0043233)	4.60×10^{-2}, 9.24×10^{-4}	30.92	13	−
		nuclear lumen (GO:0031981)	5.79×10^{-2}, 6.79×10^{-4}	20.54	6	−
		nuclear protein-containing complex (GO:0140513)	5.73×10^{-2}, 4.80×10^{-4}	21.22	6	−
		nucleolus (GO:0005730)	6.40×10^{-3}, 2.15×10^{-5}	12.19	0	−
5	Biological process	transmembrane transport (GO:0055085)	3.15×10^{-2}, 6.71×10^{-5}	23.61	47	+
		small molecule metabolic process (GO:0044281)	3.18×10^{-2}, 7.89×10^{-5}	37.06	64	+

	macromolecule metabolic process (GO:0043170)	2.28×10^{-2}, 4.05×10^{-5}	67.21	37	−
	gene expression (GO:0010467)	9.43×10^{-3}, 3.35×10^{-6}	30.70	8	−
	nucleic acid metabolic process (GO:0090304)	8.67×10^{-3}, 6.16×10^{-6}	26.70	6	−
	RNA metabolic process (GO:0016070)	1.03×10^{-2}, 1.46×10^{-5}	21.80	4	−
	RNA processing (GO:0006396)	1.03×10^{-2}, 1.10×10^{-5}	15.62	1	−
Molecular function	transmembrane transporter activity (GO:0022857)	3.29×10^{-2}, 5.43×10^{-5}	21.44	44	+
	transporter activity (GO:0005215)	5.10×10^{-2}, 4.21×10^{-5}	21.98	45	+
Cellular component	inner mitochondrial membrane protein complex (GO:0098800)	4.54×10^{-2}, 1.14×10^{-3}	6.18	17	+
	mitochondrial protein-containing complex (GO:0098798)	4.26×10^{-2}, 6.42×10^{-4}	8.90	22	+
	mitochondrial inner membrane (GO:0005743)	5.17×10^{-2}, 1.13×10^{-3}	9.99	23	+
	organelle inner membrane (GO:0019866)	4.80×10^{-2}, 1.13×10^{-3}	9.99	23	+
	mitochondrial membrane (GO:0031966)	5.11×10^{-2}, 1.03×10^{-3}	11.99	26	+
	mitochondrial envelope (GO:0005740)	4.67×10^{-2}, 6.26×10^{-4}	13.44	29	+
	envelope (GO:0031975)	4.90×10^{-2}, 1.31×10^{-3}	14.17	29	+
	organelle envelope (GO:0031967)	4.61×10^{-2}, 1.31×10^{-3}	14.17	29	+
	mitochondrion (GO:0005739)	3.02×10^{-3}, 1.01×10^{-5}	31.24	60	+
	organelle membrane (GO:0031090)	4.72×10^{-2}, 8.69×10^{-4}	29.61	50	+
	membrane (GO:0016020)	7.71×10^{-4}, 1.29×10^{-6}	77.75	120	+
	integral component of membrane (GO:0016021)	1.21×10^{-2}, 1.01×10^{-4}	60.67	92	+
	intrinsic component of membrane (GO:0031224)	1.25×10^{-2}, 1.47×10^{-4}	61.40	92	+
	nucleus (GO:0005634)	3.23×10^{-3}, 1.62×10^{-5}	45.23	19	−

		nuclear lumen (GO:0031981)	4.27×10^{-2}, 7.15×10^{-4}	16.53	4	−
		nuclear protein-containing complex (GO:0140513)	1.29×10^{-2}, 1.30×10^{-4}	17.08	3	−
		ribonucleoprotein complex (GO:1990904)	2.77×10^{-3}, 1.86×10^{-5}	17.44	2	−
7	Biological process	polysaccharide metabolic process (GO:0005976)	4.67×10^{-2}, 1.66×10^{-5}	0.51	6	+
14	Biological process	ribonucleoprotein complex subunit organization (GO:0071826)	1.66×10^{-3}, 1.18×10^{-5}	6.53	23	+
		ribonucleoprotein complex assembly (GO:0022618)	2.74×10^{-3}, 2.04×10^{-5}	6.30	22	+
		RNA biosynthetic process (GO:0032774)	1.78×10^{-2}, 1.52×10^{-4}	6.08	20	+
		transcription, DNA-templated (GO:0006351)	1.71×10^{-2}, 1.52×10^{-4}	6.08	20	+
		nucleic acid-templated transcription (GO:0097659)	1.64×10^{-2}, 1.52×10^{-4}	6.08	20	+
		rRNA metabolic process (GO:0016072)	1.47×10^{-5}, 5.76×10^{-8}	12.16	39	+
		rRNA processing (GO:0006364)	4.56×10^{-5}, 2.10×10^{-7}	11.26	36	+
		ribonucleoprotein complex biogenesis (GO:0022613)	2.45×10^{-7}, 3.48×10^{-10}	17.56	54	+
		ncRNA processing (GO:0034470)	1.43×10^{-5}, 4.07×10^{-8}	14.18	43	+
		ribosome biogenesis (GO:0042254)	1.49×10^{-5}, 5.30×10^{-8}	14.41	43	+
		ncRNA metabolic process (GO:0034660)	1.30×10^{-5}, 4.16×10^{-8}	14.86	44	+
		RNA metabolic process (GO:0016070)	1.03×10^{-10}, 7.34×10^{-14}	27.01	79	+
		RNA processing (GO:0006396)	4.72×10^{-7}, 8.39×10^{-10}	19.36	56	+
		mRNA metabolic process (GO:0016071)	1.31×10^{-2}, 1.07×10^{-4}	9.68	26	+
		gene expression (GO:0010467)	2.48×10^{-11}, 8.80×10^{-15}	38.04	99	+
		nucleic acid metabolic process (GO:0090304)	2.17×10^{-8}, 2.32×10^{-11}	33.09	82	+
		cellular protein-containing complex	2.21×10^{-2}, 2.36×10^{-4}	14.63	33	+

	assembly (GO:0034622)				
	protein-containing complex assembly (GO:0065003)	2.67×10^{-2}, 2.94×10^{-4}	15.08	33	+
	cellular component biogenesis (GO:0044085)	1.45×10^{-5}, 6.18×10^{-8}	33.54	72	+
	protein-containing complex subunit organization (GO:0043933)	2.15×10^{-2}, 2.22×10^{-4}	16.88	36	+
	nucleobase-containing compound metabolic process (GO:0006139)	6.74×10^{-5}, 3.59×10^{-7}	48.85	90	+
	cellular aromatic compound metabolic process (GO:0006725)	6.77×10^{-5}, 3.37×10^{-7}	52.67	95	+
	cellular nitrogen compound metabolic process (GO:0034641)	2.14×10^{-6}, 4.55×10^{-9}	67.08	120	+
	heterocycle metabolic process (GO:0046483)	9.11×10^{-5}, 5.18×10^{-7}	52.67	94	+
	cellular component organization or biogenesis (GO:0071840)	3.66×10^{-4}, 2.34×10^{-6}	52.45	91	+
	macromolecule metabolic process (GO:0043170)	4.21×10^{-6}, 1.05×10^{-8}	83.29	138	+
	organic cyclic compound metabolic process (GO:1901360)	1.40×10^{-3}, 9.45×10^{-6}	57.40	95	+
	nitrogen compound metabolic process (GO:0006807)	2.04×10^{-4}, 1.23×10^{-6}	111.65	161	+
	cellular metabolic process (GO:0044237)	1.65×10^{-2}, 1.64×10^{-4}	137.99	178	+
	transmembrane transport (GO:0055085)	3.66×10^{-2}, 4.16×10^{-4}	29.26	11	−
	ion transmembrane transport (GO:0034220)	1.66×10^{-2}, 1.59×10^{-4}	17.11	3	−
	ion transport (GO:0006811)	9.57×10^{-3}, 7.48×10^{-5}	18.46	3	−
	cation transport (GO:0006812)	3.58×10^{-2}, 4.20×10^{-4}	13.73	2	−
Molecular process	RNA binding (GO:0003723)	1.97×10^{-6}, 3.24×10^{-9}	23.41	61	+
	nucleic acid binding (GO:0003676)	5.55×10^{-7}, 4.58×10^{-10}	38.49	86	+

	heterocyclic compound binding (GO:1901363)	3.42×10^{-6}, 8.47×10^{-9}	81.94	137	+
	organic cyclic compound binding (GO:0097159)	3.97×10^{-6}, 1.31×10^{-8}	82.39	137	+
	binding (GO:0005488)	1.01×10^{-4}, 4.17×10^{-7}	128.76	182	+
	transmembrane transporter activity (GO:0022857)	1.93×10^{-3}, 1.11×10^{-5}	26.56	6	−
	transporter activity (GO:0005215)	9.99×10^{-4}, 4.94×10^{-6}	27.24	6	−
Cellular component	RNA polymerase II, holoenzyme (GO:0016591)	1.48×10^{-2}, 6.45×10^{-4}	2.93	12	+
	DNA-directed RNA polymerase complex (GO:0000428)	3.21×10^{-3}, 1.08×10^{-4}	4.05	16	+
	nuclear DNA-directed RNA polymerase complex (GO:0055029)	3.06×10^{-3}, 1.08×10^{-4}	4.05	16	+
	RNA polymerase complex (GO:0030880)	2.92×10^{-3}, 1.08×10^{-4}	4.05	16	+
	small-subunit processome (GO:0032040)	2.14×10^{-2}, 1.00×10^{-3}	3.15	12	+
	nucleolus (GO:0005730)	1.32×10^{-6}, 1.10×10^{-8}	12.16	41	+
	preribosome (GO:0030684)	7.27×10^{-3}, 2.92×10^{-4}	6.08	19	+
	transferase complex, transferring phosphorus-containing groups (GO:0061695)	1.70×10^{-2}, 7.71×10^{-4}	6.30	18	+
	ribonucleoprotein complex (GO:1990904)	2.98×10^{-7}, 9.98×10^{-10}	21.61	60	+
	nuclear lumen (GO:0031981)	1.12×10^{-6}, 1.12×10^{-8}	20.48	55	+
	nucleoplasm (GO:0005654)	3.73×10^{-2}, 1.87×10^{-3}	6.75	18	+
	intracellular protein-containing complex (GO:0140535)	1.02×10^{-2}, 4.28×10^{-4}	10.13	25	+
	nuclear protein-containing complex (GO:0140513)	5.24×10^{-5}, 1.05×10^{-6}	21.16	50	+
	intracellular organelle lumen (GO:0070013)	1.84×10^{-6}, 2.16×10^{-8}	30.84	70	+

		membrane-enclosed lumen (GO:0031974)	1.61×10^{-6}, 2.16×10^{-8}	30.84	70	+
		organelle lumen (GO:0043233)	1.43×10^{-6}, 2.16×10^{-8}	30.84	70	+
		transferase complex (GO:1990234)	4.56×10^{-2}, 2.37×10^{-3}	11.71	25	+
		nucleus (GO:0005634)	3.18×10^{-9}, 5.33×10^{-12}	56.05	116	+
		intracellular non-membrane-bounded organelle (GO:0043232)	1.48×10^{-4}, 3.22×10^{-6}	39.62	74	+
		non-membrane-bounded organelle (GO:0043228)	1.38×10^{-4}, 3.22×10^{-6}	39.62	74	+
		catalytic complex (GO:1902494)	3.43×10^{-2}, 1.67×10^{-3}	27.24	47	+
		protein-containing complex (GO:0032991)	1.09×10^{-6}, 5.48×10^{-9}	75.64	130	+
		intracellular membrane-bounded organelle (GO:0043231)	1.99×10^{-3}, 5.99×10^{-5}	126.06	168	+
		membrane-bounded organelle (GO:0043227)	1.91×10^{-3}, 6.09×10^{-5}	126.28	168	+
		intracellular organelle (GO:0043229)	1.15×10^{-3}, 2.90×10^{-5}	137.54	182	+
		organelle (GO:0043226)	1.08×10^{-3}, 2.90×10^{-5}	137.54	182	+
		intracellular anatomical structure (GO:0005622)	1.62×10^{-3}, 4.62×10^{-5}	179.41	223	+
		membrane (GO:0016020)	9.60×10^{-7}, 6.43×10^{-9}	96.35	46	−
		integral component of membrane (GO:0016021)	8.21×10^{-6}, 1.51×10^{-7}	75.19	34	−
		intrinsic component of membrane (GO:0031224)	4.60×10^{-6}, 7.71×10^{-8}	76.09	34	−
		cell periphery (GO:0071944)	5.56×10^{-3}, 2.14×10^{-4}	20.26	5	−

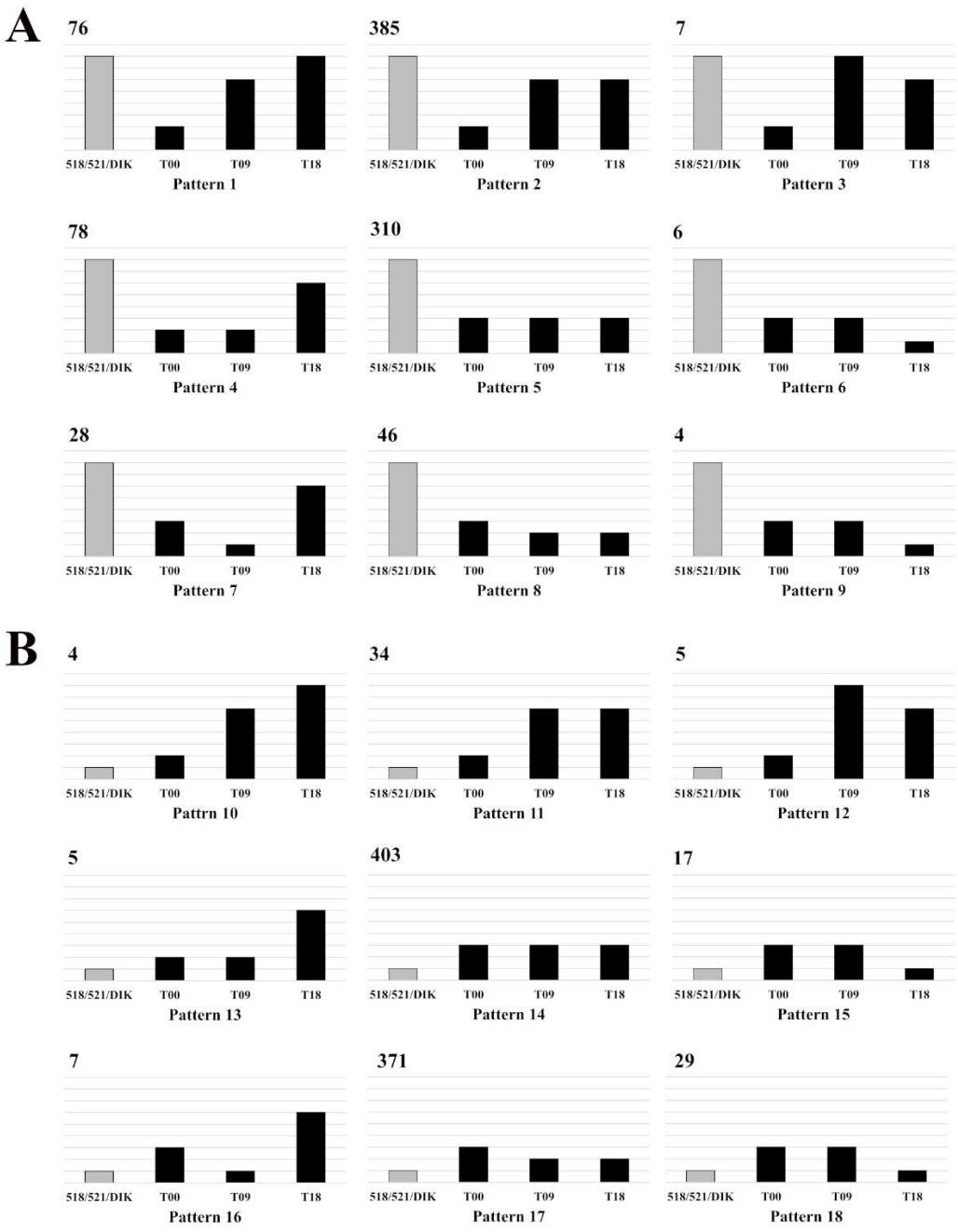

Figure 2.1. Representative transcript level change for each pattern in the 518/521/Dikaryon, T00, T09, and T18 RNA-seq libraries. Numbers in the top left of each pattern are the number of transcripts in that pattern (a) Transcript level change for transcripts downregulated at T00 compared to the haploid and dikaryon libraries. (b) Transcript level change for transcripts upregulated in the T00 library compared to the haploid and dikaryon libraries.

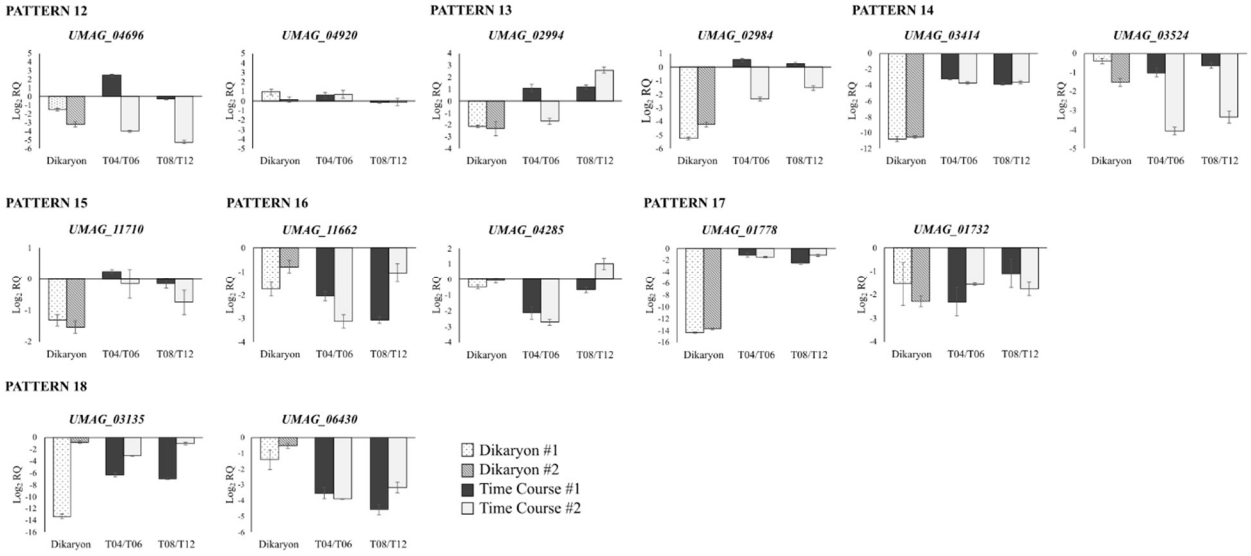

Figure 2.2. Transcript levels of genes, determined by RT-qPCR, selected from patterns 12 to 18 in the dikaryon (518 × 521) and germinating *U. maydis* teliospores at T04/T06 and T08/T12 relative to T00. Transcript levels were normalized relative to *UMAG_00175*. Error bars indicate RQ maximum and RQ minimum (95% confidence interval, n= 3).

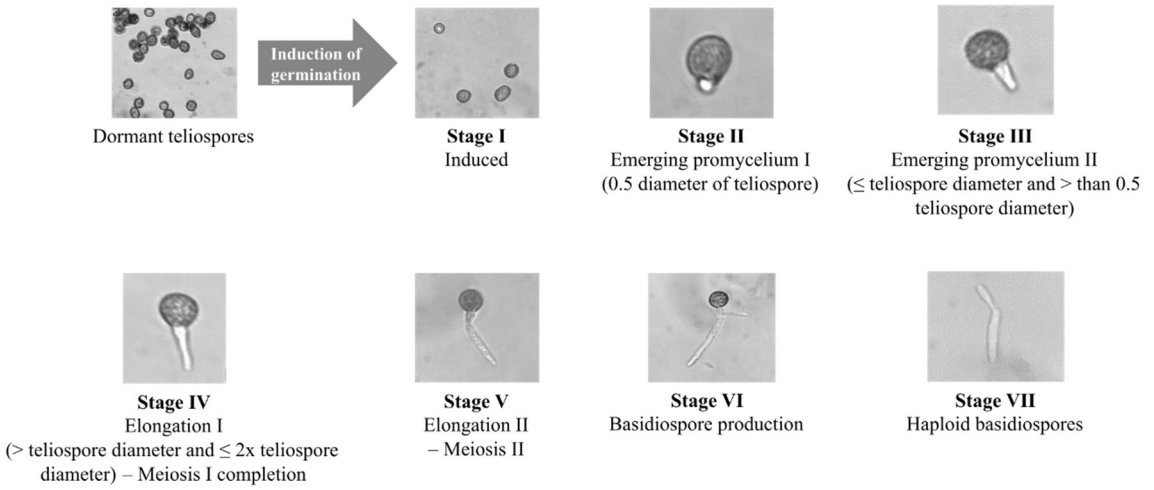

Figure 2.3. Stages of teliospore germination. Stage I are teliospores induced to germinate but are visually indistinguishable from dormant teliospores. Stage II teliospores have an emerging promycelium with a length that is less than 0.5 the diameter of the teliospore. Stage III teliospores is the second stage of the emerging promycelium where the length is equal to or less than the diameter of the teliospore and greater than 0.5 the diameter of the teliospore. Stage IV teliospores have an elongating promycelium greater than the diameter of the teliospore and less than or equal to two times the teliospore diameter. Stage V teliospores have an elongating promycelium that contains three compartments. Stage VI is the production of basidiospores on the promycelium. Stage VII is the release of the haploid basidiospores into the environment.

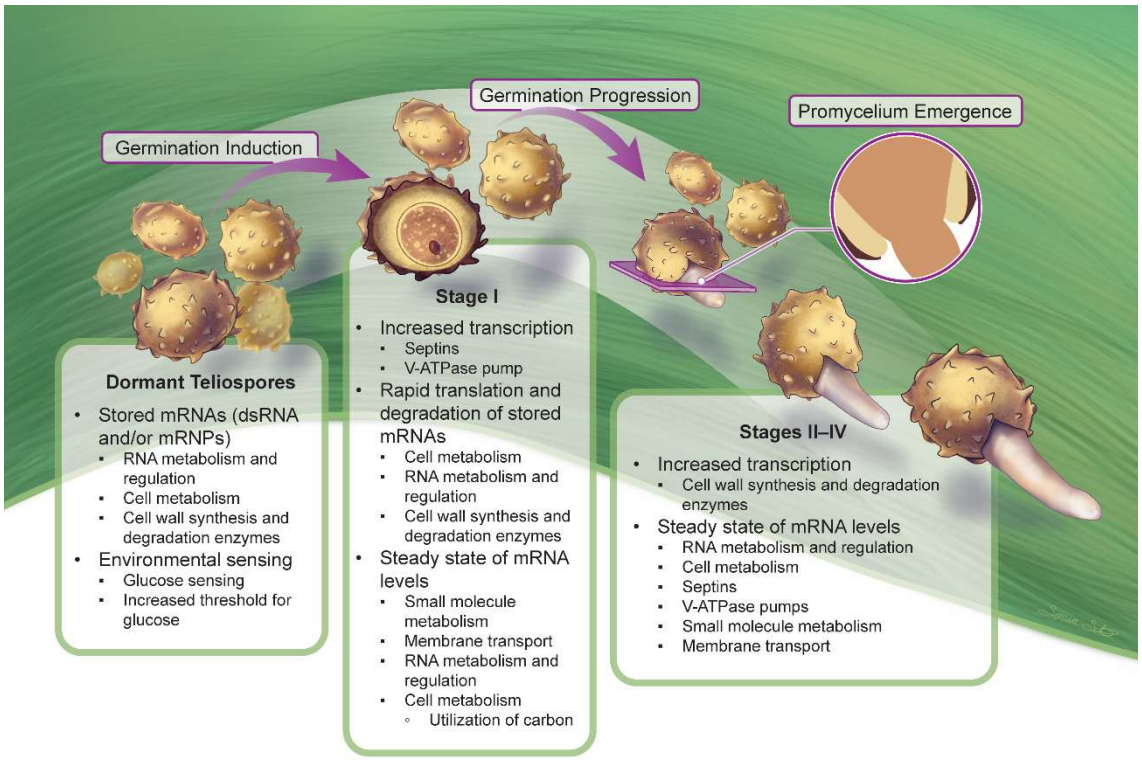

Figure 2.4. Molecular and physiological transitions during teliospore germination. Dormant teliospores are characterized by having low respiration rates and are paused at the pachytene checkpoint during meiosis. GO enrichment analysis uncovered stored mRNAs related to RNA metabolism and regulation (full list of GO terms can be found in Table 2.4), cell wall synthesis and degradation (GO:0005976 polysaccharide metabolic process), and cell metabolism (GO:0044237 cellular metabolic process). Stage I germinating teliospores are indistinguishable from dormant teliospores but are stimulated to germinate in the presence of a carbon source (*e.g.* sucrose). At this stage there is an increase in respiration rate, meiosis resumes, and the inner cell wall is thinned at the location of subsequent promycelium development. During this stage, there is also an increased transcription of septins (GO:0005856 cytoskeleton) and components of V-ATPase pumps (GO:0098796 membrane protein complex). Stored mRNAs are rapidly translated and degraded. A steady state of mRNA transcription, translation, and degradation is established (GO:0044281 small molecule metabolic process, GO:0055085 transmembrane transport, GO:0044237 cellular metabolic process). As the teliospore enters Stage II, the outer cell walls crack open to allow the promycelium to emerge (insert). While germination progresses through Stages II to IV, respiration plateaus and meiosis I is completed. There is increased transcription of cell wall synthesis and degradation enzymes (GO:0005976 polysaccharide metabolic process). A steady state of mRNA transcription, translation, and degradation is established for genes involved in RNA metabolism and regulation (refer to Table 4 for GO terms), cell metabolism (GO:0044237 cellular metabolic process, GO:0044281 small molecule metabolic process), organization of the cytoskeleton (GO:0005856 cytoskeleton), and

membrane proteins (GO:0098796 membrane protein complex, GO:0055085 transmembrane transport).

SUPPLEMENTARY MATERIALS

Table S2.1. Identification of gene transcript patterns during teliospore germination.

This is a PDF file containing Supplementary Table S2.1. It is a large dataset that lists the 1,815 transcripts that are significantly different at T00 when compared to the haploid and dikaryon RNA-seq libraries. The dataset includes the pattern identification, gene ID, normalized expression values for each RNA-seq library, and the calculated fold changes of each transcript versus the other cell types. The file name of this PDF file is “Chapter 2 – Supplementary Table S2-1.pdf”.

Table S2.2. Reference gene list for GO enrichment analysis.

This is a PDF file containing Supplementary Table S2.2. This contains the reference gene list used to perform the statistical overrepresentation test in the PANTHER Classification System. The file name of this PDF file is “Chapter 2 – Supplementary Table S2-2.pdf”.

Table S2.3. Sequences of SYBR Green RT-qPCR primers used in this study.

Primer	Primer Sequence (5'-to-3')
UMAG_00175	F: CGGTCTCGGTATCAAGTC R: AAGCAGATTGGTCGGAAG
UMAG_01732	F: TTCGCCTGCTCAATCAAT R: TCCAAGACCAAGTATGTAACG
UMAG_01778	F: GCAAATGGTGGTATGGTC R: GCTTATTTCGTGTCCTTCAT
UMAG_02984	F: CTTCCGTGATTGCTTGAC R: CAGATTGGCTATGGTGAC
UMAG_02994	F: CTACTAACAACGACGGATG R: GTCTTCCACGCAACTATC
UMAG_03135	F: CTTGCTGCTGCTCACATC R: CTCCACCGTCCAGAAGAT
UMAG_03414	F: GCTGGTGCTTACATCTTG R: GGCTGAATCCTCTTGTGA
UMAG_03524	F: GCTTTCGGGTATTCTCAAC R: AAGATGTGCTGGTGGTAG
UMAG_04285	F: GCTCAAGGTGGAACATCT R: GTCAATCACAGGCGTCTT
UMAG_04696	F: CGCAACCTTTATCACCTTC R: CACCGCTTCGATAGATGT
UMAG_04920	F: AGACCTCAAGTGGAACAA R: GTCCAGAATCACCAACATT
UMAG_06430	F: CTTGCTGAACACCACGAT R: CGAAGAGATGACAGATGCTA
UMAG_11662	F: ACTACTGCTTTGACGATTTC R: TTGTTGACGGTTGGATAGA
UMAG_11710	F: GTATCACGAGCAGAAGTTG R: CGGTCTTGAATGTGGTATC

Table S2.4. PANTHER statistical overrepresentation test results. Results of the GO term enrichment analysis performed in the PANTHER classification system.

This is a PDF file containing Supplementary Table S2.4. It is a large dataset that contains the results of the PANTHER statistical overrepresentation test performed. The dataset contains the pattern ID for the gene, ontology type, GO term, gene ID, the PANTHER family/subfamily the gene belongs to, and the PANTHER protein class of the gene. The file name of this PDF file is “Chapter 2 – Supplementary Table S2-4.pdf”.

REFERENCES

Alvarez-Tabarés I, Pérez-Martín J. 2010. Septins from the phytopathogenic fungus *Ustilago maydis* are required for proper morphogenesis but dispensable for virulence. PloS One. 5(9):e12933.

Bainbridge BW. 1971. Macromolecular composition and nuclear division during spore germination in *Aspergillus nidulans*. Microbiology. 66(3):319–325.

Banuett F, Herskowitz I. 1996. Discrete developmental stages during teliospore formation in the corn smut fungus, *Ustilago maydis*. Development. 122(10):2965–2976.

Banuett F, Quintanilla Jr RH, Reynaga-Peña CG. 2008. The machinery for cell polarity, cell morphogenesis, and the cytoskeleton in the Basidiomycete fungus *Ustilago maydis*—a survey of the genome sequence. Fungal Genet Biol. 45:S3–S14.

Beck ZT, Cloutier SC, Schipma MJ, Petell CJ, Kit W, Ma, Tran EJ. 2014. Regulation of glucose-dependent gene expression by the RNA helicase Dbp2 in *Saccharomyces cerevisiae*. Genetics. 198(3):1001–1014.

Bowman EJ, Bowman BJ. 2010. Vacuoles in filamentous fungi. Cellular and Molecular Biology of Filamentous Fungi. Washington (DC): American Society for Microbiology. p. 179–190.

Boyce KJ, Chang H, D'Souza CA, Kronstad JW. 2005. An *Ustilago maydis* septin is required for filamentous growth in culture and for full symptom development on maize. Eukaryot Cell. 4(12):2044–2056.

Brefort T, Doehlemann G, Mendoza-Mendoza A, Reissmann S, Djamei A, Kahmann R. 2009. *Ustilago maydis* as a pathogen. Annu Rev Phytopathol. 47:423–445.

Caltrider PG, Gottlieb D. 1963. Respiratory activity and enzymes for glucose catabolism in fungus spores. Phytopathology. 53(9):1021–1030.

Caltrider PG, Gottlieb D. 1966. Effect of sugars on germination and metabolism of teliospores of *Ustilago maydis*. Phytopathology. 56(5):479–484.

Chypre M, Zaidi N, Smans K. 2012. ATPcitrate lyase: A mini-review. Biochem Biophys Res Co. 422(1):1–4.

Deveau A, Kohler A, Frey-Klett P, Martin F. 2008. The major pathways of carbohydrate metabolism in the ectomycorrhizal basidiomycete *Laccaria bicolor* S238N. New Phytol. 180(2):379–390.

Donaldson ME, Meng S, Gagarinova A, Babu M, Lambie SC, Swiadek AA, Saville BJ. 2013. Investigating the *Ustilago maydis*/*Zea mays* pathosystem: transcriptional responses and novel functional aspects of a fungal calcineurin regulatory B subunit. Fungal Genet Biol. 58–59:91–104.

Donaldson ME, Ostrowski LA, Goulet KM, Saville BJ. 2017. Transcriptome analysis of smut fungi reveals widespread intergenic transcription and conserved antisense transcript expression. BMC Genomics. 18(1):340.

Donaldson ME, Saville BJ. 2013. *Ustilago maydis* natural antisense transcript expression alters mRNA stability and pathogenesis. Mol Microbiol. 89(1):29–51.

Duran R. 1972. Aspects of teliospore germination in North American smut fungi. II. Can J Botany. 50(12):2569–2574.

Duvezin-Caubet S, Rak M, Lefebvre-Legendre L, Tetaud E, Bonnefoy N, Di Rago J-P. 2006. A "petite obligate" mutant of *Saccharomyces cerevisiae*: Functional mtDNA is lethal in cells lacking the δ subunit of mitochondrial F1-ATPase. J Biol Chem. 281(24):16305–16313.

Fairman-Williams ME, Guenther U-P, Jankowsky E. 2010. SF1 and SF2 helicases: family matters. Curr Opin Struc Biol. 20(3):313–324.

Gottlieb D, Caltrider PG. 1963. Synthesis of enzymes during the germination of fungus spores. Nature. 197:916.

Graham SO. 1960. The morphology and a chemical analysis of the teliospore of the dwarf bunt fungus, *Tilletia contraversa*. Mycologia. 52(1):97–118.

Griffin DH. 1994. Spore dormancy and germination. Fungal Physiology. New York (NY): John Wiley & Sons; p. 375–398.

Harris RA, Bowker-Kinley MM, Huang B, Wu P. 2002. Regulation of the activity of the pyruvate dehydrogenase complex. Adv Enzyme Regul. 42:249–259.

Helfer S. 2014. Rust fungi and global change. New Phytol. 201(3):770–780.

Ho EC, Cahill MJ, Saville BJ. 2007. Gene discovery and transcript analyses in the corn smut pathogen *Ustilago maydis*: expressed sequence tag and genome sequence comparison. BMC Genomics. 8:334.

Jankowsky E. 2011. RNA helicases at work: binding and rearranging. Trends Biochem Sci. 36(1):19–29.

Jia C, Zhang K, Zhang D, Yu Q, Zhao Q, Xiao C, Dong Y, Chu M, Li M. 2018. Roles of VPH2 and VMA6 in localization of V-ATPase subunits, cell wall functions and filamentous development in *Candida albicans*. Fungal Genet Biol. 114:1–11.

Kämper J, Kahmann R, Bolker M, Ma LJ, Brefort T, Saville BJ, Banuett F, Kronstad JW, Gold SE, Muller O et al. 2006. Insights from the genome of the biotrophic fungal plant pathogen *Ustilago maydis*. Nature. 444(7115):97–101.

Langner T, Öztürk M, Hartmann S, Cord-Landwehr S, Moerschbacher B, Walton JD, Göhre V. 2015. Chitinases are essential for cell separation in *Ustilago maydis*. Eukaryot Cell. 14(9):846–857.

Lin F, Davies F, Tripathi R, Raghu K, Gottlieb D. 1971. Ribonucleic acids in spore germination of *Ustilago maydis*. Phytopathology. 61:645–648.

Linder P, Fuller-Pace FV. 2013. Looking back on the birth of DEAD-box RNA helicases. BBA -Gene Regul Mech. 1829(8):750–755.

Liu G, Yang Y, Yang G, Duan S, Yuan P, Zhang S, Li F, Gao X-D, Nakanishi H. 2022. Triosephosphate isomerase and its product glyceraldehyde-3-phosphate are involved in the regulatory mechanism that suppresses exit from the quiescent state in yeast cells. Microbiol Spectrum. 10(4):e00897-00822.

Livak KJ, Schmittgen TD. 2001. Analysis of relative gene expression data using real-time quantitative PCR and the $2^{-\Delta\Delta CT}$ method. Methods. 25(4):402–408.

Mattick J, Amaral P. 2022. RNA, the epicenter of genetic information: a new understanding of molecular biology. 1st ed. Boca Raton: CRC Press.

Mi H, Ebert D, Muruganujan A, Mills C, Albou L-P, Mushayamaha T, Thomas PD. 2021. PANTHER version 16: a revised family classification, tree-based classification tool, enhancer regions and extensive API. Nucl Acids Res. 49(D1):D394–D403.

Mi H, Muruganujan A, Huang X, Ebert D, Mills C, Guo X, Thomas PD. 2019. Protocol Update for large-scale genome and gene function analysis with the PANTHER classification system (v.14.0). Nat Protoc. 14(3):703–721.

Moffatt BA, Ashihara H. 2002. Purine and pyrimidine nucleotide synthesis and metabolism. The Arabidopsis Book. 2002(1).

Morrison EN, Donaldson ME, Saville BJ. 2012. Identification and analysis of genes expressed in the *Ustilago maydis* dikaryon: uncovering a novel class of pathogenesis genes. Can J Plant Pathol. 34(3):417–435.

Neupane P, Bhuju S, Thapa N, Bhattarai HK. 2019. ATP synthase: structure, function and inhibition. Biomol Concepts. 10(1):1–10.

O'Donnell KL, McLaughlin DJ. 1984. Ultrastructure of meiosis in *Ustilago maydis*. Mycologia. 76(3):468–485.

Ostrowski LA, Saville BJ. 2017. Natural antisense transcripts are linked to the modulation of mitochondrial function and teliospore dormancy in *Ustilago maydis*. Mol Microbiol. 103(5):745–763.

Ostrowski LA, Seto AM, Saville B. 2018. Investigating teliospore germination using microrespiration analysis and microdissection. J Vis Exp. (135):e57628.

Piepenbring M, Hagedorn G, Oberwinkler F. 1998. Spore Liberation and Dispersal in Smut Fungi. Botanica Acta. 111(6):444–460.

Ramberg JE, McLaughlin DJ. 1980. Ultrastructural study of promycelial development and basidiospore initiation in *Ustilago maydis*. Can J Bot. 58(14):1548–1561.

Rane HS, Bernardo SM, Raines SM, Binder JL, Parra KJ, Lee SA. 2013. *Candida albicans VMA3* is necessary for V-ATPase assembly and function and contributes to secretion and filamentation. Euk Cell. 12(10):1369–1382.

Roeder GS, Bailis JM. 2000. The pachytene checkpoint. Trends Genet. 16(9):395–403.

Sacadura NT, Saville BJ. 2003. Gene expression and EST analyses of *Ustilago maydis* germinating teliospores. Fungal Genet Biol. 40(1):47–64.

Saville BJ, Donaldson ME, Doyle CE. 2012. Chapter 22, Investigating host induced meiosis in a fungal plant pathogen. In: Andrew S, editor. Meiosis - molecular mechanisms and cytogenetic diversity. Rijeka: InTech.

Schachtschabel D, Arentshorst M, Lagendijk EL, Ram AFJ. 2012. Vacuolar H+-ATPase plays a key role in cell wall biosynthesis of *Aspergillus niger*. Fungal Genet Biol. 49(4):284–293.

Seto AM. 2013. Analysis of gene transcripts during *Ustilago maydis* teliospore dormancy and germination [Master's Thesis]. Peterborough, ON: Trent University.

Tripathi RK, Gottlieb D. 1974. Sequential biosynthesis of ribonucleic acids during germination of teliospores of *Ustilago maydis*. Mycologia. 66(3):413–421.

Walker GM, White NA. 2017. Introduction to fungal physiology. In: Kavanagh K. Fungi: Biology and applications. Hoboken (NJ): Wiley. p. 1–35.

Xing Z, Wang S, Tran EJ. 2017. Characterization of the mammalian DEAD-box protein DDX5 reveals functional conservation with *S. cerevisiae* ortholog Dbp2 in transcriptional control and glucose metabolism. RNA. 23(7):1125–1138.

Zahiri AR, Babu MR, Saville BJ. 2005. Differential gene expression during teliospore germination in *Ustilago maydis*. Mol Genet Genomics. 273(5):394–403.

CHAPTER 3

PREFACE

Title: Investigating Teliospore Germination Using Microrespiration Analysis and Microdissection

Authors: Lauren A. Ostrowski*, Amanda M. Seto*, and Barry J. Saville

Reference: Published in *Journal of Visualized Experiments* (2018) 135(e57628) doi:10.3791/57628

Video URL: https://www.jove.com/video/57628

2024 Impact Factor: 1.0

Contributions: A.M.S. and L.A.O. contributed equally to this study and are designated as co-first authors (*). B.J.S. conceived, directed, and obtained funding for the research presented in this study. A.M.S. performed the microrespiration experiments with teliospores, developed the microdissection method, and identified the stages of teliospore germination. L.A.O. conducted the statistical analysis of the microrespiration experiments and performed the preliminary microrespiration experiments with haploid cells. A.M.S. created Table 3.1, Figures 3.2, and 3.3. L.A.O. created Figure 3.1. L.A.O. drafted the introduction. A.M.S. and L.A.O. drafted relevant portions of the protocol, representative results, and discussion. A.M.S., L.A.O., and B.J.S. edited the manuscript prior to submission.

CHAPTER 3

Investigating Teliospore Germination Using Microrespiration Analysis and Microdissection

Published in *Journal of Visualized Experiments* (2018), 135(e57628)

doi:10.3791/57628

Video URL: https://www.jove.com/video/57628

SUMMARY

Smut fungi cause many devastating agricultural diseases. They are dispersed as dormant teliospores that germinate in response to environmental cues. We outline two methods to investigate molecular changes during germination: measuring respiration increase to detect metabolic activation and assessing changing molecular events by isolating teliospores at distinct morphological stages.

ABSTRACT

Smut fungi are the etiological agents of several devastating agricultural diseases. They are characterized by the production of teliospores, which are thick-walled dispersal agents. Teliospores can remain dormant for decades. The dormancy is characterized by low metabolic rates, paused macromolecular biosynthesis and greatly reduced levels of respiration. Upon receiving required environmental signals, teliospores germinate to produce haploid cells, which can initiate new rounds of infection. Teliospore germination is characterized by the resumption of macromolecular biosynthesis, increased respiration and dramatic morphological changes. In order to precisely measure changes in cellular respiration during the early stages of germination we have developed a simple protocol

employing a Clark-type respirometer. The later stages of germination are distinguished by specific morphological changes, but germination is asynchronous. We developed a microdissection technique that enables us to collect teliospores at distinct germination stages.

Keywords: *Ustilago maydis*, teliospores, dormancy, germination, respiration, microdissection

INTRODUCTION

The smut fungi (*Ustilaginales*) consist of over 1,600 species that infect grasses including the important cereal crops of corn, barley, and wheat, causing billions of dollars in crop losses annually[1]. These fungi are characterized by the production of teliospores, which have darkly pigmented cell walls and are the dispersal agents. Teliospores function to shield genetic material during the stresses of dispersal between host plants, and can persist in a dormant state for years[2]. As such, teliospores are an essential component of disease spread.

In order to study teliospore biology, our laboratory utilizes the model smut fungus *Ustilago maydis*, which is the causal agent of the disease 'common smut of corn'. Mature *U. maydis* teliospores are characterized by growth arrest, reduced cellular metabolism, and low levels of cellular respiration[3]. In favorable environmental conditions (*e.g.*, the presence of specific sugars), *U. maydis* teliospores germinate and complete meiosis, producing basidiospores which can initiate new rounds of infection. Germination is characterized by increased respiration, the return to metabolic activity, and the progression through observable morphological stages of germination[4].

The initial stage of germination includes increased respiration and metabolic function, however there are no morphological indications of change. The original measurements of respiratory change in *U. maydis* were carried out over 50 years ago, measuring oxygen consumption manometrically with a Warburg flask apparatus[5]. We have developed a new, simple method of studying precise changes in respiration during teliospore germination by measuring oxygen consumption over a time course of germination using a Clark-type microrespirometer. We previously used this method to study changes in respiratory rate between wild-type *U. maydis* haploid cells and mutants

with defective mitochondria[6], and have adapted the protocol here to study changes in teliospore respiration during germination. This provides a means of accurately identifying the timing of respiration change so that we can target teliospores at the appropriate time after the initiation of germination to investigate early molecular events. The progression of germination can be followed microscopically once the promycelia emerges from the teliospore, but the asynchronous nature inhibited the isolation of enough teliospores at a given stage for investigation. We developed a microdissection technique similar to those used for *in vitro* fertilization to physically collect teliospores at distinct morphological stages of germination.

PROTOCOL

3.1 Corn Cob Infection

3.1.1 Grow *Zea mays* (cv. Golden Bantam) until cobs are formed and have started to silk (approximately 60 days).

3.1.2 Culture compatible haploid *U. maydis* strains using standard protocols as previously described[7].

3.1.3 Infect corn cobs using standard protocols as previously described[7].

3.2 Teliospore Harvesting

3.2.1 Autoclave equipment (Büchner funnels, Büchner flasks, blenders, 250 mL centrifuge bottles, flat spatulas, and water) using a standard dry cycle with at least 30 min sterilization at 121 °C (standard liquid cycle for water).

3.2.2 Remove infected cobs from plants (approximately 28–35 days post infection) using a razor and set the cobs on a tray covered in bench protector.

3.2.3 Remove the tumours from cobs with a razor blade and collect in a beaker.

3.2.4 Fill a 250 mL laboratory blender cup with tumours until approximately 1/3 full and add autoclaved dH_2O until the blender cup is approximately 3/4 full. Disrupt the tumours by pulsing the blender at low, until homogenized.

3.2.5 Connect the vacuum pump to a water trap and then to a 1 L Büchner flask.

3.2.6 Insert large Büchner funnel into flask and line the bottom of the Büchner funnel with four layers of cheesecloth.

3.2.7 Turn on the vacuum pump.

3.2.8 Pour a portion of the homogenized tumours through the cheesecloth and scrape with a spatula.

3.2.9 Pour some dH_2O into the cheesecloth in order to flush the teliospores through.

3.2.10 Repeat until the dH_2O coming through the cheesecloth is clear.

3.2.11 Wring out the cheesecloth containing the homogenized tumour material into the filter to ensure maximum teliospore recovery.

3.2.12 When the 1 L Büchner flask is getting close to full, empty it into a large Erlenmeyer flask and set it aside.

3.2.13 Put a new piece of cheesecloth into the filter and repeat the steps (3.2.7–3.2.12) until all of the tumours have been disrupted and filtered.

3.2.14 Pour the filtered teliospores into autoclaved 250 mL centrifuge bottles and centrifuge at 1,000 × *g* for 5 min, and decant the supernatant.

3.2.15 Repeat step 3.2.14 until all of the filtered teliospores are pelleted by centrifugation.

3.2.16 Suspend pellets in a small amount of water and transfer to 50 mL centrifuge tubes.

3.2.17 Centrifuge the tubes at 1,000 × *g* for 5 min, and decant the supernatant.

3.2.18 Suspend the pellet with approximately 50 mL dH_2O, centrifuge the tubes at 1000 × *g* for 5 min, and decant the supernatant. Gently scrape off the gray top layer with a spatula and dispose of it. Repeat until there is no longer a top gray layer on top.

3.2.19 Dry samples overnight in a vacuum desiccator.

3.2.20 Store dried teliospores at 4 °C until use.

3.2.21 If desired, treat teliospores with copper sulphate[8] before inducing to germinate. If they are not treated, then perform thorough microscopic analysis of the teliospores to confirm the sample represents pure teliospores and is devoid of bacterial or other contaminations.

3.2.21.1 Weigh out approximately 50 mg of teliospores in a 1.5 mL microcentrifuge tube.

3.2.21.2 Add approximately 1.0 mL 0.75% $CuSO_4$ to the 1.5 mL microcentrifuge tube containing the teliospores. Pipette up and down to suspend the teliospores in the $CuSO_4$ solution followed by agitating the sample for 3 h.

3.2.21.3 Centrifuge the sample at 2,500 × *g* for 5 min and remove the supernatant. Resuspend the teliospore pellet with sterile water, repeat the centrifugation, and remove the supernatant.

3.2.21.4 Repeat step 3.2.21.3 two more times.

3.3 Teliospore Viability and Germination Test

3.3.1 Weigh out approximately 10 mg of *U. maydis* teliospores in a 1.5 mL microcentrifuge tube to assess their viability and the timing of germination.

3.3.2 In a biosafety cabinet, prepare potato dextrose broth (PDB; 24 g/L) supplemented with streptomycin sulfate (160 µg/mL).

3.3.3 Suspend the teliospores in 500 µL of PDB. Gently pipette to mix and break up all clumps of teliospores.

3.3.4 Transfer the teliospore suspension to an autoclaved 250 mL Erlenmeyer flask containing 10 mL of the PDB.

3.3.5 Incubate the flask at 28 °C shaking at 90 rpm for 12–16 h.

3.3.6 In a biosafety cabinet, remove a 20 µL sample of the teliospores induced to germinate and prepare a microscope slide.

3.3.7 Using a microscope, visually assess stages of germination that are present and the presence of bacterial contamination.

3.3.7.1 Count the number of teliospores at stages I through V using a hemocytometer and determine the percent that have germinated.

3.3.7.2 If only stage I teliospores are present, continue to incubate the flask for a total of 24 h before assessing teliospore germination. Continue incubation for a maximum of 48 h before deeming the sample non-viable.

3.3.7.3 If bacterial contamination is present, supplement the PDB with kanamycin sulfate (50 µg/mL) as well as streptomycin sulfate (160 µg/mL) and then repeat steps 3.3.1 to 3.3.7. If bacterial contamination persists, treat teliospores with copper sulfate and repeat steps 3.3.1 to 3.3.7.

3.4 Induction of Germination for Respiration Monitoring

3.4.1 Weigh equal amount (*e.g.* 50 mg) of teliospores for each respiration experiment.

3.4.2 In a biosafety cabinet, add teliospores to an autoclaved respiration chamber.

3.4.3 Fill the chamber with PDB (24 g/L) supplemented with streptomycin sulfate (160 µg/mL) and kanamycin sulfate (50 µg/mL).

3.4.4 Pipette up and down to create a teliospore suspension.

3.4.5 Place chamber lid in chamber to create air tight seal.

3.5 Obtaining Oxygen Consumption Rate (OCR) Measurements

3.5.1 Place the chamber in the chamber rack inside water bath (preheated to 28 °C).

3.5.2 Place O_2 probe inside opening of the chamber.

3.5.3 Monitor the data points appearing in real time on the "SensorTrace Rate" program, and let the probe stabilize (~3 min after the probe is placed in the chamber).

3.5.4 Click "measure" to measure O_2 levels continuously for 6 h with measurements recorded at 2 s intervals.

3.5.5 Stop the measurement, repeat steps 3.4.1 to 3.5.4 for each sample to be analyzed.

3.5.6 Export the data to Microsoft Excel by clicking "File | Export | Save as .xls".

3.6 Data Analysis

3.6.1 Calculate OCR

3.6.1.1 In the exported Excel file under the Within_Rates tab, record the "Rate" for each chamber measurement (nmol/h).

3.6.1.2 For each experimental sample, subtract the "Rate" of the blank chamber from the "Rate" of the experimental sample chamber to obtain a corrected OCR value, and take the absolute value of this number.

3.6.1.3 Calculate the total OCR per mg of teliospores by dividing the corrected absolute OCR value by the cellular mass used.

3.6.1.4 Average replicate "OCR per mg of teliospores" values for each strain.

3.6.2 Analyze the data using appropriate statistical method (*e.g.*, student's *t*-test, analysis of variance) using Microsoft Excel or other statistical software.

3.6.3 To graph raw data, calculate the percentage of oxygen remaining for each time-point you wish to graph. Divide first reading by itself and multiply by 100 (100% oxygen remaining), then divide each subsequent reading by the first reading, and multiply by 100 to obtain the percent of oxygen remaining in the chamber.

3.7 Induction of Teliospore Germination to Isolate Teliospores at Distinct Stages of Germination

3.7.1 Prepare PDB (24 g/L) supplemented with streptomycin sulfate (160 µg/mL) in a biosafety cabinet.

3.7.2 Place approximately 10 mg of *U. maydis* teliospores into a 1.5 mL microcentrifuge tube.

3.7.3 Suspend the teliospores in 500 µL PDB. Gently pipette to mix until there are no clumps of teliospores in the medium.

3.8 Preparation of Petri Dish and Micromanipulator

3.8.1 Prepare a Petri dish (57 cm^2) by pipetting rows of droplets for microcapillary preparation and sample collection.

3.8.1.1 Pipette 5 µL (×4) dH_2O droplets across the top of the petri dish.

3.8.1.2 Pipette 2 µL (×3) of RNA stabilization solution on the petri dish to be used for sample collection.

3.8.1.3 Pipette 5 µL (×30) droplets of germinating teliospores on the petri dish.

3.8.2 Add 15 mL of mineral oil to the Petri dish. Ensure that all droplets are covered by oil before proceeding.

3.8.3 Prepare a microcapillary with a 15 µm inner diameter, 1 mm flange, 55 mm length, and a 20° tip angle by placing it in the microcapillary holder and submerging it in

the mineral oil where capillary action will allow the mineral oil to enter the microcapillary. Release the pressure in the microcapillary before bringing it to the water droplet. Aspirate to prepare the microcapillary with water.

3.9 Isolation of Stage-specific Germinating Teliospores

3.9.1 Using the controls of the micromanipulator, move the prepared microcapillary to one of the germination droplets. Penetrate the droplet, lower the microcapillary, and bring the mouth of the microcapillary up to a germinating teliospore at the stage of germination of interest.

3.9.2 Slowly aspirate to capture the germinating teliospore. Stop aspirating once the teliospore has entered the microcapillary. Repeat until there are approximately five teliospores in the microcapillary.

3.9.3 Raise the microcapillary with the micromanipulator and bring it to the collection droplet of RNA stabilization solution. Penetrate the droplet and inject the teliospores into the droplet.

3.9.4 Repeat steps 3.9.1 to 3.9.3 until approximately 1,000 teliospores have been captured.

3.10 Recovery of Collection Droplet

3.10.1 Pipette up the collection droplet and transfer it to the lid of an RNase/DNase-free 2.0 mL microcentrifuge tube. Carefully remove mineral oil with a pipette without disturbing the collection droplet.

3.10.2 Use teliospores for downstream applications such as RNA isolation.

REPRESENTATIVE RESULTS

Using the Clark-type microrespirometer-based method of measuring changes in respiration during teliospore dormancy and germination, we confirmed that dormant teliospores exhibit a low level of respiration (~1075 μmol/h/mg) compared to germinating teliospores (~2614 μmol/h/mg; Figure 3.1A). This represents a ~2.4-fold change in average rate of respiration between dormant teliospores and teliospores that have been induced to germinate. In addition, we have identified that teliospores that have been induced to germinate have a ~45 min delay in oxygen uptake (Figure 3.1B). This is indicated by the ~30 min delay in oxygen uptake (Figure 3.1B) in addition to the ~15 min delay between the induction of germination and start of oxygen measurements. This identifies a time point to begin assessing molecular changes in the germinating teliospores that are not visibly changing.

Subsequent changes during germination can be observed microscopically. Five stages of germination were determined. Stage I of germination represents teliospores that have been induced to germinate but remain indistinguishable from dormant teliospores. Stage II teliospores have an emerging promycelium with a length that is less than or equal to the diameter of the teliospore. Stage III teliospores have promycelia that are greater than the teliospore diameter. Stage IV of germination is the initial budding of basidiospores from the promycelia, and Stage V are the resulting haploid basidiospores that divide by budding (Figure 3.2). Using the microdissection technique that we have developed, we have successfully isolated 500 to 1,000 germinating teliospores for downstream applications such as RNA isolation for RT-PCR or RNA-Seq (Table 3.1). Figure 3.3 shows the general set up of the Petri dish for microdissection and the steps for microdissection using a micromanipulator.

DISCUSSION

Basidiomycete biotrophic plant pathogens cause billions of dollars in crop losses annually. The vast majority of these pathogens produce teliospores that are integral to fungal dispersal and sexual reproduction. Gaining knowledge of the development and germination of teliospores is critical to understanding the spread of the devastating diseases caused by these fungi. In order to identify molecular changes at key control points we have devised a method to identify the timing of physiological shifts and another to isolate teliospores at distinct stages of germination. Seto *et al.* (unpublished) noted five stages of teliospore germination by light microscopy (Figure 3.2). In order to investigate physiological activation during Stage I and to assess respiration rate during germination, we used a Clark-type microrespirometer to precisely measure changes in oxygen consumption. Our sample data indicate that our method is precise and highly reproducible. Our findings confirm that germinating *U. maydis* teliospores exhibit a drastic increase in cellular respiration compared to un-induced dormant teliospores. For the first time, we have identified that *U. maydis* teliospores that have been induced to germinate exhibit a ~45 min delay in oxygen uptake. This suggests that *U. maydis* teliospores may require some time to process germination signals (*e.g.*, the presence of sugars) before responding, that increased oxygen uptake is not among the very immediate responses to germination signals or that our assay was not sensitive enough to detect the minimal change in initial oxygen uptake.

Previous studies examining respiration rates of smut teliospores[3] relied on a Warburg flask apparatus to measure oxygen levels manometrically[5]. Briefly, this method measures oxygen consumption and CO_2 production by detecting changes in pressure in an

enclosed flask through the direct observation of fluid level changes in the manometer arm. The experiments can be difficult to set up, and measurements can be imprecise. The apparatus must be attended throughout the period of measurement and, extensive calculations are required to estimate OCR. Our protocol makes use of technological advances, eliminating the requirement for the user to remain by the apparatus for the duration of the experiment, take measurements by eye, and use extensive mathematical formulas. Others have used early Clark-type respirometers to measure OCR of *Neurospora crassa*[9] and *Botryodpilodia theobromae*[10] spores, however, these early instruments permitted continuous measurements for a maximum of 20 min. This limitation would not have allowed the identification of the ~45 min delay in oxygen uptake we observed with the newer model respirometer. Our protocol has made data interpretation simpler, as the readout is the concentration of oxygen remaining in the chamber, which can be directly graphed without any calculations or data manipulation. In addition, it is possible to take continuous measurements (every 2 s) for an indefinite amount of time until available oxygen is completely depleted. This permits the identification of small changes in respiration over a long period of time. Therefore, we have improved upon earlier techniques and developed a simple, precise, and reproducible method to measure oxygen consumption of fungal spores. To our knowledge, this is the first study to use a modern Clark-type respirometer to study respiration of dormant versus germinating teliospores of smut fungi.

Despite the ease and simplicity of this protocol, optimization is required and there are biological realities that limited the analysis. First, appropriate sample sizes must be identified to achieve reasonable OCRs. Too much sample can lead to premature crashing

of oxygen levels, and too little sample can result in the inability to observe meaningful changes in oxygen consumption. Second, it is imperative to allow the probe time to stabilize (~3 min) to provide accurate initial data. Lastly, it is important to supplement germination medium with antibacterial agents (*e.g.*, streptomycin sulfate) in order to ensure bacterial contamination does not alter OCR readings. The biological limitations we faced were a low germination rate over the time course of measurement, (~1%) as determined by observing visual morphological changes. Determining spore viability would allow this rate determination to be converted to a rate per spore number and isolating teliospores with higher rates of germination would lead to higher OCRs. The asynchronous germination of *U. maydis* teliospores[11] is a reality that must be accounted for and may have contributed to an inability to detect oxygen consumption earlier in germination.

In order to improve the accuracy and precision of measuring changes in teliospore respiration, future adaptations to this method could include measuring OCR on a single cell-basis. Micromanipulation techniques could be used to isolate a single teliospore, which can then be induced to germinate, and its respiration rate can be monitored. This could improve resolution, providing information regarding the OCR during the dormancy-germination shift per teliospore, rather than per mg of teliospores. In addition, this would solve the confounding issue of asynchronous germination.

For later stages of germination, we developed a micromanipulation method to isolate teliospores at common stages of germination. This allowed the creation of relatively synchronous teliospore populations for analysis. Various methods for isolating single microorganisms have

been described and have been improved upon over the years[12]. These methods include the dilution of spore suspensions to obtain single microorganisms, semi-mechanical methods with the use of microcapillaries to obtain spores that are transferred to medium for culturing, and mechanical methods which use micromanipulators. Previous methods that we used to obtain teliospores at the same stage of germination include counterflow centrifugal elutriation and filtering germinating teliospores through a nylon membrane with a specific pore size. Using these methods allowed us to enrich for germinating teliospores, however, our samples still contained teliospores in various stages of germination[13]. Current technology for micromanipulation of single microorganisms has improved with the introduction of higher magnification and instruments for fine control of capillary needles, aspiration, and transfer of microorganisms. Previous micromanipulation techniques have focused on isolating single cells for culturing or for use in single cell PCR applications[14]. The use of micromanipulators to isolate single fungal spores has not previously been established. A previous method for isolating single fungal spores involved the use of fine forceps or needles to pick small pieces of solid medium containing germinating spores[15]. Micromanipulation with the use of micromanipulators is widely used in yeast studies where clusters of ascospores can be separated following sporulation in culture on agar medium for meiotic genetic analysis[16]. We have developed a method which combines the micromanipulation technique for bacterial cells[14] and *in vitro* fertilization methods for isolating germinating teliospores. We have shown that hundreds of common germination stage teliospores can be obtained with this technique. These samples can be used for downstream expression studies using techniques such as RT-qPCR or RNA-seq. Obtaining a population of teliospores in which germination is synchronized permits the analysis of

specific changes in gene expression that occurs during early, mid and later stages of teliospore germination.

Microdissection of stage specific germinating teliospores may require experience in set up and recognizing the different stages of germination, however, this experience can be obtained quickly through practice. There are several steps that must be followed for successful microdissection followed by RNA isolation. First, germination medium must be supplemented with antibiotics (*e.g.*, streptomycin sulfate) to suppress the growth of bacterial contamination when germination is initiated as well as during collection of germinating teliospores. Second, it is important to use a stabilization solution to stabilize and protect RNA for isolation. The RNA stabilization solution also prevents collected teliospores from progressing to the next germination stage while collecting additional teliospores. Thirdly, it is important to remove the mineral oil once the collection droplet has been recovered to ensure successful RNA extraction. Lastly, we have noticed some loss of RNA quality if isolated teliospores are stored in RNA stabilization solution for an extended period of time; therefore, it is recommended that RNA is isolated immediately following collection of germination stage specific teliospores. A limitation of the method is that the Stage I teliospores collected could contain dormant, dead, and induced to germinate teliospores as these three stages are morphologically indistinguishable. In addition, when collecting Stage III teliospores, a mixture of teliospores in meiosis I or meiosis II could be obtained. One way to aid in distinguishing between truly dormant and dead teliospores could be to determine the viability of the sample. A method for assessing fungal spore viability using live/dead cell viability assays may be able to assess percentage of viable teliospores from which more informative germination rates could be

determined[17]. In addition, nucleus staining with DAPI, for example, could be used to visualize the events of meiosis that are occurring during Stage III and the transition to Stage IV in order to further characterize teliospores morphologically at Stage III. This would aid in the collection of teliospores in only one stage of germination when using our microdissection method.

In conclusion, we have developed a simple, precise and reproducible method of measuring the changes in cellular respiration that occur during the dormancy-germination shift of *Ustilago maydis* teliospores. In addition, we have developed a method for collecting specific stages of germinating teliospores that could be used for downstream applications, such as RNA-seq. Our methods can be adapted to accommodate various cell-types and species. We anticipate that improvements to our techniques will facilitate the detection of respiratory changes on a single spore level as well as further defining the events that are occurring in the later stages of germination.

DISCLOSURES

The authors have no competing financial interests or other conflicts of interest to disclose.

ACKNOWLEDGEMENTS

We would like to thank Dr. Paul Frost for use of his microrespirometer, and Nicole Wagner and Alex Bell for technical assistance. This work was funded by an NSERC grant to B.J.S.

TABLES AND FIGURES

Table 3.1. Number of germinating teliospores successfully isolated for each germination stage in a standard isolation experiment. The table illustrates average numbers of teliospores that have been isolated using microdissection for Stages I through III before collection for downstream applications.

Germination Stage	Number of germinating teliospores isolated
Stage I	1,000
Stage II	500
Stage III	650

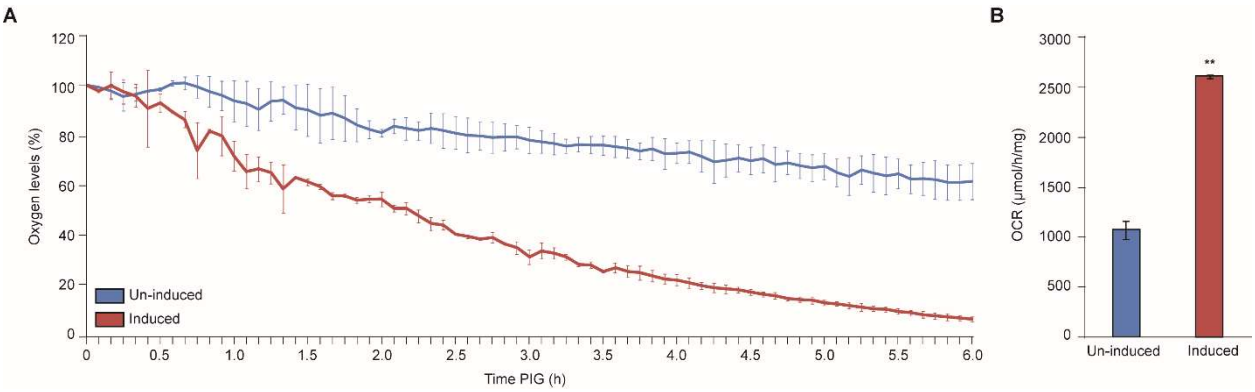

Figure 3.1. Time course of oxygen consumption during teliospore germination. Dormant teliospores were induced to germinate, and oxygen levels were recorded continually for 6 h using a Clark-type microrespirometer. Un-induced dormant teliospores were used as a control, and all measurements were normalized to a blank sample. (A) Data represented as average OCR. (B) Raw data plotted to obtain respiration curves, permitting the detection of changes in OCR during the time course. Teliospores that have been induced to germinate consume oxygen at an average rate 2.4-fold faster than un-induced dormant teliospores (p <0.01; Student's t-test). PIG: post-induction of germination.

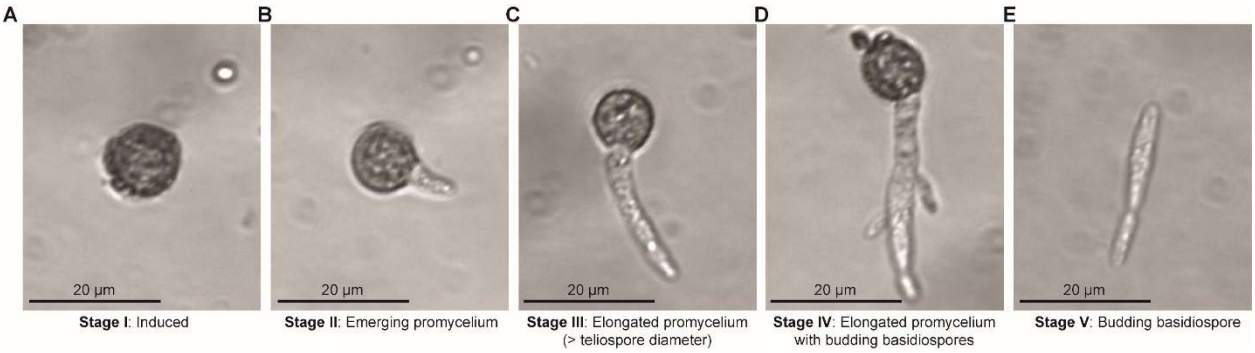

Figure 3.2. Stages of teliospore germination. Stages I through V teliospore germination are illustrated (A–E). Scale bar = 20 µm.

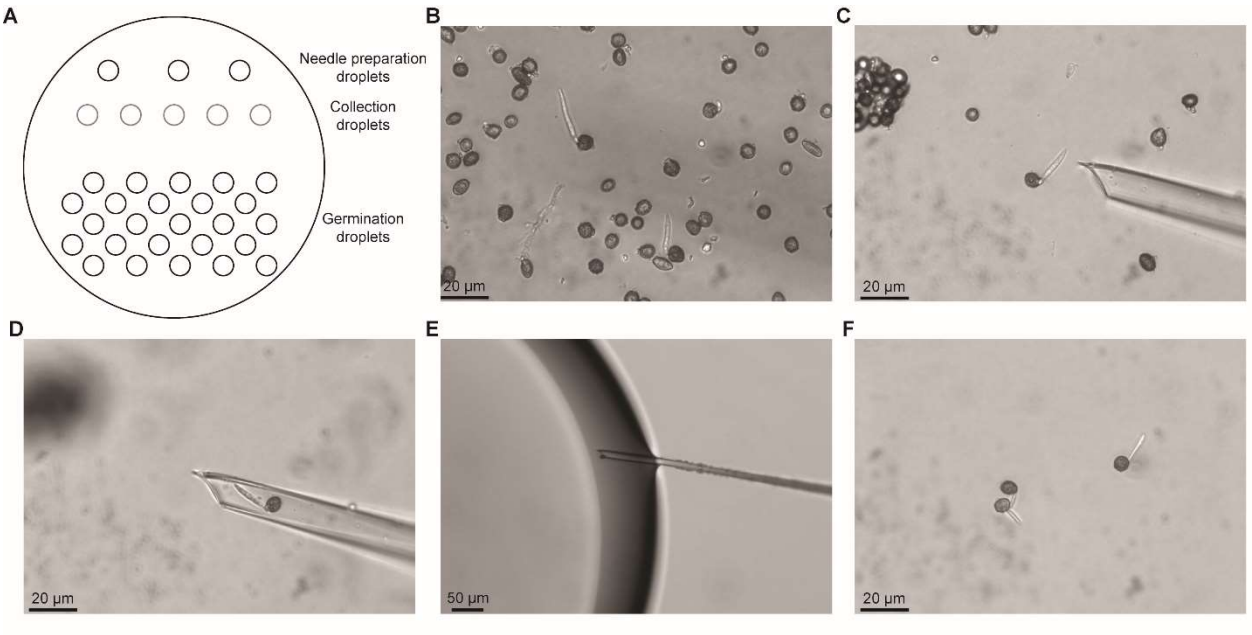

Figure 3.3. Microdissection to isolate distinct morphological stages of germinating teliospores. The general set up of a Petri dish for microdissection and the steps for isolating teliospore at stage III of germination are illustrated. (A) Illustration of a Petri dish set up with rows of droplets containing either sterile water, RNA stabilization solution, or germinating teliospores. Following germination induction, teliospores were isolated at specific stages of germination using microdissection. (B) A germination droplet containing induced to germinate teliospores in Stages I through III. (C) A prepared microcapillary was brought up to a Stage III teliospore for collection through aspiration. (D) The Stage III teliospore in a glass microcapillary is removed from the germination droplet and moved to a collection droplet. (E) The microcapillary was inserted into the collection droplet containing RNA stabilization solution and the Stage III teliospore was injected into the droplet. (F) A collection of Stage III teliospores in the RNA stabilization solution. Scale bar = 20 µm (A–D, F) and 50 µm (E).

REFERENCES

1. Saville, B. J., Donaldson, M. E., Doyle, C. E. in *Meiosis - Molecular Mechanisms and Cytogenetic Diversity*. (ed A. Swan) 411–460 InTech (2012).

2. Christensen, J. J. in *Monograph Number 2*. The American Phytopathological Society, Worcester, MA (1963).

3. Caltrider, P. G., Gottlieb, D. Respiratory activity and enzymes for glucose catabolism in fungus spores. *Phytopathology.* **53** (9), 1021–1030 (1963).

4. Allen, P. J. Metabolic aspects of spore germination in fungi. *Annual Review of Phytopathology.* **3** (3), 313–342 (1965).

5. Warburg, O. Metabolism of tumours. *Biochemische Zeitschrif.* **142**, 317–333 (1923).

6. Ostrowski, L. A., Saville, B. J. Natural antisense transcripts are linked to the modulation of mitochondrial function and teliospore dormancy in *Ustilago maydis*. *Molecular Microbiology.* **103** (5), 745–763 (2017).

7. Morrison, E. N., Donaldson, M. E., Saville, B. J. Identification and analysis of genes expressed in the *Ustilago maydis* dikaryon: Uncovering a novel class of pathogenesis genes. *Canadian Journal of Plant Pathology.* **34** (3), 417–435 (2012).

8. Doyle, C. E., Kitty Cheung, H. Y., Spence, K. L., Saville, B. J. Unh1, an *Ustilago maydis* Ndt80-like protein, controls completion of tumor maturation, teliospore development, and meiosis. *Fungal Genetics and Biology.* **94** 54–68 (2016).

9. Stade, S., Brambl, R. Mitochondrial biogenesis during fungal spore germination: Respiration and cytochrome c oxidase in *Neurospora crassa*. *Journal of Bacteriology.* **147** (3), 757–767 (1981).

10. Brambl, R. Characteristics of developing mitochondrial genetic and respiratory functions in germinating fungal spores. *Biochimica et Biophysica Acta (BBA) - Bioenergetics.* **396** (2), 175–186 (1975).

11. Sacadura, N. T., Saville, B. J. Gene expression and est analyses of *Ustilago maydis* germinating teliospores. *Fungal Genetics and Biology.* **40** (1), 47–64 (2003).

12. Hildebrand, E. M. Techniques for the isolation of single microorganisms. *The Botanical Review.* **4** (12), 627–664 (1938).

13. Seto, A. M. *Analysis of gene transcripts during Ustilago maydis teliospore dormancy and germination* Master of Science thesis, Trent University, (2013).

14. Fröhlich, J., König, H. in *Soil Biology - Intestinal Microorganisms of Termites and Other Invertebrates* (ed H & Varma König, A.) 425–437 Springer (2006).

15 Choi, Y.-W., Hyde, K. D., Ho, W. Single spore isolation of fungi. *Fungal Diversity.* **3** 29–38 (1999).

16 Sherman, F. Getting started with yeast. *Guide to Yeast Genetics and Molecular and Cell Biology, Pt B*. **350** 3–41 (2002).

17 Chen, C. Y., Séguin-Swartz, G. A rapid method for assessing the viability of fungal spores. *Canadian Journal of Plant Pathology.* **24** (2), 230–232 (2002).

CHAPTER 4

PREFACE

Title: Annotation and functional predictions of RNA helicases in *Ustilago maydis*

Authors: Amanda M. Seto and Barry J. Saville

Reference: Published in *IMA Fungus* (2025), 16: e151785

doi: https://doi.org/10.3897/imafungus.16.151785

2024 Impact Factor: 6.2

Contributions: B.J.S. conceived, directed, and obtained funding for the research presented in this study. A.M.S. conducted the literature search for known RNA helicases, performed the reciprocal BLASTp to identify RNA helicases in *Ustilago maydis*, *Ustilago hordei*, and *Sporisorium reilianum*, performed and analysed the STRING searches, constructed the phylogenetic trees, created Tables 4.1–4.9, S4.1, Figures 4.1–4.6, S4.1–S4.6, and drafted the initial manuscript. B.J.S. edited the initial manuscript. A.M.S. and B.J.S. edited the manuscript prior to submission.

CHAPTER 4

Annotation and functional predictions of RNA helicases in *Ustilago maydis*

Published in *IMA Fungus* (2025), **16**: e151785

doi: https://doi.org/10.3897/imafungus.16.151785

ABSTRACT

RNA helicases are conserved enzymes found in both prokaryotes and eukaryotes. They function in all aspects of RNA metabolism and have been found to affect various aspects of cellular and metabolic processes. They also have roles in some cancers and diseases. Research of RNA helicases in fungi indicates their conserved role in RNA metabolism, and that their dysregulation can affect fungal growth. However, the roles of RNA helicases in fungal plant pathogenesis have received limited investigation despite the increased knowledge of how RNA helicases modulate gene expression and disease progression. We used the basidiomycete plant pathogen *Ustilago maydis* as a model to identify 46 RNA helicases. We review the roles of RNA helicases in RNA metabolism, cellular growth and homeostasis, and metabolism. Then we utilized available *U. maydis* transcriptome data and current research to hypothesize potential functions of RNA helicases in fungal plant pathology. The roles include influencing cell growth, modulating stress response, virulence and disease progression, as well as fungal spore dormancy and germination. Understanding the roles RNA helicases have in gene regulation can aid in developing methods for mitigating disease spread in fungal plant pathogens.

Keywords: RNA helicases; smut fungi; *Ustilago maydis*; genome annotation; control of pathogenic development

INTRODUCTION

Helicases are conserved enzymes that utilize ATP to bind and remodel nucleic acids. These proteins are found in both prokaryotes and eukaryotes, and many have conserved functions across species. DNA helicases are involved in many cellular processes including DNA replication and repair. RNA helicases are involved in all aspects of RNA metabolism such as transcription, splicing, ribosome biogenesis, and translation (Singleton et al. 2007). A considerable amount of research supports the roles of RNA helicases in cellular metabolism, growth, and viability. The increased understanding of how defective helicases affect cellular processes has also led to identifying their role in some cancers and diseases (Fairman-Williams et al. 2010; Cai et al. 2017). In fungi, functional analysis of RNA helicase has been extensively conducted in the budding yeast *Saccharomyces cerevisiae*. Investigating their roles in yeast RNA metabolism led to identifying RNA helicases with roles in cellular growth, metabolism, and stress response. Limited investigations of pathogenic fungi have revealed roles in virulence (Panepinto et al. 2005; Bleichert and Baserga 2007; Delaney et al. 2013; Bohnsack et al. 2023). In all of these roles the helicases act to unwind double-stranded RNA (dsRNA).

The separation of RNA-RNA and RNA-DNA duplexes by RNA helicases may also involve displacing proteins from RNA, acting as RNA clamps, and annealing RNA strands. Some RNA helicases are essential proteins and defects can impact cell viability (Bleichert and Baserga 2007; Jankowsky 2011; Linder and Jankowsky 2011). This indicates possible roles in cellular growth and homeostasis. In fungi, it has also been found that some RNA helicases may modulate the expression of subsets of genes which may influence stress response or virulence. For example, in *Cryptococcus neoformans*, the RNA helicase Vad1

regulates several virulence-associated genes (Panepinto et al. 2005). Characterization of Ski2 deletion mutants in *C. neoformans* showed decreased virulence, increased resistance to azoles, and sensitivity to high temperatures and osmotic stress (Li et al. 2022). In *Neurospora crassa*, the RNA helicase FRH forms a complex with FRQ and CK1a to regulate the circadian clock (Cheng et al. 2005; Lauinger et al. 2014). For *S. cerevisiae*, the nutrient stress response is modulated by the RNA helicase Dbp2 (Beck et al. 2014) through its interaction with *SKS1*, a gene that encodes a protein responsible for yeast adaptation to low glucose conditions (Paul et al. 2025). Despite the current knowledge of RNA helicases in fungi, limited research has been conducted on their functions in phytopathogenic fungi. Their roles in fungal growth, virulence, pathogenesis, and spore dormancy have not been considered in the literature and experimental investigations have been limited in the smuts and rusts of the Basidiomycota.

In this review, we utilize the smut fungus *Ustilago maydis* to identify potential RNA helicases of interest and hypothesize their roles in the fungal life cycle. It is a member of the Basidiomycota and belongs to the *Ustilaginales* which consists of over 1,500 species. These species are important plant pathogens responsible for infecting members of the plant family Poaceae which includes many cereal crops. *Ustilago maydis* infects the aerial portions of maize causing common smut of maize. These infections lead to millions of dollars in lost food production (Martínez-Espinoza et al. 2002; Brefort et al. 2009). Although its agricultural impact is not as significant as the rust fungi, *U. maydis* is considered one of the top ten fungal pathogens of scientific importance and is a model for studying plant-pathogen interactions (Dean et al. 2012). This review highlights the functions of RNA helicases in RNA metabolism, identifies RNA helicases in *U. maydis*,

and identifies RNA helicases that have the potential to affect fungal growth, metabolism, stress response, pathogenesis, and teliospore dormancy and germination.

CHARACTERISTICS OF SF1 AND SF2 RNA HELICASE SUPERFAMILIES

Currently, six helicase superfamilies that contain both DNA and RNA helicases have been identified (Fig. 4.1A). The largest helicase superfamilies are superfamilies 1 (SF1) and 2 (SF2). The majority of eukaryotic RNA helicases are found in SF2. The remaining superfamilies (SF3–6) represent enzymes that typically function in DNA metabolism (Singleton et al. 2007; Fairman-Williams et al. 2010). Superfamily 3 (SF3) helicases are found in DNA and RNA viruses (Hickman and Dyda 2005), superfamily 4 (SF4) helicases are found in bacteria and bacteriophages (O'Donnell and Li 2018), superfamily 5 (SF5) contains the bacterial RNA helicase Rho which is responsible for transcription termination (Selvaratnam et al. 2025), and superfamily 6 (SF6) helicases are also known as the AAA+ superfamily and are involved in DNA metabolism (Ilves et al. 2010). The classification of helicases was first determined through sequence and structure motifs described by Gorbalenya and Koonin (1993) and further structural and functional analysis conducted by Singleton et al. (2007). These sequence motifs make up the helicase core that contains two RecA-like domains. The functions of these motifs are: ATP binding and hydrolysis, RNA binding, interdomain contacts, and coordinating ATP and RNA binding (Bleichert and Baserga 2007; Fairman-Williams et al. 2010). For RNA helicases, the helicase core is characterized by approximately 14 sequence motifs, as illustrated in Fig. 4.1B. Some sequence motifs are conserved in all RNA helicases (I, II, and VI) whereas others are present in a subset of RNA helicases (Fairman-Williams et al. 2010; Sloan and Bohnsack

2018). Our review focuses on fungal RNA helicases found in the SF1 and SF2 superfamilies.

Sequence and structural analyses conducted by Gorbalenya and Koonin (1993) and Singleton et al. (2007) identified three families of helicases within SF1. The families are UvrD/Rep-like, Pif1-like, and Upf1-like helicases. The UvrD/Rep-like family consists primarily of DNA helicases found in bacteria and a few eukaryotes (Gilhooly et al. 2013). Pif1-like helicases are found in both eukaryotes and prokaryotes. This family includes DNA helicases that promote nuclear and mitochondrial genome stability, and DNA repair (Bochman et al. 2010; Gilhooly et al. 2013). SF1 RNA helicases belong to the Upf1-like family of helicases. They are conserved RNA helicases that function during nonsense-mediated RNA decay and prevent genome instability during transcription (Mischo et al. 2011; Gupta and Li 2018). These RNA helicases contain sequence domains that are conserved among the UPf1-like RNA helicases and not found in other RNA helicase families (Fig. 4.1B). The subdomains 1B and 1C are in conserved locations within the RNA helicase core (Fairman-Williams et al. 2010). The 1B subdomain forms a β-barrel fold and 1C forms an α-helical fold within the helicase core, contributing to modulating conformational changes to the RNA helicase (Gowravaram et al. 2018; Kanaan et al. 2018). Motif IIIa is specific to SF1 RNA helicases and serves as a stacking platform for adenine in ATP through the conserved tyrosine residue (Fairman-Williams et al. 2010).

The SF2 superfamily of RNA helicases is the largest superfamily containing 10 families of helicases (Fig. 4.1A). These families were identified by Fairman-Williams et al. (2010) through sequence and phylogenetic analysis. Family members of SF2 include RecG-like, RecQ-like, Rad3/XPD, DEAD-box, DEAH/RHA, Ski2-like, RIG-I-like,

Swi/Snf, NS3/NPH-II, and Type 1 restriction enzymes. The RecG-like helicases are found in prokaryotes, RecQ-like and Rad3/XPD families contain DNA helicases, NS3/NPH-II family are viral RNA helicases, and Type 1 restriction enzymes are members of the restriction-modification system found in bacteria. Fungal SF2 RNA helicases are found in the remaining families (Fairman-Williams et al. 2010; Byrd and Raney 2012).

The DEAD-box family is the largest family of helicases with conservation in prokaryotes and eukaryotes. DEAD-box RNA helicases contain a helicase core that consists of 12 sequence motifs. The defining motif of this family is motif II containing the amino acid sequence motif Asp-Glu-Ala-Asp (DEAD) (Fairman-Williams et al. 2010; Jankowsky 2011; Linder and Jankowsky 2011; Byrd and Raney 2012). Many DEAD-box helicases bind to RNA in an ATP-dependent manner. They function to modulate structured RNAs by disrupting secondary and tertiary structures and can disrupt RNA-protein interactions in RNPs. DEAD-box RNA helicases can separate RNA duplexes anywhere by disrupting the duplex which then accelerates the separation. This is accomplished in an ATP-dependent manner but is limited to short duplexes (Yang et al. 2007). Structurally, DEAD-box RNA helicases contain an α-helix, called α-helix 8, located at the end of motif II (Fig. 4.1B). This structure is proposed to control access to the binding site when the helicase is in the ADP state. When ATP binds to the RNA helicase, a conformational change is induced which moves α-helix 8 out of the binding site to interact with the conserved Arginine in motif V (Schütz et al. 2010; Cordin et al. 2012).

The DEAH/RNA Helicase A (RHA) family contains spliceosomal and RHA-group subfamilies of RNA helicases. The spliceosomal RNA helicases are involved in pre-mRNA splicing and RHA-group RNA helicases function during transcription, RNA export, and

translation. The conserved sequence motifs in DEAH/RHA RNA helicases differ from DEAD-box RNA helicases and DEAD-box RNA helicases contain a more variable C-terminal domain than DEAH/RHA RNA helicases (Fig. 4.1B). The C-terminal domain of DEAH/RHA RNA helicases is conserved with the organization of the following subdomains: winged helix, helix bundle, and oligosaccharide-binding fold. The organization of these subdomains dictates the formation of a strong bond between the RNA helicase and RNA, and the translocating action of DEAH/RHA RNA helicases (De Bortoli et al. 2021). The Q-motif, which is involved in ATP binding, is absent in DEAH/RHA RNA helicases (Fairman-Williams et al. 2010). Structurally, DEAH/RHA RNA helicases contain two β-hairpins (Fig. 4.1B), one in the RecA-like domain 1 located between motifs Ib and Ic and the second in RecA-like domain 2 between motifs Vb and VI (Cordin and Beggs 2013; He et al. 2017). The first β-hairpin is an extension of motif Ib, is unique and conserved in DEAH/RHA RNA helicases, and is responsible for unwinding RNA in a 3'-to-5' direction (He et al. 2017). The β-hairpin located in RecA-like domain 2 is longer than the β-hairpin found in the same position of Ski2-like RNA helicases. Structural analysis indicates that when the RNA helicase is in the ADP state, the β-hairpin blocks access to the nucleic acid binding cavity. This cavity is formed by the two RecA-like domains, the helix bundle, and the winged helix. A conformational change occurs when ATP binds to the RNA helicase, releasing the β-hairpin from the cavity. This conformational change allows the RecA-like domain 2 to bind to the 5' end of the RNA duplex. In the proposed model for strand separation, the β-hairpin is responsible for slicing through the RNA duplex, while the helix bundle pulls the single-stranded RNA through the cavity. The OB-fold is located

at the cavity entrance and provides a docking platform for other binding proteins (He et al. 2010; Walbott et al. 2010; He et al. 2017).

The Ski2-like family of SF2 RNA helicases is divided into two subfamilies that contain the Ski2 and Brr2 RNA helicases. This is a small family of RNA helicases, and their structure makes them distinct from other SF2 RNA helicases. Ski2-like RNA helicases, like DEAH/RHA RNA helicases, have a shorter β-hairpin between sequence motifs Va and VI (Fig. 4.1B). The β-hairpin structure has been proposed to function similarly to its counterpart in DEAH/RHA RNA helicases by assisting in unwinding duplexes by positioning itself between the two strands (reviewed in Fairman-Williams et al. 2010; Johnson and Jackson 2013). At the C-terminal, Ski2-like RNA helicases have a conserved winged helix and a Sec63 domain (Fig. 4.1B). The Sec63 domain contains a helix bundle (HB), helix-loop-helix (HLH), and immunoglobulin-like (IG) domains. It is unique to this family of RNA helicases and may contribute to substrate binding regulation by forming a tunnel for RNA to bind and be translocated during unwinding (Cordin and Beggs 2013).

IDENTIFICATION OF *Ustilago maydis* RNA HELICASES

RNA helicases in *U. maydis* and their putative functions have not been previously investigated. Our interest in the function of *U. maydis* RNA helicases stemmed from previous research in our laboratory that suggested some gene transcripts are stabilized in the dormant teliospore through the formation of dsRNAs. During teliospore germination, these stabilized transcripts would need to be unwound and made available for translation (Donaldson and Saville 2013; Ostrowski and Saville 2017). It was proposed that RNA

helicases may modulate the availability of mRNAs by unwinding the dsRNAs in the teliospore after germination initiation. We identified putative *U. maydis* RNA helicases and proposed functions inferred by homology to previously characterized RNA helicases in other model organisms. We then identified RNA helicases with proposed contributions to fungal development and growth based on current research in other eukaryotes.

Putative *U. maydis* RNA helicases were identified utilizing previously characterized RNA helicases in the species *Saccharomyces cerevisiae*, *Caenorhabditis elegans*, *Drosophila melanogaster*, *Mus musculus*, and *Homo sapiens* (Jankowsky 2011; Bourgeois et al. 2016). We compared the known protein sequences of these RNA helicases to those of *U. maydis* by performing reciprocal BLASTp to identify putative *U. maydis* RNA helicases. Using this approach, 46 RNA helicases were identified in *U. maydis* (Table 1). In comparison to other species, there are approximately 41 in *S. cerevisiae* and 70 in *H. sapiens* (Bohnsack et al. 2023). Plant species such as *Arabidopsis thaliana*, *Zea mays*, and *Oryza sativa* contain more than 150 RNA helicases (Li et al. 2023). The 46 *U. maydis* RNA helicases are divided into both the SF1 and SF2 families, where four are found in the SF1 Upf1-like RNA helicases and 42 in the SF2 superfamily. The 42 RNA helicases in the SF2 superfamily are found in the DEAD-box, DEAH/RHA, and Ski2-like families. We did not identify any *U. maydis* RNA helicases belonging to the RIG-I-like family. This is unsurprising as the RIG-I-like helicases typically function as viral sensors and are involved in the antiviral immune response (Byrd and Raney 2012). In addition, DICER1 in eukaryotes is classified as a RIG-I-like helicase due to its helicase domain (Table 4.1), however we did not expect to find a *U. maydis* ortholog as it lacks the RNA interference machinery (Nakayashiki et al. 2006). Further classifications of *U. maydis* RNA helicases

were determined through phylogenetic analyses using protein sequences from *U. maydis*, *Sporisorium reilianum*, *Ustilago hordei*, *S. cerevisiae*, *Schizosaccharomyces pombe*, *N. crassa*, *C. elegans*, *H. sapiens*, *Dictyostelium discoideum*, and *A. thaliana*. Protein sequences were aligned in Jalview v2.11 (Waterhouse et al. 2009) using the JABAWS service to perform MUSCLE alignment under default settings (Edgar 2004; Troshin et al. 2011). Maximum likelihood phylogenetic trees were constructed for each family of RNA helicases (Figs 4.2–4.5).

There are four SF1 Upf1-like RNA helicases in *S. cerevisiae* and eight in *H. sapiens* (Table 4.1). Our analysis identified four Upf1-like RNA helicases in *U. maydis*. Three are putative orthologs to the characterized SF1 RNA helicases Sen1 (UMAG10602), Upf1 (UMAG_11428), and Hcs1 (UMAG_01122). The phylogenetic analysis identified the remaining RNA helicase as a putative basidiomycete-specific SF1 RNA helicase (UMAG_10130) (Fig. 4.2).

Of the 42 SF2 RNA helicases, our investigation identified 27 *U. maydis* DEAD-box RNA helicases (Table 4.1), where 25 are conserved and have orthologs in other eukaryotes (Fig. 4.3). In *S. cerevisiae*, there are 26 DEAD-box RNA helicases compared to the 33 in *H. sapiens*. The remaining two DEAD-box RNA helicases (UMAG_05873 and UMAG_00835) are basidiomycete-specific (Fig. 4.3). Many of these RNA helicases function in one aspect of RNA metabolism, however, there are a few that function in multiple areas of RNA metabolism.

A total of 10 DEAH/RHA RNA helicases were identified in *U. maydis* based on our sequence (Table 4.1) and phylogenetic (Fig. 4.4) analyses compared to the seven in *S. cerevisiae* and 15 in *H. sapiens*. Of the 10, six are spliceosomal DEAH RNA helicases and

the remaining four are RHA-group RNA helicases. The phylogenetic tree (Fig. 4.4) suggests a fungal-specific DEAH/RHA RNA helicase with no orthologs in the eukaryotes included in our phylogenetic analysis. This fungal-specific RNA helicase was identified as YLR419W in *S. cerevisiae* and UMAG_11114 in *U. maydis*.

The last family of SF2 RNA helicases are the Ski2-like RNA helicases. Data from *S. cerevisiae* identifies four Ski2-like SF2 RNA helicases (Brr2, Slh1, Mtr4, and Ski2). Suv3 was originally categorized as Ski2-like but has since been removed after further structural analysis (reviewed in Johnson and Jackson 2013). *Ustilago maydis* has orthologs to all five Ski2-like RNA helicases (Fig. 4.5).

FUNCTIONS OF RNA HELICASES AND THEIR POTENTIAL ROLES IN *Ustilago maydis*

RNA helicases function in all aspects of RNA metabolism with demonstrated roles during transcription, pre-mRNA splicing, ribosome biogenesis, RNA export, translation, and RNA degradation (Bleichert and Baserga 2007; Jankowsky 2011; Linder and Jankowsky 2011). Despite their widespread role in RNA metabolism, some RNA helicases have specific roles while others have more than one function (Jankowsky 2011). Several *H. sapiens* studies show that upregulation or downregulation of RNA helicases contributes to the development of several diseases and different forms of cancer. Other studies indicate that RNA helicases could be used as therapeutic targets for drug delivery and identifying specific diseases (Shadrick et al. 2013; Zhang and Li 2021). Fungal studies have shown their importance in cellular growth, metabolism, virulence, and stress response (Cheng et al. 2005; Panepinto et al. 2005; Beck et al. 2014; Lauinger et al. 2014; Li et al. 2022; Ying et al. 2022; Paul et

al. 2025). Based on the current research, we predict that RNA helicases may have further roles in fungal plant pathology.

A STRING analysis was conducted for each *U. maydis* gene to predict protein-protein interactions (Table S4.1) and infer their possible functions. The STRING database (v. 12.0) contains known and predicted protein interactions, and a confidence score is calculated based on available evidence from other species (Szklarczyk et al. 2023). We also conducted a gene transcript analysis based on the transcriptomic data from the *U. maydis* haploid, and dikaryon cultures, as well as dormant and germinating teliospores (Donaldson et al. 2017; Seto et al. 2025), and transcript patterns during *U. maydis* pathogenesis (Lanver et al. 2018). This analysis allowed us to make predictions on the possible roles RNA helicases have during *U. maydis* growth, development, and pathogenesis.

The analysis of the *in planta*, biotrophic growth, transcript data from Lanver et al. (2018) is summarized in Table 4.2. Lanver et al. (2018) identified 14 modules which represented groups of co-expressed genes during *U. maydis* pathogenesis. We found that of the 14 modules, the *U. maydis* RNA helicases are found in nine of the modules. A description of the nine expression profiles is summarized in Table 4.2. Most RNA helicases can be found in the green-yellow and yellow modules indicating that the activity of these RNA helicases may be important during the early stages of biotrophic development and during metabolic and cellular shifts during pathogenesis. The transcriptome data from Donaldson et al. (2017) and Seto et al. (2025) were used to determine if the RNA helicase transcript levels were enhanced in the *U. maydis* haploid, dikaryon, or teliospore. RNA helicases with specific transcript patterns during specific stages of the fungal life cycle are of particular interest. For example, a group of RNA helicases were found to be upregulated

in the dormant teliospore compared to the haploid and dikaryon cell types and have specific changes in transcript levels during teliospore germination. Some of these RNA helicases may be stored in the dormant teliospore or have roles in stabilizing mRNAs in the dormant teliospore or translating mRNAs during germination (Seto et al. 2025).

In the following sections, we highlight the functions of RNA helicases in RNA metabolism. We then utilized the STRING and gene transcript analyses to identify specific RNA helicases with potential roles in the biology of phytopathogenic fungi. This has allowed us to identify 28 RNA helicases that may impact *U. maydis* growth, pathogenesis, stress response, and/or teliospore dormancy and germination.

Transcription

Transcription is broken down into three basic steps: initiation, elongation, and termination. Initiation begins when the RNA polymerase recognizes the promoter sequence located upstream of the coding region for RNA on a DNA template. Elongation involves the synthesis of the RNA transcript until the RNA polymerase encounters the termination sequence. Termination is the dissociation of the RNA polymerase from the DNA template and the release of the RNA transcript. During transcription, the nascent RNA transcript is subjected to folding and transcription elongation can vary in speed which facilitates interactions with RNA binding proteins and RNA helicases which can influence the folding (reviewed in Pan and Sosnick 2006). Six RNA helicases have functions during transcription and are summarized in Table 4.3. *Ustilago maydis* RNA helicases with predicted roles in transcription are orthologs to the *S. cerevisiae* RNA helicases Sen1, Dbp2, and the *H. sapiens* RNA helicases DHX9, DDX23, and DDX39.

UMAG_10602 was identified as an RNA helicase that may function during pathogenic development. It is the ortholog to the SF1 Upf1-like RNA helicase Sen1 in *S. cerevisiae* and SETX in *H. sapiens* (Fig. 4.2, Table 4.1). STRING analysis predicts a conserved role in transcription. Depletion or mutation of SETX has been found to impact the expression of a subset of genes that encode cytoskeleton components, autophagy regulation, and lysosomal degradation (Richard et al. 2021; Giannini and Porrua 2024). The transcriptome analysis of data from Donaldson et al. (2017) and Seto et al. (2025) indicates that the gene transcript is present in all *U. maydis* cell types and during teliospore dormancy and germination. During *U. maydis* infection, the transcript is present in the cyan/tumour module (Table 4.2). Genes contained in this module are induced after biotrophic establishment and at the onset of tumour induction (Lanver et al. 2018). This transcript pattern for *UMAG_10602* suggests a role in ensuring genome integrity during the transcription of key genes for tumour growth and development. We predict that *UMAG_10602* mutants will impact pathogenic development and may result in decreased pathogenesis.

Pre-mRNA splicing

Eukaryotic precursor messenger RNA (pre-mRNA) is subjected to splicing before becoming a functional mRNA. This process is highly regulated and involves two consecutive transesterification steps that are catalyzed by the spliceosome. Regulation and efficiency of splicing ensures intron removal and fusion of exons to form mature mRNA. During splicing, the spliceosome undergoes structural changes mediated by RNA helicases. The identified *U. maydis* helicases that are predicted to be involved in these processes are listed in Table 4.4. Most of these RNA helicases act as chaperones to modulate the structure

of the mRNA or a ribonucleoprotein (RNP) attached to the mRNA (Liu and Cheng 2015). A total of eight RNA helicases are required for splicing and are Sub2, Prp5, Prp28, Brr2, Prp2, Prp16, Prp22, and Prp43 in *S. cerevisiae*. In general, these RNA helicases act as chaperones that modulate the structure of the RNA or RNP (Liu and Cheng 2015) and their specific functions are listed in Table 4.4. Other RNA helicases that may function during pre-mRNA splicing are Dbp2 and Ded1 in *S. cerevisiae*, and DHX9, DHX35, DDX41, DDX48, and DDX54 in *H. sapiens*. The *U. maydis* orthologs of these proteins and summaries of their functions are indicated in Table 4.4.

The splicing pathway begins with the assembly of the spliceosome which is initiated with recognition and binding of snRNA U1 at the 5' splice site. This results in the formation of the commitment complex 1 (CC1) and the prespliceosome where the snRNA U2 binds to the branch point sequence (Liu and Cheng 2015). The two DEAD-box RNA helicases that are involved in this process are Sub2 and Prp5 in *S. cerevisiae* and *H. sapiens* orthologs DDX39 and DDX46 (Bleichert and Baserga 2007; Liu and Cheng 2015). The *U. maydis* orthologs of these helicases are UMAG_11769 and UMAG_01174. There is evidence that DDX5 and DDX17 may assist this process in *H. sapiens* (Hönig et al. 2002; Lee 2002) and the *U. maydis* ortholog to these proteins is UMAG_10095.

The second step of the splicing pathway is spliceosome activation which involves recruitment of the U4/U6.U5 tri-snRNP and the pre-mRNA undergoes additional conformational changes. The structural changes and binding of snRNPs result in a stable structure which forms the basis of the catalytic core of the spliceosome (Liu and Cheng 2015). The DEAD-box RNA helicases Prp28 in *S. cerevisiae*, DDX23 in *H. sapiens*, *U. maydis* ortholog UMAG_10666, and the Ski2-like RNA helicase Brr2 in *S. cerevisiae*, *U.*

maydis ortholog UMAG_03738, (Liu and Cheng 2015; Bourgeois et al. 2016) modulate this process.

Two catalytic reactions occur after spliceosome activation. These reactions require the function of two RNA helicases. These have been identified as the SF2 DEAH RNA helicase Prp2 and SF2 DEAD-box RNA helicase Prp16 in *S. cerevisiae*, DHX16 and DDX38 in *H. sapiens* (Liu and Cheng 2015; Bourgeois et al. 2016), *U. maydis* orthologs UMAG_10095 and UMAG_04188. After the completion of mRNA splicing, the spliceosome is disassembled, and mature mRNA is released. Two SF2 DEAH RNA helicases are required for this to occur. These RNA helicases are Prp22 and Prp43 in *S. cerevisiae*, DHX8 and DHX15 in *H. sapiens* (Liu and Cheng 2015; Bourgeois et al. 2016). The *U. maydis* orthologs to these proteins are UMAG_03936 and UMAG_11281. It is notable that some helicases have more than one role in pre-mRNA splicing.

The transcript analysis of the *U. maydis* RNA helicases predicted to be involved in pre-mRNA splicing revealed five RNA helicases that may modulate pathogenesis, growth, and teliospore formation and germination. These RNA helicases are *UMAG_04587*, *UMAG_10666*, *UMAG_01174*, *UMAG_11913*, and *UMAG_06129*. The transcripts of these RNA helicases are found in the haploid, dikaryon, cell types, and during teliospore dormancy and germination (Donaldson et al. 2017; Seto et al. 2025). The RNA helicases *UMAG_04587* and *UMAG_01174* are found in the Lanver et al. (2018) cyan module, representing the tumour development module. *UMAG_10666* is the only RNA helicase found in the burlywood module, and *UMAG_11913* is found in the light-cyan module (Table 4.2). The *UMAG_06129* transcript is upregulated in the dormant teliospore, and the

transcript remains unchanged during germination (Seto et al. 2025). It is the only RNA helicase in the Lanver et al. (2018) salmon module (Table 4.2).

UMAG_04587 is a putative RNA helicase that had orthologs in the basidiomycete fungi and animals, however, there were no orthologs in the ascomycete fungi that we included in our analysis (Fig. 4.3). The STRING analysis suggests that UMAG_04587 interacts with proteins involved in pre-mRNA splicing (Table S4.1) which is consistent with other DDX41 orthologs. In *H. sapiens*, DDX41 may modulate the expression of a subset of proteins at the posttranslational level (Peters et al. 2017). In *D. melanogaster*, the ortholog Abstrakt is involved in the posttranscriptional regulation of the gene Insc by binding to the mRNA. Loss of Abstrakt resulted in decreased Insc protein levels and defects in cell polarity and cell division (Irion et al. 2004). DDX41 also has a role in the innate immune response and as an antiviral factor against viral infections. It accomplishes this by sensing viral DNA and DNA:RNA duplexes and responds by modulating nucleic acids to signal an immune response in the host (Li et al. 2018; Soponpong et al. 2018; Liu et al. 2019; Winstone et al. 2024). If *UMAG_04587* functions like a viral sensor, it may have a role in detecting and responding to mycovirus infections. The presence of the transcript in the cyan/tumour module during pathogenesis (Lanver et al. 2018) (Table 4.2) suggests that *UMAG_04587* may have an enhanced role during the onset of tumour formation *in planta*, possibly modulating gene expression at either the posttranscriptional or posttranslational level. We hypothesize that if *UMAG_04587* functions to modulate cell polarity during growth, deletion mutants will show growth defects.

The STRING analysis predicted that UMAG_10666 interacts with other spliceosomal proteins suggesting a functional role in pre-mRNA splicing in *U. maydis*

(Table S4.1). This RNA helicase is the ortholog to Prp28 in *S. cerevisiae* and DDX23 in *H. sapiens* (Fig. 4.3 and Table 4.1). The *C. elegans* ortholog DDX-23 is required for embryonic and post-embryonic development, and cell differentiation possibly by modulating specific RNA-protein interactions (Konishi et al. 2008; Chu et al. 2016). If the function of this RNA helicase is conserved, *UMAG_10666* may modulate a specific subset of genes during key transitions of the life cycle. This transcript profile during pathogenesis suggests that enhanced levels of *UMAG_10666* may be necessary for splicing transcripts that are required for the early stages of pathogenesis and/or modulating RNA-protein interactions and splicing of genes that function during the onset of tumour formation.

UMAG_01174 was identified as the putative ortholog to Prp5/DDX46 (Fig. 4.3). The STRING analysis predicts that UMAG_01174 interacts with proteins involved in pre-mRNA splicing (Table S4.1). Interestingly, STRING also predicts an interaction with the uncharacterized protein UMAG_11076. This protein is the putative ortholog to the *S. cerevisiae* protein Urn1 which has a role in cell cycle progression (Niu et al. 2008). Similarly, DDX46 has been shown to have a role in cell proliferation and cell cycle progression pathways (Li et al. 2016). If the role of this RNA helicase is conserved across species, UMAG_01174 may contribute to the progression of the cell cycle and proliferation in *U. maydis* cells. This is another RNA helicase present in the cyan/tumour module during pathogenesis (Lanver et al. 2018) (Table 4.2). This suggests that the activity of this RNA helicase may modulate the splicing of gene transcripts encoding proteins or directly modulate proteins that contribute to *U. maydis* growth and inducing tumour development.

The putative SF2 RNA helicase UMAG_11913 was identified as the ortholog to DHX35 in *H. sapiens* (Fig. 4.4, Table 4.1). The STRING analysis suggests that

UMAG_11913 interacts with other spliceosomal proteins, further indicating a conserved function across species (Table S4.1). Functional characterization of UMAG_11913 may confirm its role in the *U. maydis* spliceosome. In *Magnaporthe oryzae*, another fungal plant pathogen, *MoDHX35* deletion mutants showed reduced appressorium formation and reduced virulence (Ying et al. 2022). The *UMAG_11913* transcript is found in the light-cyan module during *U. maydis* pathogenesis indicating that the transcript is upregulated during the early stages of pathogenesis, decreases, and is followed by an increase (Lanver et al. 2018). We hypothesize that if the underlying molecular control of *UMAG_11913* is similar to *MoDHX35*, then the formation of the *U. maydis* appressorium may be affected, resulting in reduced pathogenesis. The creation of *UMAG_11913* deletion strains should be created in order to determine if there is a shared phenotype with *M. oryzae*. A similarity would indicate a conserved function of this RNA helicase in fungal plant pathogens.

Fal1, the budding yeast ortholog of UMAG_06129, is an essential protein whereas in fission yeast deletion mutants of the ortholog are viable (Kressler et al. 1997; Kim et al. 2010). Our STRING analysis of UMAG_06129 (Table S4.1) predicts protein-protein interactions with components of the splicing machinery and during ribosomal biogenesis. Interestingly, *S. pombe* Fal1 interacts with the protein Red5, a subunit of the MTREC complex, to regulate the splicing of meiosis transcripts. Meiosis transcripts are unspliced and are targeted for degradation during mitosis. It is the interaction between Fal1 and Red5 that facilitates the splicing of meiosis genes during meiosis (Marayati et al. 2016). The *U. maydis* genome contains orthologs to Red5, most of the components of the MTREC complex, and the EJC. So UMAG_06129 may function similarly to the *S. pombe* ortholog in identifying meiosis transcripts and facilitating their translation during meiosis. The

UMAG_06129 transcript is upregulated in the dormant teliospore when compared to the haploid and dikaryon cell types (Seto et al. 2025). It is the only RNA helicase found in the salmon module, which contains genes that are upregulated following tumour formation and remain upregulated during teliospore development (Table 4.2) (Lanver et al. 2018). This transcript pattern suggests the presence of a subset of genes for teliospore development, entry into dormancy, and the pause during meiosis. *UMAG_06129* may aid in the translation of these genes and the progression of the early stages of meiosis before teliospore dormancy. Functional characterization would assess this putative function in *U. maydis*. If this RNA helicase functions like its *S. pombe* ortholog, it may also impact teliospore formation and germination which occur concurrently with meiosis in *U. maydis*.

RNA export

After splicing, the mRNA undergoes additional modifications and binding of proteins to make it competent for nuclear export. This requires the recruitment of several adaptor proteins and these proteins rely on several RNA helicases to facilitate their recruitment, protein dissociation, or mRNA remodelling in both the nucleus and cytoplasm (Iglesias and Stutz 2008; Bourgeois et al. 2016). The RNA helicases Sub2, Dbp2, and Dbp5 in *S. cerevisiae* were identified as having a role in facilitating RNA export from the nucleus and the *U. maydis* orthologs of these are UMAG_11769, UMAG_10095, and UMAG_03765 (Table 4.5).

Transcriptome analysis of the three *U. maydis* RNA helicases predicted to be involved in RNA export revealed that both *UMAG_11769* and *UMAG_03765* have transcript levels that are not significantly different between cell types and during teliospore dormancy and germination (Donaldson et al. 2017; Seto et al. 2025). Both transcripts are

also found in the yellow module during pathogenesis, indicating co-expression with genes involved in cellular metabolism (Table 4.2) (Lanver et al. 2018). The *UMAG_10095* transcript was found to be upregulated in the dormant teliospore where the transcript remains unchanged during teliospore germination (Seto et al. 2025). During pathogenesis, *UMAG_10095* is present in the green-yellow module (Table 4.2) (Lanver et al. 2018) representing gene transcripts that increase and peak at 2 dpi and then decrease during the late stages of pathogenesis (Table 4.2). *UMAG_11769* and *UMAG_10095* were identified with possible roles in *U. maydis* growth, pathogenesis, and regulation of teliospore dormancy and germination.

UMAG_11769 was previously described by Feldbrügge et al. (2008) as the putative ortholog to the *S. cerevisiae* RNA helicase Sub2 and DDX39A/DDX39B in *H. sapiens* (Fig. 4.3, Table 4.1). Our STRING analysis predicts protein-protein interactions with proteins involved in spliceosome assembly and the export of polyadenylated mRNAs (Table S4.1), suggesting a conserved function across eukaryotes. The *Danio rerio* ortholog, Ddx39ab, is required for the development of the heart, trunk muscles, and eyes in the embryo. The RNA helicase was found to bind to a specific subset of epigenetic regulatory factors that regulate the development of these tissues. The loss of *ddx39ab* resulted in abnormal pre-mRNA splicing resulting in the misregulation of these developmental genes (Zhang et al. 2018). The *H. sapiens* orthologs, DDX39A and DDX39B (Fig. 4.3, Table 4.1), function in the mRNA export machinery and are linked to the mitotic progression of the cell. It has been suggested that these RNA helicases may function to regulate gene expression of regulators of mitosis and that each RNA helicase may regulate different sets of genes required for various cellular processes (Yamazaki et al. 2010). If *UMAG_11769*

functions similarly to *DDX39*, we predict that deletion mutants will have growth and mitotic defects.

The STRING analysis for the Dbp2 putative ortholog UMAG_10095 predicted interactions with proteins involved in transcription, splicing, ribosome biogenesis, RNA export, and RNA degradation (Table S4.1). This suggests that the function of this RNA helicase is conserved across eukaryotes. In the yeast and mammalian orthologs, Dbp2/DDX5, is linked to maintaining cellular homeostasis. It has a conserved role in sensing glucose levels and promoting glycolysis during cellular growth (Beck et al. 2014; Xing et al. 2017). More recently, it was shown that Dbp2 can modulate the stress response to low glucose levels by binding to specific mRNAs to retain them in the nucleus, preventing export, and promoting their degradation in nutrient-rich conditions. In low nutrient conditions, Dbp2 moves to the cytoplasm to allow export of these mRNAs from the nucleus to the cytoplasm for translation (Paul et al. 2025). We previously hypothesized that the upregulation of *UMAG_10095* in dormant and germinating teliospores would allow *U. maydis* to detect shifts in glucose levels and link this detection to a shift in RNA processing (Seto et al. 2025). Dpb2 in *S. cerevisiae* is a nonessential gene (Bond et al. 2001; Cloutier et al. 2012), and we predict that deletion of *UMAG_10095* in *U. maydis* will be nonlethal. However, we predict that *U. maydis* deletion and overexpression mutants will have a slow growth phenotype as seen in *S. cerevisiae DBP2* mutants (Cloutier et al. 2012). Finally, we hypothesize that *UMAG_10095* deletion mutants may be impaired in teliospore germination.

Ribosome biogenesis

Approximately 20 different RNA helicases are involved in ribosome biogenesis where each helicase has a specific function during the process. The *U. maydis* orthologs of these RNA helicases are listed in Table 4.6. The first step of ribosome biogenesis is the transcription of rRNA. The large primary rRNA transcript, called the 35S pre-rRNA transcript in *S. cerevisiae*, is transcribed by RNA polymerase I and contains the 18S, 5.8S, and 25S/28S rRNAs. The 5S rRNA is transcribed by RNA polymerase III separately from the 35S pre-rRNA. Processing of the pre-rRNA transcript involves cleavage of the pre-rRNA at sites in the external and internal transcribed spacers (ETS and ITS) by endonucleases and exonucleases which produces mature rRNAs (Martin et al. 2013; Rodríguez-Galán et al. 2013).

The ribosome is comprised of the large and small subunits. The large subunit, known as the 60S in eukaryotes, consists of the 25S/28S, 5.8S, 5S rRNAs and 46 ribosomal proteins (Martin et al. 2013). The SF2 DEAD-box RNA helicases that are involved in processing the 60S subunit are Dbp2, Dbp3, Dbp6, Dbp7, Dbp9, Dbp10, Drs1, Mak5, Mtr4, and Spb4 in *S. cerevisae*. The 40S in eukaryotes is the small ribosomal subunit which is comprised of the 18S rRNA and 33 other ribosomal proteins. Seven different RNA helicases are involved in processing the 40S and are Dbp4, Dbp8, Dhr1, Dhr2, Fal1, Rok1, and Rrp3. Two RNA helicases, Prp43 and Has1, are involved in processing both the 60S and 40S subunit (Martin et al. 2013; Rodríguez-Galán et al. 2013). There is the suggestion that Ded1 in *S. cerevisiae*, may have a function during ribosome biogenesis. The protein has been detected with pre-ribosomal particles, however, its actual function is not currently understood (Krogan et al. 2004; Sharma and Jankowsky 2014). Table 4.6 summarizes the specific functions of these RNA helicases during ribosome biogenesis.

Many of the RNA helicases involved in ribosome biogenesis are essential proteins. We utilized the current knowledge of these RNA helicases and the *U. maydis* transcriptome data to identify nine RNA helicases with potential roles in the *U. maydis* life cycle. The *UMAG_11989*, *UMAG_30170*, *UMAG_10683*, and *UMAG_11281* gene transcripts were not significantly different across all cell types and during teliospore dormancy and germination (Donaldson et al. 2017; Seto et al. 2025). During pathogenesis, they are found in the green-yellow (*UMAG_11989*, *UMAG_30170*, and *UMAG_10683*) and green modules (*UMAG_11281*) (Table 4.2). The gene transcripts for *UMAG_10410*, *UMAG_05214*, *UMAG_01732*, *UMAG_10241*, and *UMAG_5200* were found to be upregulated in the dormant teliospore compared to the haploid and dikaryon cell types (Seto et al. 2025). They can be found in the green (*UMAG_05214*), green-yellow (*UMAG_10410*, *UMAG_10241*), yellow (*UMAG_01732*), and magenta (*UMAG_05200*) modules during pathogenesis (Table 4.2). We predict that these RNA helicases will have roles in *U. maydis* growth, pathogenesis, stress response, and teliospore dormancy.

The *U. maydis* ortholog to *S. cerevisiae* RNA helicase Has1 was identified as UMAG_10410 (Fig. 4.3, Table 4.1). Based on the STRING analysis, its role in rRNA processing is predicted to be conserved (Table S4.1). Has1 is an essential protein in *S. cerevisiae*, and we predict deletion of UMAG_10410 will result in a lethal phenotype. The zebrafish ortholog DDX18 was suggested to be involved in cell cycle progression in developing zebrafish. The loss of the RNA helicase results in cell cycle arrest and disruption of hematopoiesis (Payne et al. 2011). In human lung cancer cells, DDX18 depletion results in cell cycle arrest at the G1 phase and overexpression increases cell proliferation (Feng et al. 2024). We predict that altering the expression of *UMAG_10410*

will lead to growth defects. Based on the pathogenesis transcriptome data from Lanver et al. (2018), the peak of the *UMAG_10410* transcript level at 2 dpi would correspond to the shift to cell proliferation following cell cycle arrest before appressoria penetration. This transcript pattern suggests *UMAG_10410* may have a role during key developmental shifts in the *U. maydis* growth within the plant. We also note that the transcript is upregulated in the dormant teliospore and remains upregulated at a steady state during teliospore germination (Seto et al. 2025). This transcript pattern suggests that *UMAG_10410* has an enhanced role during the exit from dormancy to germination possibly through maintaining genome stability or regulating DNA repair during this developmental switch.

UMAG_11989 is the ortholog to *S. cerevisiae* RNA helicase *DBP4* and *DDX10* in *H. sapiens*. Overexpression of the *H. sapiens* ortholog DDX10 results in the proliferation of several types of cancer (Yassin et al. 2010; Zhou et al. 2022). In colorectal cancer cells, DDX10 was shown to interact with the ribosomal protein RPL35, which is a component of the 60S subunit. The overexpression of this RNA helicase resulted in alternative splicing of RPL35 mRNA which then affected the downstream E2F pathway, a pathway that regulates the cell cycle and cancer development (Zhou et al. 2022). *Ustilago maydis* contains the ortholog to RPL35 (UMAG_11625), indicating the potential for UMAG_11989 to function similarly. Based on *U. maydis* transcriptome data, *UMAG_11989* may have an enhanced role during the early stages of pathogenesis, possibly during the establishment of biotrophic development after the dikaryotic filaments penetrate the plant host. It is hypothesized that it enhances the expression of a subset of genes required for cell cycle progression. If *UMAG_11989* regulates the cell cycle through its

interaction with other proteins, altering its expression may affect the growth of *U. maydis* cells and impact its growth within plant tissue.

In *H. sapiens*, cell homeostasis can be disrupted by unscheduled R-loop formation. The RNA helicase DDX47 resolves R-loop formation by unwinding these DNA:RNA hybrids (Marchena-Cruz et al. 2023). The ortholog of this in *U. maydis* was identified as UMAG_05214 and in *S. cerevisiae* Rrp3 (Fig. 4.3, Table 4.1). We previously identified *UMAG_05214* with upregulated transcript levels in the dormant teliospore and remained at a steady state during germination (Seto et al. 2025). This suggests that *UMAG_05214* may have an enhanced role during germination and hypothesize that it may function to regulate R-loop formation during transcription. *UMAG_05214* may have an additional role in promoting the transcription of genes involved in maintaining cellular homeostasis in other cell types. Disruption in the function of this RNA helicase in *U. maydis* may cause irregular cell growth and dysregulation of cellular metabolism. Functional characterization is required to determine the impact of *UMAG_05214* on teliospore germination and *U. maydis* growth.

UMAG_10683 was identified as the putative *U. maydis* Rok1/DDX52 ortholog (Fig. 4.2, Table 4.1). Our STRING analysis predicts that UMAG_10683 is involved in processing rRNA suggesting that its function is conserved. In *C. elegans*, DDX-52 loss of function mutants were resistant to hypoxia, experienced arrested early development, and cell death occurred at high temperatures (Itani et al. 2021). In *S. cerevisiae*, Rok1 is an essential protein which functions to regulate cell cycle progression (Song et al. 1995; Giaever et al. 2002; Jeon and Kim 2010). *Saccharomyces cerevisiae* cells with disrupted or overexpressed Rok1 are arrested at the G1/S phase of the cell cycle. This suggested that

the protein levels of Rok1 regulate ribosome biogenesis at the beginning of the cell cycle (Jeon and Kim 2010). We hypothesize that deletion of *UMAG_10683* will be lethal. If *UMAG_10683* functions similarly to its orthologs, altering the expression will result in defects in cell cycle progression and altered growth rates. During *U. maydis* pathogenesis, the gene transcript increases and peaks at 2 dpi, indicating that the enhanced transcription of *UMAG_10683* may aid in the translation of genes during this stage of pathogenesis.

In *S. cerevisiae*, RNA helicase Dbp3 null mutants were observed to have increased thermotolerance, oxidative stress resistance, DNA stress, and endoplasmic reticulum stress resistance (Delaney et al. 2013). The *Arabidopsis thaliana* orthologs are negative regulators of stress-responsive transcription activators (Kant et al. 2007; Khan et al. 2014). Overexpression studies of *S. cerevisiae DBP3* suggested a role in protein secretion in fungal cells (Chen et al. 2023). Our phylogenetic and sequence analysis identified UMAG_01732 as the ortholog to Dbp3 in *S. cerevisiae* and STRS1 in *A. thaliana*. We did not identify orthologs in any other species we used in our analysis (Fig. 4.3, Table 4.1). Our STRING analysis predicted interactions with proteins involved in ribosome biogenesis (Table S4.1), suggesting that this RNA helicase has a conserved function in fungi and plants. The *UMAG_01732* gene transcript is upregulated in the dormant teliospore and decreased during teliospore germination (Seto et al. 2025). This transcript pattern suggested this RNA helicase may be involved in the transition from a dormant state to one of high metabolic activity. We had named this RNA helicase *udbp3* and created deletion mutants in the compatible haploid strains, 518 and 521 (Seto and Saville 2025). Deletion mutants were viable and showed no significant difference in dikaryon formation, pathogenesis, or teliospore formation and germination. We found that the deletion mutants

were more tolerant to osmotic stress (Seto and Saville 2025). It was concluded that *udbp3* may be a negative regulator of osmotic stress response by regulating a subset of stress responsive genes during teliospore dormancy (Seto and Saville 2025). Future work should focus on creating overexpression mutants to determine if it functions similarly to *DBP3*. *udbp3* may have a similar role in regulating the protein secretion pathway to ensure the development and growth of the promycelium during teliospore germination.

Our STRING analysis for UMAG_03170 (Table S4.1) predicts that this putative RNA helicase functions during the synthesis of ribosomal subunits, suggesting a conserved role across eukaryotes. Its orthologs Drs1 in *S. cerevisiae* and DDX27 in *H. sapiens* (Fig. 4.3, Table 4.1) have demonstrated roles during ribosome biogenesis (Table 4.6). The zebrafish ortholog, DDX27, contributes to the processing of ribosomal subunits. It was also found that DDX27 regulates the translation of genes that contribute to muscle growth (Bennett et al. 2018). During *in planta* infection, the gene transcript is found in the green-yellow module (Table 4.2) (Lanver et al. 2018). Increased transcription of *UMAG_03170* may indicate an increased requirement for ribosomes and may be involved in translating a subset of genes required for later stages of pathogenesis.

UMAG_11281 is the putative ortholog to the protein Prp43 in *S. cerevisiae*. It is predicted to interact with proteins involved in splicing (Table S4.1). One notable interaction is with the *U. maydis* protein UMAG_01091, an rRNA processing protein called SAS10. The *S. cerevisiae* SAS10 ortholog has been shown to have a role in processing the 18S rRNA and has been linked to cell cycle progression (Bernstein and Baserga 2004). During *U. maydis* pathogenesis, the transcript is found in the green module where the transcript level is low during early pathogenesis, increases, and remains upregulated during late

pathogenesis (Table 4.2) (Lanver et al. 2018). This suggests an increased requirement for this RNA helicase during the later stages of pathogenesis. It may aid in cell cycle progression, during *in planta* growth, by modulating specific RNPs or facilitating protein-protein interactions during the synthesis of the 18S rRNA.

The *S. cerevisiae* RNA helicase Dbp8 functions during the processing of the 40S ribosomal subunit. The *U. maydis* ortholog, UMAG_10241, is predicted to interact with proteins involved in rRNA processing (Table S4.1). One predicted interaction is with the *U. maydis* ortholog for Esf2, suggesting that UMAG_10241 may function similarly to the *S. cerevisiae* ortholog. Esf2 is an RNA binding protein capable of enhancing the activity of Dbp8 and guiding it to its binding site (Granneman et al. 2006). The *H. sapiens* ortholog, DDX49, regulates the export of mRNAs and pre-ribosomal RNA levels which results in regulation of cell proliferation (Awasthi et al. 2018). The *UMAG_10241* transcript is upregulated in the dormant teliospore compared to the haploid and dikaryon cell types and decreases during teliospore germination (Seto et al. 2025). The activity of this RNA helicase may be required to aid in the transition from dormancy to germination by promoting and regulating the translation of genes involved in cellular and metabolic activity.

UMAG_05200 in *U. maydis* is the putative ortholog to the *S. cerevisiae* SF2 DEAD-box RNA helicase Dbp10 (Fig. 4.3, Table 4.1). STRING analysis predicts that UMAG_05200 interacts with proteins involved in ribosomal biogenesis (Table S4.1) suggesting that its function is conserved across eukaryotes. In *S. cerevisiae*, the helicase activity of Dbp10 is required to induce conformational changes to the pre-rRNA during the maturation of the 60S subunit (Burger et al. 2000; Mitterer et al. 2023). Knockdown and

overexpression studies of the ortholog DDX54 in *H. sapiens* cell lines revealed that this RNA helicase responds to DNA damage by binding to pre-mRNAs involved in the DNA damage response pathway to increase their splicing rate to promote cell survival (Milek et al. 2017). The *UMAG_05200* transcript is upregulated in the dormant teliospore and the transcript level is maintained during teliospore germination (Seto et al. 2025). This upregulation during teliospore dormancy may indicate that the transcript is stored and is required during germination to respond to potential DNA damage. DNA damage can be caused by genotoxic stressors, such as UV exposure and ionizing irradiation, which can cause a reduction in fungal spore germination (reviewed in Braga et al. 2015). In the soilborne protozoan *Spongospora subterranean*, there is an enrichment of DNA repair genes during spore germination (Balotf et al. 2021). We hypothesize that *UMAG_05200* functions during teliospore germination to protect the growing promycelium by regulating genes that respond to DNA damage.

Translation

Messenger RNAs (mRNAs) are exported to the cytoplasm and are translated to produce proteins. Translation involves several binding proteins and regulatory elements. The untranslated regions (UTR) of mRNAs, the 5’ cap, and the poly(A) tail contain control elements that regulate translation. Translation initiation starts with the 40S ribosomal subunit binding near or at the 5’ cap of the mRNA where the 5’ UTR is scanned for the initiation codon. After the initiation codon is identified, initiation factors are released and the 60S ribosomal subunit is recruited to form the 80S ribosome to begin elongation (reviewed in Wilkie et al. 2003). The translation process involves the function of the following RNA helicases: DDX48, DHX29, and DHX9 in *H. sapiens*, and Tif1/Tif2, Ded1,

Dbp5, Dhh1, Hcs1 and Slh1 in *S. cerevisiae*. The *U. maydis* orthologs to these proteins are listed in Table 4.7. These RNA helicases may function to remodel the mRNA, unwind secondary structures, and recruit proteins to initiate translation termination.

Our STRING analysis (Table S2.1) for the *U. maydis* protein UMAG_04665, the putative ortholog to *S. cerevisiae* RNA helicase Dhr1, predicted a protein-protein interaction with the translation elongation factor eEF3 (UMAG_04152). A protein-protein interaction between Dhr1 and eEF3 was reported in *S. cerevisiae* (Sturm et al. 2017) however, whether Dhr1 serves a function during translation has yet to be determined. RNA helicase activity from Dhr1 may be required to remodel the mRNA to bind or displace eEF3 from the mRNA.

Of the RNA helicases that function in translation, we identified five with potential roles in the *U. maydis* life cycle. These RNA helicases are *UMAG_04080*, *UMAG_10655*, *UMAG_05482*, *UMAG_00574*, and *UMAG_01122*. The transcripts for *UMAG_10655*, *UMAG_05482*, and *UMAG_00574* are found in all cell types (Donaldson et al. 2017; Seto et al. 2025). During pathogenesis, these gene transcripts are found in the yellow module (Table 4.2). *UMAG_04080* and *UMAG_01122* transcripts are upregulated in the dormant teliospore (Donaldson et al. 2017; Seto et al. 2025) and are found in the magenta and cyan modules respectively (Table 4.2). Combining the transcriptome data and current research on their orthologs indicate that these RNA helicases may have roles in *U. maydis* growth, pathogenesis, stress response, and teliospore dormancy and germination.

Extensive research has been conducted on the *S. cerevisiae* RNA helicase Ded1 and its ortholog DDX3 in *H. sapiens*. The *U. maydis* ortholog is identified as UMAG_04080 and its function in RNA metabolism is predicted to be conserved based on our STRING

analysis (Table S4.1). *UMAG_04080* was identified as an RNA helicase with gene transcript levels upregulated in the dormant teliospore, decreased once germination was initiated, and that did not change significantly during the remainder of the germination time course (Seto et al. 2025). This transcript pattern suggested that *UMAG_04080* may have a function during the exit from teliospore dormancy to germination. Deletion mutants in *U. maydis* are nonviable, however, mutants were created in which *UMAG_04080* was expressed in an ectopic location under a carbon sensitive promoter and the *UMAG_04080* was deleted from its native locus. We have subsequently named this RNA helicase *uded1* in *U. maydis* (Seto and Saville 2025). Characterization of these mutants showed that when grown on solid medium, slow growth and mycelial growth phenotypes were observed. Normal budding haploid growth was restored when the solid medium was supplemented with the sugar alcohol sorbitol (Seto and Saville 2025). Sorbitol is an osmoprotectant that is often added to medium for cultivating fungi with fragile cell walls (Górka-Nieć et al. 2010). Overexpression of *DED1* in *S. cerevisiae* can cause growth defects and can drive stress granule formation by binding to mRNAs to repress translation and sequestering these mRNAs in the stress granules (Aryanpur et al. 2017; Aryanpur et al. 2022). In *S. pombe*, overexpression of *ded1* interferes with the response of the MAPK pathway by negatively regulating the cell cycle response to osmotic stressors (Forbes et al. 1998). Upregulation of *uded1* impacts *U. maydis* growth and may impact the MAPK pathway, contributing to the observed slow growth phenotype and mycelial growth. The restoration of budding growth in the presence of sorbitol suggests that the altered expression of *uded1* may result in a defect in the formation of the cell wall, which makes them more sensitive to osmotic stress, or there is an impairment in mitotic division (Seto and Saville 2025). We

hypothesized that *uded1* functions to repress translation during teliospore dormancy by binding to mRNAs to create an mRNP that is stabilized. The mRNP is stored and disassembled when germination is initiated to make mRNAs available for translation (Seto and Saville 2025).

UMAG_10655 was identified as the putative *U. maydis* ortholog to Dhh1 in *S. cerevisiae* (Feldbrügge et al. 2008). Our STRING analysis (Table S4.1) predicts that UMAG_10655 interacts with proteins involved in P-body and stress granule assembly, suggesting that the *U. maydis* ortholog may function similarly to Dhh1 in other organisms. The *C. neoformans* ortholog, Vad1, was found to regulate stress response and the expression of a subset of virulence genes (Panepinto et al. 2005). It was identified as a central regulator of virulence genes and promotes resistance to the host immune response (Qiu et al. 2013). During pathogenesis, the transcript is found in the yellow module (Table 4.2) and is co-expressed with genes involved in metabolism and cellular activity (Lanver et al. 2018). The function of *UMAG*_10655 is predicted to be similar to its orthologs in that it may respond to environmental stressors or changes in the host plant defence system to regulate translation of a subset of genes, enhancing successful penetration of the plant to cause disease.

The putative eIF4A ortholog in *U. maydis* is UMAG_05482 (Fig. 4.3, Table 4.1) and the STRING analysis (Table S4.1) suggests a conserved function in translation initiation. eIF4A is a subunit of the eIF4F complex which is a component of the translational machinery. Heat shock disassembles the eIF4F complex which causes translation repression of mRNAs such as housekeeping genes. eIF4G and eIF4E assemble to form mRNPs sequestered in heat stress granules. eIF4A is unaffected by heat shock

stress and functions independently to promote the translation of mRNAs that respond to heat stress (Desroches Altamirano et al. 2024). We hypothesize that altering the expression of *UMAG_05482* may impact the heat stress response of *U. maydis*. During pathogenesis, the transcript is found in the yellow module (Table 4.2). In this module, there is an increase in gene transcripts that pertain to protein catabolism and autophagy (Lanver et al. 2018). This transcript profile suggests that the enhancement of *UMAG_05482* during the early stages of pathogenesis is likely to facilitate the translation of specific genes required for this stage of pathogenesis.

UMAG_00574 was identified as the putative ortholog to the *H. sapiens* RNA helicases DHX29 and DHX57. An ortholog in the ascomycete fungi was not found however, orthologs were found in the basidiomycetes (Fig. 4.4). The STRING analysis for UMAG_00574 predicted protein-protein interactions with ribosomal and translation initiation proteins (Table S4.1). Three interesting protein-protein interactions predicted by STRING are with the proteins UMAG_03144, UMAG_10988, and UMAG_04249. The KEGG pathway for these proteins indicates that they are involved in endocytosis. This suggests that RNA helicase activity may be involved in assembling the endocytic machinery. DHX29 binds to the 40S ribosomal subunit to induce conformational changes which allows the ribosome to position itself correctly on mRNAs containing highly structured 5’ UTRs (Pisareva et al. 2008). Messenger RNAs that contain highly structured 5’ UTRs are typically highly regulated and require different layers of gene expression control (Leppek et al. 2018). *UMAG_00574* is found in the yellow module during pathogenesis (Table 4.2) and may function to efficiently regulate the translation of regulatory genes, such as metabolic and cellular activity genes also found in this module.

For example, the endocytic pathway contributes to the early stages of *U. maydis* pathogenesis (Fuchs and Steinberg 2005; Fuchs et al. 2006) and UMAG_00574 may contribute to regulating the translation of genes involved in this pathway.

Protein sequence and phylogenetic analysis identified UMAG_01122 as the ortholog to *S. cerevisiae* Hcs1 and *H. sapiens* IGHMBP2 (Table 4.1, Fig. 4.2). It is a member of the SF1 superfamily of Upf1-like RNA helicases however there are limited studies on the function of this RNA helicase. Currently, Hcs1/IGHMBP2 has been demonstrated to interact with the translational machinery and is suggested to function during translation but its exact role is less understood (de Planell-Saguer et al. 2009; Guenther et al. 2009; Jankowsky 2011; Bourgeois et al. 2016). Our STRING analysis predicts UMAG_01122 interacts with UMAG_10602, the putative ortholog to Sen1/SETX (Table S4.1) suggesting an additional in role in transcription. Transcriptome analysis during *U. maydis* pathogenesis indicates that the transcript is in the cyan/tumour development module (Table 4.2) (Lanver et al. 2018) and upregulated in the dormant teliospore (Donaldson et al. 2017; Seto et al. 2025). If *UMAG_01122* functions during translation, it may aid in translating genes required for tumour and teliospore development and then its transcript is stored in the dormant teliospore. During teliospore germination UMAG_01122 could interact with UMAG_10602 to regulate gene expression of a subset of genes or aid in maintaining genome stability and prevent R-loop formation during transcription.

RNA degradation

Degradation of RNA is a highly efficient and conserved process that involves numerous enzymes, where many have the same targets. This process removes byproducts that are released during RNA processing such as excised introns, controls gene expression by

removal of mRNAs, and is a quality control mechanism to remove defective RNAs and RNPs (Parker 2012). There are three enzyme classes capable of RNA degradation. These enzyme classes are endonucleases, 5' exonucleases, and 3' exonucleases. RNA degradation also depends on the action of helicases, polymerases, and chaperones (Houseley and Tollervey 2009). RNA helicases that function during RNA degradation are Dhh1, Ski2, Upf1, Dbp2, and Mtr4 in *S. cerevisiae*. Their *U. maydis* orthologs and specific functions are summarized in Table 4.8.

RNA decay for many mRNAs is initiated by the shortening of the poly(A) tail, called deadenylation. This is not a uniform process, and the transition is reflective of the changes in mRNP composition or RNA structure. Once the poly(A) tail is five to fifteen adenosines long, degradation is triggered (Decker and Parker 1994). RNA degradation occurs in one of two major pathways. The most common pathway is removing the 5' cap by the decapping enzyme Dcp1/Dcp2 which initiates degradation in the 5'-to-3' direction by the enzyme Xrn1. This process may involve the function of RNA helicase Dhh1 in *S. cerevisiae* (Fischer and Weis 2002; Sweet et al. 2012), *U. maydis* ortholog UMAG_10655. Degradation in the 3'-to-5' direction is the second pathway that involves the exosome and other cofactors. The exosome requires interaction with several Ski proteins, one of which is RNA helicase Ski2 in *S. cerevisiae* (Anderson and Parker 1998; Parker 2012; Johnson and Jackson 2013). The *U. maydis* Ski2 ortholog was previously identified as UMAG_00393 (Feldbrügge et al. 2008).

The quality control pathways ensure that defective RNAs are identified and directed to the degradation pathway. The non-sense mediated decay (NMD) pathway is one surveillance pathway responsible for degrading mRNAs with aberrant translation

termination. NMD pathway activation is facilitated through the function of RNA helicase Upf1. The *U. maydis* ortholog was previously identified as UMAG_11428 (Feldbrügge et al. 2008; Martinez-Montiel et al. 2016). Once activated, the NMD machinery is assembled and stabilized on the mRNA with the function of RNA helicase Dbp2 (Xing et al. 2019). The mRNA is subjected to rapid deadenylation and increased rates of 3'-to-5' degradation (Parker, 2012). Another quality control pathway is the no-go decay (NGD) pathway. This pathway degrades mRNAs that are stalled during translation from the result of strong stem loops, rare codons, or sites of depurination. Targets for the NGD pathway are subjected to endonucleolytic cleavage followed by the 3' mRNA fragment being degraded by Xrn1 and the 5' mRNA fragment being degraded by the exosome (Parker, 2012). The last quality control pathway is the non-stop decay (NSD) pathway. mRNAs that lack a translation termination codon are subjected to this pathway. It is triggered when the ribosome reaches the 3' end of the mRNA and termination of translation cannot be achieved (Parker 2012).

Our transcriptome analysis identified *UMAG_00393* as an RNA helicase with the potential to function during the *U. maydis* pathogenesis and stress response. The transcript is present in all cell types and during teliospore germination (Donaldson et al. 2017; Seto et al. 2025) and found in the yellow module during pathogenesis (Table 4.2) (Lanver et al. 2018). Our analysis identified it as the ortholog to Ski2 (Fig. 4.5, Table 4.1). UMAG_00393 is predicted to function in RNA degradation based on the STRING results (Table S4.1). In *C. neoformans*, Ski2 deletion mutants were sensitive to high temperatures due to defects in the cell wall integrity. The cell walls of these mutants had an abnormal distribution of chitin, suggesting that Ski2 may have a role in chitin production. Additionally, these deletion mutants had decreased virulence and increased sensitivity to osmotic stress and

drugs that inhibited ribosomal function (Li et al. 2022). We hypothesize that *UMAG_00393* deletion mutants will have an attenuated response to osmotic stress and cell wall defects. This transcript profile indicates an increased requirement for *UMAG_00393* during the early stages of pathogenesis, likely to support the increased transcription and translation of RNAs for cellular growth and metabolism within the plant.

Mitochondrial RNA processing

The mitochondrial genome requires the function of several factors for maintenance and expression. Many proteins that are essential to mitochondrial function are encoded by nuclear genes and imported into the mitochondria. The mitochondrial genome itself also encodes proteins that are essential to mitochondrial function. The expression and regulation of nuclear and mitochondrial genes are coordinated by an active RNA processing system that balances the rate of RNA synthesis and degradation (Nicholls et al. 2013; Markov et al. 2014). The processing and maturation of mitochondrial mRNA in humans is more straightforward than in *S. cerevisiae*. Human mitochondrial mRNA does not require a splicing machinery as genes do not contain introns. The transcripts are polyadenylated by the mitochondrial poly(A) polymerase and are not capped at the 5' end (Nicholls et al. 2013). In *S. cerevisiae*, transcribed mitochondrial DNA contains long 3' UTR and is not polyadenylated. Transcripts can contain introns and a splicing machinery to excise the introns is required. The machinery responsible for the transcription and splicing of these transcripts includes the function of RNA helicase Mss116 (Niemer et al. 1995; Minczuk et al. 2002; Markov et al. 2014). Mitochondria also possess a degradation system which also requires the function of RNA helicase Suv3 in *S. cerevisiae* (Dziembowski et al. 2003; Guo et al. 2011; Szczesny et al. 2013). The *U. maydis* mitochondrial genome has genes that

contain introns (Pfeifer et al. 2012) and may require the function of RNA helicases such as Mss116 and Suv3 during RNA processing. Table 4.9 indicates the *U. maydis* orthologs and outlines the specific functions of the *S. cerevisiae* RNA helicases in the mitochondria.

RNA helicases with unknown functions

Our sequence and phylogenetic analyses identified several RNA helicases that are either fungal specific or their function is unknown. We identified the SF1 Upf1-like RNA helicase UMAG_10130 (Figs 4.1, 4.6), and the SF2 DEAD-box RNA helicases UMAG_00835 and UMAG_05873 (Figs 4.3, 4.6) as putative basidiomycete-specific RNA helicases. The SF2 DEAH RNA helicase YLF419W in *S. cerevisiae* only has orthologs in the fungal species we assessed and the *U. maydis* putative ortholog is UMAG_11114 (Figs 4.4, 4.6).

The *U. maydis* gene *UMAG_10130* is a SF1 Upf1-like RNA helicase and the phylogenetic analysis shows a separate clade containing genes in the other basidiomycete fungi, *S. reilianum*, *U. hordei*, and *C. neoformans*, but not with any other species we assessed (Figs 4.2, 4.6). Sequence analysis indicates that UMAG_10130 contains sequence motifs typical of RNA helicases in the SF1 Upf1-like family, indicating that a helicase core is present. UMAG_10130 and its basidiomycete orthologs have not been characterized within their respective organisms. The STRING analysis (Table S4.1) predicts putative protein-protein interactions with the same proteins as UMAG_11428, the ortholog to Upf1. Upf1 is an RNA helicase that functions during RNA degradation where it activates the NMD pathway. UMAG_10130 may function similarly to UMAG_11428 in the NMD pathway. The gene transcript is found in all *U. maydis* cell types (Donaldson et al. 2017; Seto et al. 2025) and is found in the magenta module during pathogenesis (Table 4.2). The magenta module contains genes that have a significant role during the early stages of

pathogenesis, more specifically during the establishment and maintenance of biotrophy (Lanver et al. 2018). The *UMAG_10130* transcript is found in a different module from *UMAG_11428*, suggesting that it may assist in the degradation of a specific subset of genes during this stage of pathogenesis that is different from those targeted by *UMAG_11428*.

The phylogenetic analysis identified two SF2 DEAD-box RNA helicases with no other closely related orthologs other than those found in the Basidiomycota. These RNA helicases have been identified as UMAG_05873 and UMAG_00835 (Figs4. 3, 4.6) and are uncharacterized proteins in *U. maydis*. Our findings suggest that these RNA helicases are basidiomycete-specific RNA helicases, however, more fungal species would need to be assessed for this interpretation to be conclusive. Sequence analysis revealed that both genes have a helicase core containing several canonical RNA helicase sequence motifs typical of this RNA helicase family (data not shown). The STRING analysis predicts that UMAG_05873 interacts with translational pathway proteins (Table S4.1) suggesting a role in translation. Analysis of the *UMAG_05873* transcript during *in planta* infection places the transcript in the magenta module (Lanver et al. 2018). This module is correlated to biotrophic establishment and maintenance. The enhancement of this RNA helicase during this stage of pathogenesis suggests it may function to aid in the translation of transcripts required for changes in growth of the mycelium during pathogenesis that may be specific to basidiomycetes. STRING analysis for UMAG_00835 predicts protein-protein interactions with ribosome biogenesis proteins suggesting a role in processing and assembling ribosomes (Table S4.1). The *UMAG_00835* transcript is present in the cyan/tumour module during *in planta* growth which contains genes that respond to nutrient limitations on the plant surface (Table 4.2). The transcript is upregulated in the dormant

teliospore and is decreased during germination (Seto et al. 2025). This transcript pattern suggests that *UMAG_00835* is stored and is immediately translated during germination. Its presence in the Lanver et al. (2018) cyan/tumour module suggests that this RNA helicase may respond to changes in external nutrients. We hypothesize that when dormant teliospores are in a nutrient-rich environment, a decrease in this RNA helicase during germination promotes the translation of genes for cellular growth.

An RHA-group SF2 DEAH RNA helicase YLF419W in *S. cerevisiae* was identified by Jankowsky (2011). Our analysis identified UMAG_11114 as the *U. maydis* ortholog. This RNA helicase is largely uncharacterized. Based on current research, it is a nonessential gene (Shiratori et al. 1999; Colley et al. 2000) and the protein has been found in both the mitochondria (Sickmann et al. 2003) and cytoplasm (Huh et al. 2003). YLF419W has protein sequence similarities to ancient eukaryotic retinoblastoma (Rb) protein, suggesting that YLF419W evolved from an ancient Rb gene, lost its Rb function, and instead gained the function as an RNA helicase (Takemura 2005). Our phylogenetic analysis (Figs 4.4, 4.6) shows that YLF419W clusters with putative RNA helicases in other fungal species.

UMAG_11114 was identified as an RNA helicase that currently has an unknown function. The *N. crassa* ortholog was identified as *msp-8* (NCU01143), and its putative function is in pre-mRNA splicing (Adhvaryu et al. 2016). Our STRING analysis predicted protein-protein interactions with the same proteins as *UMAG_00574*, suggesting that this RNA helicase may have a redundant function. During *U. maydis* pathogenesis, the *UMAG_11114* transcript is in the yellow module (Table 4.2). This transcript pattern indicates upregulation of the transcript during the mid to later stages of pathogenesis. This suggests a role in supporting post-transcriptional regulation of highly metabolic and

cellular activity genes (Lanver et al. 2018). Further functional characterization in *U. maydis* is required to determine the role this RNA helicase has in RNA metabolism and if there is an impact on the progression of pathogenesis.

CONCLUSIONS

Annotating the RNA helicases of the basidiomycete *U. maydis* allowed the identification of their functions in relation to gene regulation and response to environmental factors. This provided insights into their potential roles during fungal growth and development. For pathogenic fungi, RNA helicases have the potential to modulate disease progression within their host. Our analysis identified 46 RNA helicases within *U. maydis*. Through a comprehensive review of the current research on their orthologs, we were able to make predictions of their functions and roles in the life cycle. We identified 28 RNA helicases that may contribute to *U. maydis* growth, stress response, pathogenesis, or teliospore dormancy and germination. Further characterization of these RNA helicases and their influence on the various aspects of the fungal life cycle and pathogenicity can aid in developing methods for mitigating or preventing fungal diseases.

ACKNOWLEDGEMENTS

The authors have no support to report.

ADDITIONAL INFORMATION

Conflict of Interest

The authors have declared that no competing interests exist.

Ethical Statement

No ethical statement was reported.

Funding

Funding for this project was awarded by the Natural Sciences and Engineering Research Council (NSERC) of Canada to B.J.S.

Author Contributions

The investigation, methodology for gathering and analyzing literature, formal analysis of data, visualization of data, and writing of the original draft was undertaken by A.M.S. Conceptualization of this review, supervision, funding acquisition, and the writing – review and editing was provided by B.J.S.

TABLES AND FIGURES

Table 4.1. RNA helicases in *U. maydis* and their orthologs in *S. cerevisiae*, *C. elegans*, *D. melanogaster*, *M. musculus*, and *H. sapiens*.

Superfamily	Family	*U. maydis*	*S. cerevisiae*	*C. elegans*	*D. melanogaster*	*M. musculus*	*H. sapiens*
SF1	Upf1-like	UMAG_10602	Sen1	eri-7	CG7504	Setx	SETX
		UMAG_11428	Upf1	smg-2	Upf1	Upf1	UPF1
		UMAG_01122	Hcs1	Y106G6D.5		IGHMBP2	IGHMBP2
		UMAG_10130					
					CG6701	MOV10	MOV10
					armi	Mov10l1	MOV10L1
			Ecm32				
				C44H9.4	Helz	Helz Helz2	HELZ HELZ2
				emb-4	CG14729	Aqr	AQR
SF2	DEAD-box	UMAG_05482	Tif1 Tif2	inf-1 F57B9.3	eIF4A	Ddx2a Ddx2b	DDX2A DDX2B
		UMAG_06129	Fal1	F33D11.10 Y65B4A.6	eIF4A-III	DDX48	DDX48
		UMAG_10655	Dhh1	cgh-1	me3B	DDX6	DDX6
				mel-46	Gem3	DDX20	DDX20
		UMAG_03765	Dbp5	ddx-19	DBP80	DDX19a DDX19b	DDX19A DDX19B
		UMAG_11769	Sub2	hel-1	Hel25E	DDX39A DDX39B	DDX39A DDX39B
		UMAG_05873					
		UMAG_10410	Has1	B0511.6	CG6375	DDX18	DDX18
		UMAG_11989	Dbp4	ddx-10	CG5800	DDX10	DDX10
				Y55F3BR.1	CG9054	DDX1	DDX1
		UMAG_03268	Spb4	ZK512.2	DDX55	DDX55	DDX55
		UMAG_06228	Dbp7		CG8611	DDX31	DDX31
		UMAG_05214	Rrp3	T26G10.1	CG9253	DDX47	DDX47
		UMAG_10241	Dbp8	H20J04.4	DBP45A	DDX49	DDX49
		UMAG_03170	Drs1	ddx-27	Rs1	DDX27	DDX27
		UMAG_05200	Dbp10	Y94H6A.5	CG32344	DDX54	DDX54

	UMAG_04080	Ded1 Dbp1	laf-1 vbh-1	Belle	DDX3X DDX3Y D1Pas1	DDX3X DDX3Y
			glh-1 glh-2	Vasa	DDX4	DDX4
	UMAG_10095	Dbp2	ddx-17	Rm62	DDX5 DDX17	DDX5 DDX17
				CG7878		DDX53
					DDX43	DDX43
	UMAG_01732	Dbp3				
	UMAG_04587		sacy-1	abs	DDX41	DDX41
	UMAG_10666	Prp28	ddx-23	CG10333	DDX23	DDX23
			C46F11.4	DmRH27	DDX42	DDX42
	UMAG_01174	Prp5	ddx-46	CG6227	DDX46	DDX46
	UMAG_10683	Rok1	ddx-52	DmRH17	DDX52	DDX52
	UMAG_03892	Dbp9	C24H12.4	CG1666	DDX56	DDX56
	UMAG_00921	Dbp6	ZK686.2	Dbp73D	DDX51	DDX51
					Ddx21	DDX21
					Ddx50	DDX50
	UMAG_00242	Mak5	F55F8.2			DDX24
					DDX59	DDX59
	UMAG_00652 UMAG_06314	Mss116				
		Mrh4		Dbp21E2	DDX28	DDX28
	UMAG_00835					
DEAH/ RHA	UMAG_10915	Prp2	mog-4	CG10689	DHX16	DHX16
	UMAG_04188	Prp16	mog-1	CG32604	DHX38	DHX38
	UMAG_03936	Prp22	mog-5	CG8241	DHX8	DHX8
	UMAG_11281	Prp43	ddx-15	CG11107	DHX15 DHX32	DHX15 DHX32
	UMAG_00419	Dhr2	let-355			DHX33
	UMAG_11913		ddx-35			DHX35
	UMAG_00574			CG9323 CG1582	DHX29 DHX57	DHX29 DHX57
	UMAG_11114	YLR419 W				
	UMAG_05767		rha-1	mle	DHX9	DHX9

							DHX30
						DHX36	DHX36
		UMAG_04665	Dhr1	rha-2	kurz	DHX37	DHX37
				smgl-2	CG32533	DHX34	DHX34
						DHX40	DHX40
	Ski2-like	UMAG_00393	Ski2	skih-2	tst	SkiV2l	SKIV2L
		UMAG_11667	Mtr4	mtr-4	mtr4	SKIV2L2	MTREX
		UMAG_03738	Brr2	snrp-200	CG5931	Snrnp200	SNRNP200
		UMAG_00282	Slh1	Y54E2A.4	obe	Ascc3	ASCC3
		UMAG_04997	Suv3	C08F8.2	Suv3	Supv3l1	SUPV3L1
				C28H8.3		DDX60	DDX60
				dcr-1	dcr1	Dicer1	DICER1
				drh-1		DDX58 Ifih1	DDX58 IFIH1
							DHX58

Table 4.2. *Ustilago maydis* RNA helicase gene transcript levels during *in planta* pathogenesis. The modules that the RNA helicases belonged to were identified from the Lanver et al. (2018) transcriptomic data.

UMAG ID	RNA helicase ortholog	Function	Lanver et al. (2018) module	Expression module description
UMAG_10666	Prp28/DDX23	Pre-mRNA splicing	burlywood	Increased at 0.5 dpi, decreases at 2 dpi, and maintained expression
UMAG_10602	Sen1/SETX	Transcription	cyan	Tumour module – increased and maintained expression after biotrophic establishment
UMAG_11428	Upf1	RNA degradation	cyan	
UMAG_01122	Hcs1/IGHMBP2	Translation	cyan	
UMAG_01174	Prp5/DDX46	Pre-mRNA splicing	cyan	
UMAG_04587	DDX41	Pre-mRNA splicing	cyan	
UMAG_00921	Dbp6/DDX51	Ribosome biogenesis	cyan	
UMAG_03268	Spb4/DDX55	Ribosome biogenesis	green	Increases until 1 dpi, decreased and maintained expression between 2–12 dpi
UMAG_05214	Rrp3/DDX47	Ribosome biogenesis	green	
UMAG_11281	Prp43/DHX15	Pre-mRNA splicing, ribosome biogenesis	green	
UMAG_10410	Has1/DDX18	Ribosome biogenesis	green-yellow	Expression peaks at 2 dpi, followed by decrease and is maintained
UMAG_11989	Dbp4/DDX10	Ribosome biogenesis	green-yellow	
UMAG_06228	Dbp7/DDX31	Ribosome biogenesis	green-yellow	
UMAG_10241	Dbp8/DDX49	Ribosome biogenesis	green-yellow	
UMAG_03170	Drs1/DDX27	Ribosome biogenesis	green-yellow	
UMAG_10095	Dbp2/DDX5/DDX17	Transcription, pre-mRNA splicing, ribosome biogenesis, RNA export,	green-yellow	

		RNA degradation		
UMAG_03892	Dbp9/DDX56	Ribosome biogenesis	green-yellow	
UMAG_00242	Mak5/DDX24	Ribosome biogenesis	green-yellow	
UMAG_10683	Rok1/DDX52	Ribosome biogenesis	green-yellow	
UMAG_04665	Dhr1/DHX37	Ribosome biogenesis	green-yellow	
UMAG_11667	Mtr4/MTREX	Ribosome biogenesis, RNA degradation	green-yellow	
UMAG_00835	Unknown	Unknown	light-cyan	Expression decreases at 2 dpi followed by increase at 4 dpi, and is maintained
UMAG_10915	Prp2/DHX16	Pre-mRNA splicing	light-cyan	
UMAG_04188	Prp16/DHX38	Pre-mRNA splicing	light-cyan	
UMAG_03936	Prp22/DHX8	Pre-mRNA splicing	light-cyan	
UMAG_11913	DHX35	Pre-mRNA splicing	light-cyan	
UMAG_03738	Brr2/SNRNP200	Pre-mRNA splicing	light-green	Expressed during the early stages of pathogenesis, followed by decrease
UMAG_00282	Slh1/HELC1	Translation	light-green	
UMAG_10130	Unknown	Unknown	magenta	Increase in expression between 0.5–2 dpi and is maintained
UMAG_05873	Unknown	Unknown	magenta	
UMAG_05200	Dbp10/DDX54	Ribosome biogenesis, pre-mRNA splicing	magenta	
UMAG_04080	Ded1/DDX3	Pre-mRNA splicing, ribosome biogenesis, translation,	magenta	
UMAG_05767	DHX9	Transcription, pre-mRNA splicing, translation	magenta	

UMAG_06129	Fal1/DDX48	Pre-mRNA splicing, ribosome biogenesis, translation	salmon	Decreased during early stages followed by increase after 2 dpi
UMAG_05482	eIF4A/DDX2	Translation initiation	yellow	Increase in expression and peaks at 2 dpi followed by a decreased expression that is maintained
UMAG_10655	Dhh1/DDX6	Translation, RNA degradation	yellow	
UMAG_03765	Dbp5/DDX19	RNA export, translation	yellow	
UMAG_11769	Sub2/DDX39	Pre-mRNA splicing, RNA export	yellow	
UMAG_01732	Dbp3	Ribosome biogenesis	yellow	
UMAG_00652	Mss116	Mitochondrial RNA processing	yellow	
UMAG_06314	Mss116	Mitochondrial RNA processing	yellow	
UMAG_00574	DHX29/DHX57	Translation	yellow	
UMAG_11114	YLR419W	Unknown	yellow	
UMAG_00419	Dhr2/DHX32	Ribosome biogenesis	yellow	
UMAG_00393	Ski2/SkiV2	RNA degradation	yellow	
UMAG_04997	Suv3/SUV3	Mitochondrial RNA processing	yellow	

Table 4.3. Functions of RNA helicases during RNA transcription. Orthologs for *U. maydis*, *S. cerevisiae*, and *H. sapiens* are listed.

Superfamily	Family	RNA helicase orthologs			RNA helicase function during transcription	References
		U. maydis	*S. cerevisiae*	*H. sapiens*		
SF1	Upf1-like	UMAG_10602	Sen1	SETX	Regulation of R-loops formation and genome stability; Sen1-dependent pathway to aid in RNA polymerase dissociation from DNA template	Mischo et al. (2011); Hazelbaker et al. (2013); Groh et al. (2017); Hegazy et al. (2020); Aiello et al. (2022)
SF2	DEAD-box	UMAG_10666	Prp28	DDX23	DDX23 suppresses R-loop accumulation by removing RNA polymerase II during transcription elongation	Sridhara et al. (2017)
		UMAG_11769	Sub2	DDX39B	DDX39B removes unscheduled R-loops during transcription by unwinding RNA:DNA hybrids	Pérez-Calero et al. (2020)
		UMAG_10410	Has1	DDX18	Interacts with PARP-1 and R-loops to mediate DNA damage and maintain genome stability	Lin et al. (2022)
		UMAG_10095	Dbp2	DDX5 DDX17	A dsRNA-dependent ATPase that is recruited to the chromatin to facilitate RNA	Cloutier et al. (2012); Ma et al. (2013); Ma et al. (2016);

				structural rearrangements	Xing et al. (2019)
DEAH/RHA	UMAG_05767		DHX9	DHX9 with PARP1 to maintain genome stability and prevent DNA damage caused by R-loop formation	Cristini et al. (2018)

Table 4.4. Functions of RNA helicases during pre-mRNA splicing. Orthologs for *U. maydis*, *S. cerevisiae*, and *H. sapiens* are listed.

Superfamily	Family	RNA helicase orthologs			RNA helicase function during pre-mRNA splicing	References
		U. maydis	*S. cerevisiae*	*H. sapiens*		
SF2	DEAD-box	UMAG_11769	Sub2	DDX39A DDX39B	Responsible for the displacement and recruitment of specific RNPs at the pre-mRNA intron branch site; DDX39A and DDX39B regulate alternative splicing	Luo et al. (2001); Liu and Cheng (2015); Banerjee et al. (2024)
		UMAG_01174	Prp5	DDX46	Interacts with snRNP U2 to mediate conformation changes and stabilization; Release of Prp5 signals the recruitment of the U4/U6.U5 tri-snRNP; DDX46 induces pre-mRNA conformational changes for splicing	Liu et al. (2007); Liang and Cheng (2015); Bourgeois et al. (2016)
		UMAG_10666	Prp28	DDX23	Destabilizes the interaction between snRNP U1 and the 5' splice site and allows for U6 to bind to the site; May proofread the 5' splice site during spliceosome assembly	Liu and Cheng (2015); Bourgeois et al. (2016)

UMAG_04188	Prp16	DDX38	Induces spliceosome conformational changes before initiation of the second catalytic reaction; Displaces proteins associated with the spliceosome causing the catalytic core to be less rigid to allow for contact with the 3’ splice site; Prp16 functions with Prp22 to remove stalled spliceosomes and repress suboptimal splicing sites to allow for alternative splice site selection	Liu and Cheng (2015); Robert-Paganin et al. (2015); Bourgeois et al. (2016); Semlow et al. (2016)
UMAG_10095	Dbp2	DDX5 DDX17	DDX5 mediates the interaction between U1 and the 5’ splice site; Serves as a bridge for communication between the splice site and the U4/U6.U5 tri-snRNP DDX17 assists the U1 in recognizing the 5’ splice site and facilitates alternative splicing in select human genes	Hönig et al. (2002); Lee (2002); Liu (2002)

	UMAG_04080	Ded1 Dbp1	DDX3	Interacts with the spliceosome however exact role is not fully understood	Jamieson et al. (1991)
	UMAG_04587		DDX41	DDX41 and the *C. elegans* ortholog sacy-1 interact with spliceosome components and can affect alternative splicing	Polprasert et al. (2015); Tsukamoto et al. (2020); Andreou (2021)
	UMAG_06129	Fal1	DDX48	DDX48 facilitates the assembly of the exon junction complex	Linder and Jankowsky (2011)
	UMAG_5200	Dbp10	DDX54	DDX54 binds to introns that contain a weak 3' splice site to increase the splicing rate	Rodríguez-Galán et al. (2013); Milek et al. (2017)
DEAH/RHA	UMAG_10915	Prp2	DHX16	Remodels the spliceosome into its catalytically active form with cofactor Spp2; ATPase activity destabilizes the snRNPU2 from the spliceosome to expose the branchpoint	Liu and Cheng (2015); Bourgeois et al. (2016)
	UMAG_03936	Prp22	DHX8	Facilitates the release of mature mRNA by disrupting RNA-RNA or RNA-protein interactions; Capable of discarding aberrant	Robert-Paganin et al. (2015); Semlow et al. (2016)

					spliceosomes from pre-mRNA; Prp22 and Prp16 function together to repress suboptimal splicing sites and aid in alternative splice site selection	
		UMAG_11281	Prp43	DHX15	Mediates disassembly of the spliceosome after splicing completion or removal of an impaired or arrested spliceosome	Liu and Cheng (2015)
		UMAG_05767		DHX9	Binds to pre-mRNA and snRNPs that are components of the splicing machinery suggesting a possible role during splicing	Lee and Pelletier (2016)
		UMAG_11913		DHX35	DHX35 interacts with other spliceosome proteins	Sales-Lee et al. (2021)
	Ski2-like	UMAG_03738	Brr2	SNRNP200	Brr2 is a component of the snRNP U5 and mediates the unwinding of U4/U6 to release U4 during spliceosome activation; Regulates other splicing factors by	Liu and Cheng (2015)

					serving as a platform for their recruitment; Promotes protein-protein interactions; Capable of inducing structural changes to the pre-mRNA	

Table 4.5. Functions of RNA helicases during RNA export. Orthologs in *U. maydis*, *S. cerevisiae*, and *H. sapiens* are listed.

Superfamily	Family	RNA helicase orthologs			RNA helicase function during RNA export	References
		U. maydis	*S. cerevisiae*	*H. sapiens*		
SF2	DEAD-box	UMAG_11769	Sub2	DDX39A DDX39B	Responsible for recruiting the protein Yra1 to the mRNA and is then displaced to allow the mRNP to dock onto the nuclear pore complex	Luo et al. (2001); Sträßer and Hurt (2001); Noble et al. (2011)
		UMAG_10095	Dbp2	DDX5 DDX17	Aids in the assembly of Yra1, Nab2, and Mex67 on the poly(A)+ tail by unwinding and remodelling the mRNA duplex	Ma et al. (2013); Xing et al. (2019)
		UMAG_03765	Dbp5	DDX19A DDX19B DDX25	Dbp5 initiates mRNA remodelling when an mRNP is exported through the nuclear pore	Tran et al. (2007); Noble et al. (2011)

Table 4.6. Functions of RNA helicases during ribosome biogenesis. Orthologs in *U. maydis*, *S. cerevisiae*, and *H. sapiens* are listed.

Superfamily	Family	RNA helicase orthologs			RNA helicase function during ribosome biogenesis	References
		U. maydis	*S. cerevisiae*	*H. sapiens*		
SF2	DEAD-box	UMAG_10095	Dbp2	DDX5 DDX17	Dbp2 facilitates structural rearrangements of the pre-rRNA; DDX5 and DDX17 are capable of displacing snoRNA U8 from the pre-rRNA	Bond et al. (2001); Jalal et al. (2007)
		UMAG_01732	Dbp3		Facilitate access to the A_3 cleavage site of ITS1 in the 27S A2 pre-rRNA for the RNase MRP complex	Weaver et al. (1997)
		UMAG_00921	Dbp6	DDX51	Dbp6 facilitates structural rearrangements of the pre-rRNA to allow for efficient assembly of the 60S ribosomal subunit DDX51 promotes the displacement of proteins during the processing of the 3' end of the 28S rRNA	Kressler et al. (1998); Srivastava et al. (2010); Martin et al. (2013); Rodríguez-Galán et al. (2013)
		UMAG_06228	Dbp7	DDX31	Dbp7 remodels the 35S pre-rRNA which allows for the attachment and release of proteins during the maturation of the pre-rRNA DDX31 regulates rRNA transcription	Fukawa et al. (2012); Aquino et al. (2021)

UMAG_03892	Dbp9	DDX56	May modulate pre-rRNA rearrangements during 18S rRNA maturation DDX56 may function during the maturation of pre-rRNA during maturation of the 60S ribosomal subunit	Zirwes et al. (2000); Daugeron et al. (2001); Rodríguez-Galán et al. (2013)
UMAG_5200	Dbp10	DDX54	Bind to pre-rRNA to induce conformational changes or act as a chaperone for other proteins to facilitate cleavage	Burger et al. (2000); Rodríguez-Galán et al. (2013); Mitterer et al. (2023)
UMAG_03170	Drs1	DDX27	Drs1 is tightly associated with Dbp6, Dbp7, Dbp9, Mak5, and Has1 during synthesis of the 60S ribosomal subunit DDX27 associates with pre-rRNA to recruit the protein complex PeBoW	Ripmaster et al. (1992); Bernstein et al. (2006); Martin et al. (2013); Kellner et al. (2015)
UMAG_00242	Mak5	DDX24	Mak5 may function within a protein cluster or creates a stable association between ribosomal proteins during 60S assembly DDX24 interacts with MDM2 to mediate ubiquitylation and degradation of p53 to increase transcription of	Zagulski et al. (2003); Pratte et al. (2013); Yamauchi et al. (2014)

			the 47S transcript	
UMAG_11667	Mtr4	MTREX	Functions within the TRAMP complex that contributes to the polyadenylation of 3’ ends of snoRNAs and rRNAs by modulating the activity of the TRAMP complex by unwinding the RNA to generate longer stretches of ssRNA; Can impact RNA binding, ATP affinity, rate of adenylation, and TRAMP dissociation	Jia et al. (2011); Martin et al. (2013); Rodríguez-Galán et al. (2013)
UMAG_03268	Spb4	DDX55	Spb4 interacts with Pwp2 to facilitate the processing of the 35S pre-rRNA during the early and late stages of maturation DDX55 remodels pre-rRNA during the maturation process	Sachs and Davis (1990); de la Cruz et al. (1998a); Dosil and Bustelo (2004); García-Gómez et al. (2011); Choudhury et al. (2021)
UMAG_11989	Dbp4	DDX10	May facilitate the release of snoRNAs from pre-rRNA	Savitsky et al. (1996); Koš and Tollervey (2005)
UMAG_10241	Dbp8	DDX49	Dbp8 is involved in the maturation of the 18S rRNA DDX49 binds to regulatory regions to provide stability to the rRNA	Daugeron and Linder (2001); Granneman et al. (2006); Awasthi et al. (2018)
UMAG_06129	Fal1	DDX48	Fal1 may function during	Kressler et al. (1997);

				the maturation of the 18S rRNA DDX48 may remodel or promote unwinding when a secondary structure is encountered	Alexandrov et al. (2011); Rodríguez-Galán et al. (2013); Choe et al. (2014)
	UMAG_10683	Rok1	DDX52	Facilitates the release of snoRNAs from pre-rRNA which allows access to cleavage sites	Venema et al. (1997); Bohnsack et al. (2008); Martin et al. (2013); Rodríguez-Galán et al. (2013)
	UMAG_05214	Rrp3	DDX47	Mediates structural changes that allow for snoRNAs to bind and cleavage to the pre-rRNA	O'Day et al. (1996); Sekiguchi et al. (2006); Martin et al. (2013); Rodríguez-Galán et al. (2013)
	UMAG_10410	Has1	DDX18	Coordinates the assembly of proteins on the pre-rRNA to allow for cleavage to occur	Martin et al. (2013); Rodríguez-Galán et al. (2013)
	UMAG_04080	Ded1 Dbp1	DDX3	Protein detected with pre-ribosomal particles, but function is unknown	Krogan et al. (2004); Sharma and Jankowsky (2014)
DEAH/RHA	UMAG_04665	Dhr1	DHX37	Remodels pre-rRNA for processing and releases U3 to allow for cleavage to occur in the 5’ ETS and ITS1	Colley et al. (2000); Choudhury et al. (2019)
	UMAG_ 00419	Dhr2	DHX32	Dhr2 initiates cleavage at site	Colley et al. (2000);

					A_0 of the 5' ETS region of the pre-rRNA DHX32 interacts with pre-rRNA processing proteins during rRNA maturation	Choque et al. (2011); Martin et al. (2013)
		UMAG_11281	Prp43	DHX15	May displace snoRNAs from the pre-rRNA and modulate structural changes to the transcript	Rodríguez-Galán et al. (2013)

Table 4.7. Functions of RNA helicases that are involved in translation. Orthologs in *U. maydis*, *S. cerevisiae*, and *H. sapiens* are listed.

Superfamily	Family	RNA helicase orthologs			RNA helicase function during translation	References
		U. maydis	*S. cerevisiae*	*H. sapiens*		
SF1	Upf1-like	UMAG_01122	Hcs1	IGHMBP2	Exact function during translation is unknown; IGHMBP2 is found to bind to the 80S ribosome and tRNA and co-localizes with eIF4G2 and rRNA in the cytoplasm	de Planell-Saguer et al. (2009); Guenther et al. (2009); Jankowsky (2011); Bourgeois et al. (2016)
SF2	DEAD-box	UMAG_06129	Fal1	DDX48	DDX48 may remodel or promote unwinding of seconding structures to allow the 40S to scan for the translation initiation codon	Choe et al. (2014)
		UMAG_05482	eIF4A	eIF4AI eIF4AII	Component of the eIF4F complex that modulates interactions between the 5' cap and the poly(A) tail eIF4A unwinds secondary structures on the 5' UTR to allow for ribosome attachment	Li et al. (1999); Svitkin et al. (2001); Shen and Pelletier (2020)
		UMAG_04080	Ded1 Dbp1	DDX3	Uses clamping abilities to pause and/or stabilize the	Hilliker et al. (2011); Geissler et al. (2012); Sen et al.

				ribosome; Capable of resolving structured 5' UTRs to initiate translation; Interacts with eIF4G in stress granules to promote and repress translation	(2015); Yeter-Alat et al. (2023)
	UMAG_03765	Dbp5	DDX19A DDX19B DDX25	Remodels the mRNA and recruits the protein eRF1 to bind to the stop codon to initiate the process of translation termination	Gross et al. (2007); Mikhailov a et al. (2017)
	UMAG_10655	Dhh1	DDX6	Dhh1 may sense a slowing ribosome and is recruited to modulate the mRNA to repress translation DDX6 may remodel mRNPs by binding to stem-loop structures in the 3' UTR of the mRNA	Fischer and Weis (2002); Carroll et al. (2011); Sweet et al. (2012); Wang et al. (2015); Shen and Pelletier (2020)
DEAH/RHA	UMAG_05767		DHX9	May recognize post-transcriptional control elements in the 5' region of the mRNA and induce conformational changes for efficient translation	Hartman et al. (2006)

	UMAG_00574		DHX29 DHX57	DHX29 is required for efficient translation of mRNAs with highly structured 5' UTRs by binding to the 40S subunit and inducing conformation al changes that allows for the ribosome to position correctly on the mRNA	Pisareva et al. (2008)
Ski2-like	UMAG_00282	Slh1	HELC1/AS CC3	Slh1 inhibits the translation of mRNAs that lack a poly(A) tail; Induce conformation al changes that allow for the ribosome quality control complex to access defective polypeptide chains for degradation	Searfoss and Wickner (2000); Daugeron et al. (2011); Sitron et al. (2017)

Table 4.8. RNA helicases that are involved in RNA degradation. Orthologs in *U. maydis*, *S. cerevisiae*, and *H. sapiens* are listed.

Superfamily	Family	RNA helicase orthologs			RNA helicase function during RNA degradation	References
		U. maydis	*S. cerevisiae*	*H. sapiens*		
SF1	Upf1-like	UMAG_11428	Upf1	UPF1	Is recruited to mRNAs that contain a long 3' UTR and interacts with NCBP1 to begin the initial steps of the NMD pathway	Hogg and Goff (2010); Imamachi et al. (2012); Ganesan et al. (2022)
SF2	DEAD-box	UMAG_10655	Dhh1	DDX6	Dhh1 activates decapping of the 5' end by modulating the structure of the mRNA to facilitate access for Dcp1	Fischer and Weis (2002); Sweet et al. (2012)
		UMAG_10095	Dbp2	DDX5 DDX17	May act as an RNA binding protein to facilitate or stabilize the assembly of the NMD machinery on the mRNA	Xing et al. (2019)
	Ski2-like	UMAG_00393	Ski2	SkiV2	Ski2 unwinds secondary structures and resolve RNPs at the 3' end of the mRNA for exosome access	Anderson and Parker (1998); Johnson and Jackson (2013)
		UMAG_11667	Mtr4	MTREX	Mtr4 may target aberrant precursor 5.8S rRNA for degradation; May function to unwind RNA to generate long stretches of sRNA to allow the exosome to access	de la Cruz et al. (1998b); Jia et al. (2011)

Table 4.9. RNA helicases that are involved in mitochondrial RNA processing. Orthologs for *U. maydis*, *S. cerevisiae*, and *H. sapiens* are listed.

Superfamily	Family	RNA helicase orthologs			RNA helicase function during mitochondrial RNA processing	References
		U. maydis	*S. cerevisiae*	*H. sapiens*		
SF2	DEAD-box	UMAG_00652 UMAG_06314	Mss116		Modulates mitochondrial transcription and is involved in the splicing of group I and II mitochondrial introns	Niemer et al. (1995); Minczuk et al. (2002); Markov et al. (2014)
	Ski2-like	UMAG_04997	Suv3	SUV3	Is involved in the processing of the r1 intron in the precursor of the mitochondrial 21S rRNA; Functions within the mitochondrial degradosome to unwind dsRNA	Stepien et al. (1995); Dziembowski et al. (2003); Guo et al. (2011)

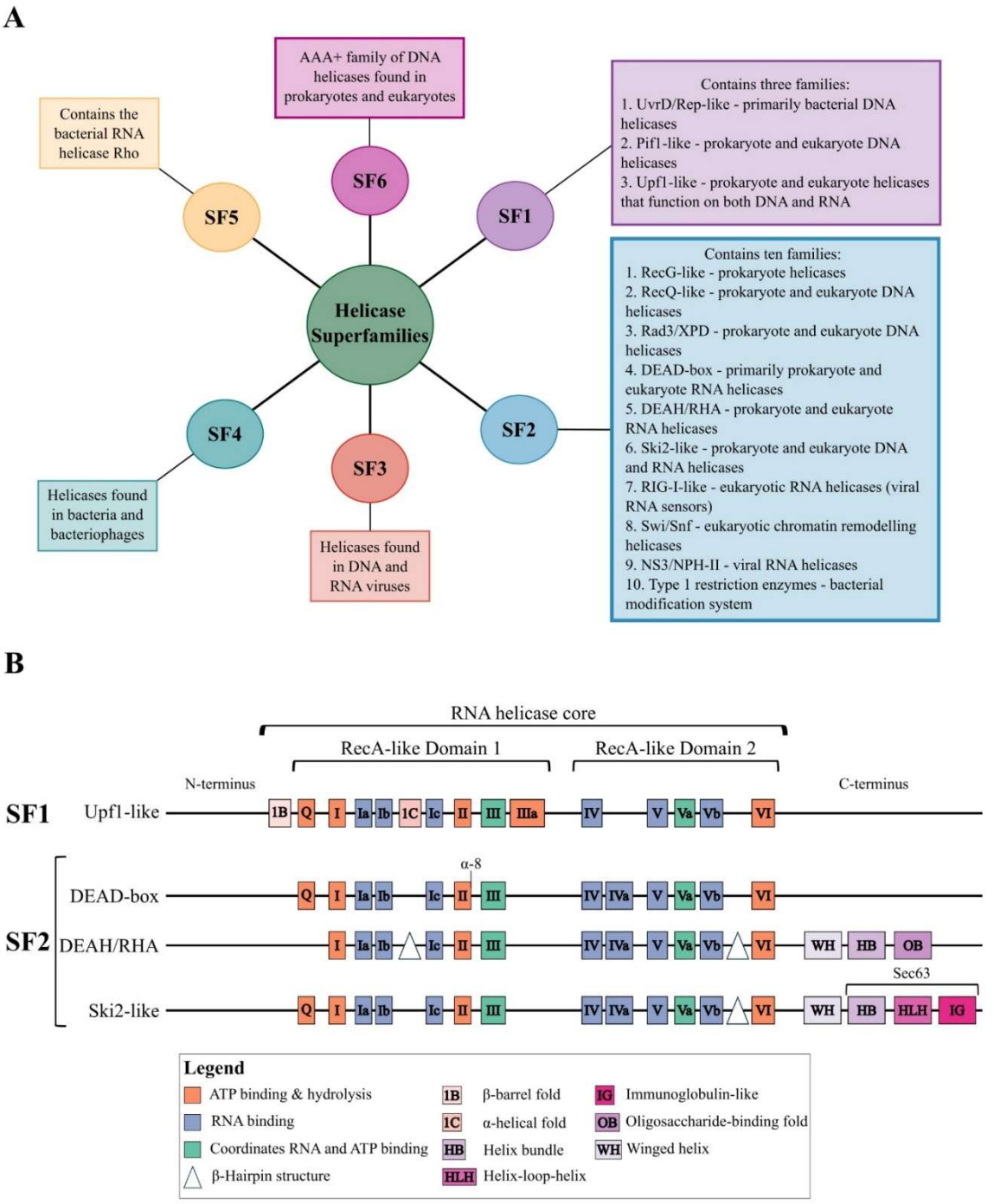

Figure 4.1. Helicase superfamilies and characteristics of SF1 and SF2 RNA helicases: **A** Summary of the six helicase superfamilies found in prokaryotes and eukaryotes; **B** The characteristics of the N-terminus, C-terminus domains, and RNA helicase core of SF1 and SF2 RNA helicases. The SF1 and SF2 RNA helicases have two RecA-like domains containing specific sequence motifs. These sequence motifs are coloured according to their biochemical functions: orange, ATP binding and hydrolysis; blue, RNA binding; green, coordination between RNA and ATP binding. The N-terminus and C-terminus of RNA helicases contain some conserved domains that are indicated however, variability in these

regions provides specificity to the RNA helicase. The α-8 represents the conserved α-helix at the end of motif II. The triangle represents the position of the β-hairpin structure motif. Abbreviations: HB, helix bundle containing the ratchet helix; HLH, helix-loop-helix; IG, immunoglobulin-like; OB, oligosaccharide-binding fold; WH, winged helix. The distance between domains and sequence motif sizes is not to scale.

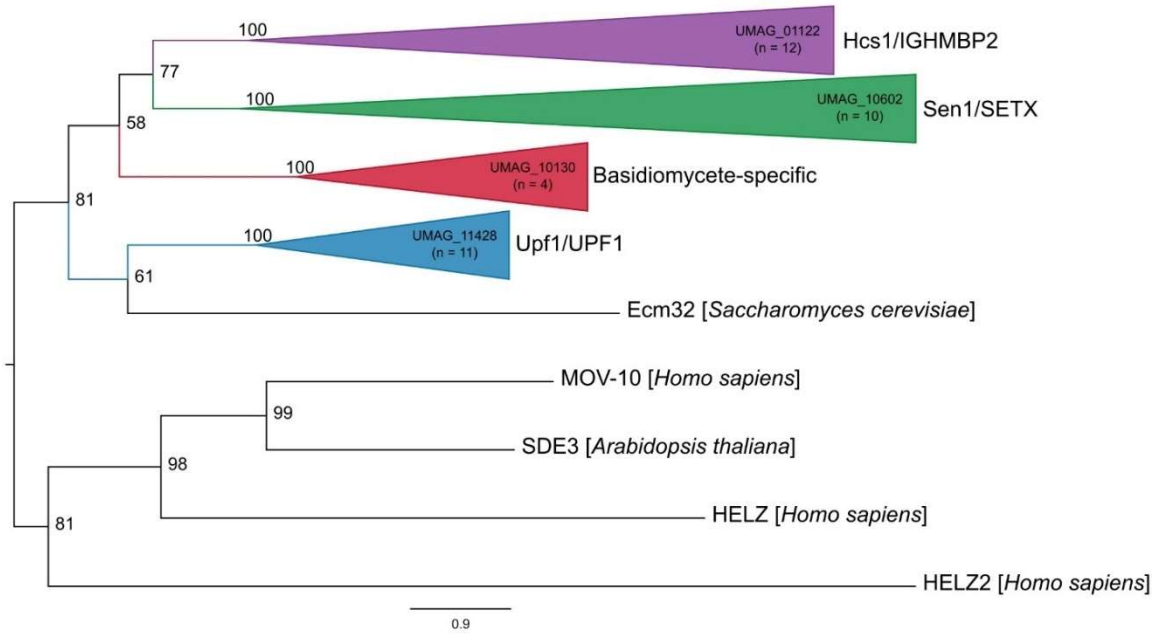

Figure 4.2. Maximum likelihood phylogenetic tree of SF1 RNA helicases. The phylogenetic tree was created with orthologs from *U. maydis*, *S. reilianum*, *U. hordei*, *C. neoformans*, *S. cerevisiae*, *S. pombe*, *N. crassa*, *A. thaliana*, *C. elegans*, *D. discoideum*, and *H. sapiens* using W-IQ-Tree multicore version 1.6.12 with default settings (Trifinopoulos et al. 2016), 1000 ultrafast bootstrap alignments, and approximate Bayes test. The tree was visualized with FigTree v1.4.4 (http://tree.bio.ed.ac.uk/software/figtree/), rooted at the midpoint, and the bootstrap value is indicated for each node. Phylogenetic groups containing an RNA helicase ortholog in *U. maydis* were collapsed and colour-coded. The *U. maydis* RNA helicase and the number of sequences for each clade are identified for each collapsed group. Each collapsed group was named after the *S. cerevisiae* and *H. sapiens* orthologs. The scale bar indicates the expected number of substitutions per amino acid. The original phylogenetic tree is supplementary Figure S4.1 and contains all gene names and organisms used in this analysis.

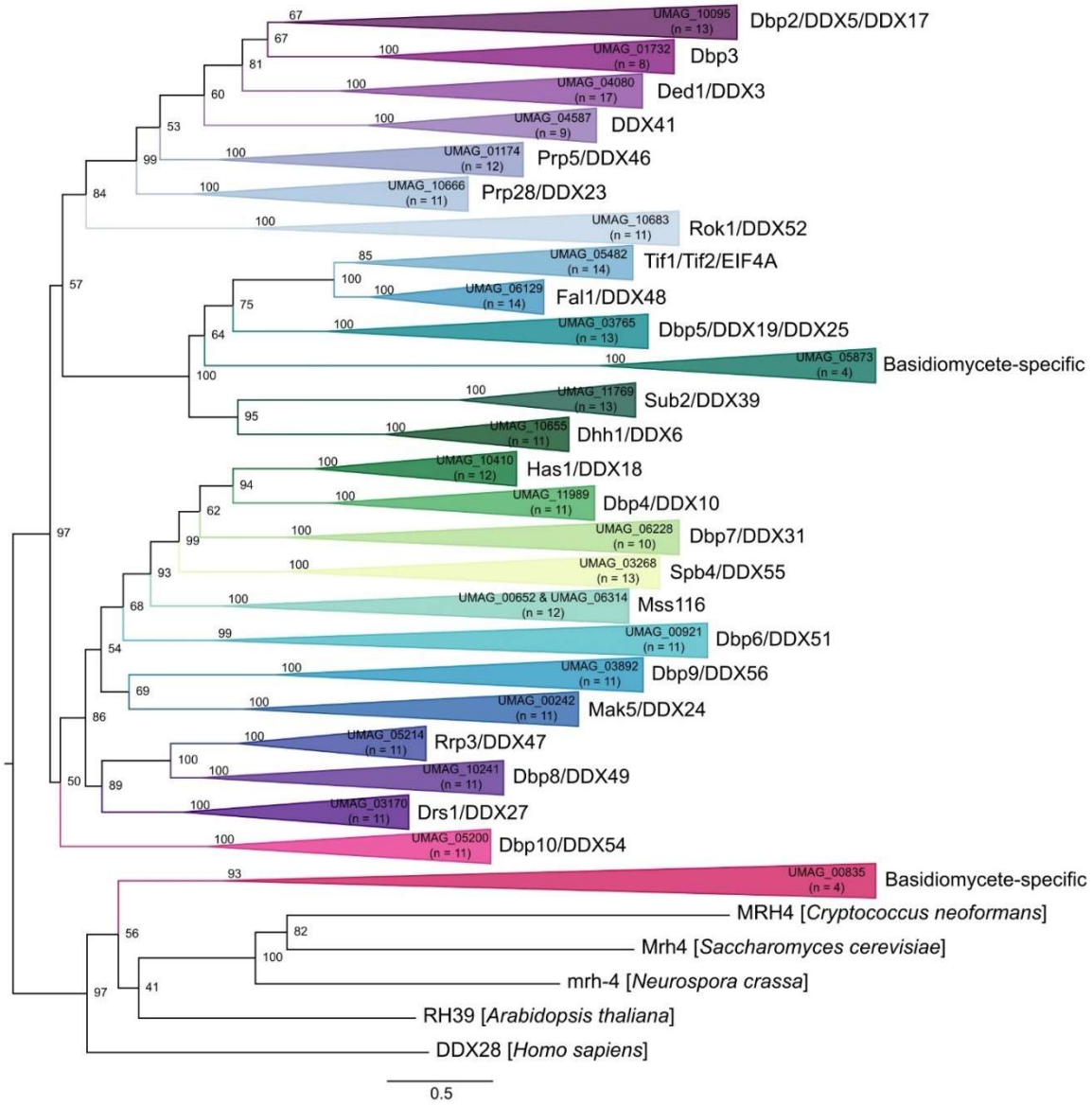

Figure 4.3. Maximum likelihood phylogenetic tree of SF2 DEAD-box RNA helicases. The phylogenetic tree was created with orthologs from *U. maydis*, *S. reilianum*, *U. hordei*, *C. neoformans*, *S. cerevisiae*, *S. pombe*, *N. crassa*, *A. thaliana*, *C. elegans*, *D. discoideum*, and *H. sapiens* using W-IQ-Tree multicore version 1.6.12 with default settings (Trifinopoulos et al. 2016), 1000 ultrafast bootstrap alignments, and approximate Bayes test. The tree was visualized with FigTree v1.4.4 (http://tree.bio.ed.ac.uk/software/figtree/), rooted at the midpoint, and the bootstrap value is indicated for each node. Phylogenetic groups containing an RNA helicase ortholog in *U. maydis* were collapsed and colour-coded. The *U. maydis* RNA helicase and the number of sequences for each clade are identified for each collapsed group. Each collapsed group was named after the *S. cerevisiae* and *H. sapiens* orthologs. The scale bar indicates the expected number of substitutions per amino acid. The original phylogenetic tree is supplementary Figure S4.2 and contains all gene names and organisms used in this analysis.

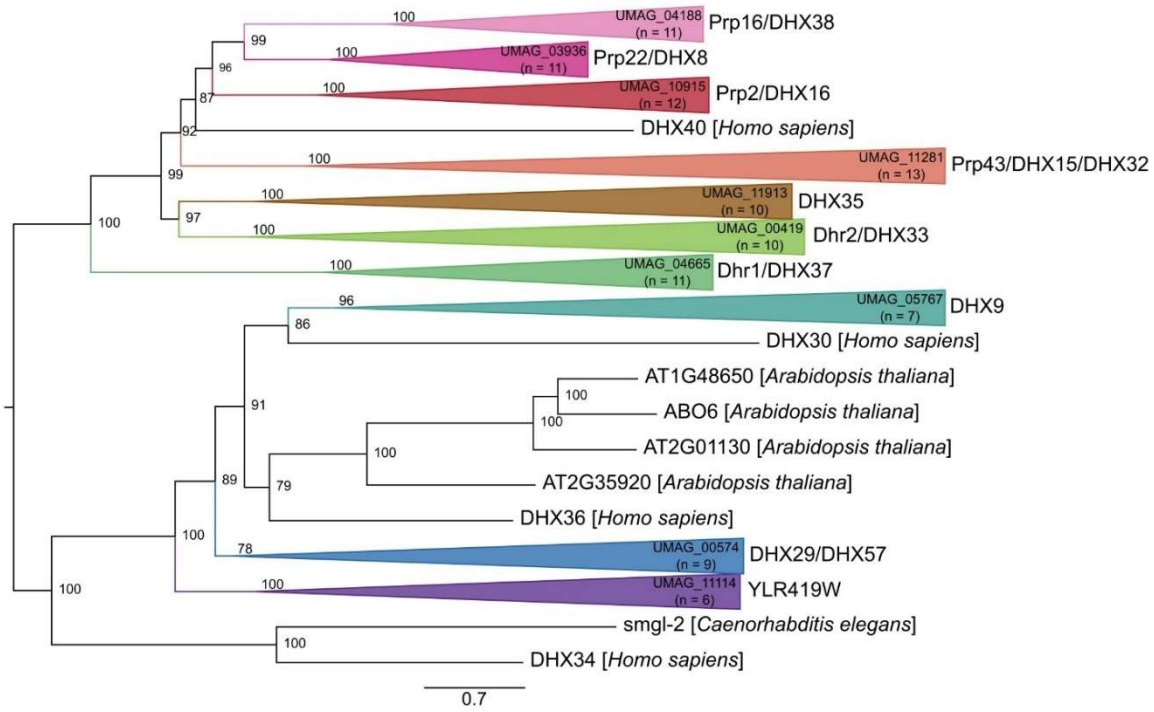

Figure 4.4. Maximum likelihood phylogenetic tree of SF2 DEAH/RHA RNA helicases. The phylogenetic tree was created with orthologs from *U. maydis*, *S. reilianum*, *U. hordei*, *C. neoformans*, *S. cerevisiae*, *S. pombe*, *N. crassa*, *A. thaliana*, *C. elegans*, *D. discoideum*, and *H. sapiens* using W-IQ-Tree multicore version 1.6.12 with default settings (Trifinopoulos et al. 2016), 1000 ultrafast bootstrap alignments, and approximate Bayes test. The tree was visualized with FigTree v1.4.4 (http://tree.bio.ed.ac.uk/software/figtree/), rooted at the midpoint, and the bootstrap value is indicated for each node. Phylogenetic groups containing an RNA helicase ortholog in *U. maydis* were collapsed and colour-coded. The *U. maydis* RNA helicase and the number of sequences for each clade are identified for each collapsed group. Each collapsed group was named after the *S. cerevisiae* and *H. sapiens* orthologs. The scale bar indicates the expected number of substitutions per amino acid. The original phylogenetic tree is supplementary Figure S4.3 and contains all gene names and organisms used in this analysis.

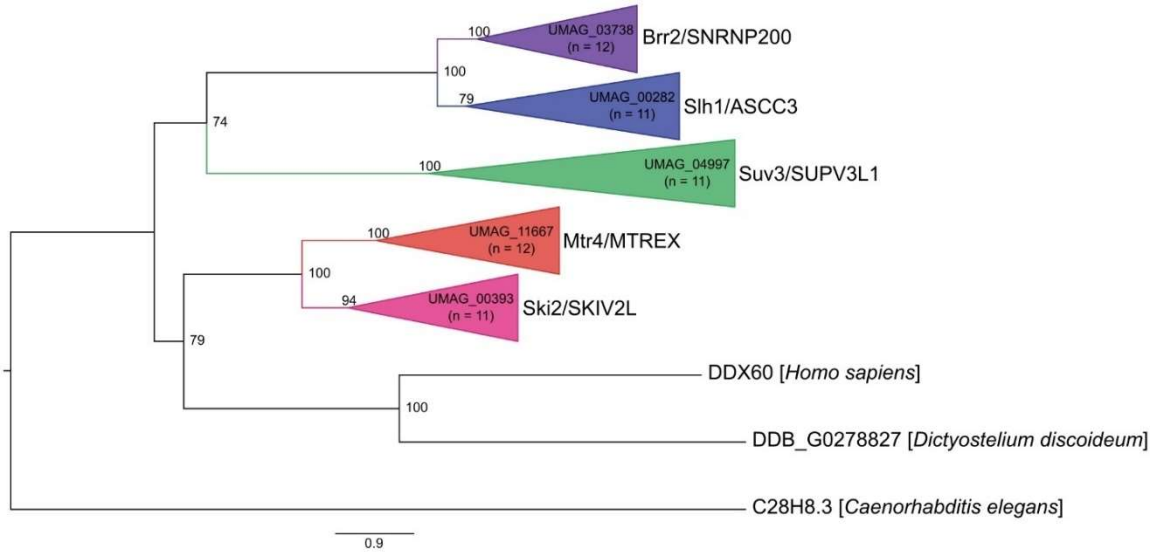

Figure 4.5. Maximum likelihood phylogenetic tree of SF2 Ski2-like RNA helicases. The phylogenetic tree was created with orthologs from *U. maydis*, *S. reilianum*, *U. hordei*, *C. neoformans*, *S. cerevisiae*, *S. pombe*, *N. crassa*, *A. thaliana*, *C. elegans*, *D. discoideum*, and *H. sapiens* using W-IQ-Tree multicore version 1.6.12 with default settings (Trifinopoulos et al. 2016), 1000 ultrafast bootstrap alignments, and approximate Bayes test. The tree was visualized with FigTree v1.4.4 (http://tree.bio.ed.ac.uk/software/figtree/), rooted at the midpoint, and the bootstrap value is indicated for each node. Phylogenetic groups containing an RNA helicase ortholog in *U. maydis* were collapsed and colour-coded. The *U. maydis* RNA helicase and the number of sequences for each clade are identified for each collapsed group. Each collapsed group was named after the *S. cerevisiae* and *H. sapiens* orthologs. The scale bar indicates the expected number of substitutions per amino acid. The original phylogenetic tree is supplementary Figure S4.4 and contains all gene names and organisms used in this analysis.

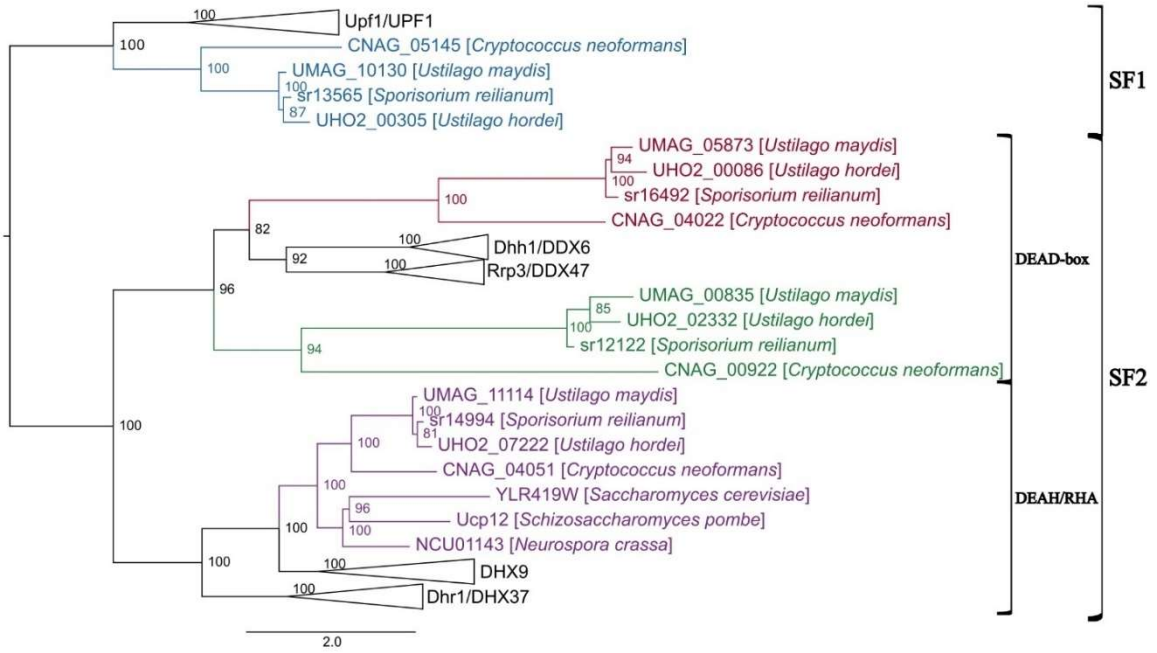

Figure 4.6. Maximum likelihood phylogenetic tree of RNA helicases with unknown function. The phylogenetic tree was created with orthologs of RNA helicases with unknown functions from *U. maydis*, *S. reilianum*, *U. hordei*, *C. neoformans*, *S. cerevisiae*, *S. pombe*, *N. crassa*, *A. thaliana*, *C. elegans*, *D. discoideum*, and *H. sapiens* using W-IQ-Tree multicore version 1.6.12 with default settings (Trifinopoulos et al. 2016), 1000 ultrafast bootstrap alignments, and approximate Bayes test. The tree was visualized with FigTree v1.4.4 (http://tree.bio.ed.ac.uk/software/figtree/), rooted with the SF1 clade as the outgroup, and the bootstrap value is indicated for each node. Phylogenetic groups containing known RNA helicases were collapsed and named after their *S. cerevisiae* and *H. sapiens* orthologs. Clades coloured in blue, red, green, and purple indicate RNA helicases with unknown functions. The scale bar indicates the expected number of substitutions per amino acid. The raw phylogenetic tree is supplementary Figure S4.5 and contains all gene names and organisms used in this analysis.

SUPPLEMENTARY MATERIALS

Table S4.1. Results of predicted functional protein partners for each RNA helicase identified in *Ustilago maydis*. The predicted functional partners were determined by performing a STRING analysis for each RNA helicase in the STRING database (https://string-db.org/).

This is a PDF file containing Supplementary Table S4.1. It is a large dataset containing the results of the STRING analysis performed on all 46 RNA helicases. The table consists of the RNA helicase and lists its predicted functional partner. The UMAG description, KEGG pathway, KEGG BRITE, and STRING score are listed for each predicated functional partner. The file name of this PDF file is “Chapter 4 – Supplementary Table S4-1.pdf”.

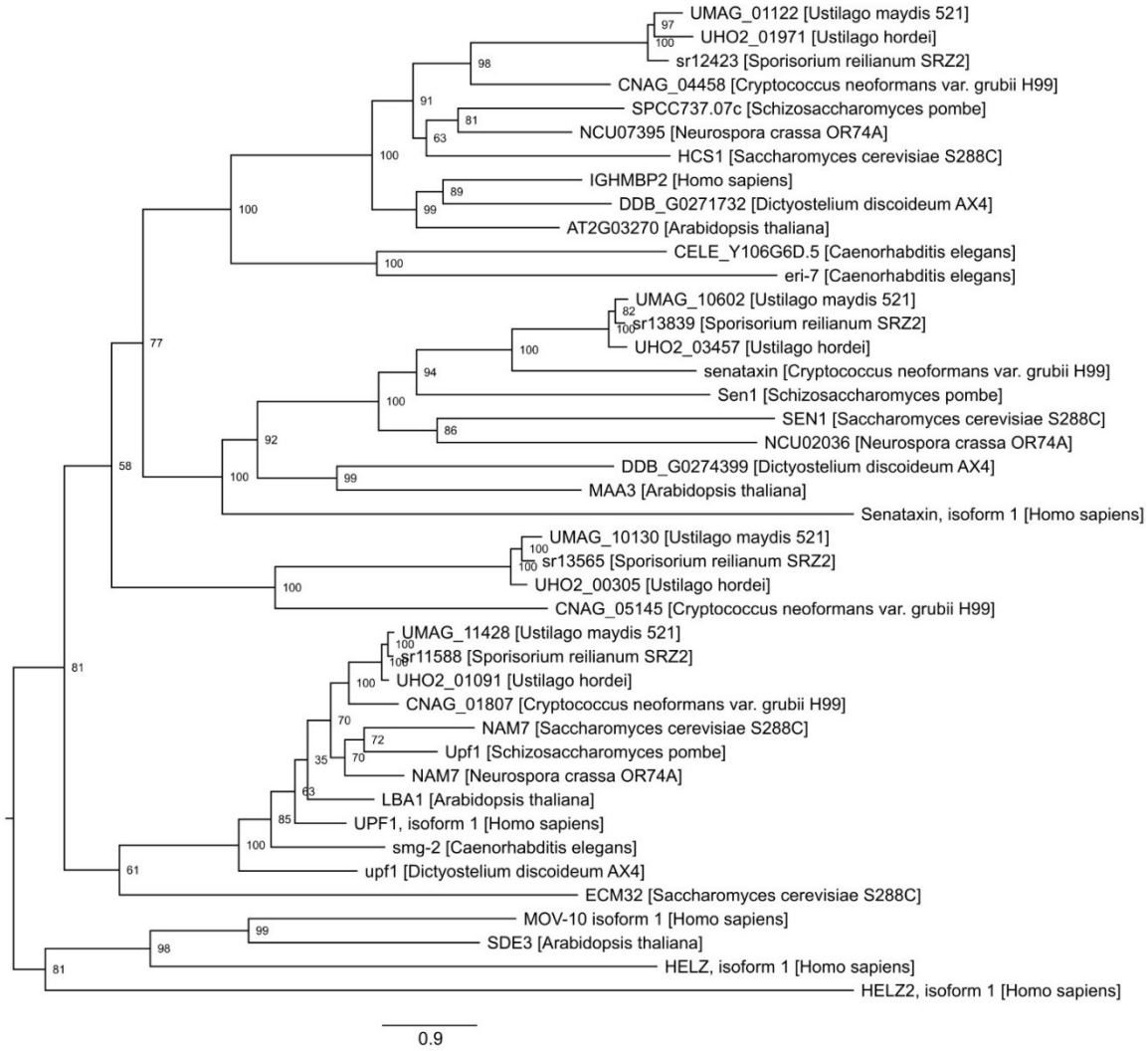

Figure S4.1. The original maximum likelihood phylogenetic tree of SF1 Upf1-like RNA helicases. The phylogenetic tree was created with orthologs from *U. maydis*, *S. reilianum*, *U. hordei*, *C. neoformans*, *S. cerevisiae*, *S. pombe*, *N. crassa*, *A. thaliana*, *C. elegans*, *D. discoideum*, and *H. sapiens* using W-IQ-Tree multicore version 1.6.12 with default settings (Trifinopoulos et al. 2016), 1000 ultrafast bootstrap alignments, and approximate Bayes test. The tree was visualized with FigTree v1.4.4 (http://tree.bio.ed.ac.uk/software/figtree/), rooted at the midpoint, and the bootstrap value is indicated for each node. The scale bar indicates the expected number of substitutions per amino acid.

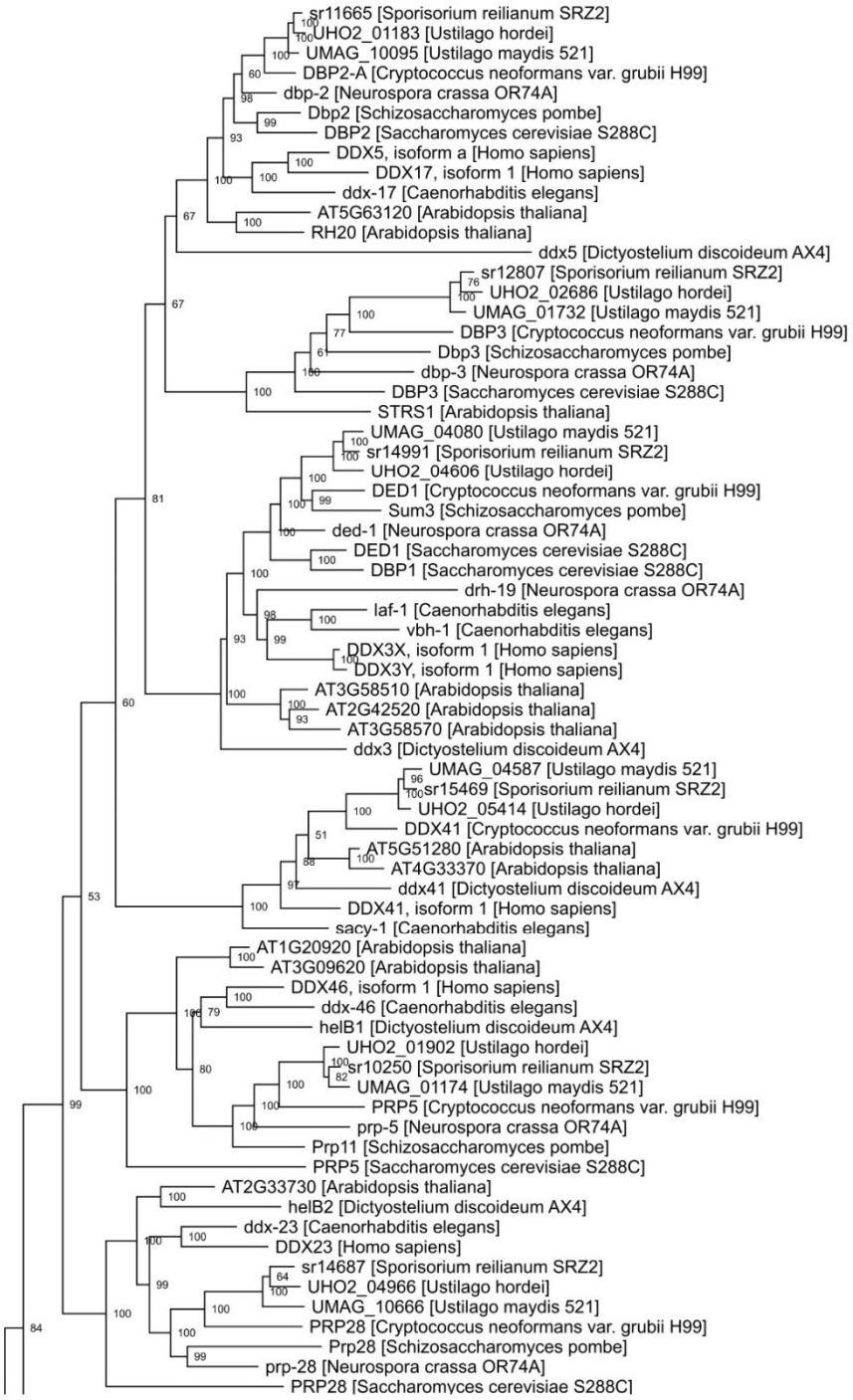
sr11665 [Sporisorium reilianum SRZ2]
UHO2_01183 [Ustilago hordei]
UMAG_10095 [Ustilago maydis 521]
DBP2-A [Cryptococcus neoformans var. grubii H99]
dbp-2 [Neurospora crassa OR74A]
Dbp2 [Schizosaccharomyces pombe]
DBP2 [Saccharomyces cerevisiae S288C]
DDX5, isoform a [Homo sapiens]
DDX17, isoform 1 [Homo sapiens]
ddx-17 [Caenorhabditis elegans]
AT5G63120 [Arabidopsis thaliana]
RH20 [Arabidopsis thaliana]
ddx5 [Dictyostelium discoideum AX4]
sr12807 [Sporisorium reilianum SRZ2]
UHO2_02686 [Ustilago hordei]
UMAG_01732 [Ustilago maydis 521]
DBP3 [Cryptococcus neoformans var. grubii H99]
Dbp3 [Schizosaccharomyces pombe]
dbp-3 [Neurospora crassa OR74A]
DBP3 [Saccharomyces cerevisiae S288C]
STRS1 [Arabidopsis thaliana]
UMAG_04080 [Ustilago maydis 521]
sr14991 [Sporisorium reilianum SRZ2]
UHO2_04606 [Ustilago hordei]
DED1 [Cryptococcus neoformans var. grubii H99]
Sum3 [Schizosaccharomyces pombe]
ded-1 [Neurospora crassa OR74A]
DED1 [Saccharomyces cerevisiae S288C]
DBP1 [Saccharomyces cerevisiae S288C]
drh-19 [Neurospora crassa OR74A]
laf-1 [Caenorhabditis elegans]
vbh-1 [Caenorhabditis elegans]
DDX3X, isoform 1 [Homo sapiens]
DDX3Y, isoform 1 [Homo sapiens]
AT3G58510 [Arabidopsis thaliana]
AT2G42520 [Arabidopsis thaliana]
AT3G58570 [Arabidopsis thaliana]
ddx3 [Dictyostelium discoideum AX4]
UMAG_04587 [Ustilago maydis 521]
sr15469 [Sporisorium reilianum SRZ2]
UHO2_05414 [Ustilago hordei]
DDX41 [Cryptococcus neoformans var. grubii H99]
AT5G51280 [Arabidopsis thaliana]
AT4G33370 [Arabidopsis thaliana]
ddx41 [Dictyostelium discoideum AX4]
DDX41, isoform 1 [Homo sapiens]
sacy-1 [Caenorhabditis elegans]
AT1G20920 [Arabidopsis thaliana]
AT3G09620 [Arabidopsis thaliana]
DDX46, isoform 1 [Homo sapiens]
ddx-46 [Caenorhabditis elegans]
helB1 [Dictyostelium discoideum AX4]
UHO2_01902 [Ustilago hordei]
sr10250 [Sporisorium reilianum SRZ2]
UMAG_01174 [Ustilago maydis 521]
PRP5 [Cryptococcus neoformans var. grubii H99]
prp-5 [Neurospora crassa OR74A]
Prp11 [Schizosaccharomyces pombe]
PRP5 [Saccharomyces cerevisiae S288C]
AT2G33730 [Arabidopsis thaliana]
helB2 [Dictyostelium discoideum AX4]
ddx-23 [Caenorhabditis elegans]
DDX23 [Homo sapiens]
sr14687 [Sporisorium reilianum SRZ2]
UHO2_04966 [Ustilago hordei]
UMAG_10666 [Ustilago maydis 521]
PRP28 [Cryptococcus neoformans var. grubii H99]
Prp28 [Schizosaccharomyces pombe]
prp-28 [Neurospora crassa OR74A]
PRP28 [Saccharomyces cerevisiae S288C]

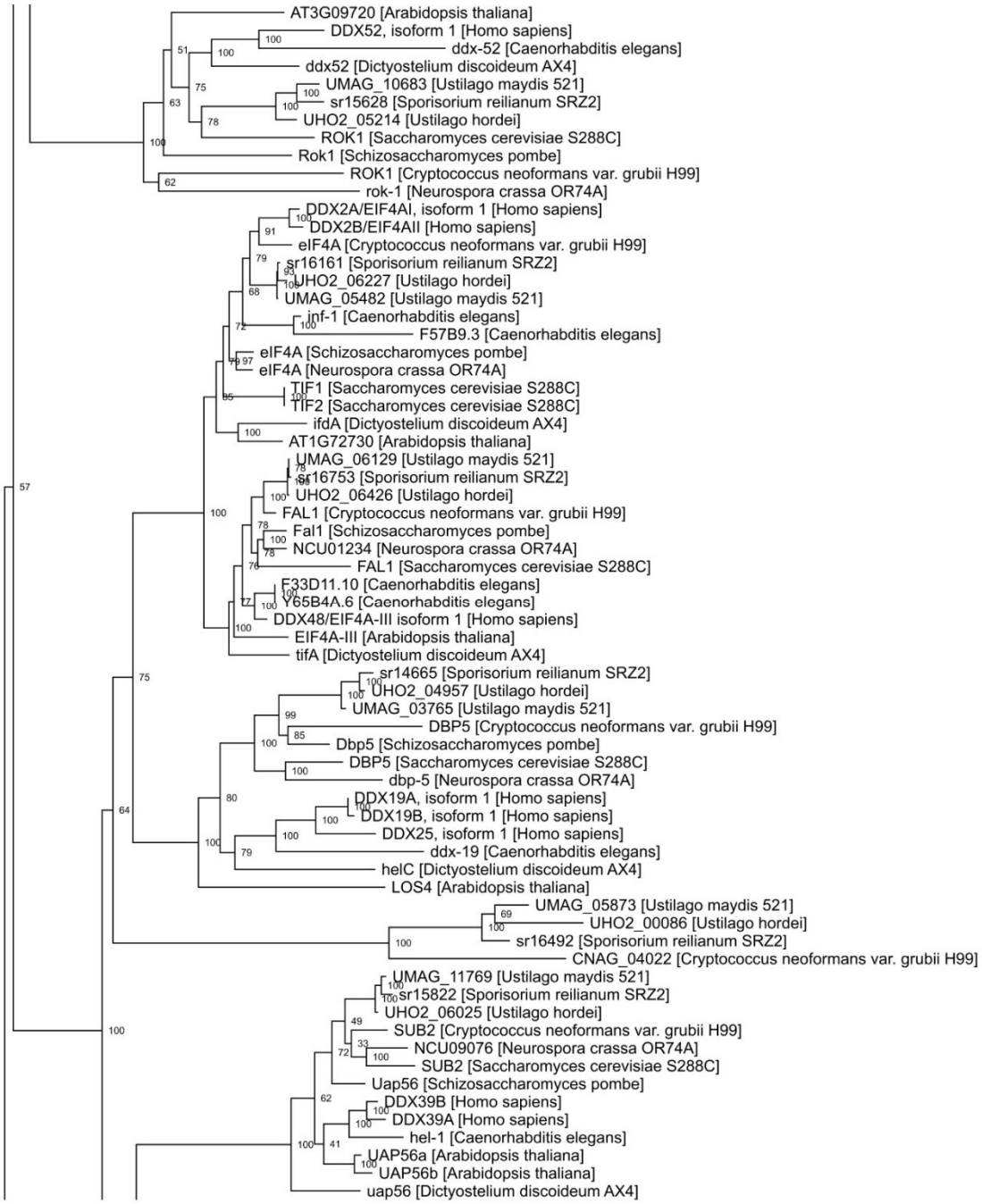
AT3G09720 [Arabidopsis thaliana]
DDX52, isoform 1 [Homo sapiens]
ddx-52 [Caenorhabditis elegans]
ddx52 [Dictyostelium discoideum AX4]
UMAG_10683 [Ustilago maydis 521]
sr15628 [Sporisorium reilianum SRZ2]
UHO2_05214 [Ustilago hordei]
ROK1 [Saccharomyces cerevisiae S288C]
Rok1 [Schizosaccharomyces pombe]
ROK1 [Cryptococcus neoformans var. grubii H99]
rok-1 [Neurospora crassa OR74A]
DDX2A/EIF4AI, isoform 1 [Homo sapiens]
DDX2B/EIF4AII [Homo sapiens]
eIF4A [Cryptococcus neoformans var. grubii H99]
sr16161 [Sporisorium reilianum SRZ2]
UHO2_06227 [Ustilago hordei]
UMAG_05482 [Ustilago maydis 521]
inf-1 [Caenorhabditis elegans]
F57B9.3 [Caenorhabditis elegans]
eIF4A [Schizosaccharomyces pombe]
eIF4A [Neurospora crassa OR74A]
TIF1 [Saccharomyces cerevisiae S288C]
TIF2 [Saccharomyces cerevisiae S288C]
ifdA [Dictyostelium discoideum AX4]
AT1G72730 [Arabidopsis thaliana]
UMAG_06129 [Ustilago maydis 521]
sr16753 [Sporisorium reilianum SRZ2]
UHO2_06426 [Ustilago hordei]
FAL1 [Cryptococcus neoformans var. grubii H99]
Fal1 [Schizosaccharomyces pombe]
NCU01234 [Neurospora crassa OR74A]
FAL1 [Saccharomyces cerevisiae S288C]
F33D11.10 [Caenorhabditis elegans]
Y65B4A.6 [Caenorhabditis elegans]
DDX48/EIF4A-III isoform 1 [Homo sapiens]
EIF4A-III [Arabidopsis thaliana]
tifA [Dictyostelium discoideum AX4]
sr14665 [Sporisorium reilianum SRZ2]
UHO2_04957 [Ustilago hordei]
UMAG_03765 [Ustilago maydis 521]
DBP5 [Cryptococcus neoformans var. grubii H99]
Dbp5 [Schizosaccharomyces pombe]
DBP5 [Saccharomyces cerevisiae S288C]
dbp-5 [Neurospora crassa OR74A]
DDX19A, isoform 1 [Homo sapiens]
DDX19B, isoform 1 [Homo sapiens]
DDX25, isoform 1 [Homo sapiens]
ddx-19 [Caenorhabditis elegans]
helC [Dictyostelium discoideum AX4]
LOS4 [Arabidopsis thaliana]
UMAG_05873 [Ustilago maydis 521]
UHO2_00086 [Ustilago hordei]
sr16492 [Sporisorium reilianum SRZ2]
CNAG_04022 [Cryptococcus neoformans var. grubii H99]
UMAG_11769 [Ustilago maydis 521]
sr15822 [Sporisorium reilianum SRZ2]
UHO2_06025 [Ustilago hordei]
SUB2 [Cryptococcus neoformans var. grubii H99]
NCU09076 [Neurospora crassa OR74A]
SUB2 [Saccharomyces cerevisiae S288C]
Uap56 [Schizosaccharomyces pombe]
DDX39B [Homo sapiens]
DDX39A [Homo sapiens]
hel-1 [Caenorhabditis elegans]
UAP56a [Arabidopsis thaliana]
UAP56b [Arabidopsis thaliana]
uap56 [Dictyostelium discoideum AX4]

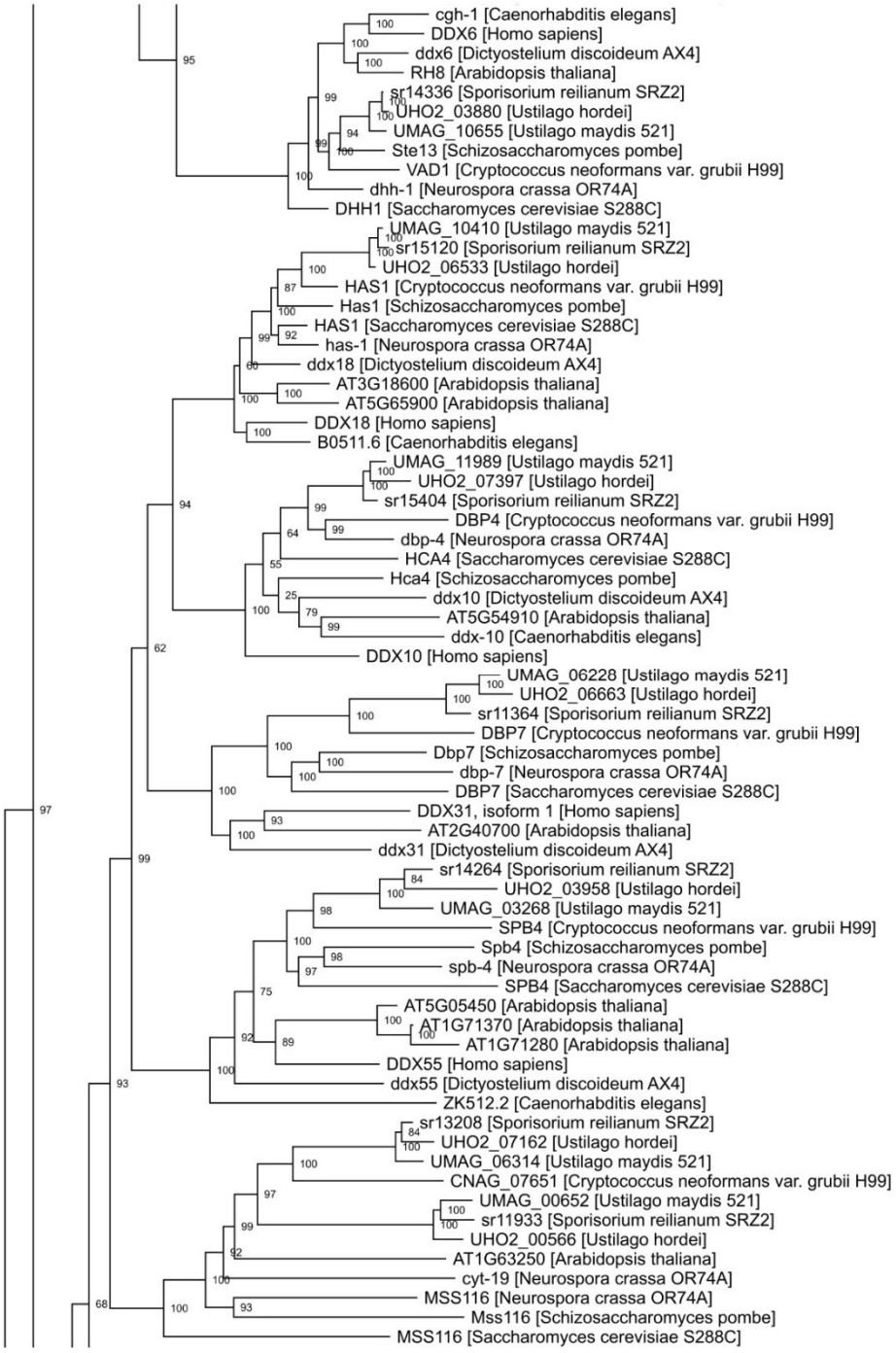
cgh-1 [Caenorhabditis elegans]
DDX6 [Homo sapiens]
ddx6 [Dictyostelium discoideum AX4]
RH8 [Arabidopsis thaliana]
sr14336 [Sporisorium reilianum SRZ2]
UHO2_03880 [Ustilago hordei]
UMAG_10655 [Ustilago maydis 521]
Ste13 [Schizosaccharomyces pombe]
VAD1 [Cryptococcus neoformans var. grubii H99]
dhh-1 [Neurospora crassa OR74A]
DHH1 [Saccharomyces cerevisiae S288C]
UMAG_10410 [Ustilago maydis 521]
sr15120 [Sporisorium reilianum SRZ2]
UHO2_06533 [Ustilago hordei]
HAS1 [Cryptococcus neoformans var. grubii H99]
Has1 [Schizosaccharomyces pombe]
HAS1 [Saccharomyces cerevisiae S288C]
has-1 [Neurospora crassa OR74A]
ddx18 [Dictyostelium discoideum AX4]
AT3G18600 [Arabidopsis thaliana]
AT5G65900 [Arabidopsis thaliana]
DDX18 [Homo sapiens]
B0511.6 [Caenorhabditis elegans]
UMAG_11989 [Ustilago maydis 521]
UHO2_07397 [Ustilago hordei]
sr15404 [Sporisorium reilianum SRZ2]
DBP4 [Cryptococcus neoformans var. grubii H99]
dbp-4 [Neurospora crassa OR74A]
HCA4 [Saccharomyces cerevisiae S288C]
Hca4 [Schizosaccharomyces pombe]
ddx10 [Dictyostelium discoideum AX4]
AT5G54910 [Arabidopsis thaliana]
ddx-10 [Caenorhabditis elegans]
DDX10 [Homo sapiens]
UMAG_06228 [Ustilago maydis 521]
UHO2_06663 [Ustilago hordei]
sr11364 [Sporisorium reilianum SRZ2]
DBP7 [Cryptococcus neoformans var. grubii H99]
Dbp7 [Schizosaccharomyces pombe]
dbp-7 [Neurospora crassa OR74A]
DBP7 [Saccharomyces cerevisiae S288C]
DDX31, isoform 1 [Homo sapiens]
AT2G40700 [Arabidopsis thaliana]
ddx31 [Dictyostelium discoideum AX4]
sr14264 [Sporisorium reilianum SRZ2]
UHO2_03958 [Ustilago hordei]
UMAG_03268 [Ustilago maydis 521]
SPB4 [Cryptococcus neoformans var. grubii H99]
Spb4 [Schizosaccharomyces pombe]
spb-4 [Neurospora crassa OR74A]
SPB4 [Saccharomyces cerevisiae S288C]
AT5G05450 [Arabidopsis thaliana]
AT1G71370 [Arabidopsis thaliana]
AT1G71280 [Arabidopsis thaliana]
DDX55 [Homo sapiens]
ddx55 [Dictyostelium discoideum AX4]
ZK512.2 [Caenorhabditis elegans]
sr13208 [Sporisorium reilianum SRZ2]
UHO2_07162 [Ustilago hordei]
UMAG_06314 [Ustilago maydis 521]
CNAG_07651 [Cryptococcus neoformans var. grubii H99]
UMAG_00652 [Ustilago maydis 521]
sr11933 [Sporisorium reilianum SRZ2]
UHO2_00566 [Ustilago hordei]
AT1G63250 [Arabidopsis thaliana]
cyt-19 [Neurospora crassa OR74A]
MSS116 [Neurospora crassa OR74A]
Mss116 [Schizosaccharomyces pombe]
MSS116 [Saccharomyces cerevisiae S288C]

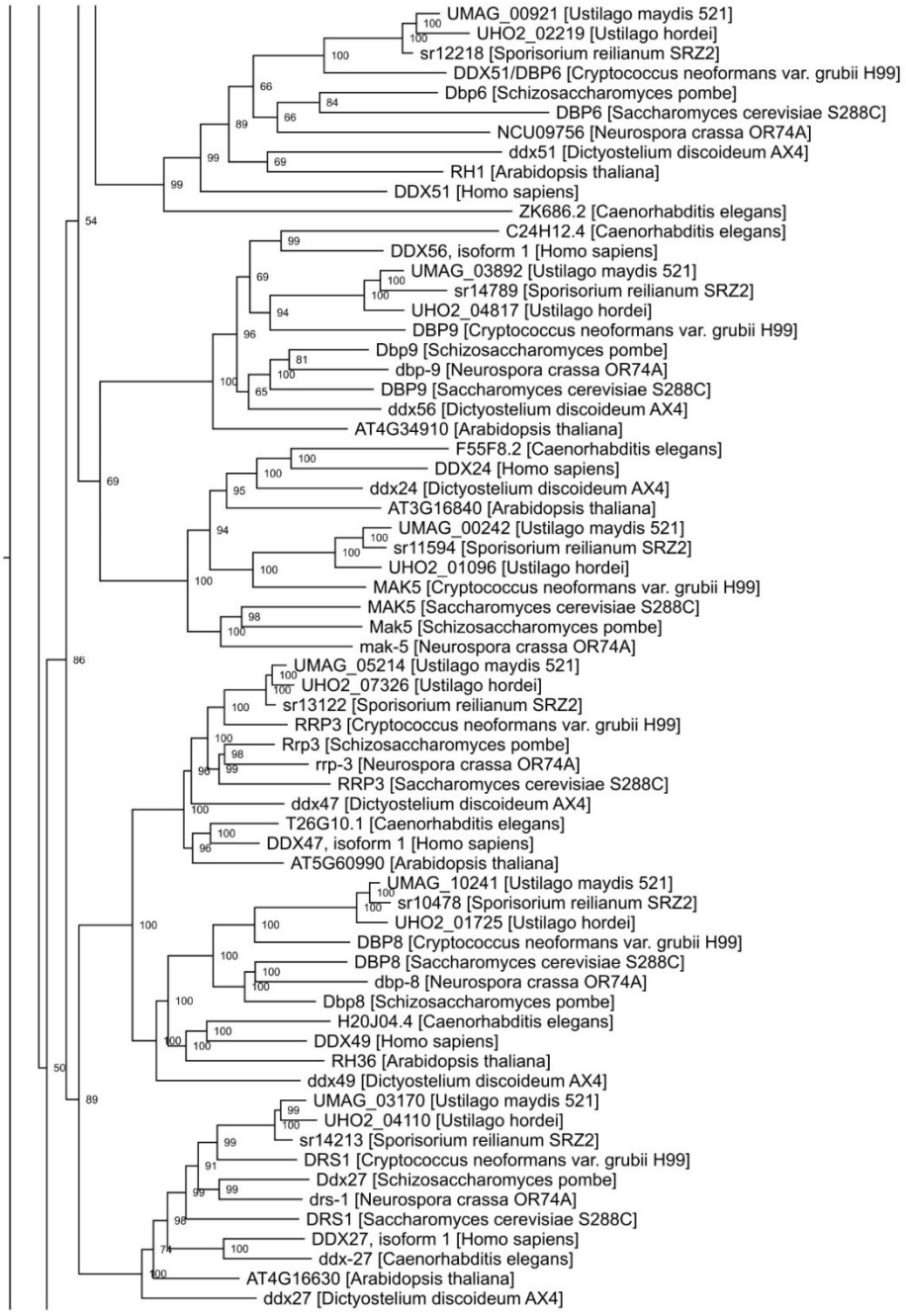
UMAG_00921 [Ustilago maydis 521]
UHO2_02219 [Ustilago hordei]
sr12218 [Sporisorium reilianum SRZ2]
DDX51/DBP6 [Cryptococcus neoformans var. grubii H99]
Dbp6 [Schizosaccharomyces pombe]
DBP6 [Saccharomyces cerevisiae S288C]
NCU09756 [Neurospora crassa OR74A]
ddx51 [Dictyostelium discoideum AX4]
RH1 [Arabidopsis thaliana]
DDX51 [Homo sapiens]
ZK686.2 [Caenorhabditis elegans]
C24H12.4 [Caenorhabditis elegans]
DDX56, isoform 1 [Homo sapiens]
UMAG_03892 [Ustilago maydis 521]
sr14789 [Sporisorium reilianum SRZ2]
UHO2_04817 [Ustilago hordei]
DBP9 [Cryptococcus neoformans var. grubii H99]
Dbp9 [Schizosaccharomyces pombe]
dbp-9 [Neurospora crassa OR74A]
DBP9 [Saccharomyces cerevisiae S288C]
ddx56 [Dictyostelium discoideum AX4]
AT4G34910 [Arabidopsis thaliana]
F55F8.2 [Caenorhabditis elegans]
DDX24 [Homo sapiens]
ddx24 [Dictyostelium discoideum AX4]
AT3G16840 [Arabidopsis thaliana]
UMAG_00242 [Ustilago maydis 521]
sr11594 [Sporisorium reilianum SRZ2]
UHO2_01096 [Ustilago hordei]
MAK5 [Cryptococcus neoformans var. grubii H99]
MAK5 [Saccharomyces cerevisiae S288C]
Mak5 [Schizosaccharomyces pombe]
mak-5 [Neurospora crassa OR74A]
UMAG_05214 [Ustilago maydis 521]
UHO2_07326 [Ustilago hordei]
sr13122 [Sporisorium reilianum SRZ2]
RRP3 [Cryptococcus neoformans var. grubii H99]
Rrp3 [Schizosaccharomyces pombe]
rrp-3 [Neurospora crassa OR74A]
RRP3 [Saccharomyces cerevisiae S288C]
ddx47 [Dictyostelium discoideum AX4]
T26G10.1 [Caenorhabditis elegans]
DDX47, isoform 1 [Homo sapiens]
AT5G60990 [Arabidopsis thaliana]
UMAG_10241 [Ustilago maydis 521]
sr10478 [Sporisorium reilianum SRZ2]
UHO2_01725 [Ustilago hordei]
DBP8 [Cryptococcus neoformans var. grubii H99]
DBP8 [Saccharomyces cerevisiae S288C]
dbp-8 [Neurospora crassa OR74A]
Dbp8 [Schizosaccharomyces pombe]
H20J04.4 [Caenorhabditis elegans]
DDX49 [Homo sapiens]
RH36 [Arabidopsis thaliana]
ddx49 [Dictyostelium discoideum AX4]
UMAG_03170 [Ustilago maydis 521]
UHO2_04110 [Ustilago hordei]
sr14213 [Sporisorium reilianum SRZ2]
DRS1 [Cryptococcus neoformans var. grubii H99]
Ddx27 [Schizosaccharomyces pombe]
drs-1 [Neurospora crassa OR74A]
DRS1 [Saccharomyces cerevisiae S288C]
DDX27, isoform 1 [Homo sapiens]
ddx-27 [Caenorhabditis elegans]
AT4G16630 [Arabidopsis thaliana]
ddx27 [Dictyostelium discoideum AX4]

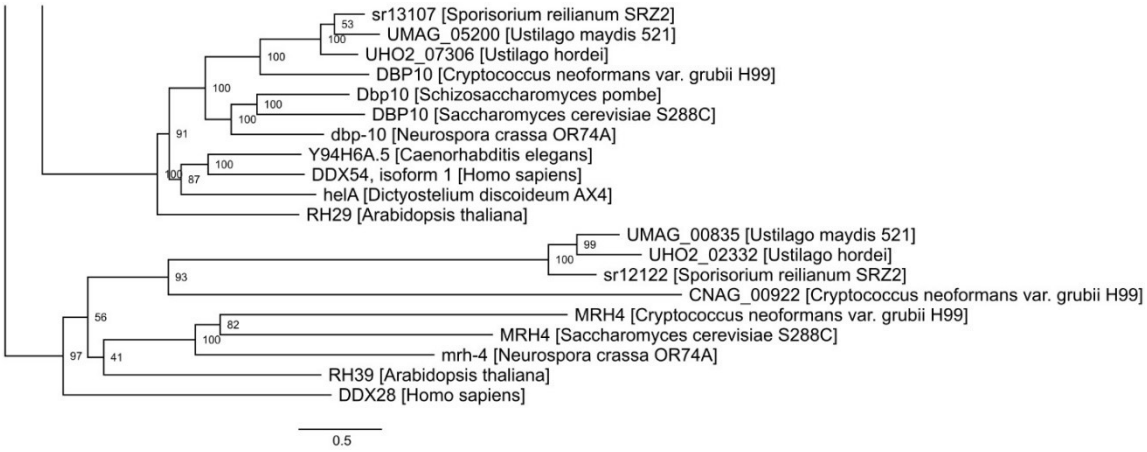

Figure S4.2. The original maximum likelihood phylogenetic tree of SF2 DEADbox RNA helicases. The phylogenetic tree was created with orthologs from *U. maydis*, *S. reilianum*, *U. hordei*, *C. neoformans*, *S. cerevisiae*, *S. pombe*, *N. crassa*, *A. thaliana*, *C. elegans*, *D. discoideum*, and *H. sapiens* using W-IQ-Tree multicore version 1.6.12 with default settings (Trifinopoulos et al. 2016), 1000 ultrafast bootstrap alignments, and approximate Bayes test. The tree was visualized with FigTree v1.4.4 (http://tree.bio.ed.ac.uk/software/figtree/), rooted at the midpoint, and the bootstrap value is indicated for each node. The scale bar indicates the expected number of substitutions per amino acid.

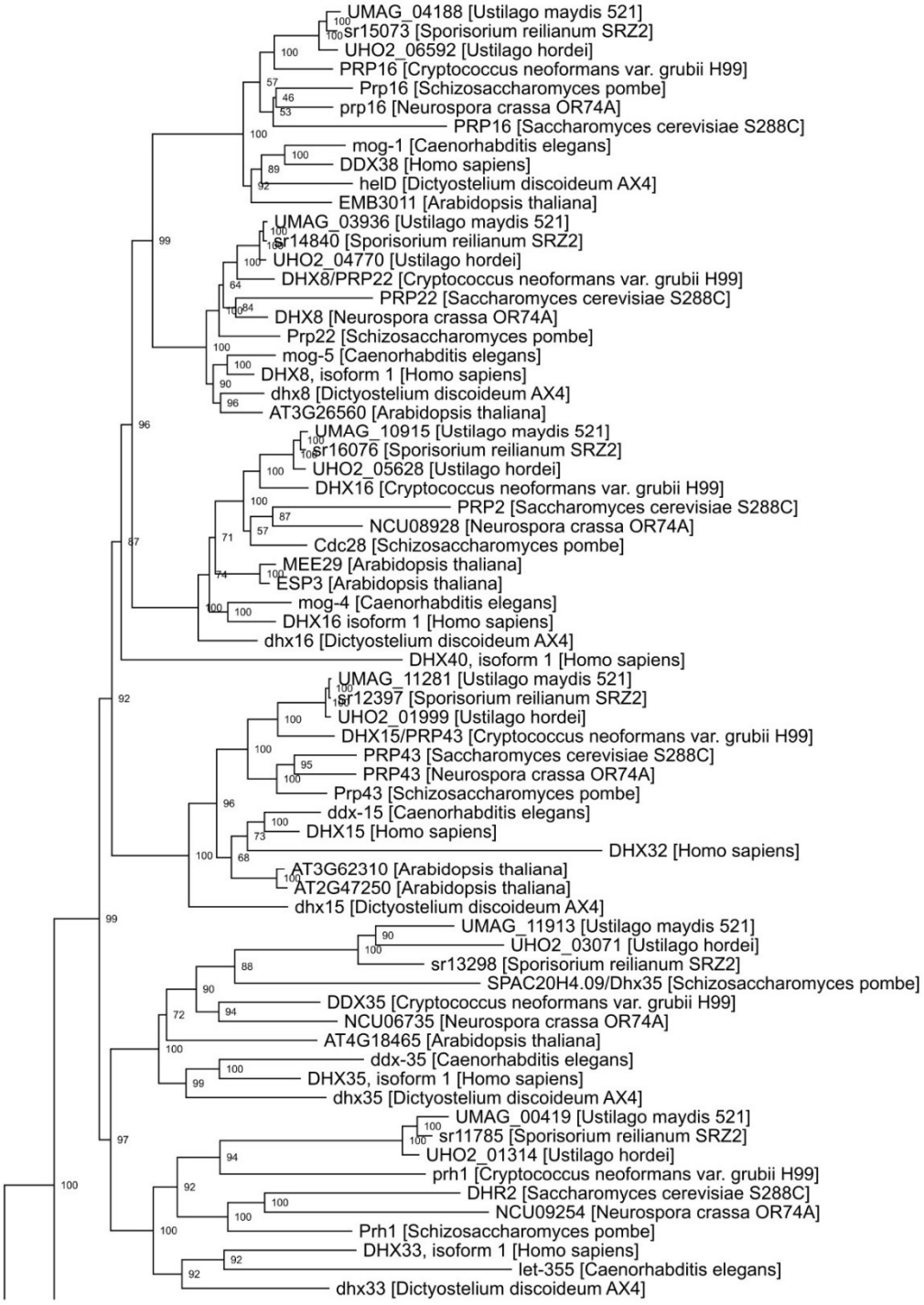
UMAG_04188 [Ustilago maydis 521]
sr15073 [Sporisorium reilianum SRZ2]
UHO2_06592 [Ustilago hordei]
PRP16 [Cryptococcus neoformans var. grubii H99]
Prp16 [Schizosaccharomyces pombe]
prp16 [Neurospora crassa OR74A]
PRP16 [Saccharomyces cerevisiae S288C]
mog-1 [Caenorhabditis elegans]
DDX38 [Homo sapiens]
helD [Dictyostelium discoideum AX4]
EMB3011 [Arabidopsis thaliana]
UMAG_03936 [Ustilago maydis 521]
sr14840 [Sporisorium reilianum SRZ2]
UHO2_04770 [Ustilago hordei]
DHX8/PRP22 [Cryptococcus neoformans var. grubii H99]
PRP22 [Saccharomyces cerevisiae S288C]
DHX8 [Neurospora crassa OR74A]
Prp22 [Schizosaccharomyces pombe]
mog-5 [Caenorhabditis elegans]
DHX8, isoform 1 [Homo sapiens]
dhx8 [Dictyostelium discoideum AX4]
AT3G26560 [Arabidopsis thaliana]
UMAG_10915 [Ustilago maydis 521]
sr16076 [Sporisorium reilianum SRZ2]
UHO2_05628 [Ustilago hordei]
DHX16 [Cryptococcus neoformans var. grubii H99]
PRP2 [Saccharomyces cerevisiae S288C]
NCU08928 [Neurospora crassa OR74A]
Cdc28 [Schizosaccharomyces pombe]
MEE29 [Arabidopsis thaliana]
ESP3 [Arabidopsis thaliana]
mog-4 [Caenorhabditis elegans]
DHX16 isoform 1 [Homo sapiens]
dhx16 [Dictyostelium discoideum AX4]
DHX40, isoform 1 [Homo sapiens]
UMAG_11281 [Ustilago maydis 521]
sr12397 [Sporisorium reilianum SRZ2]
UHO2_01999 [Ustilago hordei]
DHX15/PRP43 [Cryptococcus neoformans var. grubii H99]
PRP43 [Saccharomyces cerevisiae S288C]
PRP43 [Neurospora crassa OR74A]
Prp43 [Schizosaccharomyces pombe]
ddx-15 [Caenorhabditis elegans]
DHX15 [Homo sapiens]
DHX32 [Homo sapiens]
AT3G62310 [Arabidopsis thaliana]
AT2G47250 [Arabidopsis thaliana]
dhx15 [Dictyostelium discoideum AX4]
UMAG_11913 [Ustilago maydis 521]
UHO2_03071 [Ustilago hordei]
sr13298 [Sporisorium reilianum SRZ2]
SPAC20H4.09/Dhx35 [Schizosaccharomyces pombe]
DDX35 [Cryptococcus neoformans var. grubii H99]
NCU06735 [Neurospora crassa OR74A]
AT4G18465 [Arabidopsis thaliana]
ddx-35 [Caenorhabditis elegans]
DHX35, isoform 1 [Homo sapiens]
dhx35 [Dictyostelium discoideum AX4]
UMAG_00419 [Ustilago maydis 521]
sr11785 [Sporisorium reilianum SRZ2]
UHO2_01314 [Ustilago hordei]
prh1 [Cryptococcus neoformans var. grubii H99]
DHR2 [Saccharomyces cerevisiae S288C]
NCU09254 [Neurospora crassa OR74A]
Prh1 [Schizosaccharomyces pombe]
DHX33, isoform 1 [Homo sapiens]
let-355 [Caenorhabditis elegans]
dhx33 [Dictyostelium discoideum AX4]

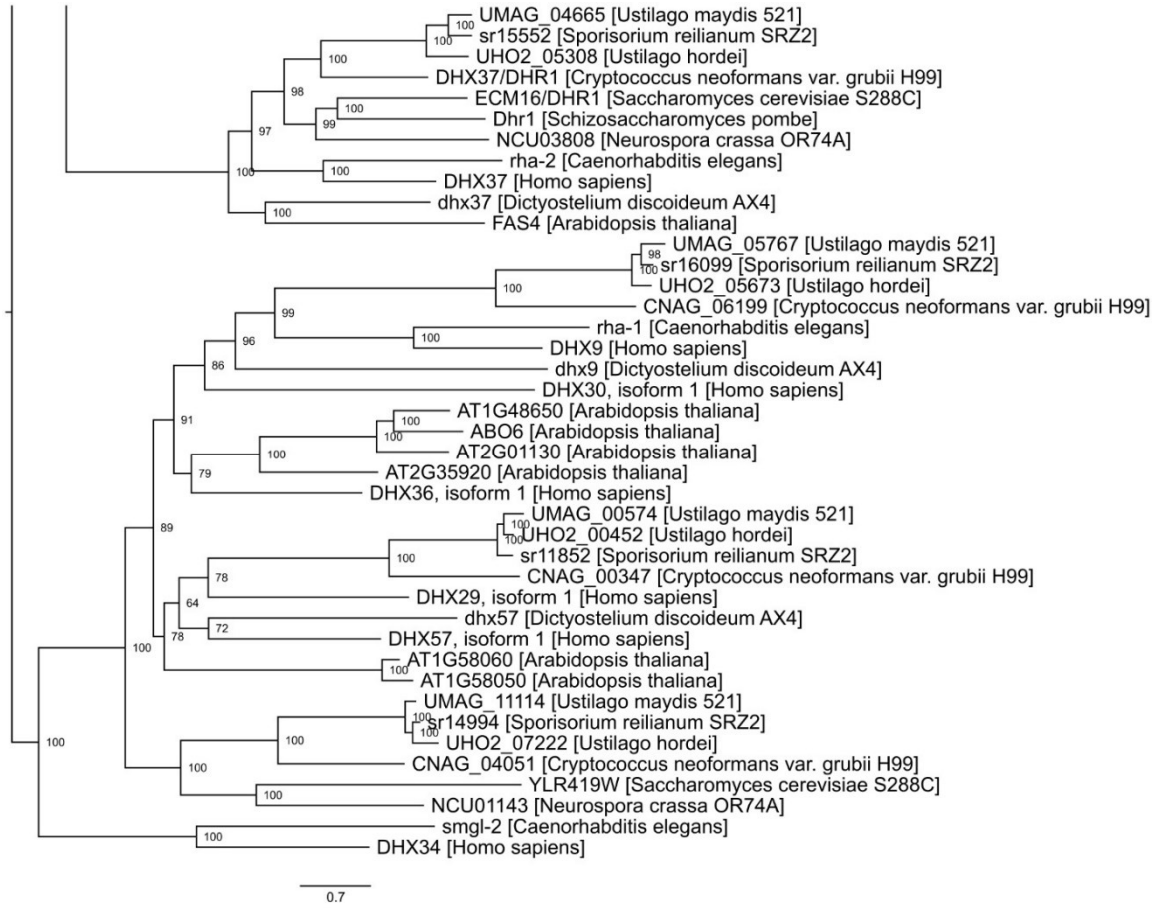

Figure S4.3. The original maximum likelihood phylogenetic tree of SF2 DEAH RNA helicases. The phylogenetic tree was created with orthologs from *U. maydis*, *S. reilianum*, *U. hordei*, *C. neoformans*, *S. cerevisiae*, *S. pombe*, *N. crassa*, *A. thaliana*, *C. elegans*, *D. discoideum*, and *H. sapiens* using W-IQ-Tree multicore version 1.6.12 with default settings (Trifinopoulos et al. 2016), 1000 ultrafast bootstrap alignments, and approximate Bayes test. The tree was visualized with FigTree v1.4.4 (http://tree.bio.ed.ac.uk/software/figtree/), rooted at the midpoint, and the bootstrap value is indicated for each node. The scale bar indicates the expected number of substitutions per amino acid.

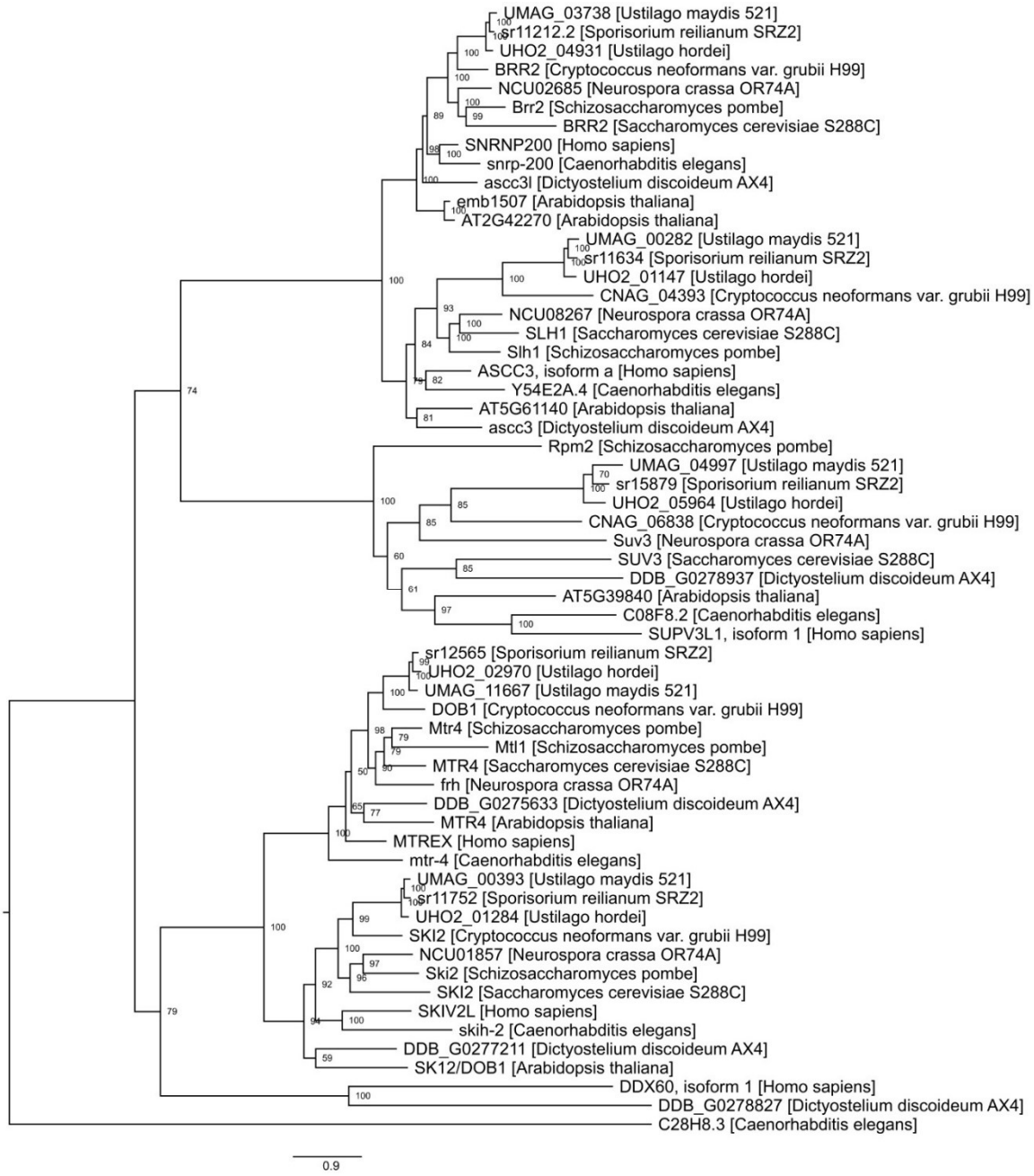

Figure S4.4. The original maximum likelihood phylogenetic tree of SF2 Ski2-like RNA helicases. The phylogenetic tree was created with orthologs from *U. maydis*, *S. reilianum*, *U. hordei*, *C. neoformans*, *S. cerevisiae*, *S. pombe*, *N. crassa*, *A. thaliana*, *C. elegans*, *D. discoideum*, and *H. sapiens* using W-IQ-Tree multicore version 1.6.12 with default settings (Trifinopoulos et al. 2016), 1000 ultrafast bootstrap alignments, and approximate Bayes test. The tree was visualized with FigTree v1.4.4 (http://tree.bio.ed.ac.uk/software/figtree/), rooted at the midpoint, and the bootstrap value is indicated for each node. The scale bar indicates the expected number of substitutions per amino acid.

REFERENCES

Adhvaryu K, Firoozi G, Motavaze K, Lakin-Thomas P (2016) PRD-1, a Component of the Circadian System of *Neurospora crassa*, Is a Member of the DEAD-box RNA Helicase Family. Journal of Biological Rhythms 31: 258–271. doi:10.1177/0748730416639717.

Aiello U, Challal D, Wentzinger G, Lengronne A, Appanah R, Pasero P, Palancade B, Libri D (2022) Sen1 is a key regulator of transcription-driven conflicts. Molecular Cell 82: 2952–2966.e2956. doi:https://doi.org/10.1016/j.molcel.2022.06.021.

Alexandrov A, Colognori D, Steitz JA (2011) Human eIF4AIII interacts with an eIF4G-like partner, NOM1, revealing an evolutionarily conserved function outside the exon junction complex. Genes & Development 25: 1078–1090.

Anderson JSJ, Parker R (1998) The 3′ to 5′ degradation of yeast mRNAs is a general mechanism for mRNA turnover that requires the SKI2 DEVH box protein and 3′ to 5′ exonucleases of the exosome complex. The EMBO Journal 17: 1497–1506.

Andreou AZ (2021) DDX41: a multifunctional DEAD-box protein involved in pre-mRNA splicing and innate immunity. Biological Chemistry 402: 645–651. doi:doi:10.1515/hsz-2020-0367.

Aquino GRR, Hackert P, Krogh N, Pan KT, Jaafar M, Henras AK, Nielsen H, Urlaub H, Bohnsack KE, Bohnsack MT (2021) The RNA helicase Dbp7 promotes domain V/VI compaction and stabilization of inter-domain interactions during early 60S assembly. Nature Communications 12: 6152. doi:10.1038/s41467-021-26208-9.

Aryanpur PP, Mittelmeier TM, Bolger TA (2022) The RNA Helicase Ded1 Regulates Translation and Granule Formation during Multiple Phases of Cellular Stress Responses. Molecular and Cellular Biology 42: e00244-00221. doi:10.1128/MCB.00244-21.

Aryanpur PP, Regan CA, Collins JM, Mittelmeier TM, Renner DM, Vergara AM, Brown NP, Bolger TA (2017) Gle1 regulates RNA binding of the DEAD-box helicase Ded1 in its complex role in translation initiation. Molecular and Cellular Biology 37: e00139-00117.

Awasthi S, Verma M, Mahesh A, K. Khan MI, Govindaraju G, Rajavelu A, Chavali PL, Chavali S, Dhayalan A (2018) DDX49 is an RNA helicase that affects translation by regulating mRNA export and the levels of pre-ribosomal RNA. Nucleic Acids Research 46: 6304–6317.

Balotf S, Tegg RS, Nichols DS, Wilson CR (2021) Spore Germination of the Obligate Biotroph Spongospora subterranea: Transcriptome Analysis Reveals Germination

Associated Genes. Frontiers in Microbiology 12: 691877. doi:10.3389/fmicb.2021.691877.

Banerjee S, Nagasawa Chloe K, Widen Steven G, Garcia-Blanco Mariano A (2024) Parsing the roles of DExD-box proteins DDX39A and DDX39B in alternative RNA splicing. Nucleic Acids Research: doi:10.1093/nar/gkae431.

Banuett F, Herskowitz I (1996) Discrete developmental stages during teliospore formation in the corn smut fungus, *Ustilago maydis*. Development 122: 2965–2976.

Beck ZT, Cloutier SC, Schipma MJ, Petell CJ, Kit W, Ma, Tran EJ (2014) Regulation of glucose-dependent gene expression by the RNA helicase Dbp2 in *Saccharomyces cerevisiae*. Genetics 198: 1001–1014. doi:10.1534/genetics.114.170019.

Bennett AH, O'Donohue M-F, Gundry SR, Chan AT, Widrick J, Draper I, Chakraborty A, Zhou Y, Zon LI, Gleizes P-E, Beggs AH, Gupta VA (2018) RNA helicase, DDX27 regulates skeletal muscle growth and regeneration by modulation of translational processes. PLOS Genetics 14: e1007226. doi:10.1371/journal.pgen.1007226.

Bernstein KA, Baserga SJ (2004) The small subunit processome is required for cell cycle progression at G1. Molecular Biology of the Cell 15: 5038–5046. doi:10.1091/mbc.e04-06-0515.

Bernstein KA, Granneman S, Lee AV, Manickam S, Baserga SJ (2006) Comprehensive mutational analysis of yeast DEXD/H box RNA helicases involved in large ribosomal subunit biogenesis. Molecular and Cellular Biology 26: 1195–1208.

Bleichert F, Baserga SJ (2007) The long unwinding road of RNA helicases. Molecular Cell 27: 339–352.

Bochman ML, Sabouri N, Zakian VA (2010) Unwinding the functions of the Pif1 family helicases. DNA Repair 9: 237–249. doi:https://doi.org/10.1016/j.dnarep.2010.01.008.

Bohnsack MT, Kos M, Tollervey D (2008) Quantitative analysis of snoRNA association with pre-ribosomes and release of snR30 by Rok1 helicase. EMBO Reports 9: 1230–1236.

Bond AT, Mangus DA, He F, Jacobson A (2001) Absence of Dbp2p alters both nonsense-mediated mRNA decay and rRNA processing. Molecular and Cellular Biology 21: 7366–7379.

Bourgeois CF, Mortreux F, Auboeuf D (2016) The multiple functions of RNA helicases as drivers and regulators of gene expression. Nature Reviews Molecular Cell Biology 17: 426.

Braga GUL, Rangel DEN, Fernandes ÉKK, Flint SD, Roberts DW (2015) Molecular and physiological effects of environmental UV radiation on fungal conidia. Current Genetics 61: 405–425. doi:10.1007/s00294-015-0483-0.

Brefort T, Doehlemann G, Mendoza-Mendoza A, Reissmann S, Djamei A, Kahmann R (2009) *Ustilago maydis* as a pathogen. Annual Review of Phytopathology 47: 423–445. doi:10.1146/annurev-phyto-080508-081923.

Burger F, Daugeron M-C, Linder P (2000) Dbp10p, a putative RNA helicase from Saccharomyces cerevisiae, is required for ribosome biogenesis. Nucleic Acids Research 28: 2315–2323. doi:10.1093/nar/28.12.2315.

Byrd AK, Raney KD (2012) Superfamily 2 helicases. Frontiers in Bioscience-Landmark 17: 2070–2088. doi:10.2741/4038.

Cai W, Xiong Chen Z, Rane G, Satendra Singh S, Choo Ze, Wang C, Yuan Y, Zea Tan T, Arfuso F, Yap CT, Pongor LS, Yang H, Lee MB, Cher Goh B, Sethi G, Benoukraf T, Tergaonkar V, Prem Kumar A (2017) Wanted DEAD/H or Alive: Helicases Winding Up in Cancers. Journal of the National Cancer Institute 109: doi:10.1093/jnci/djw278.

Caltrider PG, Gottlieb D (1963) Respiratory activity and enzymes for glucose catabolism in fungus spores. Phytopathology 53: 1021–1030.

Caltrider PG, Gottlieb D (1966) Effect of sugars on germination and metabolism of teliospores of *Ustilago maydis*. Phytopathology 56: 479–484.

Carroll JS, Munchel SE, Weis K (2011) The DExD/H box ATPase Dhh1 functions in translational repression, mRNA decay, and processing body dynamics. Journal of Cell Biology 194: 527–537.

Chen N, Yang S, You D, Shen J, Ruan B, Wu M, Zhang J, Luo X, Tang H (2023) Systematic genetic modifications of cell wall biosynthesis enhanced the secretion and surface-display of polysaccharide degrading enzymes in Saccharomyces cerevisiae. Metabolic Engineering 77: 273–282. doi:https://doi.org/10.1016/j.ymben.2023.04.011.

Cheng P, He Q, He Q, Wang L, Liu Y (2005) Regulation of the *Neurospora* circadian clock by an RNA helicase. Genes & Development 19: 234–241. doi:10.1101/gad.1266805.

Choe J, Ryu I, Park OH, Park J, Cho H, Yoo JS, Chi SW, Kim MK, Song HK, Kim YK (2014) eIF4AIII enhances translation of nuclear cap-binding complex–bound mRNAs by promoting disruption of secondary structures in 5′ UTR. Proceedings of the National Academy of Sciences 111: E4577–E4586.

Choque E, Marcellin M, Burlet-Schiltz O, Gadal O, Dez C (2011) The nucleolar protein Nop19p interacts preferentially with Utp25p and Dhr2p and is essential for the production of the 40S ribosomal subunit in *Saccharomyces cerevisiae*. RNA Biology 8: 1158–1172.

Choudhury P, Hackert P, Memet I, Sloan KE, Bohnsack MT (2019) The human RNA helicase DHX37 is required for release of the U3 snoRNP from pre-ribosomal particles. RNA Biology 16: 54–68.

Choudhury P, Kretschmer J, Hackert P, Bohnsack KE, Bohnsack MT (2021) The DExD box ATPase DDX55 is recruited to domain IV of the 28S ribosomal RNA by its C-terminal region. RNA Biology 18: 1124–1135. doi:10.1080/15476286.2020.1829366.

Christensen JJ (1963) Corn smut caused by *Ustilago maydis* (Monograph No. 2). American Phytopathological Society, 41 pp.

Chu Y-D, Chen H-K, Huang T, Chan S-P (2016) A novel function for the DEAD-box RNA helicase DDX-23 in primary microRNA processing in *Caenorhabditis elegans*. Developmental Biology 409: 459–472. doi:https://doi.org/10.1016/j.ydbio.2015.11.011.

Cloutier SC, Ma WK, Nguyen LT, Tran EJ (2012) The DEAD-box RNA helicase Dbp2 connects RNA quality control with repression of aberrant transcription. Journal of Biological Chemistry 287: 26155–26166.

Colley A, Beggs JD, Tollervey D, Lafontaine DL (2000) Dhr1p, a putative DEAH-box RNA helicase, is associated with the box C+D snoRNP U3. Molecular and Cellular Biology 20: 7238–7246.

Cordin O, Beggs JD (2013) RNA helicases in splicing. RNA Biology 10: 83–95. doi:10.4161/rna.22547.

Cordin O, Hahn D, Beggs JD (2012) Structure, function and regulation of spliceosomal RNA helicases. Current Opinion in Cell Biology 24: 431–438. doi:https://doi.org/10.1016/j.ceb.2012.03.004.

Cristini A, Groh M, Kristiansen MS, Gromak N (2018) RNA/DNA hybrid interactome identifies DXH9 as a molecular player in transcriptional termination and R-loop-associated DNA damage. Cell Reports 23: 1891–1905.

Daugeron M-C, Kressler D, Linder P (2001) Dbp9p, a putative ATP-dependent RNA helicase involved in 60S-ribosomal-subunit biogenesis, functionally interacts with Dbp6p. RNA 7: 1317–1334.

Daugeron M-C, Linder P (2001) Characterization and mutational analysis of yeast Dbp8p, a putative RNA helicase involved in ribosome biogenesis. Nucleic Acids Research 29: 1144–1155.

Daugeron M-C, Prouteau M, Lacroute F, Séraphin B (2011) The highly conserved eukaryotic DRG factors are required for efficient translation in a manner redundant with the putative RNA helicase Slh1. Nucleic Acids Research 39: 2221–2233.

De Bortoli F, Espinosa S, Zhao R (2021) DEAH-Box RNA Helicases in Pre-mRNA Splicing. Trends in Biochemical Sciences 46: 225–238. doi:10.1016/j.tibs.2020.10.006.

de la Cruz J, Kressler D, Rojo M, Tollervey D, Linder P (1998a) Spb4p, an essential putative RNA helicase, is required for a late step in the assembly of 60S ribosomal subunits in *Saccharomyces cerevisiae*. RNA 4: 1268–1281.

de la Cruz J, Kressler D, Tollervey D, Linder P (1998b) Dob1p (Mtr4p) is a putative ATP-dependent RNA helicase required for the 3′ end formation of 5.8 S rRNA in *Saccharomyces cerevisiae*. The EMBO Journal 17: 1128–1140.

de Planell-Saguer M, Schroeder DG, Rodicio MC, Cox GA, Mourelatos Z (2009) Biochemical and genetic evidence for a role of IGHMBP2 in the translational machinery. Human Molecular Genetics 18: 2115–2126.

Dean R, Van Kan JA, Pretorius ZA, Hammond-Kosack KE, Di Pietro A, Spanu PD, Rudd JJ, Dickman M, Kahmann R, Ellis J, Foster GD (2012) The Top 10 fungal pathogens in molecular plant pathology. Molecular Plant Pathology 13: 414–430. doi:10.1111/j.1364-3703.2011.00783.x.

Decker CJ, Parker R (1994) Mechanisms of mRNA degradation in eukaryotes. Trends in Biochemical Sciences 19: 336–340.

Delaney JR, Ahmed U, Chou A, Sim S, Carr D, Murakami CJ, Schleit J, Sutphin GL, An EH, Castanza A, Fletcher M, Higgins S, Jelic M, Klum S, Muller B, Peng ZJ, Rai D, Ros V, Singh M, Wende HV, Kennedy BK, Kaeberlein M (2013) Stress profiling of longevity mutants identifies Afg3 as a mitochondrial determinant of cytoplasmic mRNA translation and aging. Aging Cell 12: 156–166. doi:https://doi.org/10.1111/acel.12032.

Desroches Altamirano C, Kang M-K, Jordan MA, Borianne T, Dilmen I, Gnädig M, von Appen A, Honigmann A, Franzmann TM, Alberti S (2024) eIF4F is a thermo-sensing regulatory node in the translational heat shock response. Molecular Cell 84: 1727–1741.e1712. doi:10.1016/j.molcel.2024.02.038.

Donaldson ME, Ostrowski LA, Goulet KM, Saville BJ (2017) Transcriptome analysis of smut fungi reveals widespread intergenic transcription and conserved antisense transcript expression. BMC Genomics 18: 340. doi:10.1186/s12864-017-3720-8.

Donaldson ME, Saville BJ (2013) *Ustilago maydis* natural antisense transcript expression alters mRNA stability and pathogenesis. Molecular Microbiology 89: 29–51. doi:10.1111/mmi.12254.

Dosil M, Bustelo XR (2004) Functional Characterization of Pwp2, a WD Family Protein Essential for the Assembly of the 90 S Pre-ribosomal Particle. Journal of Biological Chemistry 279: 37385–37397. doi:10.1074/jbc.M404909200.

Dziembowski A, Piwowarski J, Hoser R, Minczuk M, Dmochowska A, Siep M, van der Spek H, Grivell L, Stepien PP (2003) The Yeast Mitochondrial Degradosome: Its Composition, Interplay Between RNA Helicase And RNase Activities And The Role In Mitochondrial RNA Metabolism. Journal of Biological Chemistry 278: 1603–1611.

Edgar RC (2004) MUSCLE: multiple sequence alignment with high accuracy and high throughput. Nucleic Acids Research 32: 1792–1797. doi:10.1093/nar/gkh340.

Fairman-Williams ME, Guenther U-P, Jankowsky E (2010) SF1 and SF2 helicases: family matters. Current Opinion in Structural Biology 20: 313–324.

Feldbrügge M, Zarnack K, Vollmeister E, Baumann S, Koepke J, König J, Münsterkötter M, Mannhaupt G (2008) The posttranscriptional machinery of *Ustilago maydis*. Fungal Genetics and Biology 45: S40–S46.

Feng B, Wang X, Qiu D, Sun H, Deng J, Tan Y, Ji K, Xu S, Zhang S, Tang C (2024) DDX18 Facilitates the Tumorigenesis of Lung Adenocarcinoma by Promoting Cell Cycle Progression through the Upregulation of CDK4. International Journal of Molecular Sciences 25: 4953.

Fischer N, Weis K (2002) The DEAD box protein Dhh1 stimulates the decapping enzyme Dcp1. The EMBO Journal 21: 2788–2797.

Forbes KC, Humphrey T, Enoch T (1998) Suppressors of Cdc25p Overexpression Identify Two Pathways That Influence the G2/M Checkpoint in Fission Yeast. Genetics 150: 1361–1375. doi:10.1093/genetics/150.4.1361.

Fuchs U, Hause G, Schuchardt I, Steinberg G (2006) Endocytosis is essential for pathogenic development in the corn smut fungus *Ustilago maydis*. The Plant Cell 18: 2066–2081. doi:10.1105/tpc.105.039388.

Fuchs U, Steinberg G (2005) Endocytosis in the plant-pathogenic fungus Ustilago maydis. Protoplasma 226: 75–80. doi:10.1007/s00709-005-0109-3.

Fukawa T, Ono M, Matsuo T, Uehara H, Miki T, Nakamura Y, Kanayama H-o, Katagiri T (2012) DDX31 regulates the p53-HDM2 pathway and rRNA gene transcription through its interaction with NPM1 in renal cell carcinomas. Cancer Research 72: 5867–5877.

Ganesan R, Mangkalaphiban K, Baker RE, He F, Jacobson A (2022) Ribosome-bound Upf1 forms distinct 80S complexes and conducts mRNA surveillance. RNA 28: 1621–1642. doi:10.1261/rna.079416.122.

García-Gómez JJ, Lebaron S, Froment C, Monsarrat B, Henry Y, de La Cruz J (2011) Dynamics of the putative RNA helicase Spb4 during ribosome assembly in *Saccharomyces cerevisiae*. Molecular and Cellular Biology 31: 4156–4164.

Geissler R, Golbik RP, Behrens S-E (2012) The DEAD-box helicase DDX3 supports the assembly of functional 80S ribosomes. Nucleic Acids Research 40: 4998–5011.

Giaever G, Chu AM, Ni L, Connelly C, Riles L, Véronneau S, Dow S, Lucau-Danila A, Anderson K, André B, Arkin AP, Astromoff A, El Bakkoury M, Bangham R, Benito R, Brachat S, Campanaro S, Curtiss M, Davis K, Deutschbauer A, Entian K-D, Flaherty P, Foury F, Garfinkel DJ, Gerstein M, Gotte D, Güldener U, Hegemann JH, Hempel S, Herman Z, Jaramillo DF, Kelly DE, Kelly SL, Kötter P, LaBonte D, Lamb DC, Lan N, Liang H, Liao H, Liu L, Luo C, Lussier M, Mao R, Menard P, Ooi SL, Revuelta JL, Roberts CJ, Rose M, Ross-Macdonald P, Scherens B, Schimmack G, Shafer B, Shoemaker DD, Sookhai-Mahadeo S, Storms RK, Strathern JN, Valle G, Voet M, Volckaert G, Wang C-y, Ward TR, Wilhelmy J, Winzeler EA, Yang Y, Yen G, Youngman E, Yu K, Bussey H, Boeke JD, Snyder M, Philippsen P, Davis RW, Johnston M (2002) Functional profiling of the Saccharomyces cerevisiae genome. Nature 418: 387–391. doi:10.1038/nature00935.

Giannini M, Porrua O (2024) Senataxin: A key actor in RNA metabolism, genome integrity and neurodegeneration. Biochimie 217: 10–19. doi:https://doi.org/10.1016/j.biochi.2023.08.001.

Gilhooly NS, Gwynn EJ, Dillingham MS (2013) Superfamily 1 helicases. Frontiers in Bioscience-Scholar 5: 206–216. doi:10.2741/s367.

Gorbalenya AE, Koonin EV (1993) Helicases: amino acid sequence comparisons and structure-function relationships. Current Opinion in Structural Biology 3: 419–429.

Gowravaram M, Bonneau F, Kanaan J, Maciej VD, Fiorini F, Raj S, Croquette V, Le Hir H, Chakrabarti S (2018) A conserved structural element in the RNA helicase UPF1 regulates its catalytic activity in an isoform-specific manner. Nucleic Acids Research 46: 2648–2659. doi:10.1093/nar/gky040.

Granneman S, Lin C, Champion EA, Nandineni MR, Zorca C, Baserga SJ (2006) The nucleolar protein Esf2 interacts directly with the DExD/H box RNA helicase, Dbp8, to stimulate ATP hydrolysis. Nucleic Acids Research 34: 3189–3199.

Groh M, Albulescu LO, Cristini A, Gromak N (2017) Senataxin: genome guardian at the interface of transcription and neurodegeneration. Journal of Molecular Biology 429: 3181–3195.

Gross T, Siepmann A, Sturm D, Windgassen M, Scarcelli JJ, Seedorf M, Cole CN, Krebber H (2007) The DEAD-box RNA helicase Dbp5 functions in translation termination. Science 315: 646–649.

Guenther U-P, Handoko L, Laggerbauer B, Jablonka S, Chari A, Alzheimer M, Ohmer J, Plöttner O, Gehring N, Sickmann A (2009) IGHMBP2 is a ribosome-associated helicase inactive in the neuromuscular disorder distal SMA type 1 (DSMA1). Human Molecular Genetics 18: 1288–1300.

Guo XE, Chen C-F, Wang DD-H, Modrek AS, Phan VH, Lee W-H, Chen P-L (2011) Uncoupling the roles of the SUV3 helicase in maintenance of mitochondrial genome stability and RNA degradation. Journal of Biological Chemistry 286: 38783–38794.

Gupta P, Li Y-R (2018) Upf proteins: highly conserved factors involved in nonsense mRNA mediated decay. Molecular Biology Reports 45: 39–55. doi:10.1007/s11033-017-4139-7.

Hartman TR, Qian S, Bolinger C, Fernandez S, Schoenberg DR, Boris-Lawrie K (2006) RNA helicase A is necessary for translation of selected messenger RNAs. Nature Structural & Molecular Biology 13: 509–516.

Hazelbaker DZ, Marquardt S, Wlotzka W, Buratowski S (2013) Kinetic competition between RNA Polymerase II and Sen1-dependent transcription termination. Molecular Cell 49: 55–66.

He Y, Andersen GR, Nielsen KH (2010) Structural basis for the function of DEAH helicases. EMBO Reports 11: 180–186. doi:https://doi.org/10.1038/embor.2010.11.

He Y, Staley JP, Andersen GR, Nielsen KH (2017) Structure of the DEAH/RHA ATPase Prp43p bound to RNA implicates a pair of hairpins and motif Va in translocation along RNA. RNA 23: 1110–1124. doi:10.1261/rna.060954.117.

Hegazy YA, Fernando CM, Tran EJ (2020) The balancing act of R-loop biology: The good, the bad, and the ugly. Journal of Biological Chemistry 295: 905–913. doi:10.1074/jbc.REV119.011353.

Hilliker A, Gao Z, Jankowsky E, Parker R (2011) The DEAD-box protein Ded1 modulates translation by the formation and resolution of an eIF4F-mRNA complex. Molecular Cell 43: 962–972.

Hogg JR, Goff SP (2010) Upf1 senses 3′ UTR length to potentiate mRNA decay. Cell 143: 379–389.

Hönig A, Auboeuf D, Parker MM, O'Malley BW, Berget SM (2002) Regulation of alternative splicing by the ATP-dependent DEAD-box RNA helicase p72. Molecular and Cellular Biology 22: 5698–5707.

Houseley J, Tollervey D (2009) The many pathways of RNA degradation. Cell 136: 763–776.

Huh W-K, Falvo JV, Gerke LC, Carroll AS, Howson RW, Weissman JS, O'Shea EK (2003) Global analysis of protein localization in budding yeast. Nature 425: 686–691. doi:10.1038/nature02026.

Iglesias N, Stutz F (2008) Regulation of mRNP dynamics along the export pathway. FEBS Letters 582: 1987–1996. doi:https://doi.org/10.1016/j.febslet.2008.03.038.

Imamachi N, Tani H, Akimitsu N (2012) Up-frameshift protein 1 (UPF1): multitalented entertainer in RNA decay. Drug Discoveries & Therapeutics 6: 55–61.

Irion U, Leptin M, Siller K, Fuerstenberg S, Cai Y, Doe CQ, Chia W, Yang X (2004) Abstrakt, a DEAD Box Protein, Regulates Insc Levels and Asymmetric Division of Neural and Mesodermal Progenitors. Current Biology 14: 138–144. doi:10.1016/j.cub.2004.01.002.

Itani OA, Zhong X, Tang X, Scott BA, Yan JY, Flibotte S, Lim Y, Hsieh AC, Bruce JE, Van Gilst M, Crowder CM (2021) Coordinate Regulation of Ribosome and tRNA Biogenesis Controls Hypoxic Injury and Translation. Current Biology 31: 128–137.e125. doi:https://doi.org/10.1016/j.cub.2020.10.001.

Jalal C, Uhlmann-Schiffler H, Stahl H (2007) Redundant role of DEAD box proteins p68 (Ddx5) and p72/p82 (Ddx17) in ribosome biogenesis and cell proliferation. Nucleic Acids Research 35: 3590–3601.

Jamieson DJ, Rahe B, Pringle J, Beggs JD (1991) A suppressor of a yeast splicing mutation (prp8-l) encodes a putative ATP-dependent RNA helicase. Nature 349: 715–717.

Jankowsky E (2011) RNA helicases at work: binding and rearranging. Trends in Biochemical Sciences 36: 19–29.

Jeon S, Kim J (2010) Upstream open reading frames regulate the cell cycle-dependent expression of the RNA helicase Rok1 in Saccharomyces cerevisiae. FEBS Letters 584: 4593–4598. doi:https://doi.org/10.1016/j.febslet.2010.10.019.

Jia H, Wang X, Liu F, Guenther U-P, Srinivasan S, Anderson JT, Jankowsky E (2011) The RNA helicase Mtr4p modulates polyadenylation in the TRAMP complex. Cell 145: 890–901.

Johnson SJ, Jackson RN (2013) Ski2-like RNA helicase structures: common themes and complex assemblies. RNA Biology 10: 33–43.

Kahmann R, Kämper J (2004) Ustilago maydis: how its biology relates to pathogenic development. New Phytologist 164: 31–42. doi:https://doi.org/10.1111/j.1469-8137.2004.01156.x.

Kämper J, Kahmann R, Bolker M, Ma LJ, Brefort T, Saville BJ, Banuett F, Kronstad JW, Gold SE, Muller O, Perlin MH, Wosten HA, de Vries R, Ruiz-Herrera J, Reynaga-Pena CG, Snetselaar K, McCann M, Perez-Martin J, Feldbrugge M, Basse CW, Steinberg G, Ibeas JI, Holloman W, Guzman P, Farman M, Stajich JE, Sentandreu R, Gonzalez-Prieto JM, Kennell JC, Molina L, Schirawski J, Mendoza-Mendoza A, Greilinger D, Munch K, Rossel N, Scherer M, Vranes M, Ladendorf O, Vincon V, Fuchs U, Sandrock B, Meng S, Ho EC, Cahill MJ, Boyce KJ, Klose J, Klosterman SJ, Deelstra HJ, Ortiz-Castellanos L, Li W, Sanchez-Alonso P, Schreier PH, Hauser-Hahn I, Vaupel M, Koopmann E, Friedrich G, Voss H, Schluter T, Margolis J, Platt D, Swimmer C, Gnirke A, Chen F, Vysotskaia V, Mannhaupt G, Guldener U, Munsterkotter M, Haase D, Oesterheld M, Mewes HW, Mauceli EW, DeCaprio D, Wade CM, Butler J, Young S, Jaffe DB, Calvo S, Nusbaum C, Galagan J, Birren BW (2006) Insights from the genome of the biotrophic fungal plant pathogen *Ustilago maydis*. Nature 444: 97–101. doi:10.1038/nature05248.

Kanaan J, Raj S, Decourty L, Saveanu C, Croquette V, Le Hir H (2018) UPF1-like helicase grip on nucleic acids dictates processivity. Nature Communications 9: 3752. doi:10.1038/s41467-018-06313-y.

Kant P, Kant S, Gordon M, Shaked R, Barak S (2007) *STRESS RESPONSE SUPPRESSOR1* and *STRESS RESPONSE SUPPRESSOR2*, Two DEAD-Box RNA Helicases That Attenuate Arabidopsis Responses to Multiple Abiotic Stresses. Plant Physiology 145: 814–830. doi:10.1104/pp.107.099895.

Kellner M, Rohrmoser M, Forné I, Voss K, Burger K, Mühl B, Gruber-Eber A, Kremmer E, Imhof A, Eick D (2015) DEAD-box helicase DDX27 regulates 3′ end formation of ribosomal 47S RNA and stably associates with the PeBoW-complex. Experimental Cell Research 334: 146–159.

Khan A, Garbelli A, Grossi S, Florentin A, Batelli G, Acuna T, Zolla G, Kaye Y, Paul LK, Zhu J-K, Maga G, Grafi G, Barak S (2014) The Arabidopsis STRESS RESPONSE

SUPPRESSOR DEAD-box RNA helicases are nucleolar- and chromocenter-localized proteins that undergo stress-mediated relocalization and are involved in epigenetic gene silencing. The Plant Journal 79: 28–43. doi:https://doi.org/10.1111/tpj.12533.

Kim D-U, Hayles J, Kim D, Wood V, Park H-O, Won M, Yoo H-S, Duhig T, Nam M, Palmer G, Han S, Jeffery L, Baek S-T, Lee H, Shim YS, Lee M, Kim L, Heo K-S, Noh EJ, Lee A-R, Jang Y-J, Chung K-S, Choi S-J, Park J-Y, Park Y, Kim HM, Park S-K, Park H-J, Kang E-J, Kim HB, Kang H-S, Park H-M, Kim K, Song K, Song KB, Nurse P, Hoe K-L (2010) Analysis of a genome-wide set of gene deletions in the fission yeast *Schizosaccharomyces pombe*. Nature Biotechnology 28: 617–623. doi:10.1038/nbt.1628.

Konishi T, Uodome N, Sugimoto A (2008) The *Caenorhabditis elegans* DDX-23, a homolog of yeast splicing factor PRP28, is required for the sperm-oocyte switch and differentiation of various cell types. Developmental Dynamics 237: 2367–2377. doi:https://doi.org/10.1002/dvdy.21649.

Koš M, Tollervey D (2005) The putative RNA helicase Dbp4p is required for release of the U14 snoRNA from preribosomes in *Saccharomyces cerevisiae*. Molecular Cell 20: 53–64.

Kressler D, de la Cruz J, Rojo M, Linder P (1997) Fal1p is an essential DEAD-box protein involved in 40S-ribosomal-subunit biogenesis in *Saccharomyces cerevisiae*. Molecular and Cellular Biology 17: 7283–7294.

Kressler D, de la Cruz J, Rojo M, Linder P (1998) Dbp6p Is an Essential Putative ATP-Dependent RNA Helicase Required for 60S-Ribosomal-Subunit Assembly in *Saccharomyces cerevisiae*. Molecular and Cellular Biology 18: 1855–1865.

Krogan NJ, Peng W-T, Cagney G, Robinson MD, Haw R, Zhong G, Guo X, Zhang X, Canadien V, Richards DP, Beattie BK, Lalev A, Zhang W, Davierwala AP, Mnaimneh S, Starostine A, Tikuisis AP, Grigull J, Datta N, Bray JE, Hughes TR, Emili A, Greenblatt JF (2004) High-Definition Macromolecular Composition of Yeast RNA-Processing Complexes. Molecular Cell 13: 225–239. doi:10.1016/S1097-2765(04)00003-6.

Lanver D, Müller AN, Happel P, Schweizer G, Haas FB, Franitza M, Pellegrin C, Reissmann S, Altmüller J, Rensing SA (2018) The biotrophic development of Ustilago maydis studied by RNA-seq analysis. The Plant Cell 30: 300–323.

Lauinger L, Diernfellner A, Falk S, Brunner M (2014) The RNA helicase FRH is an ATP-dependent regulator of CK1a in the circadian clock of *Neurospora crassa*. Nature Communications 5: 3598. doi:10.1038/ncomms4598.

Lee C-G (2002) RH70, a bidirectional RNA helicase, co-purifies with U1snRNP. Journal of Biological Chemistry 277: 39679–39683.

Lee T, Pelletier J (2016) The biology of DHX9 and its potential as a therapeutic target. Oncotarget 7: 42716.

Leppek K, Das R, Barna M (2018) Functional 5' UTR mRNA structures in eukaryotic translation regulation and how to find them. Nature Reviews Molecular Cell Biology 19: 158–174. doi:10.1038/nrm.2017.103.

Li B, Li Y-M, He W-T, Chen H, Zhu H-W, Liu T, Zhang J-H, Song T-N, Zhou Y-L (2016) Knockdown of DDX46 inhibits proliferation and induces apoptosis in esophageal squamous cell carcinoma cells. Oncology Reports 36: 223–230. doi:10.3892/or.2016.4803.

Li C, Ma X, Ma L, Zhen S, Na Y, Zhang P, Zhu X (2022) The RNA helicase Ski2 in the fungal pathogen *Cryptococcus neoformans* highlights key roles in azoles resistance and stress tolerance. Medical Mycology 60: doi:10.1093/mmy/myac083.

Li Q, Imataka H, Morino S, Rogers GW, Richter-Cook NJ, Merrick WC, Sonenberg N (1999) Eukaryotic translation initiation factor 4AIII (eIF4AIII) is functionally distinct from eIF4AI and eIF4AII. Molecular and Cellular Biology 19: 7336–7346.

Li Y, Li H, Su N, Liu D, Luo R, Jin H (2018) Molecular cloning and functional characterization of duck DDX41. Developmental and Comparative Immunology 88: 183–189. doi:https://doi.org/10.1016/j.dci.2018.07.015.

Liang W-W, Cheng S-C (2015) A novel mechanism for Prp5 function in prespliceosome formation and proofreading the branch site sequence. Genes & Development 29: 81–93.

Lin W-L, Chen J-K, Wen X, He W, Zarceno GA, Chen Y, Chen S, Paull TT, Liu H-w (2022) DDX18 prevents R-loop-induced DNA damage and genome instability via PARP-1. Cell Reports 40: 111089. doi:https://doi.org/10.1016/j.celrep.2022.111089.

Linder P, Jankowsky E (2011) From unwinding to clamping—the DEAD box RNA helicase family. Nature Reviews Molecular Cell Biology 12: 505–516.

Liu J, Huang Y, Huang X, Li C, Ni Sw, Yu Y, Qin Q (2019) Grouper DDX41 exerts antiviral activity against fish iridovirus and nodavirus infection. Fish & Shellfish Immunology 91: 40–49. doi:https://doi.org/10.1016/j.fsi.2019.05.019.

Liu T, Zhang Q, Wang L, Yu L, Leng W, Yang J, Chen L, Peng J, Ma L, Dong J, Xu X, Xue Y, Zhu Y, Zhang W, Yang L, Li W, Sun L, Wan Z, Ding G, Yu F, Tu K, Qian Z, Li R, Shen Y, Li Y, Jin Q (2007) The use of global transcriptional analysis to reveal the biological and cellular events involved in distinct development phases of

Trichophyton rubrum conidial germination. BMC Genomics 8: 100. doi:10.1186/1471-2164-8-100.

Liu Y-C, Cheng S-C (2015) Functional roles of DExD/H-box RNA helicases in Pre-mRNA splicing. Journal of Biomedical Science 22: 54.

Liu Z-R (2002) p68 RNA helicase is an essential human splicing factor that acts at the U1 snRNA-5′ splice site duplex. Molecular and Cellular Biology 22: 5443–5450.

Luo M-J, Zhou Z, Magni K, Christoforides C, Rappsilber J, Mann M, Reed R (2001) Pre-mRNA splicing and mRNA export linked by direct interactions between UAP56 and Aly. Nature 413: 644–647.

Ma WK, Cloutier SC, Tran EJ (2013) The DEAD-box protein Dbp2 functions with the RNA-binding protein Yra1 to promote mRNP assembly. Journal of Molecular Biology 425: 3824–3838.

Ma WK, Paudel BP, Xing Z, Sabath IG, Rueda D, Tran EJ (2016) Recruitment, duplex unwinding and protein-mediated inhibition of the dead-box RNA helicase Dbp2 at actively transcribed chromatin. Journal of Molecular Biology 428: 1091–1106.

Marayati BF, Hoskins V, Boger RW, Tucker JF, Fishman ES, Bray AS, Zhang K (2016) The fission yeast MTREC and EJC orthologs ensure the maturation of meiotic transcripts during meiosis. RNA 22: 1349–1359. doi:10.1261/rna.055608.115.

Marchena-Cruz E, Camino LP, Bhandari J, Silva S, Marqueta-Gracia JJ, Amdeen SA, Guillén-Mendoza C, García-Rubio ML, Calderón-Montaño JM, Xue X, Luna R, Aguilera A (2023) DDX47, MeCP2, and other functionally heterogeneous factors protect cells from harmful R loops. Cell Reports 42: 112148. doi:10.1016/j.celrep.2023.112148.

Markov DA, Wojtas ID, Tessitore K, Henderson S, McAllister WT (2014) Yeast DEAD box protein Mss116p is a transcription elongation factor that modulates the activity of mitochondrial RNA polymerase. Molecular and Cellular Biology 34: 2360–2369.

Martin R, Straub AU, Doebele C, Bohnsack MT (2013) DExD/H-box RNA helicases in ribosome biogenesis. RNA Biology 10: 4–18.

Martínez-Espinoza AD, García-Pedrajas MaD, Gold SE (2002) The Ustilaginales as plant pests and model systems. Fungal Genetics and Biology 35: 1–20.

Martinez-Montiel N, Morales-Lara L, Hernández-Pérez JM, Martínez-Contreras RD (2016) *In silico* analysis of the structural and biochemical features of the NMD factor UPF1 in *Ustilago maydis*. PLOS One 11: e0148191. doi:10.1371/journal.pone.0148191.

Mi H, Thomas P (2009) PANTHER Pathway: An Ontology-Based Pathway Database Coupled with Data Analysis Tools. In: Nikolsky Y, Bryant J (Eds) Protein Networks and Pathway Analysis. Humana Press, Totowa, NJ, 123–140. doi:10.1007/978-1-60761-175-2_7.

Mikhailova T, Shuvalova E, Ivanov A, Susorov D, Shuvalov A, Kolosov PM, Alkalaeva E (2017) RNA helicase DDX19 stabilizes ribosomal elongation and termination complexes. Nucleic Acids Research 45: 1307–1318.

Milek M, Imami K, Mukherjee N, De Bortoli F, Zinnall U, Hazapis O, Trahan C, Oeffinger M, Heyd F, Ohler U (2017) DDX54 regulates transcriptome dynamics during DNA damage response. Genome Research 27: 1344–1359.

Minczuk M, Dmochowska A, Palczewska M, Stepien PP (2002) Overexpressed yeast mitochondrial putative RNA helicase Mss116 partially restores proper mtRNA metabolism in strains lacking the Suv3 mtRNA helicase. Yeast 19: 1285–1293.

Mischo HE, Gómez-González B, Grzechnik P, Rondón AG, Wei W, Steinmetz L, Aguilera A, Proudfoot NJ (2011) Yeast Sen1 helicase protects the genome from transcription-associated instability. Molecular Cell 41: 21–32.

Mitterer V, Hamze H, Kunowska N, Stelzl U, Henras Anthony K, Hurt E (2023) The RNA helicase Dbp10 coordinates assembly factor association with PTC maturation during ribosome biogenesis. Nucleic Acids Research 52: 1975–1987. doi:10.1093/nar/gkad1206.

Nicholls TJ, Rorbach J, Minczuk M (2013) Mitochondria: mitochondrial RNA metabolism and human disease. The International Journal of Biochemistry & Cell Biology 45: 845–849.

Niemer I, Schmelzer C, Boörner GV (1995) Overexpression of DEAD box protein pMSS116 promotes ATP-dependent splicing of a yeast group II intron *in vitro*. Nucleic Acids Research 23: 2966–2972.

Niu W, Li Z, Zhan W, Iyer VR, Marcotte EM (2008) Mechanisms of Cell Cycle Control Revealed by a Systematic and Quantitative Overexpression Screen in *S. cerevisiae*. PLOS Genetics 4: e1000120. doi:10.1371/journal.pgen.1000120.

Noble KN, Tran EJ, Alcázar-Román AR, Hodge CA, Cole CN, Wente SR (2011) The Dbp5 cycle at the nuclear pore complex during mRNA export II: nucleotide cycling and mRNP remodeling by Dbp5 are controlled by Nup159 and Gle1. Genes & Development 25: 1065–1077.

O'Day CL, Chavanikamannil F, Abelson J (1996) 18S rRNA processing requires the RNA helicase-like protein Rrp3. Nucleic Acids Research 24: 3201–3207.

O'Donnell KL, McLaughlin DJ (1984) Ultrastructure of meiosis in *Ustilago maydis*. Mycologia 76: 468–485. doi:10.2307/3793330.

Ostrowski LA, Saville BJ (2017) Natural antisense transcripts are linked to the modulation of mitochondrial function and teliospore dormancy in *Ustilago maydis*. Molecular Microbiology 103: 745–763. doi:10.1111/mmi.13587.

Ostrowski LA, Seto AM, Saville B (2018) Investigating teliospore germination using microrespiration analysis and microdissection. Journal of Visualized Experiments: e57628. doi:10.3791/57628.

Pan T, Sosnick T (2006) RNA folding during transcription. Annual Review of Biophysics and Biomolecular Structure 35: 161–175.

Panepinto J, Liu L, Ramos J, Zhu X, Valyi-Nagy T, Eksi S, Fu J, Jaffe HA, Wickes B, Williamson PR (2005) The DEAD-box RNA helicase Vad1 regulates multiple virulence-associated genes in *Cryptococcus neoformans*. Journal of Clinical Investigation 115: 632–641. doi:10.1172/JCI23048.

Parker R (2012) RNA degradation in *Saccharomyces cerevisae*. Genetics 191: 671–702.

Payne EM, Bolli N, Rhodes J, Abdel-Wahab OI, Levine R, Hedvat CV, Stone R, Khanna-Gupta A, Sun H, Kanki JP, Gazda HT, Beggs AH, Cotter FE, Look AT (2011) Ddx18 is essential for cell-cycle progression in zebrafish hematopoietic cells and is mutated in human AML. Blood 118: 903–915. doi:10.1182/blood-2010-11-318022.

Pérez-Calero C, Bayona-Feliu A, Xue X, Barroso SI, Muñoz S, González-Basallote VM, Sung P, Aguilera A (2020) UAP56/DDX39B is a major cotranscriptional RNA-DNA helicase that unwinds harmful R loops genome-wide. Genes & Development 34: 898–912. doi:10.1101/gad.336024.119.

Peters D, Radine C, Reese A, Budach W, Sohn D, Jänicke RU (2017) The DEAD-box RNA helicase DDX41 is a novel repressor of $p21^{WAF1/CIP1}$ mRNA translation. Journal of Biological Chemistry 292: 8331–8341. doi:10.1074/jbc.M116.772327.

Pfeifer A, Martin B, Kämper J, Basse CW (2012) The Mitochondrial LSU rRNA Group II Intron of *Ustilago maydis* Encodes an Active Homing Endonuclease Likely Involved in Intron Mobility. PLOS One 7: e49551. doi:10.1371/journal.pone.0049551.

Pisareva VP, Pisarev AV, Komar AA, Hellen CU, Pestova TV (2008) Translation initiation on mammalian mRNAs with structured 5′ UTRs requires DExH-box protein DHX29. Cell 135: 1237–1250.

Polprasert C, Schulze I, Sekeres MA, Makishima H, Przychodzen B, Hosono N, Singh J, Padgett RA, Gu X, Phillips JG (2015) Inherited and somatic defects in DDX41 in myeloid neoplasms. Cancer Cell 27: 658–670.

Pradhan A, Ma Q, de Assis LJ, Leaves I, Larcombe DE, Rodriguez Rondon AV, Nev OA, Brown AJP (2021) Anticipatory Stress Responses and Immune Evasion in Fungal Pathogens. Trends in Microbiology 29: 416–427. doi:10.1016/j.tim.2020.09.010.

Pratte D, Singh U, Murat G, Kressler D (2013) Mak5 and Ebp2 act together on early pre-60S particles and their reduced functionality bypasses the requirement for the essential pre-60S factor Nsa1. PLOS One 8: e82741.

Qiu J, Olszewski Michal A, Williamson Peter R (2013) *Cryptococcus neoformans* Growth and Protection from Innate Immunity Are Dependent on Expression of a Virulence-Associated DEAD-Box Protein, Vad1. Infection and Immunity 81: 777–788. doi:10.1128/iai.00821-12.

Richard P, Feng S, Tsai Y-L, Li W, Rinchetti P, Muhith U, Irizarry-Cole J, Stolz K, Sanz LA, Hartono S, Hoque M, Tadesse S, Seitz H, Lotti F, Hirano M, Chédin F, Tian B, Manley JL (2021) SETX (senataxin), the helicase mutated in AOA2 and ALS4, functions in autophagy regulation. Autophagy 17: 1889–1906. doi:10.1080/15548627.2020.1796292.

Ripmaster TL, Vaughn GP, Woolford JL (1992) A putative ATP-dependent RNA helicase involved in *Saccharomyces cerevisiae* ribosome assembly. Proceedings of the National Academy of Sciences 89: 11131–11135.

Robert-Paganin J, Réty S, Leulliot N (2015) Regulation of DEAH/RHA helicases by G-patch proteins. BioMed Research International 2015: 931857. doi:10.1155/2015/931857.

Rodríguez-Galán O, García-Gómez JJ, de la Cruz J (2013) Yeast and human RNA helicases involved in ribosome biogenesis: current status and perspectives. Biochimica et Biophysica Acta - Gene Regulatory Mechanisms 1829: 775–790.

Sachs A, Davis R (1990) Translation initiation and ribosomal biogenesis: involvement of a putative rRNA helicase and RPL46. Science 247: 1077–1079.

Sales-Lee J, Perry DS, Bowser BA, Diedrich JK, Rao B, Beusch I, Yates JR, Roy SW, Madhani HD (2021) Coupling of spliceosome complexity to intron diversity. Current Biology 31: 4898–4910.e4894. doi:https://doi.org/10.1016/j.cub.2021.09.004.

Saville BJ, Donaldson ME, Doyle CE (2012) Investigating host induced meiosis in a fungal plant pathogen. In: Andrew S (Ed) Meiosis - Molecular Mechanisms and Cytogenetic Diversity. InTech, Rijeka, doi:10.5772/30032.

Savitsky K, Ziv Y, Bar-Shira A, Gilad S, Tagle DA, Smith S, Uziel T, Sfez S, Nahmias J, Sartiel A, Eddy RL, Shows TB, Collins FS, Shiloh Y, Rotman G (1996) A Human Gene (DDX10) Encoding a Putative DEAD-Box RNA Helicase at 11q22–q23. Genomics 33: 199–206. doi:https://doi.org/10.1006/geno.1996.0184.

Schütz P, Karlberg T, van den Berg S, Collins R, Lehtiö L, Högbom M, Holmberg-Schiavone L, Tempel W, Park H-W, Hammarström M, Moche M, Thorsell A-G, Schüler H (2010) Comparative Structural Analysis of Human DEAD-Box RNA Helicases. PLOS One 5: e12791. doi:10.1371/journal.pone.0012791.

Searfoss AM, Wickner RB (2000) 3′ poly (A) is dispensable for translation. Proceedings of the National Academy of Sciences 97: 9133–9137.

Sekiguchi T, Hayano T, Yanagida M, Takahashi N, Nishimoto T (2006) NOP132 is required for proper nucleolus localization of DEAD-box RNA helicase DDX47. Nucleic Acids Research 34: 4593–4608.

Semlow DR, Blanco MR, Walter NG, Staley JP (2016) Spliceosomal DEAH-box ATPases remodel pre-mRNA to activate alternative splice sites. Cell 164: 985–998.

Sen ND, Zhou F, Ingolia NT, Hinnebusch AG (2015) Genome-wide analysis of translational efficiency reveals distinct but overlapping functions of yeast DEAD-box RNA helicases Ded1 and eIF4A. Genome Research 25: 1196–1205. doi:10.1101/gr.191601.115.

Seto AM, Donaldson ME, Saville BJ (2025) Exploring mechanisms of gene expression control during *Ustilago maydis* teliospore germination. Canadian Journal of Plant Pathology 47: 80–97. doi:10.1080/07060661.2024.2413557.

Seto AM, Saville BJ (2025) Characterization of RNA helicase genes in *Ustilago maydis* reveals links to stress response and teliospore dormancy [Manuscript submitted for publication]. 63 pp.

Shadrick WR, Ndjomou J, Kolli R, Mukherjee S, Hanson AM, Frick DN (2013) Discovering New Medicines Targeting Helicases: Challenges and Recent Progress. Journal of Biomolecular Screening 18: 761–781. doi:10.1177/1087057113482586.

Sharma D, Jankowsky E (2014) The Ded1/DDX3 subfamily of DEAD-box RNA helicases. Critical Reviews in Biochemistry and Molecular Biology 49: 343–360.

Shen L, Pelletier J (2020) General and Target-Specific DExD/H RNA Helicases in Eukaryotic Translation Initiation. International Journal of Molecular Sciences 21: 4402.

Shiratori A, Shibata T, Arisawa M, Hanaoka F, Marakami Y, Eki T (1999) Systematic identification, classification, and characterization of the open reading frames which

encode novel helicase-related proteins in *Saccharomyces cerevisiae* by gene disruption and Northern analysis. Yeast 15: 219–253. doi:https://doi.org/10.1002/(SICI)1097-0061(199902)15:3<219::AID-YEA349>3.0.CO;2-3.

Sickmann A, Reinders J, Wagner Y, Joppich C, Zahedi R, Meyer HE, Schönfisch B, Perschil I, Chacinska A, Guiard B, Rehling P, Pfanner N, Meisinger C (2003) The proteome of *Saccharomyces cerevisiae* mitochondria. Proceedings of the National Academy of Sciences 100: 13207–13212. doi:doi:10.1073/pnas.2135385100.

Singleton MR, Dillingham MS, Wigley DB (2007) Structure and mechanism of helicases and nucleic acid translocases. Annual Review of Biochemistry 76: 23–50.

Sitron CS, Park JH, Brandman O (2017) Asc1, Hel2, and Slh1 couple translation arrest to nascent chain degradation. RNA 23: 798–810.

Sloan KE, Bohnsack MT (2018) Unravelling the mechanisms of RNA helicase regulation. Trends in Biochemical Sciences 43: 237–250.

Song Y, Kim S, Kim J (1995) ROK1, a high-copy-number plasmid suppressor of keml, encodes a putative ATP-dependent RNA helicase in *Saccharomyces cerevisiae*. Gene 166: 151–154. doi:https://doi.org/10.1016/0378-1119(96)80010-2.

Soponpong S, Amparyup P, Tassanakajon A (2018) A cytosolic sensor, PmDDX41, mediates antiviral immune response in black tiger shrimp *Penaeus monodon*. Developmental and Comparative Immunology 81: 291–302. doi:https://doi.org/10.1016/j.dci.2017.12.013.

Sridhara SC, Carvalho S, Grosso AR, Gallego-Paez LM, Carmo-Fonseca M, de Almeida SF (2017) Transcription Dynamics Prevent RNA-Mediated Genomic Instability through SRPK2-Dependent DDX23 Phosphorylation. Cell Reports 18: 334–343. doi:10.1016/j.celrep.2016.12.050.

Srivastava L, Lapik YR, Wang M, Pestov DG (2010) Mammalian DEAD box protein Ddx51 acts in 3′ end maturation of 28S rRNA by promoting the release of U8 snoRNA. Molecular and Cellular Biology 30: 2947–2956.

Stepien PP, Kokot L, Leski T, Bartnik E (1995) The *suv3* nuclear gene product is required for the in vivo processing of the yeast mitochondrial 21s rRNA transcripts containing the r1 intron. Current Genetics 27: 234–238.

Sträßer K, Hurt E (2001) Splicing factor Sub2p is required for nuclear mRNA export through its interaction with Yra1p. Nature 413: 648–652.

Sturm M, Cheng J, Baßler J, Beckmann R, Hurt E (2017) Interdependent action of KH domain proteins Krr1 and Dim2 drive the 40S platform assembly. Nature Communications 8: 2213. doi:10.1038/s41467-017-02199-4.

Svitkin YV, Pause A, Haghighat A, Pyronnet S, Witherell G, Belsham GJ, Sonenberg N (2001) The requirement for eukaryotic initiation factor 4A (elF4A) in translation is in direct proportion to the degree of mRNA 5' secondary structure. RNA 7: 382–394.

Sweet T, Kovalak C, Coller J (2012) The DEAD-box protein Dhh1 promotes decapping by slowing ribosome movement. PLOS Biology 10: e1001342.

Szczesny RJ, Wojcik MA, Borowski LS, Szewczyk MJ, Skrok MM, Golik P, Stepien PP (2013) Yeast and human mitochondrial helicases. Biochimica et Biophysica Acta - Gene Regulatory Mechanisms 1829: 842–853.

Szklarczyk D, Kirsch R, Koutrouli M, Nastou K, Mehryary F, Hachilif R, Gable AL, Fang T, Doncheva NT, Pyysalo S, Bork P, Jensen LJ, von Mering C (2023) The STRING database in 2023: protein-protein association networks and functional enrichment analyses for any sequenced genome of interest. Nucleic Acids Research 51: D638–d646. doi:10.1093/nar/gkac1000.

Takemura M (2005) Evolutionary history of the retinoblastoma gene from archaea to eukarya. BioSystems 82: 266–272. doi:https://doi.org/10.1016/j.biosystems.2005.08.005.

Thomas PD, Ebert D, Muruganujan A, Mushayahama T, Albou L-P, Mi H (2022) PANTHER: Making genome-scale phylogenetics accessible to all. Protein Science 31: 8–22. doi:https://doi.org/10.1002/pro.4218.

Tran EJ, Zhou Y, Corbett AH, Wente SR (2007) The DEAD-box protein Dbp5 controls mRNA export by triggering specific RNA: protein remodeling events. Molecular Cell 28: 850–859.

Trifinopoulos J, Nguyen L-T, von Haeseler A, Minh BQ (2016) W-IQ-TREE: a fast online phylogenetic tool for maximum likelihood analysis. Nucleic Acids Research 44: W232–W235. doi:10.1093/nar/gkw256.

Troshin PV, Procter JB, Barton GJ (2011) Java bioinformatics analysis web services for multiple sequence alignment—JABAWS:MSA. Bioinformatics 27: 2001–2002. doi:10.1093/bioinformatics/btr304.

Tsukamoto T, Gearhart MD, Kim S, Mekonnen G, Spike CA, Greenstein D (2020) Insights into the Involvement of Spliceosomal Mutations in Myelodysplastic Disorders from Analysis of SACY-1/DDX41 in *Caenorhabditis elegans*. Genetics 214: 869–893. doi:10.1534/genetics.119.302973.

Venema J, Bousquet-Antonelli C, Gelugne J-P, Caizergues-Ferrer M, Tollervey D (1997) Rok1p is a putative RNA helicase required for rRNA processing. Molecular and Cellular Biology 17: 3398–3407.

Walbott H, Mouffok S, Capeyrou R, Lebaron S, Humbert O, van Tilbeurgh H, Henry Y, Leulliot N (2010) Prp43p contains a processive helicase structural architecture with a specific regulatory domain. The EMBO Journal 29: 2194–2204. doi:https://doi.org/10.1038/emboj.2010.102.

Wang Y, Arribas-Layton M, Chen Y, Lykke-Andersen J, Sen GL (2015) DDX6 orchestrates mammalian progenitor function through the mRNA degradation and translation pathways. Molecular Cell 60: 118–130.

Waterhouse AM, Procter JB, Martin DMA, Clamp M, Barton GJ (2009) Jalview Version 2—a multiple sequence alignment editor and analysis workbench. Bioinformatics 25: 1189–1191. doi:10.1093/bioinformatics/btp033.

Weaver PL, Sun C, Chang T-H (1997) Dbp3p, a putative RNA helicase in *Saccharomyces cerevisiae*, is required for efficient pre-rRNA processing predominantly at site A_3. Molecular and Cellular Biology 17: 1354–1365.

Wilkie GS, Dickson KS, Gray NK (2003) Regulation of mRNA translation by 5′-and 3′-UTR-binding factors. Trends in Biochemical Sciences 28: 182–188.

Xing Z, Ma WK, Tran EJ (2019) The DDX5/Dbp2 subfamily of DEAD-box RNA helicases. Wiley Interdisciplinary Reviews: RNA 10: e1519.

Xing Z, Wang S, Tran EJ (2017) Characterization of the mammalian DEAD-box protein DDX5 reveals functional conservation with *S. cerevisiae* ortholog Dbp2 in transcriptional control and glucose metabolism. RNA 23: 1125–1138.

Yamauchi T, Nishiyama M, Moroishi T, Yumimoto K, Nakayama KI (2014) MDM2 mediates nonproteolytic polyubiquitylation of the DEAD-Box RNA helicase DDX24. Molecular and Cellular Biology 34: 3321–3340.

Yamazaki T, Fujiwara N, Yukinaga H, Ebisuya M, Shiki T, Kurihara T, Kioka N, Kambe T, Nagao M, Nishida E, Masuda S (2010) The Closely Related RNA helicases, UAP56 and URH49, Preferentially Form Distinct mRNA Export Machineries and Coordinately Regulate Mitotic Progression. Molecular Biology of the Cell 21: 2953–2965. doi:10.1091/mbc.e09-10-0913.

Yang Q, Del Campo M, Lambowitz AM, Jankowsky E (2007) DEAD-Box Proteins Unwind Duplexes by Local Strand Separation. Molecular Cell 28: 253–263. doi:https://doi.org/10.1016/j.molcel.2007.08.016.

Yassin ER, Abdul-Nabi AM, Takeda A, Yaseen NR (2010) Effects of the NUP98–DDX10 oncogene on primary human CD34+ cells: role of a conserved helicase motif. Leukemia 24: 1001–1011. doi:10.1038/leu.2010.42.

Yeter-Alat H, Belgareh-Touzé N, Huvelle E, Banroques J, Tanner NK (2023) The DEAD-Box RNA Helicase Ded1 Is Associated with Translating Ribosomes. Genes 14: 1566.

Ying S, Zhang Z, Zhang Y, Hao Z, Chai R, Qiu H, Wang Y, Zhu X, Wang J, Sun G, Lin F (2022) MoDHX35, a DEAH-Box Protein, Is Required for Appressoria Formation and Full Virulence of the Rice Blast Fungus, *Magnaporthe oryzae*. International Journal of Molecular Sciences 23: 9015.

Zagulski M, Kressler D, Becam A-M, Rytka J, Herbert C (2003) Mak5p, which is required for the maintenance of the M1 dsRNA virus, is encoded by the yeast ORF YBR142w and is involved in the biogenesis of the 60S subunit of the ribosome. Molecular Genetics and Genomics 270: 216–224.

Zhang L, Li X (2021) DEAD-Box RNA Helicases in Cell Cycle Control and Clinical Therapy. Cells 10: 1540.

Zhang L, Yang Y, Li B, Scott IC, Lou X (2018) The DEAD-box RNA helicase Ddx39ab is essential for myocyte and lens development in zebrafish. Development 145: doi:10.1242/dev.161018.

Zhou X, Liu Z, He T, Zhang C, Jiang M, Jin Y, Wu Z, Gu C, Zhang W, Yang X (2022) DDX10 promotes the proliferation and metastasis of colorectal cancer cells via splicing RPL35. Cancer Cell International 22: 58. doi:10.1186/s12935-022-02478-1.

Zirwes RF, Eilbracht J, Kneissel S, Schmidt-Zachmann MS (2000) A novel helicase-type protein in the nucleolus: protein NOH61. Molecular Biology of the Cell 11: 1153–1167.

CHAPTER 5

PREFACE

Title: Characterization of RNA Helicase Genes in *Ustilago maydis* Reveals Links to Stress Response and Teliospore Dormancy

Authors: Amanda M. Seto and Barry J. Saville

Reference: Published in *International Journal of Molecular Sciences* (2025)

doi: https://doi.org/10.3390/ijms26062432

2024 Impact Factor: 4.9

Contributions: B.J.S. conceived, directed, and obtained funding for the research presented in this research. A.M.S. performed the bioinformatic analysis for Udbp3 and Uded1, created the *Ustilago maydis* strains crg1:*uded1*, Δ*uded1* crg1:*uded1*, Δ*uded1* crg1:*uded1* [pCM768], Δ*uded1* crg1:*uded1* [pCMas-ssm1], and Δ*udbp3*, carried out the seedling pathogenesis assays, plate mating assays, stress response assays, plate growth assays, microscopic analysis, collected samples and isolated RNA, performed the RT-PCRs and RT-qPCRs, conducted the S1 nuclease protection assay, created Tables 5.1, S5.1–S5.2, Figures 5.1–5.10, S5.1–S5.9, and drafted the manuscript. B.J.S. edited the initial manuscript. A.M.S. and B.J.S. edited the manuscript prior to submission.

CHAPTER 5

Characterization of RNA Helicase Genes in *Ustilago maydis* Reveals Links to Stress Response and Teliospore Dormancy

Published in *International Journal of Molecular Sciences* (2025), **26**(6): 2432

doi: https://doi.org/10.3390/ijms26062432

ABSTRACT

Fungi produce dormant structures that are responsible for protection during adverse environmental conditions and dispersal (disease spread). *Ustilago maydis*, a basidiomycete plant pathogen, is a model for understanding the molecular mechanisms of teliospore dormancy and germination. Dormant teliospores store components required for germination including mRNAs which may be stored as dsRNAs. RNA helicases are conserved enzymes that function to modulate, bind, and unwind RNA duplexes, and can displace other proteins. We hypothesize that RNA helicases function during teliospore dormancy to stabilize and/or modulate stored mRNAs. We identified the *U. maydis udbp3* and *uded1* as encoding RNA helicases of interest as they are upregulated in the dormant teliospore and decrease during germination. Experimental results suggest that *udbp3* may function as a negative regulator of osmotic stress-responsive genes and that *uded1* modulates stress response by repressing translation. The altered expression of *uded1* also results in slow growth, polarized growth, and the formation of dsRNA. Together the data supports a role for both helicases modulating gene expression, in response to stress, leading to teliospore dormancy and also modulating responses for teliospore germination.

Increasing our molecular understanding of these processes will aid in developing novel strategies to mitigate disease spread.

Keywords: Teliospore dormancy; germination; RNA helicase; stress response; *uded1*; *udbp3*, *Ustilago maydis*

INTRODUCTION

Dormancy is defined as a time of rest or pause in phenotypic development [1]. Many organisms develop dormant structures as a strategy to survive adverse environmental conditions. For example, some plants develop dormant seeds to withstand unfavourable environmental conditions until favourable conditions are met for germination to occur [2]. Some microbes utilize dormancy as a response to environmental stress. This allows for the microbe to maintain their viability until favourable growth conditions are met [3]. Fungi develop spores that enable their survival for long periods of time and their dispersal allows for disease spread. Characteristic traits of dormant fungal spores are limited cell proliferation and low metabolic activity. Once conditions are favourable, there is an irreversible transition to germination where respiration and metabolic rates increase [1]. Understanding the molecular mechanisms that occur during this transition from dormancy to germination can aid in developing methods for mitigating disease spread among fungal plant pathogens. We use the basidiomycete *Ustilago maydis* (DC.) Corda as a model for studying the teliospore transition from a dormant state to an actively germinating spore.

Ustilago maydis is a plant pathogen that infects *Zea mays* resulting in the development of the disease Common Smut of Corn. The disease is characterized by the growth of tumours that contain billions of black teliospores. These tumours crack open, releasing teliospores into the environment, enabling the spread of disease to other crops. The dormant teliospores contain three-layer thick cell walls that are melanized and echinulated [4-6]. Teliospores can remain viable for years [7] and germination is stimulated in the presence of a carbon source [8]. Germination is the irreversible transition from low to high metabolic activity where the spore utilizes its stored reserves to facilitate the

resumption of metabolism. Phenotypic development also resumes and a germ tube is produced [9]. Fungal spores contain the necessary components that are required for the initiation of germination. These components can include carbohydrates as energy reserves and stored RNAs [10]. Previous research indicates that dormant *U. maydis* teliospores contain stored RNAs bound to proteins to form a complex. These ribonucleoprotein (RNP) complexes disappear following germination and may function to protect the RNA during dormancy [11,12]. Our laboratory hypothesized that dormant *U. maydis* teliospores contain mRNAs that are stabilized by binding with complementary antisense RNAs to form double-stranded RNA (dsRNA) [13,14]. We hypothesize that RNA helicases are involved in stabilizing RNA:RNA interactions and unwinding mRNA transcripts for translation following the initiation of germination.

RNA helicases are highly conserved enzymes that function in all aspects of RNA metabolism. They are capable of driving and regulating gene expression by remodelling RNA, unwinding RNA duplexes, displacing proteins, and binding to RNA to create ribonucleoprotein (RNP) complexes [15-17]. Classification of RNA helicases is based on their sequence and structure motifs as described by Gorbalenya and Koonin [18] and further analyzed by Singleton*, et al.* [19]. A total of six helicase superfamilies have been identified with superfamilies 1 (SF1) and 2 (SF2) being the largest. The majority of eukaryotic RNA helicases can be found in SF2 [19,20].

The functional characterization of RNA helicases in several eukaryotes has revealed that these enzymes have roles in cellular and metabolic pathways. For example, the RNA helicase *VAD1* in *Cryptococcus neoformans* is associated with the regulation of several virulence genes, response to stress, and salt tolerance [21]. Deletion of the *Magnaporthe*

oryzae RNA helicase *MoDHX35* results in reduced appressoria formation and attenuated virulence [22]. Despite the vast research on the function of RNA helicases, their roles in the lifecycle of phytopathogenic fungi has not been extensively explored.

RNA-seq analysis identified several RNA helicases that are upregulated in the dormant teliospore and decrease during germination [23]. Specifically, pattern 17 contained transcripts that were upregulated in the dormant teliospore, decreased during germination, and remained decreased as germination progressed. Of the five RNA helicases identified in this pattern, the orthologs to *Saccharomyces cerevisiae DBP3* and *DED1* were selected for further characterization in *U. maydis*. In budding yeast, *DBP3* is an SF2 DEAD-box RNA helicase that is not essential for cell viability and is involved in processing the ITS1 A3 cleavage site during pre-RNA maturation [24]. Delaney*, et al.* [25] demonstrated that *DBP3* deletion mutants had increased thermotolerance and were resistant to oxidative, endoplasmic reticulum, and DNA damage stressors. This suggests that the *U. maydis* ortholog, *udbp3,* may also function in stress response. The *DED1* RNA helicase is essential with roles in translation promotion and repression [26-28]. We hypothesized that the *U. maydis* ortholog, *uded1*, is involved in repressing translation during teliospore dormancy and modulating translation when germination is initiated. The results of this study suggest that *udbp3* is a negative regulator of osmotic stress response. Upregulation of *udbp3* during dormancy may function to regulate a subset of stress-responsive genes. In contrast, *uded1* may modulate the translation of genes during dormancy and germination. This study identifies potential molecular mechanisms that are involved during teliospore dormancy and germination and offers insight into gene regulation during the transition from dormancy to germination.

RESULTS

Identification of RNA Helicases with Potential Roles During Teliospore Germination

The transcriptome data from Seto, Donaldson and Saville [23] identified five candidate RNA helicases that we hypothesized to have a role during *U. maydis* teliospore germination. These RNA helicases were found in pattern 17 of teliospore germination and have transcript levels that were decreased in the haploid and dikaryon cell types, upregulated in the dormant teliospore, and decreased during teliospore germination. This specific transcript pattern suggested a role during the exit from dormancy to germination. Candidate RNA helicases were identified as *UMAG_04080*, *UMAG_01732*, *UMAG_10241*, *UMAG_01122*, and *UMAG_00835*. Seto and Saville [29] identified these RNA helicases as orthologs to *S. cerevisiae DED1*, *DBP3*, *DBP8* and *HCS1* respectively. *UMAG_00835* is a putative basidiomycete-specific RNA helicase with possible functions in ribosome biogenesis [29]. The RNA helicases *UMAG_01732* and *UMAG_04080* were prioritized as genes of interest based on their confirmed transcript level pattern and the observations that their transcript levels were the highest in the dormant teliospore compared to the other candidates [23].

Bioinformatic analysis of *UMAG_01732* was previously performed by Seto and Saville [29] and was identified as a putative fungal- and plant-specific RNA helicase. UMAG_01732 contains a helicase core consistent with the sequence motifs previously identified in *S. cerevisiae* Dbp3 (Figure 5.1A). Weaver, Sun and Chang [24] previously identified the signalling sequence motif lysine-lysine-X (KKX) repeated several times in *S. cerevisiae* Dbp3. Our results of the protein MUSCLE alignment with putative Dbp3

orthologs indicated conservation of the KKX sequence motif, however, the repeat length of the motif differs between species. The *U. maydis* KKX motif is repeated five times compared to the 10 tandem repeats in *S. cerevisiae*. A phylogenetic tree was created from the MUSCLE alignment of known and putative Dbp3 orthologs and the closely related Dbp2/DDX17 RNA helicases. The phylogenetic tree showed two distinct clades from the SF2 DEAD-box RNA helicases (Figure 5.1B). In Figure 5.1B, the boxed region indicates the Dbp3 group of RNA helicases that contains UMAG_01732. These results are consistent with our previous phylogenetic trees that identified UMAG_01732 as a putative fungal and plant RNA helicase [29] and we have named the *U. maydis* ortholog as Udbp3.

The *S. cerevisiae* Ded1 is a well-characterized SF2 DEAD-box RNA helicase and the *H. sapiens* ortholog was identified as DDX3. Protein sequence and phylogenetic analysis conducted by Seto and Saville [29] identified UMAG_04080 as the putative ortholog. UMAG_04080 contains a helicase core consistent with known Ded1/DDX3 proteins in other organisms (Figure 5.2A). A phylogenetic tree was created with Ded1/DDX3 orthologs and the closely related Tif1/DDX2 orthologs (Figure 5.2B). The phylogenetic tree shows two distinct clades (Figure 5.2B), and the boxed region indicates the Ded1/DDX3 clade containing UMAG_04080. These results were consistent with previous results in Seto and Saville [29] and supported UMAG_04080 as an ortholog to Ded1/DDX3. We have named the *U. maydis* ortholog Uded1.

udbp3 Characterization

The ability of Δ*udbp3* mutants to form dikaryotic filaments was assessed through a mating assay. Sexually compatible haploid strains (518 and 521) were spotted on PDA plates containing charcoal. A Fuz^+ phenotype indicates successful fusion of haploid strains.

Filamentous growth was unaffected in the reciprocal (Δ*udbp3* × wt) or deletion (Δ*udbp3* × Δ*udbp3*) crosses. The deletion of *udbp3* did not affect mating ability (Figure S5.1).

A pathogenesis assay was performed to determine the ability of *udbp3* mutants to infect the plant. Golden Bantam *Z. mays* seedlings were infected with the reciprocal, deletion, or wild-type crosses. Both reciprocal and deletion strains showed no significant difference in virulence compared to wild-type infections (Figure S5.2). The infected seedlings were able to produce tumours and develop teliospores. This indicated that the deletion of *udbp3* did not affect infection, disease development, tumour formation, or teliospore development.

Teliospores were obtained from Golden Bantam *Z. mays* ears infected with the deletion (Δ*udbp3* × Δ*udbp3*) strains and germination was assessed through teliospore germination time courses. Germination was assessed at 16 h post induction of germination (PIG), germination percentage was determined, and morphology was examined with microscopy. There was no visual difference in the morphology of dormant teliospores. Teliospore germination was not affected, no visible defects of the promycelium were detected, and basidiospores were still produced suggesting that meiosis was not affected (Figure S5.3). The combined results indicated that *udbp3* was not required for the progression of teliospore germination.

Saccharomyces cerevisiae DBP3 deletion mutants have a slow-growth phenotype [24], increased thermotolerance, and were tolerant to endoplasmic reticulum (ER) stress caused by tunicamycin, oxidative stress caused by paraquat, and resistant to DNA damage caused by exposure to methyl methane sulfonate (MMS) [25]. *Ustilago maydis* Δ*udbp3* mutants were assessed for abnormalities in growth and stress response. We found no

difference in the growth of the 518Δ*udbp3* or the 521Δ*udbp3* strains when compared to the wild-type when incubated at 16 °C, 28 °C, and 37 °C (Figure S5.4). The Δ*udbp3* mutants also showed no difference, compared to wild-type strains, in growth when exposed to tunicamycin, paraquat, or MMS (Figure S5.5).

The response to osmotic stress was not previously assessed in *S. cerevisiae DBP3* mutants. The response to osmotic stress was assessed in the Δ*udbp3* mutants by spotting a 10-fold dilution series on YEPS plates containing 1 M NaCl. Of the 518Δ*udbp3* mutants, two of the biological replicates showed no difference in growth compared to 518. The 518Δ*udbp3* #1 mutant showed a slight decrease in growth compared to the other deletion biological replicates and 518 (Figure 5.3). The 521Δ*udbp3* mutants showed an increased tolerance to osmotic stress compared to 521 (Figure 5.3). The parental strains 518 and 521 are sister strains [30] and have previously described differences in growth and hormone concentrations, so the differences in osmotic stress response were not unexpected [31].

Deletion of uded1 is Detrimental to Growth

Ded1 in *S. cerevisiae* is an essential protein for cell viability. To assess the importance of *uded1* in *U. maydis*, we attempted to create *uded1* deletion mutants using the Kämper [32] homologous recombination-based method. These attempts resulted in no viable mutants. A two-step gene deletion method described by Ostrowski and Saville [14] was used to create *uded1* deletion mutants. This method involved first creating expression mutants where the ectopic expression of *uded1* was placed under the control of a carbon-sensitive inducible promoter and integrated at the *ip* locus. These expression mutants (crg1:*uded1*) were created in the sexually compatible 518 and 521 wild-type strains so that we could later assess the impact of gene alterations on the ability of the fungus to mate and infect *Z. mays*.

Homologous recombination was then used to replace the native *uded1* with a hygromycin B resistance cassette in the crg1:*uded1* strains. Growth of deletion strains (Δ*uded1* crg1:*uded1*) was observed when incubated in the presence of L-arabinose (permissive growth conditions). In repressive growth conditions, where D-glucose is the carbon source, these mutants were effectively deletion mutants (Figure 5.4A). Under repressive growth conditions, the deletion mutants showed reduced growth at the 10^{-1} and 10^{-2} dilutions compared to the wild-type and expression strains. No difference in growth was found between the 518Δ*uded1* crg1:*uded1* and 521Δ*uded1* crg1:*uded1* strains (Figure S5.6). The ability to control when the ectopically integrated *uded1* is expressed thus enabled us to determine that *uded1* is required for full cell viability and growth in *U. maydis*.

Another growth phenotype that was observed in the Δ*uded1* crg1:*uded1* mutants was the length of time mutants took to grow on solid medium in permissive conditions compared to the wild-type and expression strains. Following incubation at 28 °C for 7 days, the wild-type and crg1:*uded1* strains had significantly more growth than the Δ*uded1* crg1:*uded1* strains. The growth of the Δ*uded1* crg1:*uded1* mutant colonies were significantly smaller compared to the wild-type and expression strains (Figure 5.4B).

During our early experiments with the Δ*uded1* crg1:*uded1* mutants, a mycelial growth phenotype was observed when these strains were streaked on YEPA plates supplemented with hygromycin B. This phenotype was also observed on YEPA, DCMA, and CMA plates supplemented with and without hygromycin B. In *U.* maydis, the switch from budding haploid cells to filamentous growth is in response to environmental factors. Changes in nutrient availability [33], exposure to air [34], acidic pH [35], triacylglycerides [36], and involvement of the cyclic AMP/protein kinase A pathway [34,37]. In order to

assess the cell morphology of the Δ*uded1* crg1:*uded1* mutants, all strains were initially streaked on DCMA plates containing 1 M sorbitol. Single colonies were picked and patched onto either YEPA or YEPA containing 1 M sorbitol plates. Following a 3-day incubation at 28 °C, the 518Δ*uded1* crg1:*uded1* patches grown on YEPA appeared slightly fuzzy compared to both wild-type and 518 crg1:*uded1* strains (Figure 5.5). The 518Δ*uded1* crg1:*uded1* strains grown on YEPA with 1 M sorbitol did not differ in appearance compared to wild-type strains. The cell morphology of all strains was examined through microscopic analysis. For 518Δ*uded1* crg1:*uded1* strains grown in YEPA, a mixture of normal budding cells and cells that appear long and filament-like was observed. When the same strains are grown on YEPA with 1 M sorbitol, the cells appear indistinguishable from wild-type (Figure 5.5). This mycelial growth phenotype was also seen in the 521Δ*uded1* crg1:*uded1* mutants when grown in YEPA and normal budding was restored when cells were grown in the presence of sorbitol (Figure S5.7). This indicates that the osmotic stabilizing affects of sorbitol are required for the mutant strains to grow in a manner similar to wild-type strains.

The Ability for uded1 Mutants to Mate and Infect the Plant

A mating assay was performed to assess if the altered expression of *uded1* impacts the ability of compatible haploid cells to fuse and form a dikaryon. The dikaryon is white and appears fuzzy (Fuz^+) when spotted on medium containing charcoal. The *uded1* mutant and wild-type strains were cultured in permissive conditions (DCMA) and equal volumes of compatible haploids were mixed and spotted on PDA plates containing charcoal. Plates were incubated at room temperature for 3 days and monitored for Fuz^+ development. In general, there was no difference in dikaryon formation when wild-type was crossed with the deletion (wt × Δ*uded1* crg1:*uded1*) (Figure 5.6A). There is a reduction in the density

of Fuz$^+$ in the wt × crg1:*uded1* crosses where the spots appear less white when compared to the 518 × 521 cross. Fuz$^+$ formation is further decreased in the deletion crosses (Δ*uded1* crg1:*uded1* × Δ*uded1* crg1:*uded1*) compared to the 518 × 521 and wt × crg1:*uded1* crosses. The formation of Fuz$^+$ was detected when spots were viewed under a stereoscopic microscope (Figure S5.8). The results of the growth experiments (Figure 5.5) suggested that if mutants were grown in permissive conditions supplemented with 1 M sorbitol, an osmoprotectant, normal budding growth would result.

A second mating assay (Figure 5.6B) was conducted where all mutants and wild-type strains were cultured in DCMA containing 1 M sorbitol. The formation of Fuz$^+$ on PDA plates containing charcoal was monitored for 3 days. There was no difference in dikaryon formation when expression strains were crossed with wild-type or the deletions (wt × crg1:*uded1* or crg1:*uded1* × Δ*uded1* crg1:*uded1*) and with reciprocal crosses (wt × Δ*uded1* crg1:*uded1*). However, reduced Fuz$^+$ development was observed in all deletion crosses (Δ*uded1* crg1:*uded1* × Δ*uded1* crg1:*uded1*) (Figure 5.6B). The Δ*uded1* crg1:*uded1* × Δ*uded1* crg1:*uded1* spots appeared less dense and were smaller when compared to the 518 × 521 spot. Fuz$^+$ development in the Δ*uded1* crg1:*uded1* × Δ*uded1* crg1:*uded1* was monitored for up to 5 days at RT but there was no difference in dikaryon formation compared to 3 days (Figure S5.9). This indicates that with these growth conditions, a wild-type × mutant mating was indistinguishable from wild-type × wild-type but that mutant × mutant matings had substantially reduced Fuz$^+$.

The ability for Δ*uded1* crg1:*uded1* mutants to infect the plant was assessed through pathogenesis assays. Equal volumes of compatible haploids were mixed and injected into

7-day-old Golden Bantam seedlings. The Δ*uded1* crg1:*uded1* strains were unable to infect seedlings (Figure S5.10) and therefore teliospores could not be produced.

Transcript Levels of uded1 in Mutants Grown in Repressive and Permissive Conditions

The transcript level of *uded1* in expression and deletion mutants was assessed when grown in repressive and permissive conditions. In permissive conditions, the *uded1* transcript in the crg1:*uded1* mutants is upregulated compared to the level present in cells grown in repressive conditions and wild-type cells (Figure 5.7). The *uded1* transcript level in the 518Δ*uded1* crg1:*uded1* mutants was upregulated to an even higher degree than in the 518 crg1:*uded1* mutant (Figure 5.7A). The same transcript level trend was seen in the 521Δ*uded1* crg1:*uded1* mutants in comparison to the 521 crg1:*uded1* mutant in permissive conditions (Figure 5.7B). It is the upregulation of *uded1* that is likely contributing to the slow-growth phenotype in Figure 5.4B, a similar slow growth on overexpression was noted for *S. pombe* [26]. In addition, in *S. pombe*, the altered expression of *ded1* contributes to modulating antisense RNAs [38].

Impact of uded1 Expression on dsRNA Stability

Altered *uded1* expression and its impact on sense/antisense interactions was assessed by creating mutants that express *as-ssm1* from an autonomously replicating vector in the crg1:*uded1* mutants. The *as-ssm1* transcript was previously shown to be preferentially expressed in the dormant teliospore and its expression forms dsRNA [14]. This makes it the ideal candidate for assessing sense/antisense interactions when *uded1* expression is altered. The expression of *uded1* was altered by growing the crg1:*uded1* [pCMas-ssm1] mutants in repressive and permissive conditions to repress or activate the crg1 promoter.

An S1 nuclease protection assay was performed to determine the presence of dsRNA and assess the impact of *ssm1*/*as-ssm1* interactions when the expression of *uded1* is altered in the crg1:*uded1* [pCMas-ssm1] mutants.

Strand-specific semi-quantitative RT-PCR was used to confirm expression of the *ssm1* and *as-ssm1* transcripts in the crg1:*uded1* [pCMas-ssm1] mutants grown in repressive and permissive growth conditions (Figure 5.8). The *ssm1* transcript was detected in the empty vector ([pCM768]) control samples and the crg1:*uded1* [pCMas-ssm1] mutants grown in repressive and permissive conditions. The *as-ssm1* transcript was detected in the crg1:*uded1* [pCMas-ssm1] mutants grown in repressive and permissive conditions. Additionally, the *as-ssm1* transcript was detected at low levels in the empty vector controls. The detection of low *as-ssm1* transcript levels was also detected in the haploid cell RNA transcriptome data from Donaldson*, et al.* [39] and Seto, Donaldson and Saville [23]. An internal *UMAG_gapdh*-specific primer was included as a control to assess *UMAG_gapdh* transcript levels. It was noted that in the no first-strand primer (water-primed) samples, an RT-PCR product was produced. This is an indication of non-specific or false-priming during reverse transcription caused by the presence of hairpin structures in the RNA, as previously reported by Ho*, et al.* [40].

The upregulation of *uded1* in the crg1:*uded1* [pCMas-ssm1] mutants was verified using RT-qPCR (Figure 5.9). All three biological replicates of the 518 crg1:*uded1* [pCMas-ssm1] mutants show an upregulation of *uded1* in permissive conditions compared to growth in repressive conditions (Figure 5.9A). The same trend was observed in the 521 crg1:*uded1* [pCMas-ssm1] mutants (Figure 5.9B). One 518 crg1:*uded1* [pCM768] control

biological replicate was removed from further analysis as *uded1* was not upregulated in the permissive grown conditions compared to the repressive sample (Figure S5.11).

The S1 nuclease protection assay was used to determine differences in *ssm1*/*as-ssm1* formation when the expression of *uded1* is altered. All mutant samples expressing *as-ssm1* (crg1:*uded1* [pCMas-ssm1]) from the vector have increased resistance to S1 nuclease digestion in both repressive and permissive conditions indicating that altered expression of *uded1* has no impact on dsRNA formation (Figure 5.10). The 521 crg1:*uded1* [pCM768] empty vector controls grown in permissive conditions showed increased resistance to S1 nuclease digestion (Figure 5.10B); however, the same was not observed with the 518 crg1:*uded1* [pCM768] empty vector controls (Figure 5.10A). The formation of dsRNA in the empty vector controls suggests that upregulation of *uded1* induces conformational changes to the RNA under these conditions or that Uded1 is binding to this region of the transcript to form an mRNP.

DISCUSSION

The role of RNA helicases in fungal phytopathology is not fully understood and little is known of their roles in fungal virulence and pathogenicity. Our previous work identified 46 RNA helicases in the basidiomycete *U. maydis* [29]. We utilized the RNA-seq data from Seto, Donaldson and Saville [23] to identify candidate RNA helicases that may have a role during *U. maydis* teliospore dormancy and germination. We determined that RNA helicases that are upregulated in the dormant teliospore and then decreased once germination is initiated were RNA helicases of interest. We identified five candidate RNA helicases and focused our investigation on the RNA helicases *udbp3* and *uded1*.

The Role of udbp3 in Osmotic Stress Response

UMAG_01732 (*udbp3*) was identified as an ortholog of *DBP3* in *S. cerevisiae*. Phylogenetic analysis identified this DEAD-box RNA helicase as fungal- and plant-specific [29]. Udbp3 contains the characteristic nuclear localization signal KKX sequence motif first described by Weaver, Sun and Chang [24] in the *S. cerevisiae* ortholog. This bioinformatic analysis and the transcript pattern of interest during teliospore germination supported the creation of deletion mutants to explore its potential impact on teliospore dormancy and germination.

The deletion of *udbp3* did not adversely affect *U. maydis* virulence, pathogenicity, or teliospore germination. Mutants in *S. cerevisiae* had a slow-growth phenotype at a decreased temperature [24]; however, this was not an obvious phenotype in the *U. maydis* deletion mutants. The *S. cerevisiae DBP3* mutant had been previously characterized for its response to various stressors. The *DBP3* mutant displayed increased tolerance to ER, oxidative, and DNA stress [25]; however, this phenotype was not observed in our *U. maydis* deletion mutants. Our results suggest in the absence of *udbp3*, there is increased tolerance to osmotic stress induced by exposure to 1 M NaCl. *DBP3* orthologs have been identified in other plant species, such as *Arabidopsis thaliana*, *Glycine max*, *Oryza sativa*, *Vitis vinifera*, *Medicago truncatula*, *Malus domestica*, and *Hordeum vulgare*. Characterization of this gene in plants has been limited to *A. thaliana* and *G. max* [41,42]. In *A. thaliana*, the ortholog *strs*1 is a negative regulator of stress-responsive transcription activators and their downstream targets. This RNA helicase is downregulated by saline, osmotic, and heat stress resulting in the enhancement of transcription factors that respond to these stressors. Overexpression of *strs1* leads to decreased heat and saline tolerance [42,43]. In contrast,

the *G. max* ortholog, *GmRH*, is induced in low temperatures and during high salinity conditions. It was proposed that *GmRH* may have a function in processing RNA during low temperature and salt stress conditions [41]. The increased tolerance to osmotic stress in the Δ*udbp3* mutants suggests that in *U. maydis udbp3* may function as a negative regulator in response to stress, similar to *strs1*. The absence of *udbp3* may induce the transcription of stress-related genes and/or their transcription activators.

udbp3 is upregulated in the dormant teliospore [23] which suggests a function during teliospore dormancy. Based on our current data and previous work in Chung, Cho, Yun, Choi, So, Lee and Lee [41] and Kant, Kant, Gordon, Shaked and Barak [42], *udbp3* may function as a negative regulator of stress-related genes or their activators in response to stress in the teliospore. This would lead to the suppression of stress-related genes in the dormant teliospore. The teliospore is comprised of physical barriers to protect itself from harsh environmental conditions. The *U. maydis* teliospore cell wall is three layers thick where one layer is melanized and contains ornamentation [6,44,45]. These features allow survival of the teliospore in adverse environmental conditions, such as temperature fluctuations and UV exposure.

The DED1 Ustilago maydis Ortholog Is uded1

Our previous annotation of RNA helicases in *U. maydis* [29] and transcriptomic analyses [23] identified *UMAG_04080* as an RNA helicase of interest. It is an RNA helicase found in pattern 17 of transcript level patterns identified in Seto, Donaldson and Saville [23] where the transcript is upregulated in the dormant teliospore and decreases during germination. The protein sequence analysis and phylogenetic work (Figure 2) identified UMAG_04080 as the ortholog to Ded1 in *S. cerevisiae* and DDX3 in *H. sapiens* [29] and

therefore we named this gene *uded1*. The *S. cerevisiae DED1* is an essential gene and deletion mutants have a lethal phenotype [46]. Based on this, it was important to determine the phenotype of the *uded1* mutants. The Δ*uded1* crg1:*uded1* mutants showed that cell growth is inhibited in the absence of *uded1* expression (Figure 5.4). When these mutants are grown in permissive conditions, growth is noticeably slower than the wild-type and expression strains (Figure 5.4B). The upregulation of *uded1* in the Δ*uded1* crg1:*uded1* mutants (Figure 5.7) may contribute to a slow-growth phenotype. The upregulation is caused by the crg1 promoter which yields high levels of expression when *U. maydis* is grown in the presence of L-arabinose [47]. In *S. cerevisiae*, when Ded1 was overexpressed by a factor greater than 10, a slow-growth phenotype and an accumulation of stress granules were observed [26]. A slow-growth phenotype was not observed in the crg1:*uded1* mutants where two copies of *uded1* are present in the genome. Two copies of *uded1* did not increase the transcript level in the crg1:*uded1* mutants (Figure 5.7) to the degree that it was increased in the Δ*uded1* crg1:*uded1* mutants under permissive conditions. The higher *uded1* transcript levels may be required for inhibiting growth.

When compatible Δ*uded1* crg1:*uded1* mutants are crossed with each other, there is decreased Fuz^+ formation when compared to wt × wt, wt × Δ*uded1* crg1:*uded1*, or crg1:*uded1* × Δ*uded1* crg1:*uded1* crosses (Figure 5.6). There was greater fuz^+ formation when cultures were grown in a medium containing sorbitol (Figure 5.6B); however, it was still less dense compared to the wil-type Fuz^+ formation. Several factors may contribute to the decreased Fuz^+ formation in the deletion mutant crosses. The mating assay was performed on PDA medium containing charcoal. The primary carbon source in PDA is dextrose, which did not stimulate the crg1 promoter in the deletion mutants and therefore

overexpression of *uded1* did not influence growth. The mutants were initially cultured overnight in permissive growth conditions, which stimulated the expression of *uded1* and growth of the haploid cells long enough for fusion of the compatible strains on the PDA plates. The addition of the osmoprotectant sorbitol to the growth medium allowed normal budding growth of the Δ*uded1* crg1:*uded1* mutants. The normal growth contributed to the successful fusion of the compatible strains to form the dikaryon but then the lack of crg1 induction would mean that *uded1* is not expressed and continued growth was inhibited producing a reduced amount of Fuz^{+}.

The Δ*uded1* crg1:*uded1* mutants were unable to infect the plant. The inability of the mutants to infect *Z. mays* may be due to insufficient levels of arabinose on the plant surface to ensure ectopic expression of *uded1* from the *ip* locus. The lack of expression would be expected to reduce growth and therefore pathogenesis would not proceed. At the time of infection, the inoculum contained equal concentrations of compatible haploids that are suspended in water. The addition of arabinose to the inoculum was not explored but its addition may have provided sufficient levels of arabinose for *uded1* expression in the deletion mutants which might have allowed dikaryon formation and plant infection.

Uded1's Role in Translation Regulation

Several studies in the budding yeast show that Ded1 regulates translation [26,28]. Our initial hypothesis was that *uded1* had a role in modulating dsRNA during the exit from teliospore dormancy to germination, possibly aiding the translation of stored mRNAs in the dormant teliospore. Ostrowski and Saville [14] identified *as-ssm1* as a natural antisense transcript to a mitochondrial seryl-tRNA synthetase that is expressed in a teliospore-specific manner. The expression of *as-ssm1* forms an mRNA duplex with *ssm1* that may

stabilize the mRNA, repress translation, and prevent degradation during teliospore dormancy [14]. We used the crg1:*uded1* strains to create mutants that expressed the *as-ssm1* transcript from an autonomously replicating vector in haploid cells. We then assessed dsRNA stability in the crg1:*uded1* [pCMas-ssm1] mutants by altering the expression of *uded1* by growing the mutants in repressive and permissive conditions. Under these conditions, *as-ssm1* transcription from the autonomously replicating vector in repressive and permissive conditions was confirmed using RT-PCR (Figure 5.8). However, the genomic copy of *as-ssm1* was also detected at low levels in the vector-only (crg1:*uded1* [pCM768]) controls in repressive and permissive conditions. Reviewing data from Ostrowski and Saville [14] indicated that the *as-ssm1* transcript is teliospore-specific and is not detected in the SG200 solo-pathogenic *U. maydis* strain. However, transcriptome analysis of the data from Donaldson, Ostrowski, Goulet and Saville [39] indicated low levels of the *as-ssm1* transcript in the wild-type haploid strains 518 and 521. Therefore, detecting *as-ssm1* in the vector-only controls was not unexpected. Under the repressive growth conditions, we found no difference in dsRNA formation when the expression of *uded1* is altered (Figure 5.10). The inability to detect a difference in dsRNA formation may indicate that the expression of *as-ssm1* from the vector is driving the dsRNA formation to a high level and that the influence of *uded1* cannot be detected above this level. Interestingly, dsRNA formation was detected in the vector-only controls (crg1:*uded1* [pCM768]) when grown in permissive conditions. This detection of an impact of Uded1 on dsRNA formation may be due to the low level of *as-ssm1* in the haploid strains. This suggests that *uded1* may induce conformational changes to the mRNA to stabilize it, and/or bind to *as-ssm1*/*ssm1* to form an mRNP when *as-ssm1* and *ssm1* RNAs are expressed from

the genome at lower (wild-type) levels. Therefore, the *uded1* influence on dsRNA formation and the subsequent translation inhibition is linked to RNA levels and/or the site of transcription.

In *S. pombe*, the *uded1*ortholog enhances the antisense RNA gene silencing effect when it is co-expressed with a long antisense. It was suggested that *ded1* functions to stabilize the sense/antisense pair to suppress the expression of the gene [38]. The overexpression of Ded1 in *S. cerevisiae* results in translation repression and the formation of stress granules which contain mRNPs that are stalled in translation [26-28]. Ded1 mediates translation when the TOR pathway is inactivated [48] and it was proposed that Ded1 promotes cell survival by repressing general translation which inhibits cell growth and then promoting translation once the stressor has been removed or the cell has adapted [28]. One class of genes that are negative interactors with Ded1 under stress conditions are those involved in mitochondrial translation [49]. Although only nonessential genes were assessed, essential genes, such as the *ssm1* ortholog, may also interact with *DED1*. Given the conserved function of *DED1*/*DDX3*, *uded1* may function to repress the translation of a subset of genes through the formation of mRNPs, especially those formed during teliospore dormancy. Consistent with this, the *uded1* binding to *ssm1*/*as-smm1* to stabilize the dsRNA, observed in our experiments, may result in the creation of an mRNP that stalls translation. The resulting mRNP would likely be sequestered in an RNA granule such as a stress granule where translation could be repressed and the mRNA stabilized [50].

The Δ*uded1* crg1:*uded1* mutants have a mycelial phenotype when grown in permissive conditions. The microscopic analysis (Figure 5.5) showed a mixture of normal budding cells (cigar-shaped) and elongated cells that appear to be growing in a polarized

manner. Forbes*, et al.* [51] reported that cells appear elongated when *ded1* (*sum3*) is overexpressed in *S. pombe*. Overexpression of *ded1* may negatively regulate the cell-cycle response to osmotic stress, possibly interfering with the regulation of proteins in the MAPK pathway [51]. The *uded1* transcript is upregulated in the Δ*uded1* crg1:*uded1* mutants (Figure 5.7) and may contribute to the mycelial phenotype observed (Figure 5.5). Normal budding growth is restored in the Δ*uded1* crg1:*uded1* mutants when cells are in the presence of sorbitol, an osmoprotectant [52-54] (Figure 5.5), which suggests that altered *uded1* expression changes the cells so they are sensitive to osmotic stress. The sensitivity in the *uded1* mutants could result from a defect in the cell wall formation or impaired mitotic division.

The *U. maydis uded1* may have further functions similar to its orthologs in other fungi. Aryanpur, Mittelmeier and Bolger [28] reported that overexpression of Ded1 and oxidative stress resulted in growth defects and translational changes. In addition, an accumulation of stress granules in cells overexpressing Ded1 was observed [26]. Our study did not explore the possibility of stress granule accumulation; however, overexpression of *uded1* led to altered phenotypes in response to a stressor and future research could explore any potential link to stress granule formation in *U. maydis*.

Our results suggest a possible function for *uded1* during teliospore dormancy. The RNA-seq analysis from Seto, Donaldson and Saville [23] indicated that the transcript is upregulated in the dormant teliospore. In dormant teliospores, translation is repressed, and we infer that Uded1 levels are increased based on their transcript levels during dormancy. This translation repression may reduce cell growth and promote the entrance into a dormant state. Consistent with this is the slow-growth phenotype observed in our Δ*uded1*

crg1:*uded1* mutants where the *uded1* transcript was increased. The proposed function of the *S. pombe* Ded1 is to repress general translation leading to slowed growth with the subsequent reversal of this process in response to oxidative stress changes [28]. We hypothesize that, during teliospore formation, *uded1* is involved in repressing the translation of genes involved in cell proliferation and growth and promoting the translation of genes involved in preparing the teliospore for dormancy. Gene transcripts are stored in the dormant teliospore in the form of mRNPs with Uded1 to stabilize them, possibly in stress granules; then when the signal for germination is received, Uded1 could unwind the mRNAs and promote translation of the genes involved in cell proliferation and growth resulting in germination and promycelium formation.

In light of the presented research, we view fungal spore dormancy as a stress response. The development of fungal spores involves changes to the cytoplasm, accumulation of protective compounds, and downregulation of cellular processes that involve cell proliferation and growth [55]. These changes aid in protecting the fungus from adverse environmental conditions during liberation and dispersal. Some notable compounds that have been found in dormant fungal spores are trehalose, glycogen, and lipids [1,56,57] which may act as protective compounds and metabolism reserves during dormancy. Fungal spores are typically characterized as having low respiration rates and limited metabolic activity [8,58-60] suggesting that many of the genes involved in these biological pathways are translationally repressed. Other general features include thick cell walls, as seen with teliospores, and decreased water content [reviewed in 10]. Enzymes and pre-formed mRNAs essential for growth and metabolism are stored within the dormant fungal spore and are utilized once germination is initiated [8,10,11,58,61-63]. Previous

work by Donaldson and Saville [13] and Ostrowski and Saville [14] hypothesized that stored mRNAs in the cytoplasm of dormant teliospores were in the form of sense/antisense pairs that are stabilized with an RNA helicase such as *uded1* to form an mRNP. Teliospore germination is induced under favourable growth conditions, which we interpret as equivalent to removing the stress that the spore senses [55]. The RNA helicases we examined, *udbp3* and *uded1*, are upregulated in the dormant teliospore. Our research has uncovered that these RNA helicases are involved in responding to stresses through interacting with RNA metabolism. Specifically, *udbp3* is involved in regulating stress-responsive transcription factors or genes and *uded1* is involved in slowing growth and interacting with dsRNA also in response to stress. We propose that the *uded1* effect on growth is the result of translation repression and promotion during teliospore dormancy, and that Uded1 may function to bind and stabilize sense/antisense transcripts for storage in the dormant teliospore and then reactivate the mRNAs upon germination. Viewing the formation and germination of teliospores as a stress response involving the activity of these helicases increases our understanding of the molecular events involved during teliospore formation and germination and may aid in developing novel methods for mitigating fungal disease spread and progression.

MATERIALS AND METHODS

Ustilago maydis Strains and Growth Conditions

The *U. maydis* strains used in this study are listed in Table 1. Unless otherwise noted, all *U. maydis* strains are grown in YEPS medium (1% *w/v* yeast extract, 2% *w/v* peptone, 2% *w/v* sucrose) at 28 °C, shaking at 250 rpm. Mutant strains that contain the hygromycin

resistance cassette are grown on medium supplemented with 250 µg/mL hygromycin B (Bioshop Canada, Burlington, ON, Canada) and strains that contain the carboxin resistance cassette are grown on medium supplemented with 4 µg/mL carboxin (MilliporeSigma, Oakville, ON, Canada).

Bioinformatic Analysis

Ustilago maydis RNA helicases were previously identified by Seto and Saville [29]. The transcriptome data from Seto, Donaldson and Saville [23] was utilized to identify RNA helicases with transcript levels that were upregulated in the dormant teliospore and decreased during germination.

Identification of the RNA helicase core for Udbp3 and Uded1 was carried out by aligning protein sequences against orthologs identified by Seto and Saville [29]. Protein sequences were aligned in Jalview v2.11.2.0 [64] using the JABAWS service to perform the MUSCLE alignment under default settings [65]. The RNA helicase core sequence motifs for all RNA helicases in *S. cerevisiae* were previously compared to other orthologs in Fairman-Williams, Guenther and Jankowsky [20] and was used to identify the RNA helicase core in Udbp3 and Uded1. The aligned protein sequences were used to construct maximum likelihood phylogenetic trees using W-IQ-TREE multicore version 1.6.12 [66]. Default settings were selected, 1000 ultrafast bootstrap alignments, and approximate Bayes test were conducted. Phylogenetic trees were visualized and analyzed using FigTree v1.4.4 (available online: http://tree.bio.ed.ac.uk/software/figtree/, accessed 10 February 2023).

Creation of udbp3 Deletion Strains

Deletion constructs were created for *udbp3* utilizing the PCR-based method outlined in Kämper [32]. The plasmids pMF1-hs [32] and pMF1-c [67] (Table S5.1) were used to obtain the hygromycin (*hph*^{R}) and the carboxin resistance cassettes (*cbx*^{R}). Both resistance cassettes were PCR amplified from linearized plasmid DNA using the primers HygCarb_Out_pMF1-F and HygCarb_Out_pMF1-R (Table S5.2). The upstream and downstream flanking regions of the *udbp3* ORF were PCR amplified using primers Dbp3_LF-F and Dbp3_LF_SfiI-R(2) for the 5' flank and Dbp3_RF_SfiI(2) and Dbp3_RF-R(2) for the 3' flank (Table S5.2) to introduce the *Sfi*I restriction endonuclease cleavage site. All PCR products were purified using the PureLink PCR Purification Kit (Thermo Fisher Scientific, Mississauga, ON, Canada), digested with *Sfi*I (New England Biolabs, Whitby, ON, Canada), and gel purified with the PureLink Quick Gel Extraction Kit (Thermo Fisher Scientific, Mississauga, ON, Canada). Equal concentrations of the purified flanking regions and resistance cassette were ligated using T4 DNA ligase (New England Biolabs, Whitby, ON, Canada) and were purified using the PureLink Quick Gel Extraction Kit (Thermo Fisher Scientific, Mississauga, ON, Canada). The Hyg^R and Carb^R constructs were cloned into the pCR2.1 TOPO vector and transformed into One Shot TOP10 competent *E. coli* cells (Thermo Fisher Scientific, Mississauga, ON, Canada). Blue-white screening and kanamycin selection were utilized to select putative transformants containing the *udbp3* deletion construct. Putative bacterial transformants were cultured in LB Broth (Miller) (MilliporeSigma, Oakville, ON, Canada) containing 100 µg/mL ampicillin (BioShop Canada, Burlington, ON, Canada) overnight and plasmid DNA was isolated using the PureLink Quick Plasmid Miniprep Kit (Thermo Fisher Scientific, Mississauga, ON, Canada). Successful transformants were confirmed through sequencing

using primers in Table S5.2 using BigDye Terminator chemistry V.3.1 (Thermo Fisher Scientific, Mississauga, ON, Canada) and an automated sequencer (ABI 3730 DNA analyzer, Thermo Fisher Scientific, Mississauga, ON, Canada). Raw sequences were trimmed and assembled in SeqMan Pro V.11.2.1 using default settings, and aligned using MEGA 7 [68].

Confirmed deletion constructs were PCR amplified from pCR2.1TOPOΔUMAG_01732-HygR and pCR2.1TOPOΔUMAG_01732-CarbR using primers Dbp3_LF_Nested-F and Dbp3_RF-R (Table S5.2) and Phusion High-Fidelity DNA polymerase (Thermo Fisher Scientific, Mississauga, ON, Canada). PCR products were gel purified with the PureLink Quick Gel Extraction Kit (Thermo Fisher Scientific, Mississauga, ON, Canada). The Hyg^R deletion construct was transformed into 518 competent protoplasts and the $Carb^R$ deletion construct was transformed into 521 competent protoplasts to replace *udbp3* with the resistance cassette through homologous recombination. Competent protoplasts and *U. maydis* transformation was performed using the method of Wang*, et al.* [69] with modifications from Morrison*, et al.* [70]. Transformants were plated on DCM containing 2.0% *w/v* D-glucose (Bioshop Canada, Burlington, ON, Canada), 1 M sorbitol (Bioshop Canada, Burlington, ON, Canada), and supplemented with either 250 µg/mL hygromycin B or 4 µg/mL carboxin. Genomic DNA was isolated from successful transformants using the method described by Hoffman and Winston [71]. Putative transformants were screened with PCR and confirmed through Southern blot analysis. Southern blot analysis was conducted using the DIG High Prime DNA labelling and Detection Kit 1 (MilliporeSigma, Oakville, ON, Canada). Probes were

created for the hygromycin and carboxin resistance cassettes following the manufacturer's protocol.

Creation of an uded1 Ustilago maydis Ectopic Expression Strain

The creation of the ectopic expression construct followed the methods outlined in Ostrowski and Saville [14] which used the p123 shuttle vector (Table S5.1). The p123 vector contains ampicillin resistance for bacterial transformation and carboxin resistance targeted to *U. maydis* genome integration at the *ip* locus. The p123 vector contains the constitutive otef promoter (P_{otef}) upstream of the GFP reporter (*egfp*) [72].

The *uded1* expression construct was created to express *uded1* under an L-arabinose inducible promoter. The p123 vector was first modified by replacing P_{otef} with the crg1 promoter (P_{crg1}). P_{crg1} was PCR amplified from pMF2-1h [67] (Table S5.1) with primers crg1-KpnI-F and crg1-XmaI-R (Table S5.2) using Phusion High-Fidelity DNA Polymerase (Thermo Fisher Scientific, Mississauga, ON, Canada). These primers introduced the restriction endonuclease cleavage sites *Kpn*I and *Xma*I at the 5' and 3' ends respectively for insertion into p123 in place of P_{otef}. The PCR product and p123 were digested with *Kpn*I and *Xma*I (New England Biolabs, Whitby, ON, Canada) and purified with the PureLink Quick Gel Extraction Kit (Thermo Fisher Scientific, Mississauga, ON, Canada) following the manufacturer's protocols. The digested and purified PCR product and p123 without P_{otef} were ligated with T4 DNA ligase, transformed into Subcloning Efficiency DH5α Competent *Escherichia coli* cells (Thermo Fisher Scientific, Mississauga, ON, Canada), and plated on LB Broth (Miller) (MilliporeSigma, Oakville, ON, Canada) supplemented with 100 µg/mL ampicillin following the manufacturer's protocols. Bacterial colonies were cultured overnight in 3.0 mL of LB Broth (Miller) (MilliporeSigma, Oakville, ON, Canada)

supplemented with 100 µg/mL ampicillin and plasmid DNA was isolated using the PureLink Quick Plasmid Miniprep Kit (Thermo Fisher Scientific, Mississauga, ON, Canada) following the manufacturer's protocols. Putative transformants were verified by sequencing following the protocols outlined above and using the plasmid DNA.

The *uded1* expression construct was created using the modified p123 vector (p123+crg1). *uded1* was PCR amplified with primers UMAG_04080_NcoI-F and UMAG_04080_NotI_R from *U. maydis* gDNA using Phusion High Fidelity DNA Polymerase. Both p123+crg1 and PCR products were digested with *Nco*I-HF and *Not*I-HF (New England Biolabs, Whitby, ON, Canada). Digested products were gel purified with the PureLink Quick Gel Extraction Kit (Thermo Fisher Scientific, Mississauga, ON, Canada), followed by ligation with T4 DNA ligase (New England Biolabs, Whitby, ON, Canada). The ligated product produced the p123+crg1+*uded1* construct which was transformed into Subcloning Efficiency DH5α Competent *Escherichia coli* cells (Thermo Fisher Scientific, Mississauga, ON, Canada) and grown on LB Broth (Miller) (MilliporeSigma, Oakville, ON, Canada) plates supplemented with 100 µg/mL ampicillin with modifications to the manufacturer's protocols. Following transformation, the plated transformants were incubated at 28 °C for two days to promote slow growth of *E. coli*. Previous transformations at the recommended 37 °C incubation temperature yielded little to no transformants which suggested leaky expression of *uded1* from the plasmid resulting in the gene being toxic to *E. coli*. Bacterial colonies were cultured overnight at 28 °C in 3.0 mL of LB Broth (Miller) (MilliporeSigma, Oakville ON, Canada) supplemented with 100 µg/mL ampicillin and plasmid DNA was isolated using the PureLink Quick Plasmid Miniprep Kit (Thermo Fisher Scientific, Mississauga, ON, Canada) following the

manufacturer's protocols. The construct was verified through sequencing using the procedure above using primers listed in Table S5.2.

The confirmed construct was linearized with *Ssp*I (New England Biolabs, Whitby, ON, Canada) and purified with the PureLink PCR Purification Kit (Thermo Fisher Scientific, Mississauga, ON, Canada). The linearized construct was transformed into competent *U. maydis* 518 and 521 protoplasts for integration into the *ip* locus using the transformation protocols described above. The transformed protoplasts were plated on DCM plates containing 2.0% *w/v* D-glucose and 1 M sorbitol and supplemented with 4 µg/mL carboxin. Genomic DNA was isolated from successful transformants using the method described above. The transformants were screened for multiple p123+crg1+*uded1* insertions with PCR using the primers p123multi-F and p123multi-R (Table S5.2). Putative transformants that did not PCR amplify with these primers passed the PCR screen. Transformants that passed this screen were PCR amplified with primers umgapd-F and umgapd-R (Table S5.2) to ensure genomic DNA was amplifiable. The putative transformants were confirmed with Southern blot analysis using the DIG High Prime DNA labelling and Detection Kit 1 (MilliporeSigma, Oakville, ON, Canada) using the carboxin resistance-specific probe.

Creation of an uded1 Ustilago maydis Deletion Strain

Viable mutants could not be obtained using the traditional PCR-based method [32] to delete *uded1* to delete *uded1* suggesting that the deletion of *uded1* is lethal. Instead, the two-step gene disruption method employed by Ostrowski and Saville [14] was utilized to delete the native *uded1* from its native locus in the ectopic expression strains (518 crg1:*uded1* and 521 crg1:*uded1*).

The *uded1* deletion construct was created following the methods in Kämper [32]. The Hyg^R cassette was PCR amplified with the primers HygCarb_Out_pMF1-F and HygCarb_Out_pMF1-R (Table S5.2) from linearized pMF1-hs DNA. The 5' and 3' flanking regions of *uded1* were PCR amplified from *U. maydis* genomic DNA with the primers Ded1_LF-F and Ded1_LF_SfiI-R(2), and Ded1_RF_SfiI-F(2) and Ded1_RF-R (Table S5.2) respectively to introduce an *Sfi*I restriction endonuclease cleavage site. All PCR products were PCR purified, digested with *Sfi*I, and purified by gel extraction. Equal concentrations of the purified Hyg^R cassette, *uded1* 5' flanking region, and *uded1* 3' flanking region were ligated using T4 DNA ligase (New England Biolabs, Whitby, ON, Canada). The ligated product (~3.9 kb) was gel extracted and purified following the same method for creating the *udbp3* deletion mutants. The purified ligation product was cloned into the pCR 2.1 TOPO vector and transformed into One Shot TOP10 competent *E. coli* cells (Thermo Fisher Scientific, Mississauga, ON, Canada). Putative transformants were selected using blue-white screening and kanamycin selection. Putative transformants were confirmed by sequencing as outlined above using primers listed in Table S2.

The confirmed deletion construct was PCR amplified from the pCR2.1TOPOΔ*uded1*-HygR plasmid using nested primers Ded1_LF_Nest-F and Ded1_RF_Nest-R (Table S5.2) and Phusion High-Fidelity DNA polymerase (Thermo Fisher Scientific, Mississauga, ON, Canada). The PCR product was gel extracted and purified as described above. The purified deletion construct was transformed into 518 crg1:*uded1* and 521 crg1:*uded1* competent protoplasts to replace *uded1* at its native locus by homologous recombination. Transformants were plated on DCM plates containing 1.0% *w/v* L-arabinose (MilliporeSigma, Oakville, ON, Canada), 1 M sorbitol, and supplemented

with 250 µg/mL hygromycin B. Medium containing L-arabinose ensured ectopic expression of *uded1* at the *ip* locus to allow for growth of transformants. Genomic DNA was isolated from putative transformants following the methods above and screened by PCR using the primers 04080_LF-Seq-F1 and 04080-Seq-R1 (Table S5.2). Putative transformants that passed the PCR screen were confirmed through Southern Blot analysis using the methods outlined above. The hygromycin resistance cassette was probed following the manufacturer's protocol.

Creation of as-ssm1 Expressing Strains

The *ssm1* antisense (*as-ssm1*) was previously characterized by Ostrowski and Saville [14]. Donaldson and Saville [13] created an expression vector to express *as-ssm1* from an autonomously replicating sequence in the pCM768 vector. The pCM[as-ssm1] vector was transformed into competent 518 crg1:*uded1* and 521 crg1:*uded1* protoplasts using the García-Pedrajas*, et al.* [73] *U. maydis* transformation method. All transformed cells were plated and grown on YEPS plates supplemented with 250 µg/mL hygromycin B. DNA was isolated from putative transformants and PCR screened with primers pGAP(-79)Forward and Um12232 PCR-F to amplify the antisense transcript and HYG-Seq-F2 and HYG-Seq-R3 which amplify the Hyg^R cassette (Table S5.2) to verify successful *U. maydis* transformation. Furthermore, antisense transcript expression was confirmed via RT-PCR for all transformants.

Total RNA Isolation, RT-PCR, and RT-qPCR

Total RNA was isolated from all samples, DNaseI-treated, and screened for gDNA contamination following the methods outlined in Doyle*, et al.* [74] and Morrison,

Donaldson and Saville [70]. RNA was quantified with a NanoDrop 8000 Spectrophotometer (Thermo Fisher Scientific, Mississauga, ON, Canada) and quality was assessed by electrophoretic separation of glyoxalated RNA on an agarose gel using methods outlined in Sambrook and Russell [75]. Reverse transcription was carried out on 200 ng of DNase I-treated RNA in a 10 µL reaction using TaqMan Reverse Transcription Reagents (Thermo Fisher Scientific, Mississauga, ON, Canada). For RT-PCR, RNA was primed with oligo-d$(T)_{16}$ and for strand-specific first-strand synthesis reactions, RNA was primed with primers listed in Table S5.2. The oligo-d$(T)_{16}$ reactions were carried out under the following conditions: 25 °C for 10 min, 50 °C for 30 min, 95 °C for 10 min, followed by a 4 °C hold. Strand-specific first-strand synthesis reactions were carried out under the conditions outlined by Ho, Donaldson and Saville [40]. Following first-strand synthesis, the cDNA was diluted fourfold (1:3) with dH_2O.

Primers for all RT-PCR reactions were designed in Primer3 v4.1.0 [76-78] and are listed in Table S2. All RT-PCR reactions were performed with 2.0 µL of diluted cDNA and DreamTaq DNA Polymerase (Thermo Fisher Scientific, Mississauga, ON, Canada). PCR cycling conditions were: 95 °C for 3 min, then 35 cycles of 95 °C for 30 s, 60 °C for 30 s, and 72 °C for 1 min, then 72 °C for 10 min, followed by a 4 °C hold. One-third of the RT-PCR product was separated by agarose gel electrophoresis. Agarose gels contained 0.3 µg/mL of ethidium bromide (BioShop Canada, Burlington, ON, Canada), and PCR products were visualized under UV light.

Primers and TaqMan MGB probes for RT-qPCR were designed with Primer Express Software version 2.0 (Thermo Fisher Scientific, Mississauga, ON, Canada) using default criteria for genes *UMAG_00175* and *uded1* (Table S5.2). RT-qPCR reactions were

carried out with 2.0 µL of diluted cDNA in a 20 µL reaction with TaqMan Universal PCR Master Mix (Thermo Fisher Scientific, Mississauga, ON, Canada) on the QuantStudio 3 Real-Time PCR System (Thermo Fisher Scientific, Mississauga, ON Canada). The RT-qPCR cycling conditions were: 50 °C for 2 min, 95 °C for 10 min, followed by 40 cycles of 95 °C for 15 s and 60 °C for 1 min. Data was collected and analyzed using the QuantStudio Design & Analysis Software version 2.6.0 (Thermo Fisher Scientific, Mississauga, ON, Canada). The comparative C_T ($2^{-\Delta\Delta CT}$) method was used to analyze the results where *UMAG_00175* was set as the endogenous control. The calibrator control is specified for each experiment.

S1 Nuclease Protection Assay

RNA was isolated from as-ssm1 expressing strains that were grown and harvested from YEPS and YEPA (1% *w/v* yeast extract, 2% *w/v* peptone, 1% *w/v* L-arabinose) plates supplemented with 250 µg/mL hygromycin B. Cells were frozen in liquid nitrogen and stored at −80 °C prior to RNA extraction. The frozen cells were resuspended in TRIzol reagent (Thermo Fisher Scientific, Mississauga, ON, Canada) and transferred to 2.0 mL screw-cap tubes containing Lysing Matrix C (MP Biomedicals, Santa Ana, CA, USA). Cells were disrupted and RNA was isolated following the methods described above. All RNA samples were precipitated, DNase I-treated, and screened for gDNA contamination as described above.

S1 nuclease digestion reactions were carried out on 2.5 µg of DNase I-treated RNA and incubated at 37 °C for 30 minutes. Each reaction contained the following final concentration of S1 nuclease (Thermo Fisher Scientific, Mississauga, ON, Canada): 0, 0.01, 0.1, or 1 U/µL. The dsRNA was extracted by phenol/chloroform, precipitated with

NH_4Ac/Ethanol/GlycoBlue Coprecipitant (Thermo Fisher Scientific, Mississauga, ON, Canada) at −20 °C for at least 60 min, and resuspended in 15 µL DEPC-treated water. Strand-specific first-strand synthesis was performed on 2.0 µL of S1 trimmed RNA using tagged *ssm1* sense-specific first-strand primers that targeted either the overlapping region of the sense/antisense region (um12232_FS_Sense_Tag) or the non-overlapping region (um12232_FS_S_NO) (Table S5.2). The RT-PCRs were carried out targeting the overlapping and non-overlapping regions to determine dsRNA protection and PCR cycling was performed using 40 cycles instead of 35.

Plate Mating Assays

Plate mating assays were carried out by a modified method of Donaldson*, et al.* [79]. The *udbp3* mutant strains were grown overnight in YEPS and the *uded1* mutant strains were grown overnight in liquid DCM containing 1.0% *w/v* L-arabinose and DCM containing 1.0% *w/v* L-arabinose and 1 M sorbitol. All cells were washed and diluted to an OD_{600} of 1.0 with sterile water. Equal volumes of compatible haploids were pre-mixed and 5.0 µL were spotted on PDA (BioShop Canada, Burlington, ON, Canada) plates containing 1.0% *w/v* activated charcoal (MilliporeSigma, Oakville, ON, Canada). All plates were incubated at room temperature and filamentous growth was assessed 2–3 days post spotting.

Seedling Pathogenesis Assays

Pathogenesis assays on Golden Bantam *Z. mays* seedlings were performed following the protocols outlined in Morrison, Donaldson and Saville [70]. Disease symptoms were scored at 7, 10, and 14 days post-infection using the scoring system outlined in Cheung*, et al.* [80]. All pathogenesis assays were performed in triplicate with approximately 45 plants

per biological replicate. Statistical analysis was performed as outlined in Cheung, Donaldson, Storfie, Spence, Fetsch, Harrison and Saville [80].

Stress Response Assay

The osmotic stress response caused by NaCl was assessed in the *udbp3* deletion mutants. All strains were cultured overnight in YEPS and normalized to an OD_{600} of 1.0. Cells were pelleted, washed with sterile dH_2O, and resuspended in sterile dH_2O. A ten-fold dilution series was created for each strain and 5.0 µL of the dilution series was plated on YEPS plates containing 1 M NaCl and Minimal Medium (MM) plates containing 1.0% *w/v* D-glucose and 1 M NaCl. Plates were incubated at 28 °C for three days.

Plate Growth Assays

Mycelial growth of the *uded1* mutant strains was assessed by streaking all strains on DCM plates containing 1.0% *w/v* L-arabinose, 1 M sorbitol, and antibiotic selection. All plates were incubated at 28 °C for four days. For each *U. maydis* strain, single colonies were picked and streaked on YEPS and YEPA plates. Plates were incubated at 28 °C for three days. The growth on the plate was observed using a Leica S8 APO stereo microscope (Leica Microsystems, Concord, ON, Canada). Photographs were obtained using the Leica EC3 camera and images were analyzed using the Leica Application Suite EZ software v2.1.0 (Leica Microsystems, Concord, ON, Canada). A small portion from the middle of the growth on the plate was picked to include both budding and filamentous cells and was resuspended in 100 µL sterile dH_2O. Cells were observed using the AxioScope.A1 compound microscope (Carl Zeiss MicroImaging, Toronto, ON, Canada) and differential

interference contrast (DIC) images were created at 400× magnification using an Axiocam 208 colour camera (Carl Zeiss MicroImaging, Toronto, ON, Canada).

Supplementary Materials: The following supporting information can be downloaded at: https://www.mdpi.com/article/10.3390/ijms26062432/s1.

Author Contributions: Conceptualization, writing – review and editing, A.M.S. and B.J.S; methodology, formal analysis, writing – original draft preparation, A.M.S; resources, supervision, funding acquisition, B.J.S. All authors have read and agreed to the published version of the manuscript.

Funding: Funding for this project was awarded by the Natural Sciences and Engineering Research Council (NSERC) of Canada to B.J.S.

Institutional Review Board Statement: Not applicable

Informed Consent Statement: Not applicable

Data Availability Statement: Data is contained within the article and Supplementary Materials.

Acknowledgments: We would like to thank Scott Lambie for creating pCMas-ssm1.

Conflicts of Interest: The authors declare no conflict of interest

TABLES AND FIGURES

Table 5.1. The *Ustilago maydis* strains used in this study.

Strain	Relevant genotype*	Source
Wild-type		
518	*a2 b2*	Holliday [81]
521	*a1 b1*	Holliday [81]
uded1 Mutants		
518 crg1:*uded1*	*a2 b2* crg1:*uded1*::cbx^R	This study
521 crg1:*uded1*	*a1 b1* crg1:*uded1*::cbx^R	This study
518Δ*uded1* crg1:*uded1*	*a2 b2* Δ*uded1*::hph^R crg1:*uded1*::cbx^R	This study
521Δ*uded1* crg1:*uded1*	*a1 b1* Δ*uded1*::hph^R crg1:*uded1*::cbx^R	This study
518 crg1:*uded1* [pCM768]	*a2 b2* crg1:*uded1*::cbx^R [*pCM768*]	This study
521 crg1:*uded1* [pCM768]	*a1 b1* crg1:*uded1*::cbx^R [*pCM768*]	This study
518 crg1:*uded1* [pCMas-ssm1]	*a2 b2* crg1:*uded1*::cbx^R [*pCMas-ssm1*]	This study
521 crg1:*uded1* [pCMas-ssm1]	*a1 b1* crg1:*uded1*::cbx^R [*pCMas-sm1*]	This study
udbp3 Mutants		
518Δ*udbp3*	*a2 b2* Δ*udbp3*::hph^R	This study
521Δ*udbp3*	*a1 b1* Δ*udbp3*::cbx^R	This study

**a1 b1* = mating type loci genotype, *a2 b2* = mating type loci genotype, hph^R = hygromycin resistance, cbx^R = carboxin resistance

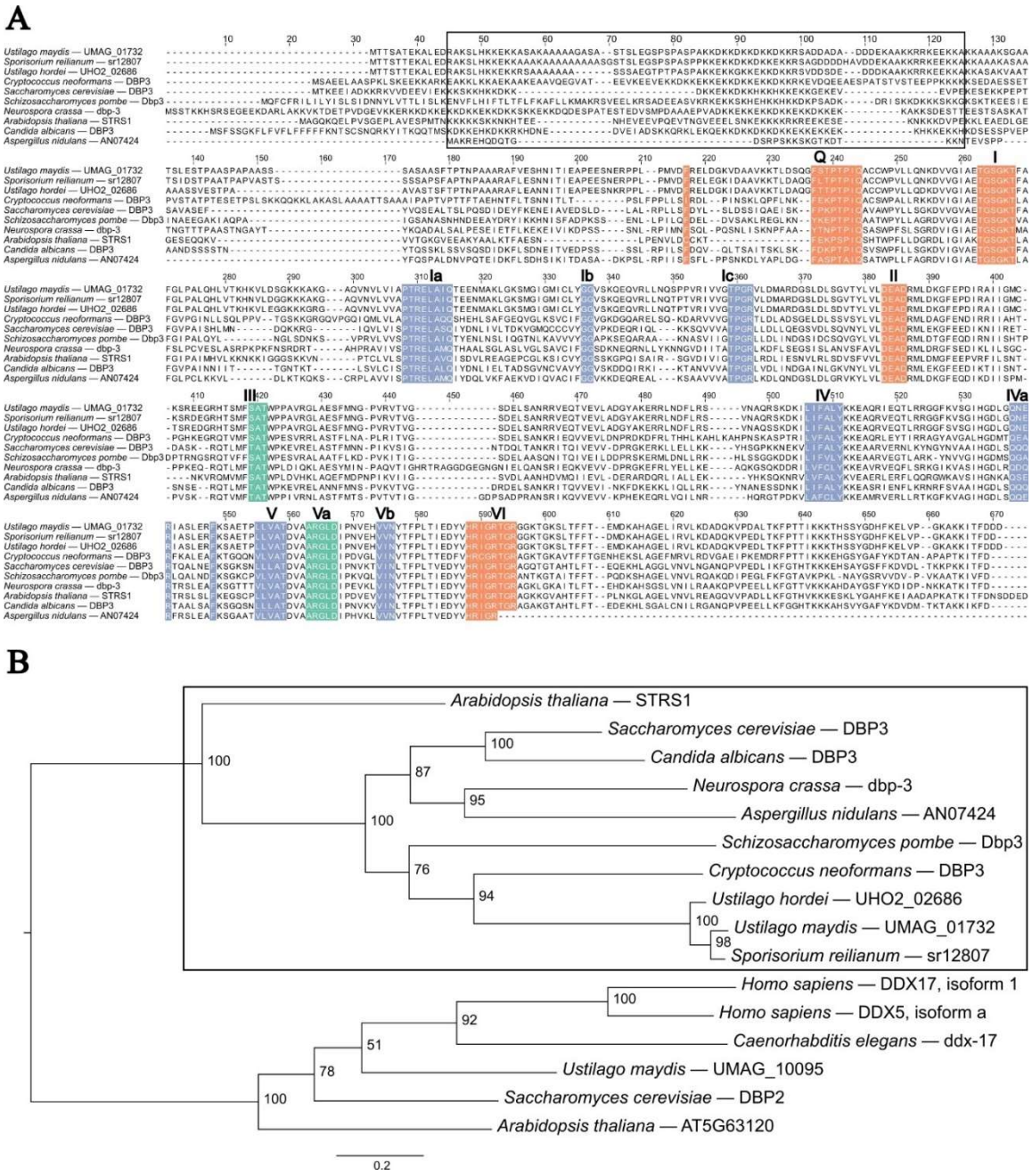

Figure 5.1. Protein sequence alignment and maximum likelihood phylogenetic tree for Udbp3 and its orthologs. (**A**) Protein sequence alignment of Udbp3 and putative orthologs. MUSCLE alignment [65] of protein sequences was performed and visualized in Jalview v2.11.2.0 [64]. The repetitive KKX sequence motif is identified by the black box. The RNA helicase core sequence motifs, indicated by bold letters and numbers, were identified based on motif identification from Fairman-Williams, Guenther and Jankowsky [20]. The coloured boxes indicate sequence motifs based on their predominant biochemical function: Orange, ATP binding and hydrolysis; Blue, nucleic acid binding; Green, coordination of NTP and nucleic acid binding site (**B**) Maximum likelihood phylogenetic tree of Udbp3 orthologs was created using W-IQ-Tree multicore version 1.6.12 with default settings [66],

1000 ultrafast bootstrap alignments, and approximate Bayes test. The tree was visualized using FigTree v1.4.4 (available online: http://tree.bio.ed.ac.uk/software/figtree/, accessed on 10 February 2023). The tree was rooted at the midpoint, the bootstrap value is indicated for each node, and the scale bar indicates the expected number of substitutions per amino acid. The protein for each organism is indicated and the black box indicates the clade of Udbp3 orthologs.

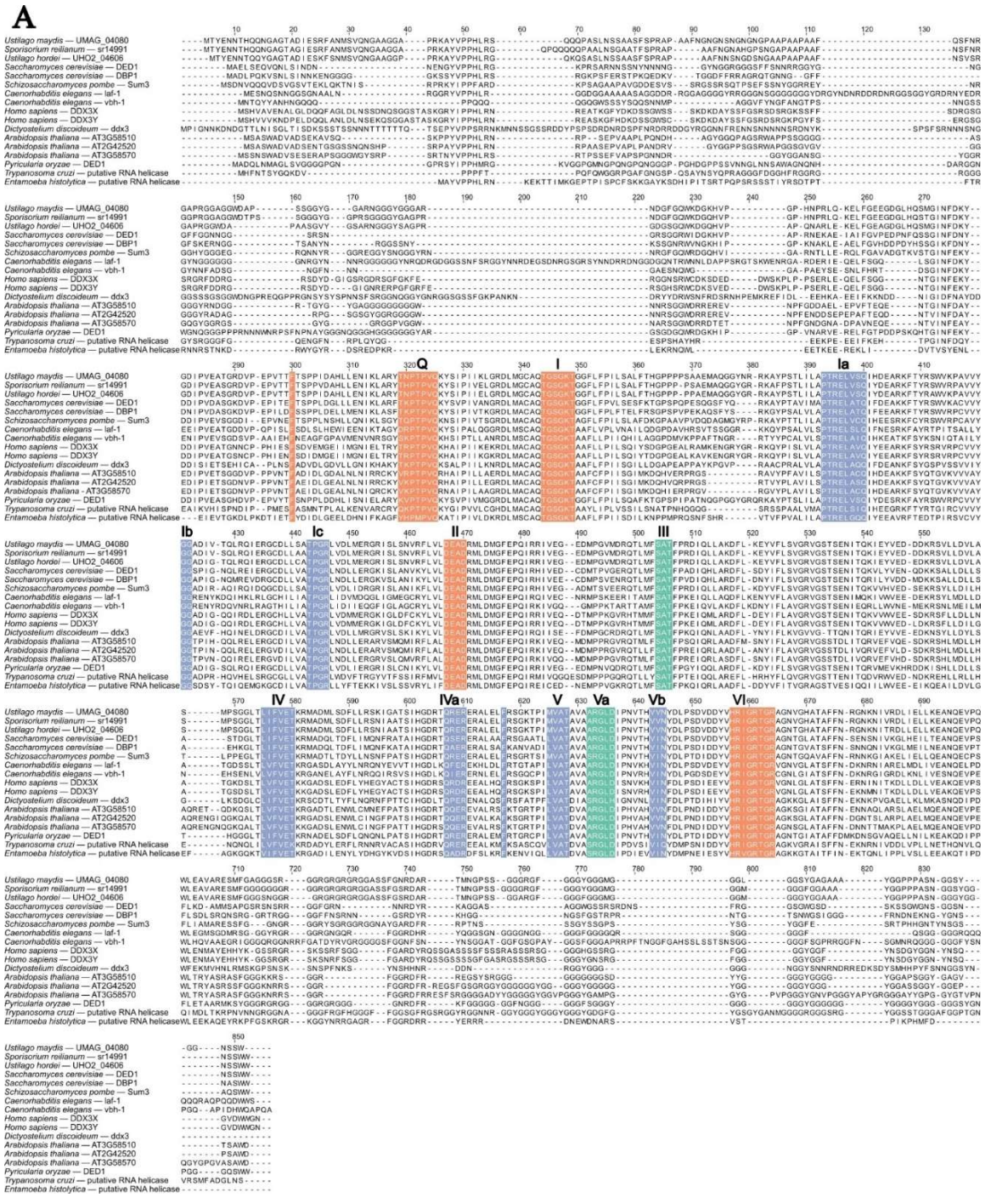

Figure 5.2 *Cont.*

B

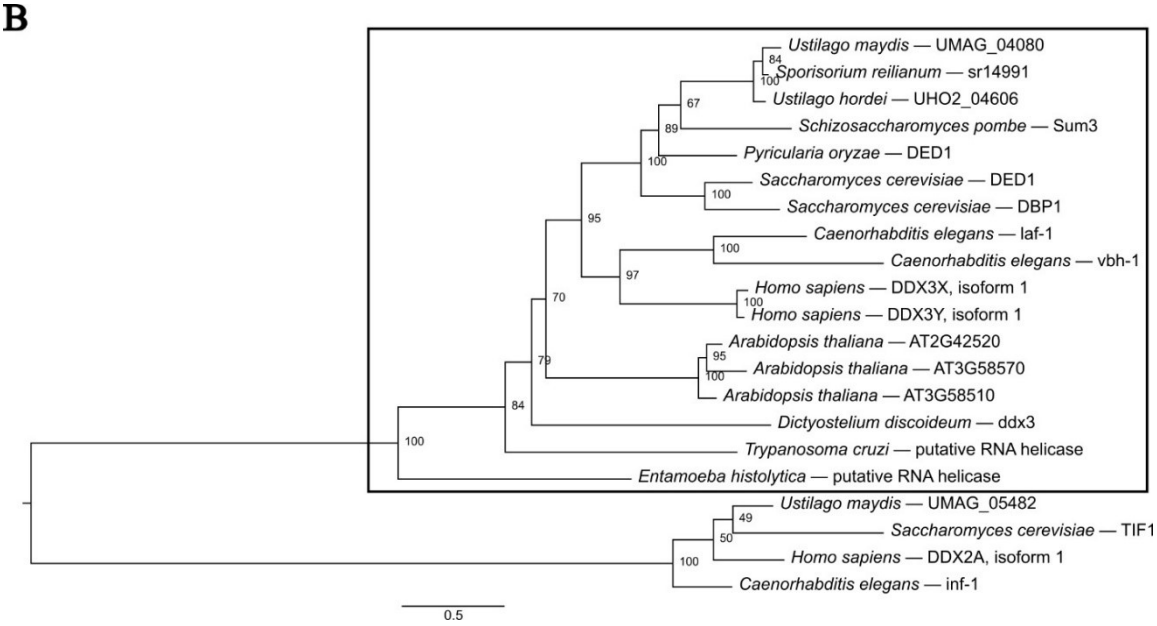

Figure 5.2. Uded1 protein sequence alignment and maximum likelihood phylogenetic tree. (**A**) MUSCLE alignment [65] of Uded1 and putative orthologs. The RNA helicase core sequence motifs, indicated in bold letters and numbers, were identified based on analysis from Fairman-Williams, Guenther and Jankowsky [20]. The coloured boxes indicate sequence motifs based on their predominant biochemical function: Orange, ATP binding and hydrolysis; Blue, nucleic acid binding; Green, coordination of NTP and nucleic acid binding site (**B**) Maximum likelihood phylogenetic tree of uded1 orthologs was constructed using W-IQ-Tree with default settings [66], 1000 ultrafast bootstrap alignments, and approximate Bayes test. The tree was visualized using FigTree v1.4.4 (available online: http://tree.bio.ed.ac.uk/software/figtree/, accessed on 10 February 2023). The tree was rooted at the midpoint, the bootstrap value is indicated for each node, and the scale bar indicates the expected number of substitutions per amino acid. The name of the protein for each organism is indicated and the box indicates the clade of Uded1 orthologs.

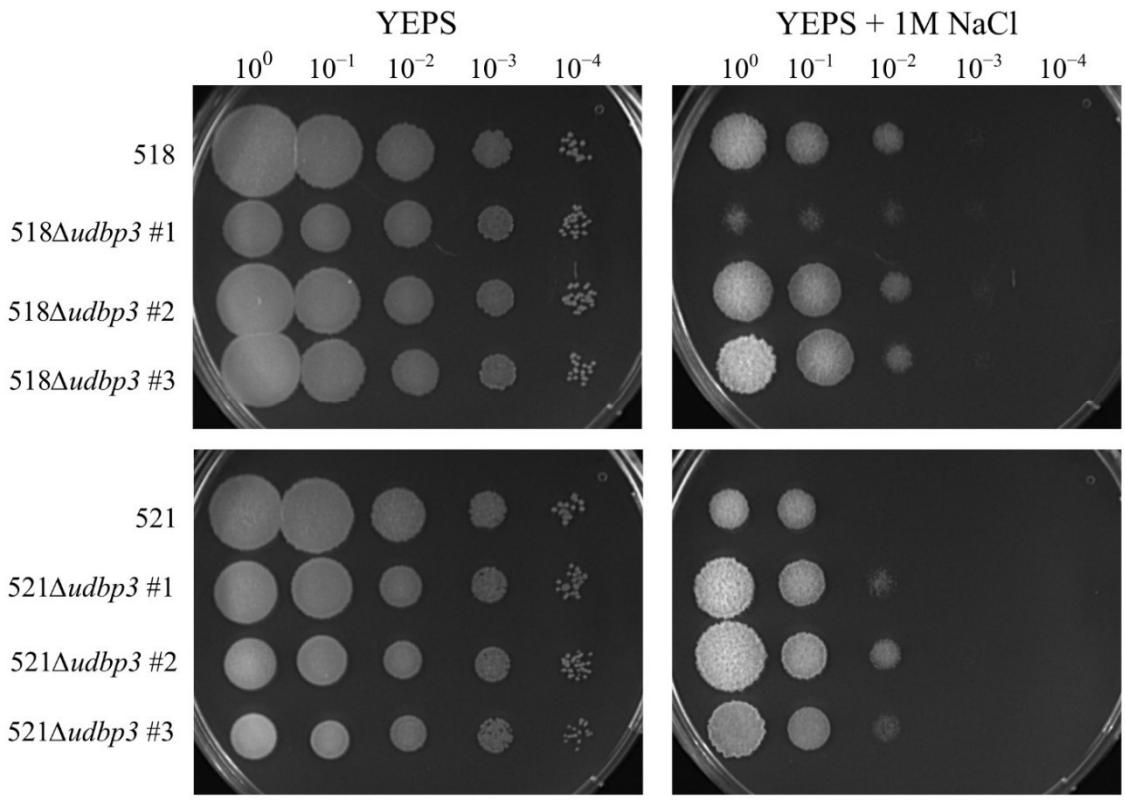

Figure 5.3. The effects of osmotic stress on Δ*udbp3* mutants. Overnight cultures were normalized to an OD_{600} = 1.0 and a 10-fold serial dilution series was created for all strains. All *U. maydis* cultures were spotted on YEPS (control plate) and YEPS containing 1 M NaCl. Plates were incubated at 28 °C and photographed after 3 days. The data shown is representative of three technical replicates of the spotting assay.

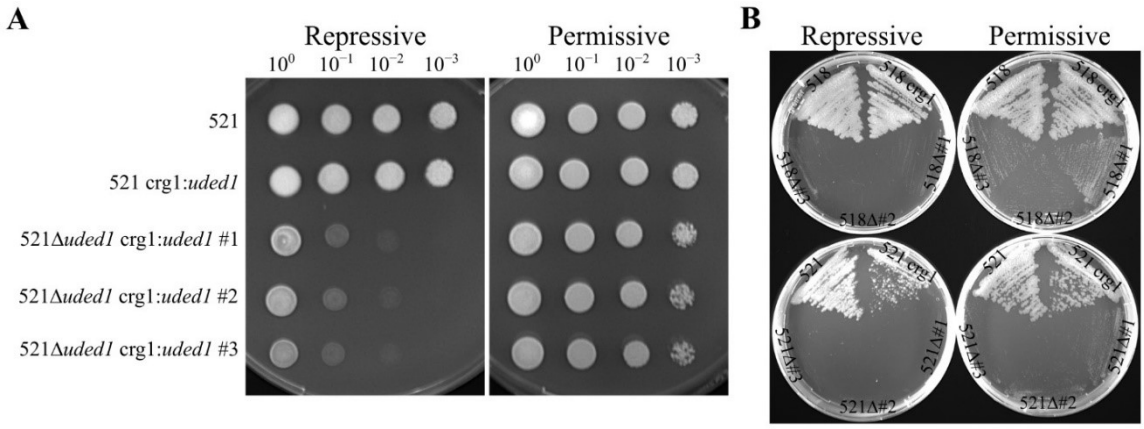

Figure 5.4. Growth of *uded1* mutants in permissive and repressive growth conditions. (**A**) A 10-fold serial dilution series was plated on MM containing 1.0% D-glucose (repressive) and MM containing 1.0% L-arabinose (permissive). Plates were incubated at 28 °C and photographs of each plate were taken after 3 days. The data shown is representative of three technical replicates of the spotting assay. (**B**) *uded1* mutants streaked onto YEPS (repressive) and YEPA (permissive) plates and incubated at 28 °C. Photographs were taken at 7 days post-incubation. Label abbreviations: crg1 delineates the crg1:*uded1* strain and Δ#1–3 delineates the Δ*uded1* crg1:*uded1* biological replicates.

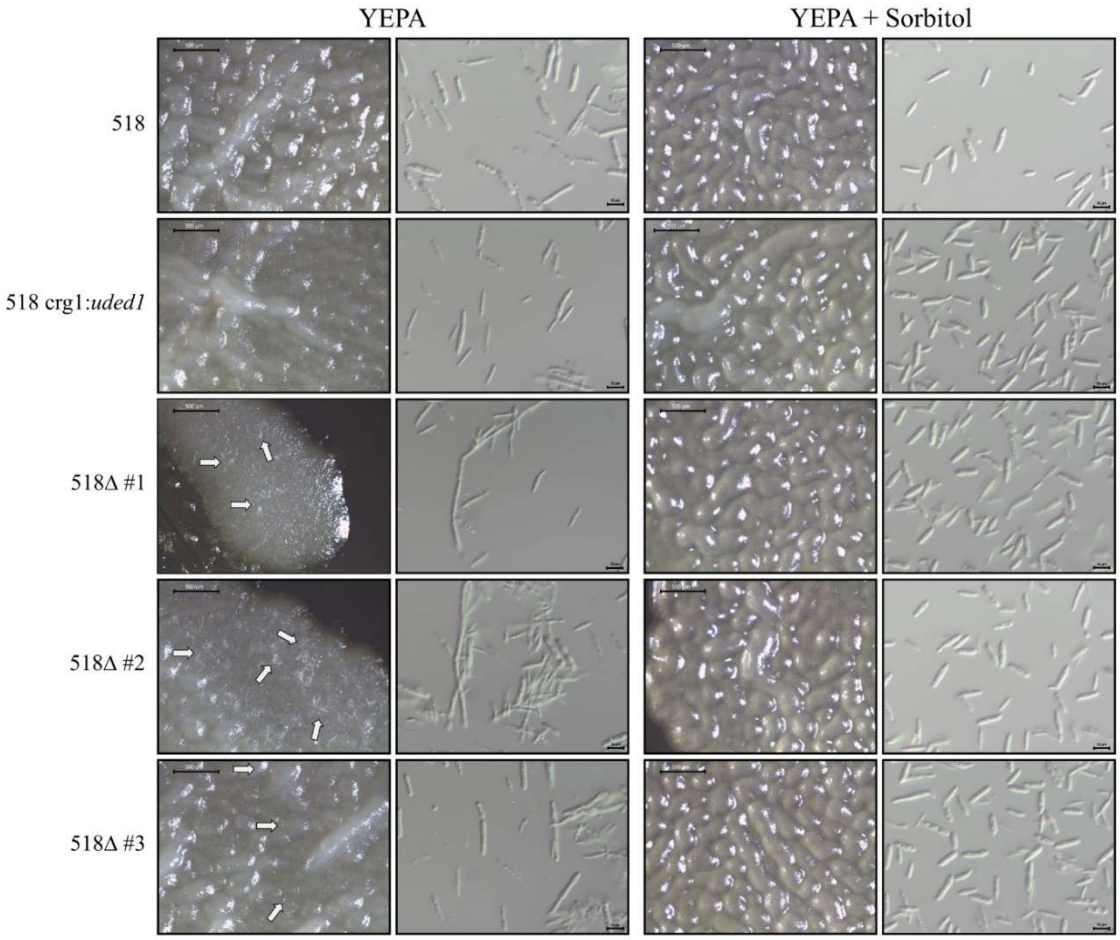

Figure 5.5. The effects of sorbitol addition to solid medium on the growth of *uded1* mutants. Single colonies of each *U. maydis* strain were streaked onto YEPA and YEPA containing 1 M sorbitol plates and incubated at 28 °C for 3 days. Microscopic images were taken of the growth on the plate (40×) and of the cells resuspended in sterile dH_2O (400× magnification). Scale bar indicates 500 µm (plate micrographs) and 10 µm (cell micrographs). Data shown is representative of three technical replicates of the growth assay. The results of the growth assay in the 521 *uded1* mutants is shown in Figure S5.7. Arrows indicate mycelial growth. Label abbreviations: Δ#1–3 delineates the Δ*uded1* crg1:*uded1* biological replicates.

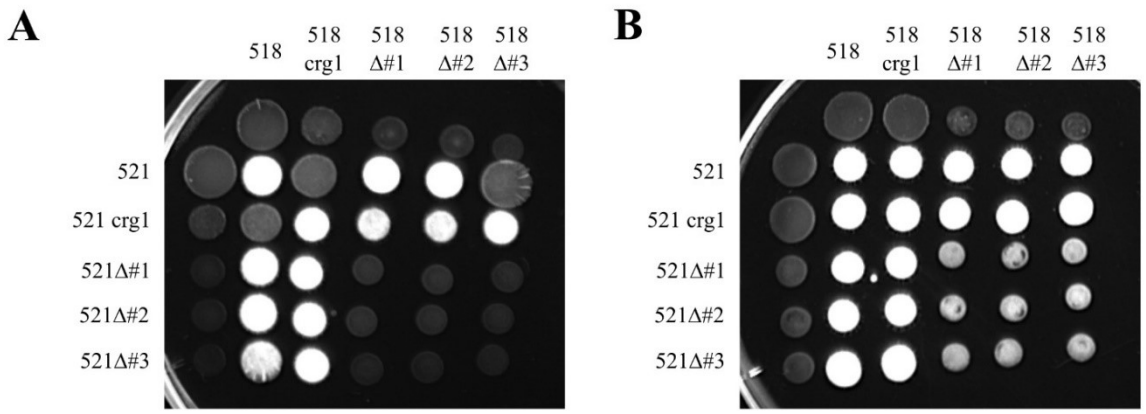

Figure 5.6. Mating assay of *uded1* mutants. (**A**) *Ustilago maydis* strains were cultured overnight in DCM containing 1.0% L-arabinose. (**B**) *Ustilago maydis* strains were cultured overnight in DCM containing 1.0% L-arabinose and 1 M sorbitol. All cultures were normalized, and compatible strains were premixed. Premixed cultures were spotted on PDA containing 1.0% activated charcoal. Plates were incubated at room temperature. Photos were taken after 3 days and the representative data of three technical replicates of the mating assay is shown. The label abbreviations are: crg1 indicates the crg1:*uded1* mutants and Δ #1–3 indicates the Δ*uded1* crg1:*uded1* mutants.

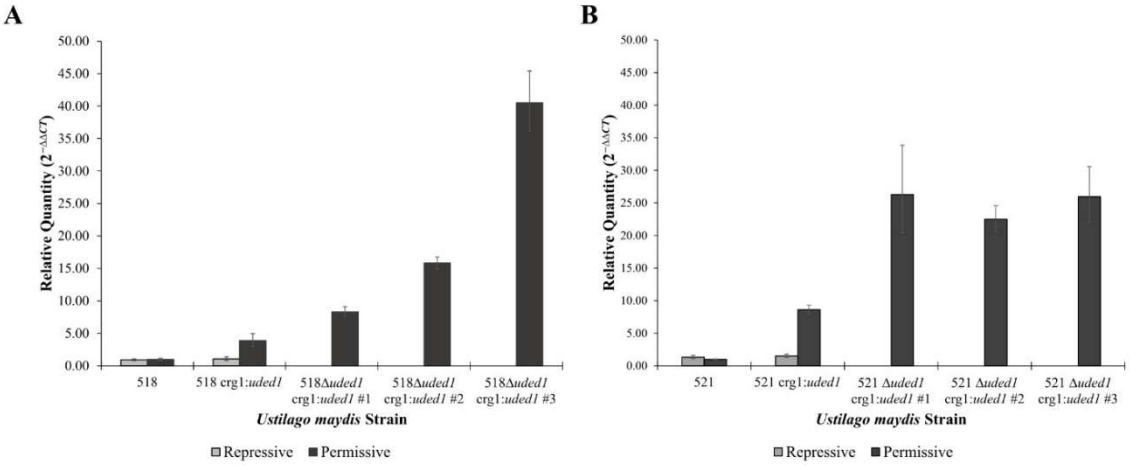

Figure 5.7. The *uded1* transcript is upregulated in the deletion strains when grown in permissive conditions. The relative quantities were determined by RT-qPCR and calculated using the comparative C_T ($2^{-\Delta\Delta CT}$) method, *UMAG_00175* was the endogenous control, and the parent strain (518 or 521) grown in repressive conditions was set as the calibrator. (**A**) 518 wild-type and mutant strains. (**B**) 521 wild-type and mutant strains. Bars indicate the RQ minimum and RQ maximum values (95% confidence interval, n = 3).

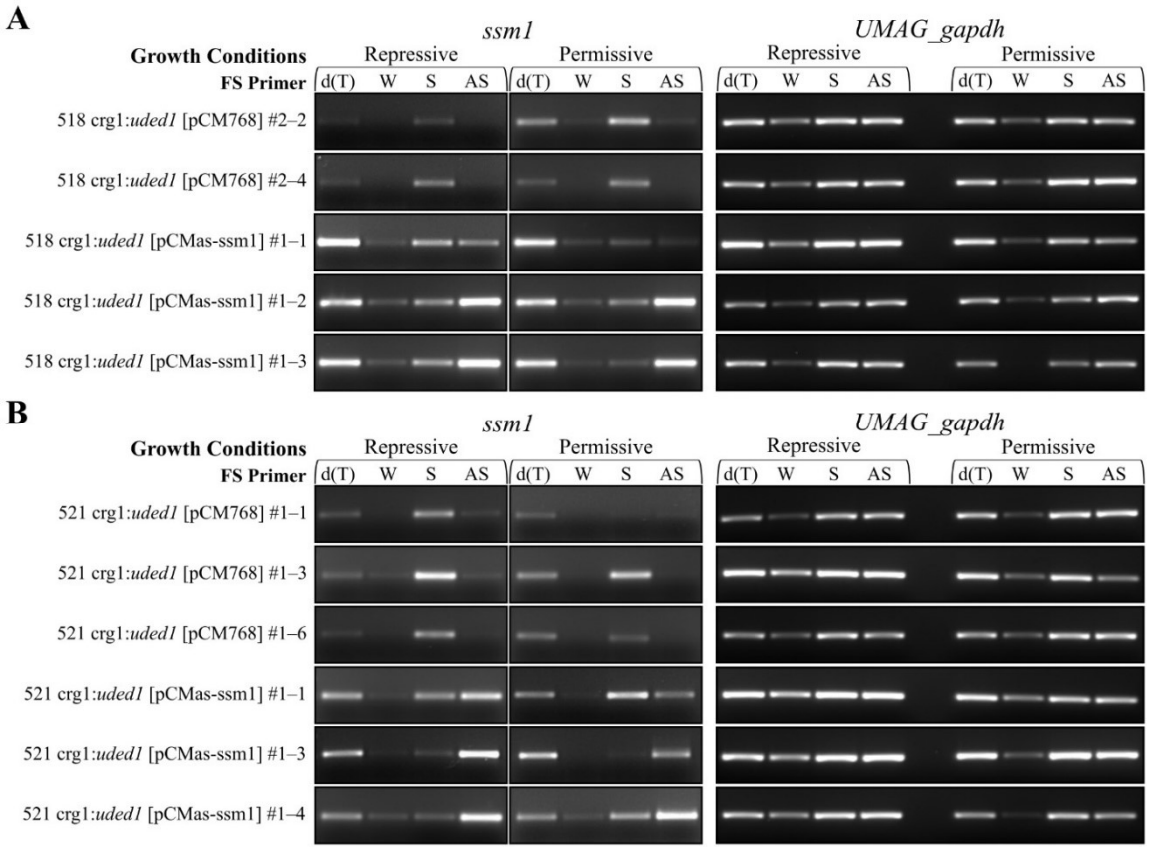

Figure 5.8. RT-PCR detection of the *ssm1* and *as-ssm1* transcripts in crg1:*uded1* mutants where *as-ssm1* is expressed from an autonomously replicating vector. (**A**) *as-ssm1* expressed in the 518 crg1: *uded1* mutant strains. (**B**) *as-ssm1* expressed in the 521 crg1:*uded1* mutant strain. RNA sources include crg1:*uded1* [pCM768] controls and crg1:*uded1* [pCMas-ssm1] strains grown in YEPS (repressive) and YEPA (permissive) medium. First-strand cDNA synthesis primers include: Oligo(dT)$_{16}$ (dT), DEPC-treated H_2O (W), *ssm1* sense-specific primer (S), and *as-ssm1* antisense-specific primer (AS). *UMAG_gapdh* was used as the housekeeping gene, a control.

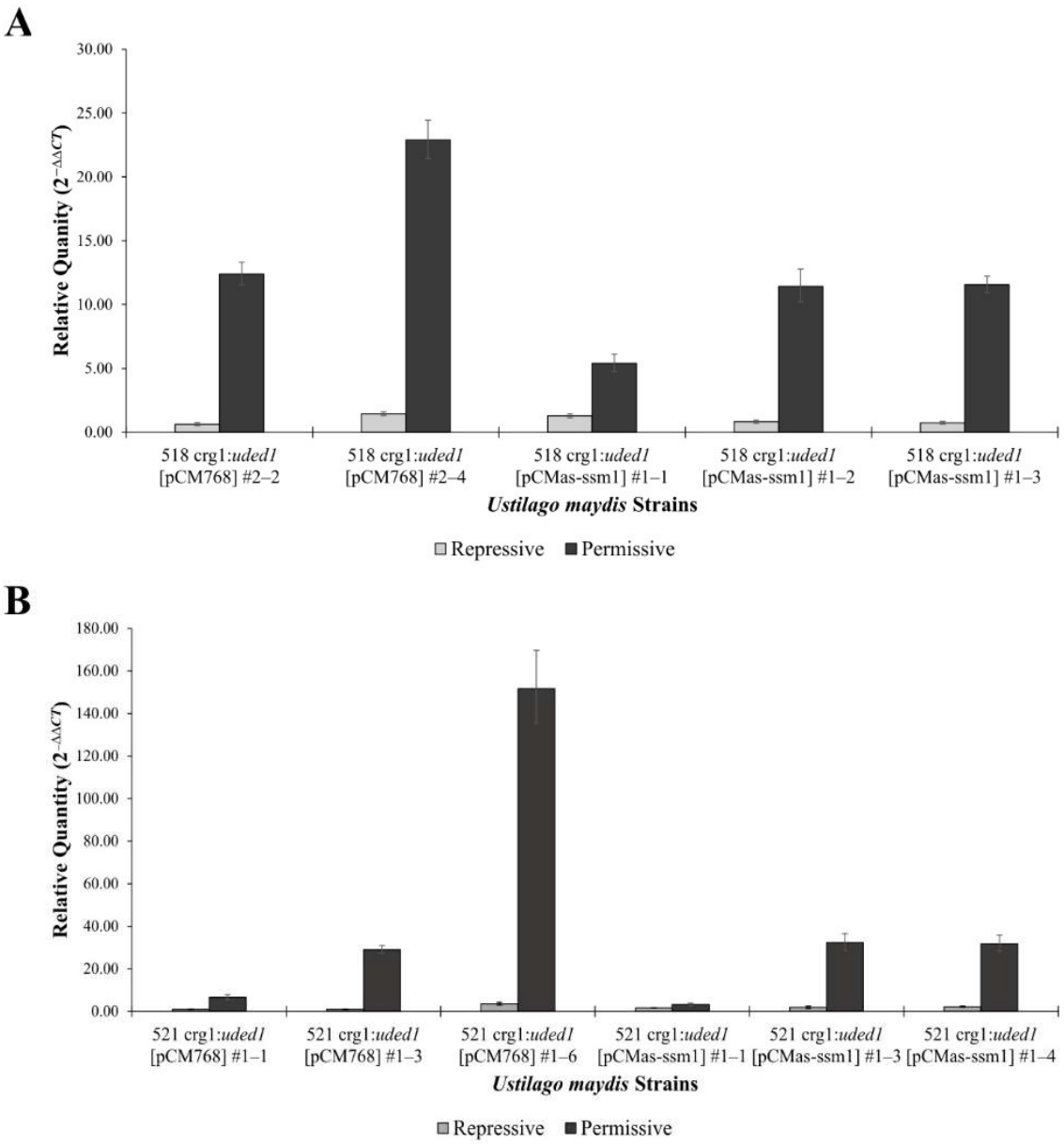

Figure 5.9. The *uded1* transcript is upregulated in the crg1:*uded1* mutants grown in permissive conditions. All *U. maydis* strains were grown in YEPS (repressive) and YEPA (permissive) medium. Relative quantities were determined by RT-qPCR and calculated using the comparative C_T ($2^{-\Delta\Delta CT}$) method, *UMAG_00175* was the endogenous control, and the parent strain (crg1:*uded1*) grown in repressive conditions was set as the calibrator. Assessment of the *uded1* transcript level in the (**A**) 518 crg1:*uded1* [pCMas-ssm1] mutants and (**B**) 521 crg1:*uded1* [pCMas-ssm1]. Bars indicate the RQ minimum and RQ maximum values (95% confidence interval, n = 3).

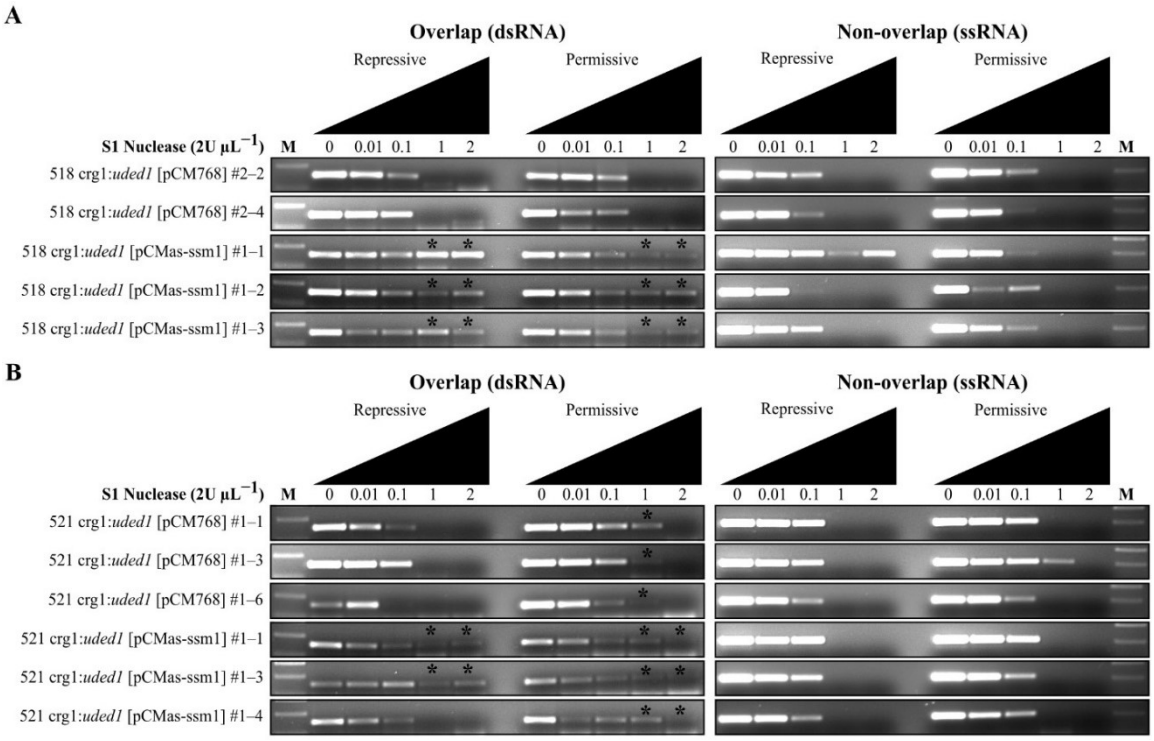

Figure 5.10. S1 nuclease protection assay of *ssm1* and *as-ssm1* interactions. The (**A**) 518 crg1:*uded1* [pCMas-ssm1] and (**B**) 521 crg1:*uded1* [pCMas-ssm1] mutants were grown in repressive (YEPS) and permissive (YEPA) medium. Increasing amounts of S1 nuclease were used to digest equal quantities of RNA. RNA sources include crg1:*uded1* [pCM768] controls and crg1:*uded1* [pCMas-ssm1] strains. A tagged *ssm1* sense-specific primer was used to generate cDNA. A *gapdh*-specific first-strand synthesis primer was included and used as an internal control to assess *UMAG_gapdh* transcript levels. A DNA molecular weight marker (M) was included. The asterisk (*) indicates increased S1 nuclease digestion resistance. The lighting of the gel images was adjusted using Inkscape v.1.3.2.

SUPPLEMENTARY MATERIALS

Table S5.1. Plasmids used in this study.

Plasmid	Relevant Primers	Cloning Sites	Source
uded1 *expression constructs*			
p123			Basse, Stumpferl and Kahmann [70]
pMF2-1h	crg1-KpnI-F crg1-XmaI-R		Brachmann, Konig, Julius and Feldbrugge [65]
p123+crg1		*Kpn*I *Xma*I	This study
p123+crg1+*uded1*	UMAG_04080_NcoI-F UMAG_04080_NotI-R	*Nco*I *Not*I	This study
uded1 *deletion constructs*			
pMF1-hs	HygCarb_Out_pMF1-F HygCarb_Out_pMF1-R		Kämper [30]
pCR2.1TOPOΔ*uded1*-HygR	Ded1_LF_Nest-F Ded1_RF_Nest-R	*Sfi*I	This study
UMAG_01732 *deletion constructs*			
pMF1-hs	HygCarb_Out_pMF1-F HygCarb_Out_pMF1-R		Kämper [30]
pMF1-c	HygCarb_Out_pMF1-F HygCarb_Out_pMF1-R		Brachmann, Konig, Julius and Feldbrugge [65]
pCR2.1TOPOΔ*UMAG_01732*-HygR	Dbp3_LF_Nested-F Dbp3_RF-R	*Sfi*I	This study
pCR2.1TOPOΔ*UMAG_01732*-CarbR	Dbp3_LF_Nested-F Dbp3_RF-R	*Sfi*I	This study
as-ssm1 *expressing plasmid*			
pCM768			Kojic and Holloman [80]
pCM[*as-ssm1*]			Donaldson and Saville (2013)

Table S5.2. Primers used in this study.

Primer	Primer Sequence (5'-to-3')[a,b]
crg1 inducible uded1 *expression strain*	
crg1-KpnI-F	ggaggtaccGCGGCCGCTACCTGGCTTATCG
crg1-XmaI-R	ggacccgggACTCAGGCCTATTATGGTATC
p123 Seq-F2	TCGGGGCTGGCTTAACTATG
crg1 Seq-F1	GTTCCTTCACGGCTGATCTC
crg1 Seq-R1	CTCTTTTCTGAACGCCTCGC
crg1 Seq-F2	TTGATGTCGCCCAACTGTTG
crg1 Seq-R2	ACTGCTCGGAAATCTCACAC
crg1 Seq-F3	AAGTGTGAGATTTCCGAGCAG
UMAG_04080_NcoI-F	ggaccatggATGACTTACGAAAACAACACAC
UMAG_04080_NotI-R	ggagcggccgcTTACCACCATGACGAGTTGC
04080-seqF1	CCAACATGTCGGTCCAGAATG
04080-seqR1	ACGGGAATGTCACCATACTTG
04080-seqF2	AGCCTGTCACTACCTTCACC
04080-seqR2	GGGGTAGCAGAGAGAAGGTC
04080-seqF3	GGTTTCGAGCCTCAGATTCG
04080-seqR3	TCTTGCCCGATCTGAAGAGC
04080-seqF4	GTCGACGACTATGTTCACCG
04080-seqR4	TTACCACCATGACGAGTTGC
uded1 *native deletion strain*	
Ded1_LF-F	TGCTGTCCATCTTGTTTCTGTG
Ded1_LF_SfiI-R(2)	gttgggccatctaggccGATGATGATGTATCAATGGTGG
Ded1_RF-R	AGAATCACGAATGCCCACAC
Ded1_RF_SfiI-F(2)	caacggcctgagtggccTCGCTGCGCATATTCGGTCG
HygCarb_Out_pMF1-F	CCTCGAGGCCTAGATGGC
HygCarb_Out_pMF1-R	ATAGGGCGAATTGGAGCTC
pCR2.1_IN_Seq-F	CTTCCGGCTCGTATGTTGTG
04080_LF-Seq-R1	ACGCCGTCTCTTCTATCCAG
UMAG_04080-LB-Nest-FOR	TGGACATGTCGTTGCTCTTTG
04080_LF-Seq-R2	GGCTGTTAGTCTGTGCTGTG
04080-LF-Seq-F1	ATTAGACTGCCACCCACTCG
HYG-Seq-R1	AGTTTGCAGAGCTTGGTGTG
HYG-Seq-F1	ATCTGACGCGAAATGTGAGC
HYG-Seq-R2	ACATATCCACGCCCTCCTAC
HYG-Seq-F2	TAGGAGGGCGTGGATATGTC
HYG-Seq-F3	GGCAAACTGTGATGGACGAC
HYG-Seq-R3	GTCAGGACATTGTTGGAGCC
HYG-Seq-F4	GTACACAAATCGCCCGCAG
HYG-Seq-R4	TTCTACACAGCCATCGGTCC

04080_RF-Seq-R1	GCTACTGCGACCGAATATGC
04080_RF-Seq-F1	AGTGCTTCTCCTCTGCTCTG
04080_RF-Seq-F2	ACCACGACTCGACTCTTACG
04080_RF-Seq-R2	AATGGGGCCGTACTACTTGC
04080_RF-Seq-F3	ACATTCATCCTCACGTTCGG
UMAG_04080-RB-Nest-REV	AAAAGAGGCGGTGACTGC
pCR2.1_IN-R	CTTAATGCGCCGCTACAGG
Ded1_LF_Nest-F	GGCGTCCCGACTATATAAACTC
Ded1_RF_Nest-R	CTCCATCTCGTTCATCAGCAC
UMAG_01732 *deletion strain*	
Dbp3_LF-F	AGCCAAGACATGCAAAGGTC
Dbp3_LF_SfiI-R(2)	gttgggccatctaggccTGTATGTAATTAGACAGATAC
Dbp3_RF_SfiI-F(2)	caacggcctgagtggccGGGTTCCACTTACTGTGTTTGG
Dpb3_RF-R(2)	AACAAGTAGGCTGTAGTTTGGC
HygCarb_Out_pMF1-F	CCTCGAGGCCTAGATGGC
HygCarb_Out_pMF1-R	ATAGGGCGAATTGGAGCTC
pCR2.1_IN_Seq-F	CTTCCGGCTCGTATGTTGTG
01732_LF-Seq-R1	GTTGCTCTTCTCGACTCCCT
01732_LF-Seq-F1	TGTGGCCGCAAGTAAGTTAG
01732_LF-Seq-R2	CTCGTTATGACAGCTCTTGGG
01732_LF-Seq-F2	CAGTAACAGACAAAGCCCGC
HYG-Seq-R1	AGTTTGCAGAGCTTGGTGTG
HYG-Seq-F1	ATCTGACGCGAAATGTGAGC
HYG-Seq-R2	ACATATCCACGCCCTCCTAC
HYG-Seq-F2	TAGGAGGGCGTGGATATGTC
HYG-Seq-F3	GGCAAACTGTGATGGACGAC
HYG-Seq-R3	GTCAGGACATTGTTGGAGCC
HYG-Seq-F4	GTACACAAATCGCCCGCAG
HYG-Seq-R4	TTCTACACAGCCATCGGTCC
CARB-Seq-F1	AATGCGCGACGAGTATTCAG
CARB-Seq-R1	TCTCCGTTCTTCACCCTAGC
CARB-Seq-F2	GTTCATACATCCACACCGACC
CARB-Seq-R2	AAAGTACAGAAGGGCAAGCG
CARB-Seq-F3	CCTCAAGTCCAACAACACCC
CARB-Seq-R3	TGGTGTCATTCTGCTTGTCG
CARB-Seq-F4	TCGTTCTTTCCTCAGCACTTC
CARB-Seq-R4	AGGGTTGAGGTTCTTGGGG
01732_RF-Seq-R1	TGTTCTGCAAAGCTTGACCTC
01732_RF-Seq-F1	AAGCTGAGAAAGATGGCCAC
01732_RF-Seq-R2	GTACCAAGCAAGCTGAGTGTG
01732_RF-Seq-F2	ACCTAGGACTCAAACTGCCC

01732_RF-Seq-F3	CTACCAACATCGTCCTGCAG
Dbp3_LF_Nested-F	GGTGTGCAGCTTCTTCCG
Dbp3_RF-R	AGTATACTGGAAGGCGCTCC
as-ssm1 *expressing strains*	
pGAP(-79)Forward	GACCTCACTCTTCAAGAACAAGC
Um12232 PCR-F	AGGCTACCTTGGGTTTGAGAA
First-strand synthesis (Sense specific)	
S2491_FS (Sense)	CCGAGATGACGACCTTCTTG
um12232_FS_Sense_Tag	cgaggatcatggtggcgaataaAGCAGCGCCTTGACAATAATA
um12232_FS_S_NO	cgaggatcatggtggcgaataaCCCTGAGCCATTTCATATCG
um12232-FS2	AGTTGACCCGTCTTACCCAG
First-strand synthesis (Antisense specific)	
as-um12232-FSb	CATAGTGACGCTGACCTCTG
RT-PCR	
umgapd	F: CATAATGTCTCAGGTCAACATCG R: GGATGTTGGAGGGGTCCT
UMAG_00175	F: TTCCTCTTCCGACCAATCTG R: TAGGTGAGGAGGGTGAGACG
UMAG_04080	F: TTCTCTCGGCTCTCTTCACC R: GAAGGTGGCTGAGAACATGAG
UMAG_01732	F: CTGACCGCATGCTAGATAAGG R: TCGTTCTGTCCTAAATCACCG
ssm1 (um12232)	F: GCACTAGGACATGCATTCCG R: CATGTCTAGCACGCGGTATG
um12232_PCR-F2	AGGCTACCTTGGGTTTGAGAAGCA
um12232_PCR-F3	GCGCACAAGCTCTCGTTTCAA
Tagged_PCR-R70	CGAGGATCATGGTGGCGAATAA
RT-qPCR	
UMAG_00175_qPCR	F: ACGCACCGAATCCGAAATC R: TGCGGTGATACTCCATGTCAA
UMAG_04080_qPCR	F: ACTTACCGCTCGTGGGTGAA R: GTAGCAGAGAGAAGGTCACATCCA
RT-qPCR TaqMan MGB Probes	
UMAG_00175_VIC	VIC-CCTCACTTGGAAGACG-MGB-NFQ
UMAG_04080_FAM	6FAM-ATTGTCACTCAGCTCCGT-MGB-NFQ

[a]Lower-case letters in primer sequences represent nucleotides not complementary to the *U. maydis* genome.

[b]Underlined letters are restriction endonuclease recognition sites.

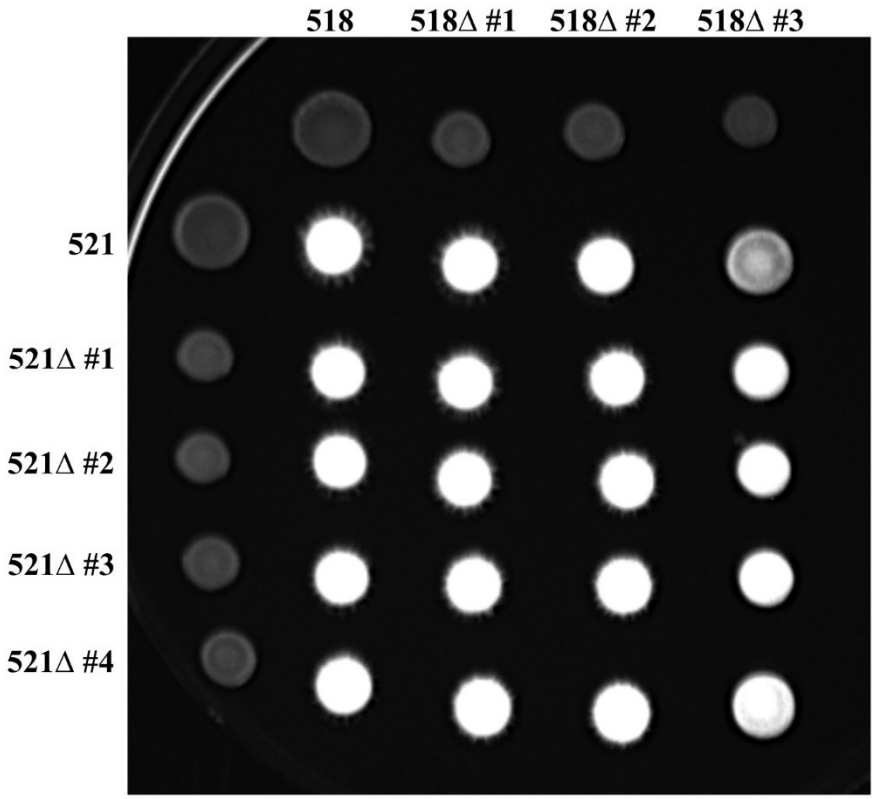

Figure S5.1. Forced dikaryon formation of *udbp3* deletion mutants. *Ustilago maydis* strains were cultured overnight in YEPS medium and normalized to an OD_{600} of 1.0. Equal volumes of compatible strains were premixed and spotted on solid PDA containing 1.0% activated charcoal. Plates were incubated at room temperature and filamentous growth was monitored for 3 days. Three technical replicates of the mating assay were performed, and the representative data is shown. The label abbreviation Δ indicates the Δ*udbp3* deletion mutant.

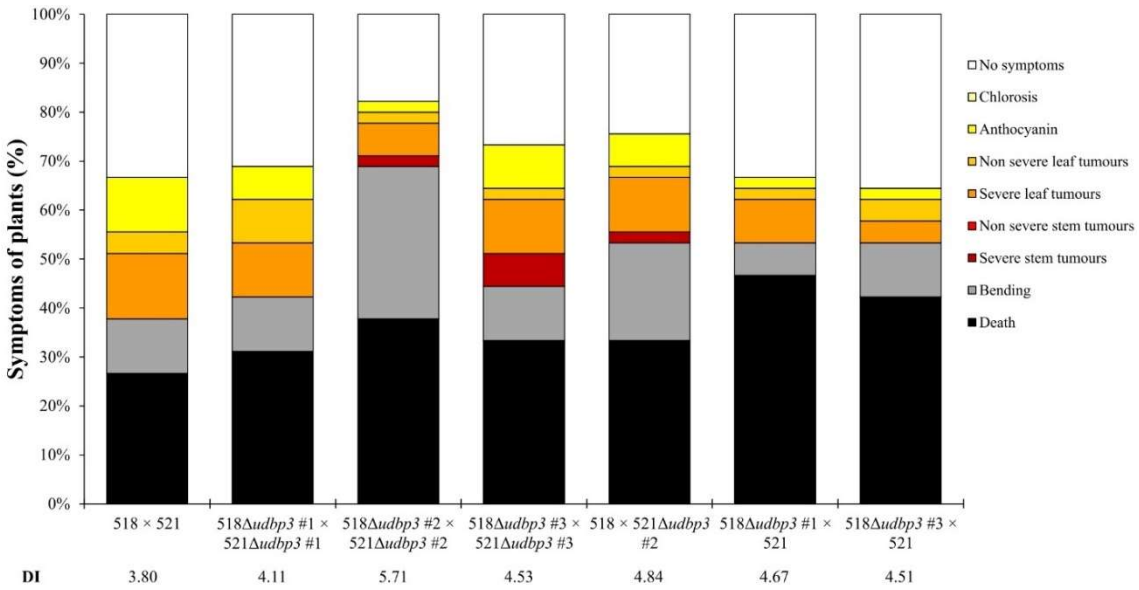

Figure S5.2. *udbp3* mutant pathogenesis assay in maize. Evaluation of virulence of *Ustilago maydis* 518 × 521 (wild-type), Δ*udbp3* × Δ*udbp3* (deletion), and Δ*udbp3* × wt (reciprocal) infections in *Zea mays*. Bars represent the percentage of plants displaying symptoms at 14 days post inoculation. Colours indicate the scored symptom ranging from mild (chlorosis) to severe symptoms (large stem tumours and plant death) as indicated in the legend. A total of 45 plants per cross were infected and the disease index (DI) is the calculated mean of the disease symptoms. Statistical differences were determined using Kruskal-Wallis test coupled with a Dunn multiple comparison ($p \leq 0.05$) and resulted in no significant difference between wild-type infections to deletion or reciprocal cross infections.

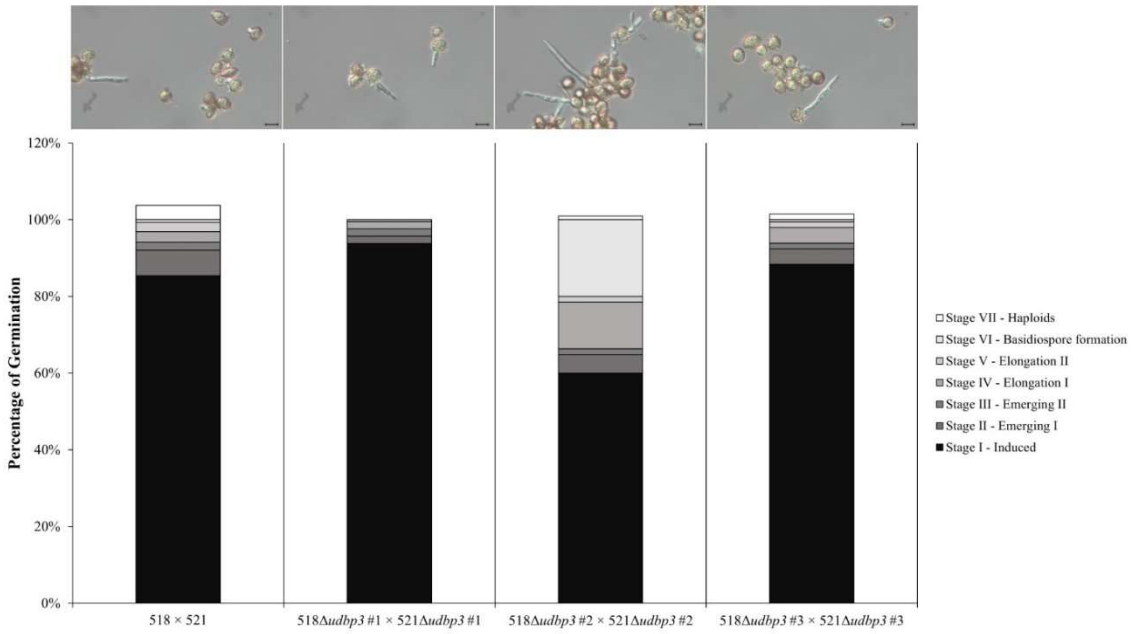

Figure S5.3. Teliospore germination test of *udbp3* deletion mutants. Teliospores were induced to germinate in YEPS Gold medium and incubated overnight. Germinating teliospores were harvested at 16 h post induction of germination for wild-type (518 × 521) and deletion (518Δ*udbp3* × 521Δ*udbp3*) crosses. Microscopic images of each sample were taken at 400× magnification and are displayed along the top. The percentage of germination was determined using a hemocytometer and stages of germination were identified based on the criteria in Seto, Donaldson and Saville [23]. Scale bar indicates 10 μm.

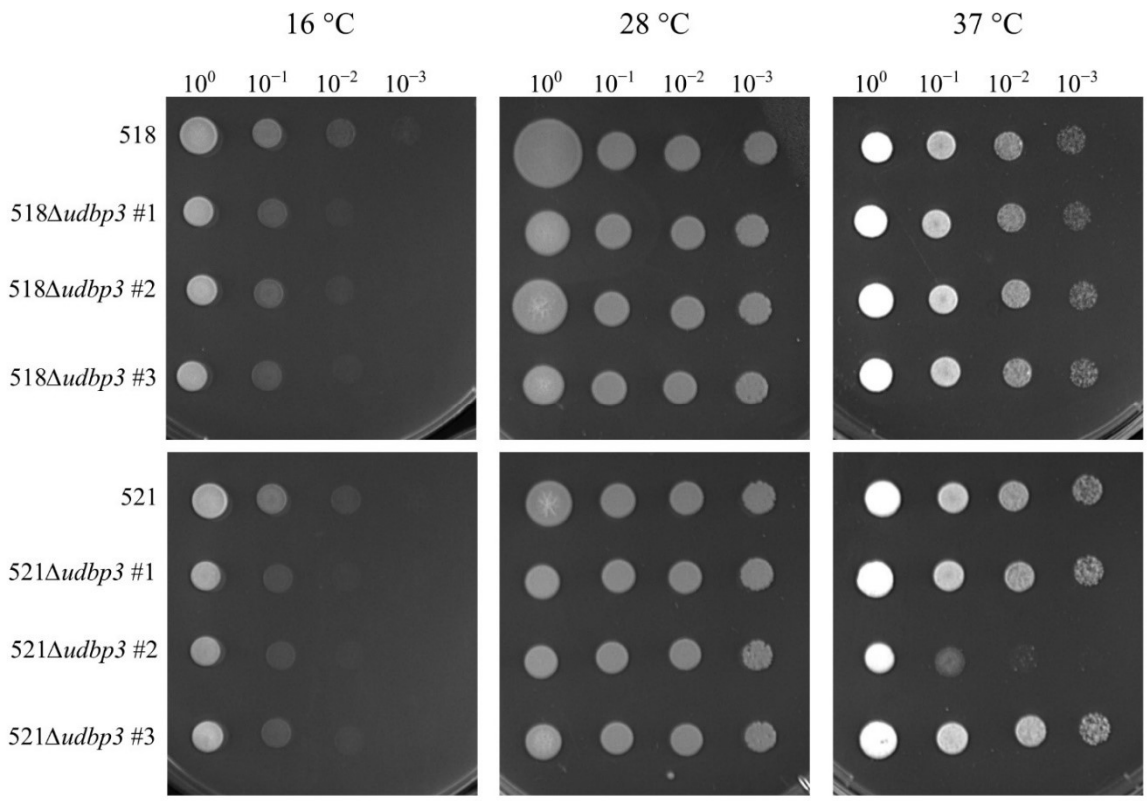

Figure S5.4. Growth of Δ*udbp3* at different temperatures. All strains were cultured overnight in YEPS Gold medium and normalized to an OD_{600} = 1.0. A 10-fold serial dilution series was created and spotted on MM medium containing 1.0% *w/v* D-glucose. Plates were incubated at either 16 °C, 28 °C, or 37 °C and monitored for 3 days. Photos were taken on the third day and the representative of three technical replicates of the spotting assay is shown.

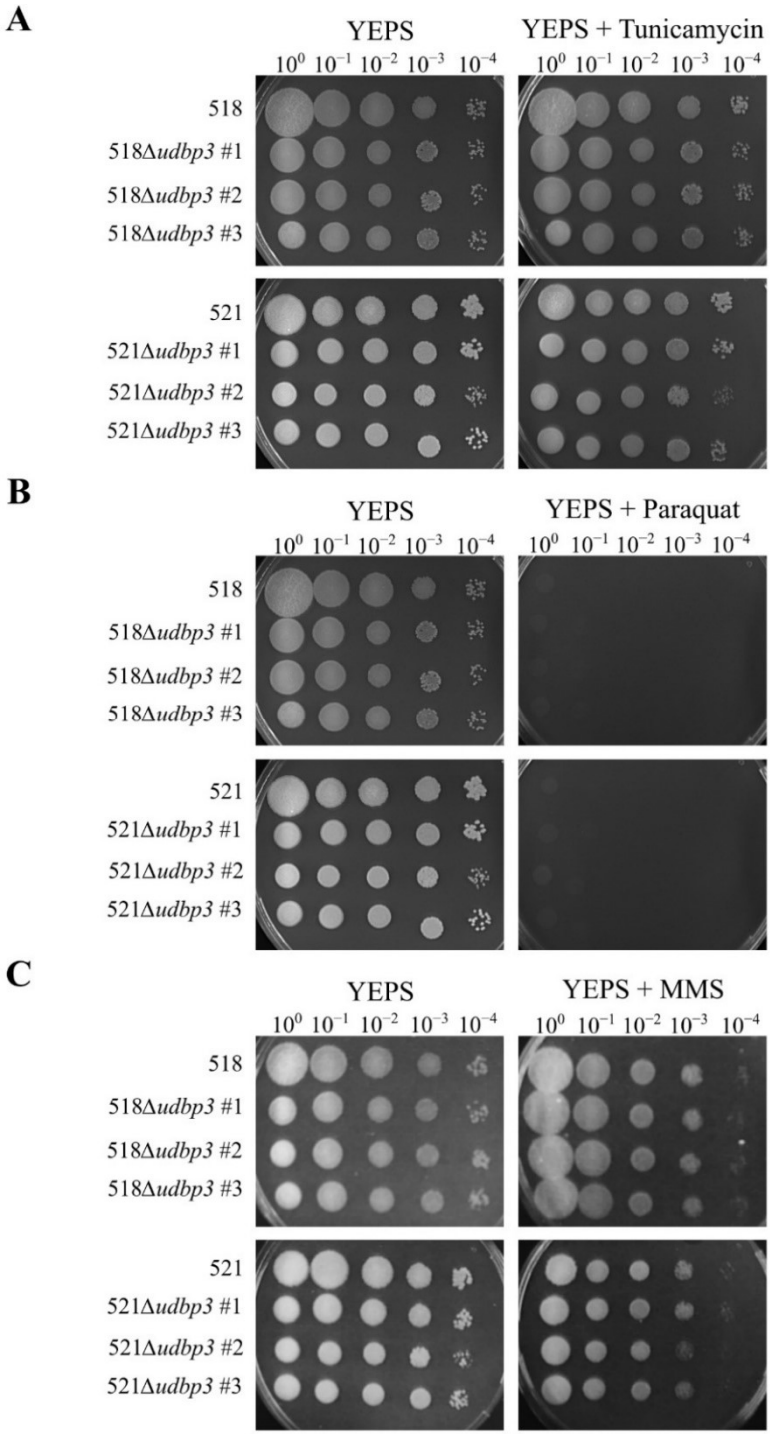

Figure S5.5. *udbp3* deletion mutants tolerance to various stressors. All *Ustilago maydis* strains were cultured overnight in YEPS Gold medium, washed, and normalized to an OD_{600} = 1.00. A 10-fold serial dilution series was created and spotted on YEPS and YEPS containing (**A**) 3 µg/mL tunicamycin, (**B**) 5 mM paraquat, and (**C**) 0.01% methyl methanesulphonate (MMS). All plates were incubated at 28 °C and monitored for 3 days. Photos were taken on the third day and the representative of three technical replicates of each spotting assay is shown.

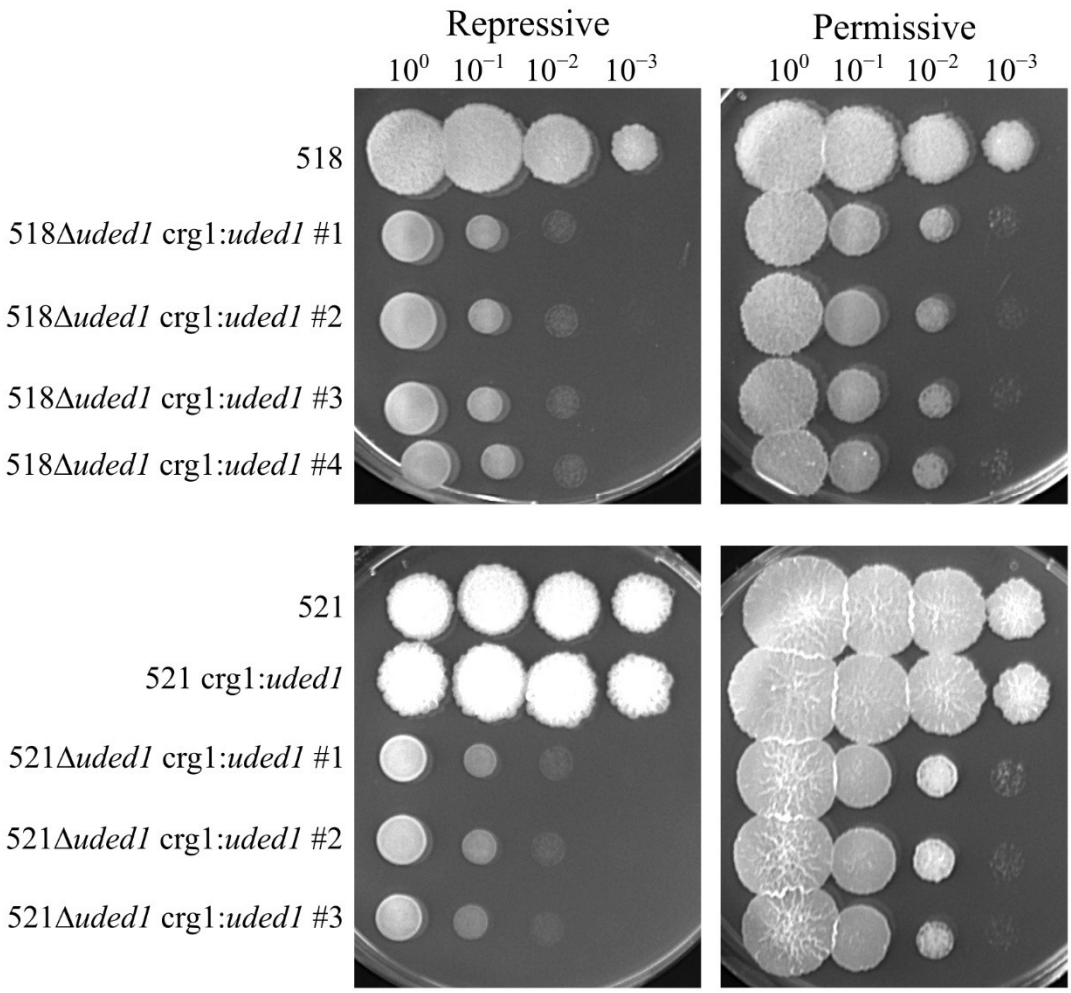

Figure S5.6. Growth of the *uded1* deletion strains in repressive and permissive growth conditions. A 10-fold serial dilution series was spotted on YEPS (repressive) and YEPA (permissive) plates. Plates were incubated at 28 °C and growth was monitored for 3 days. The data shown after 3 days of growth and is representative of three technical replicates of the spotting assay. The lighting of each photograph was adjusted using Inkscape v1.3.2.

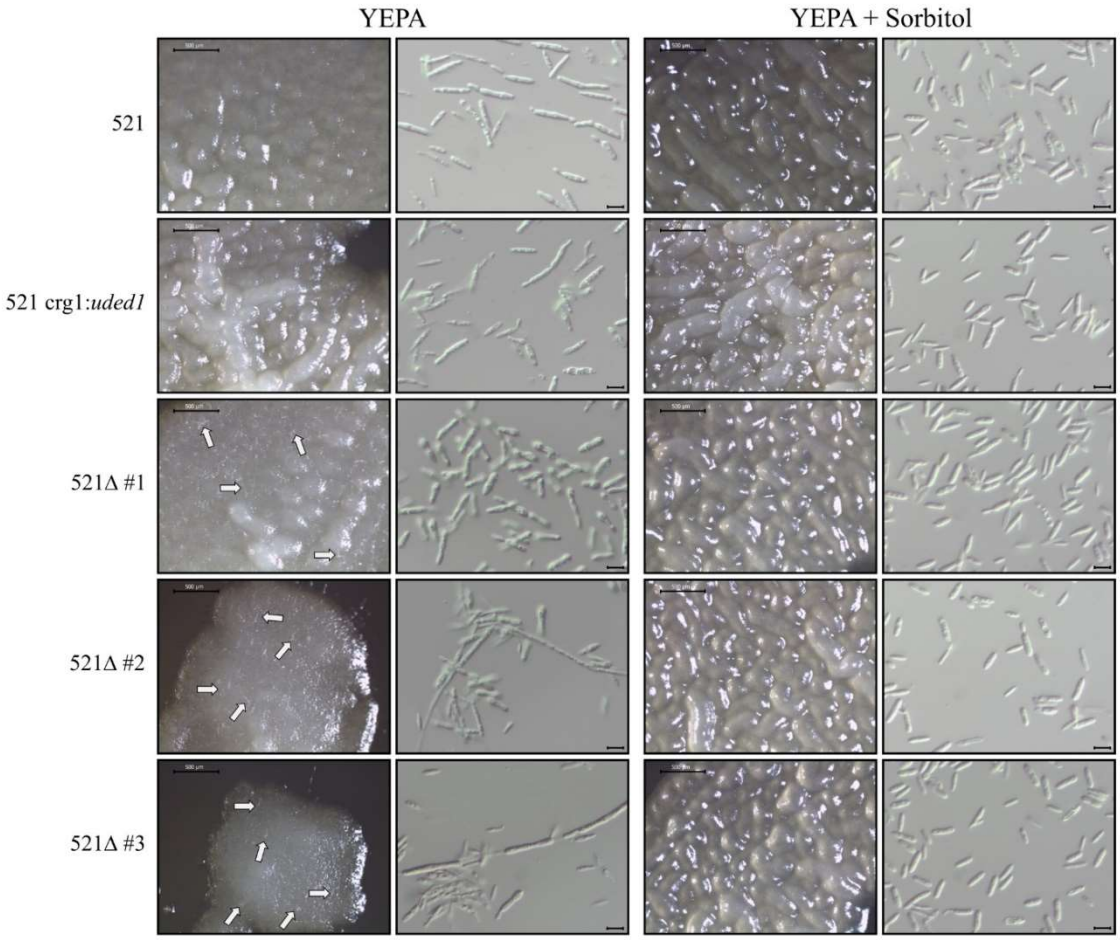

Figure S5.7. The effects of sorbitol addition to solid medium on the growth of *uded1* mutants. Single colonies of each *U. maydis* strain were streaked onto YEPA and YEPA containing 1 M sorbitol plates and incubated at 28 °C for 3 days. Microscopic images were taken of the growth on the plate (40×) and of the cells resuspended in sterile dH_2O (400× magnification). Scale bar indicates 500 µm (plate micrographs) and 10 µm (cell micrographs). Data shown is representative of three technical replicates of the growth assay. Arrows indicate mycelial growth. Label abbreviations: Δ#1–3 delineates the 521Δ*uded1* crg1:*uded1* biological replicates

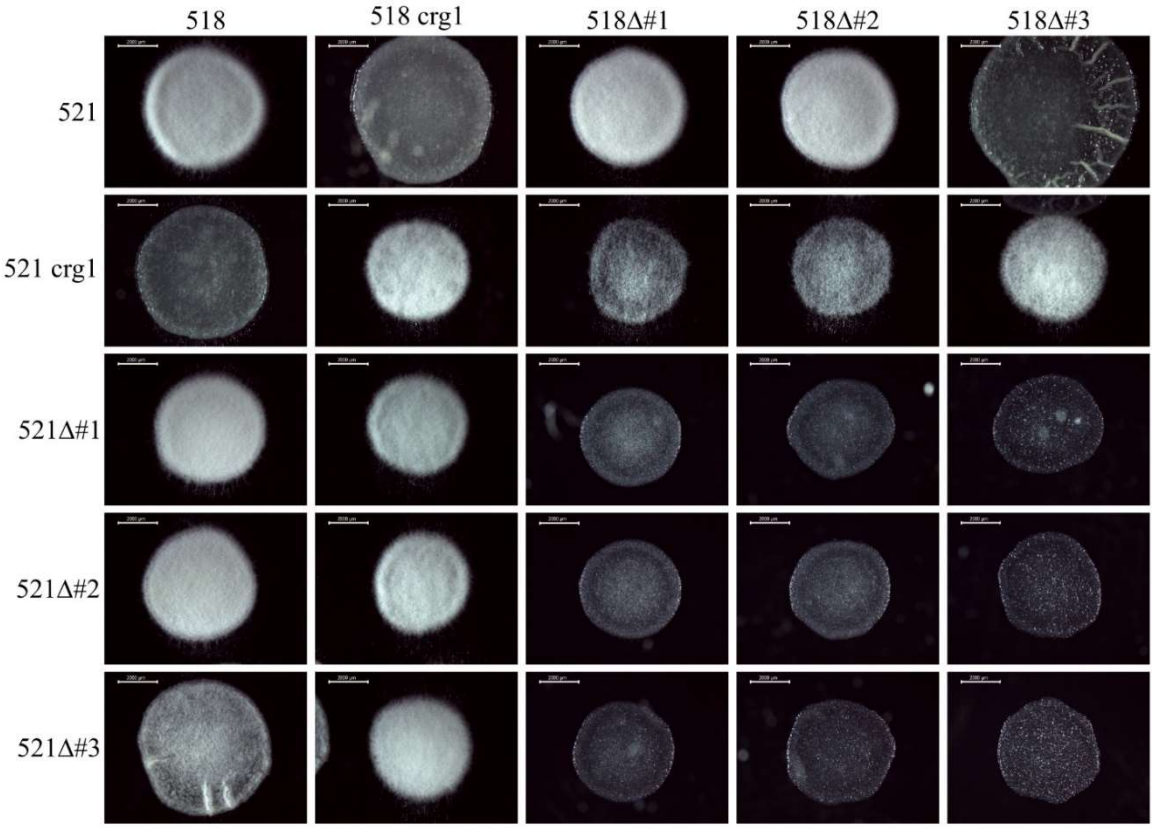

Figure S5.8. Mating assay of *uded1* mutants. All *Ustilago maydis* strains were grown overnight in DCM containing 1.0% *w/v* L-arabinose, washed, normalized to an OD_{600} of 1.0, and equal volumes of compatible strains were premixed. Premixed cultures were spotted on PDA containing 1.0% activated charcoal and incubated at room temperature for 3 days. Microscopic images of each plate were taken with a stereoscopic microscope. Scale bar = 2 mm and the representative data of three technical replicates of the mating assay is shown. The label abbreviations are: crg1 indicates the crg1:*uded1* mutants and Δ #1–3 indicates the Δ*uded1* crg1:*uded1* mutants.

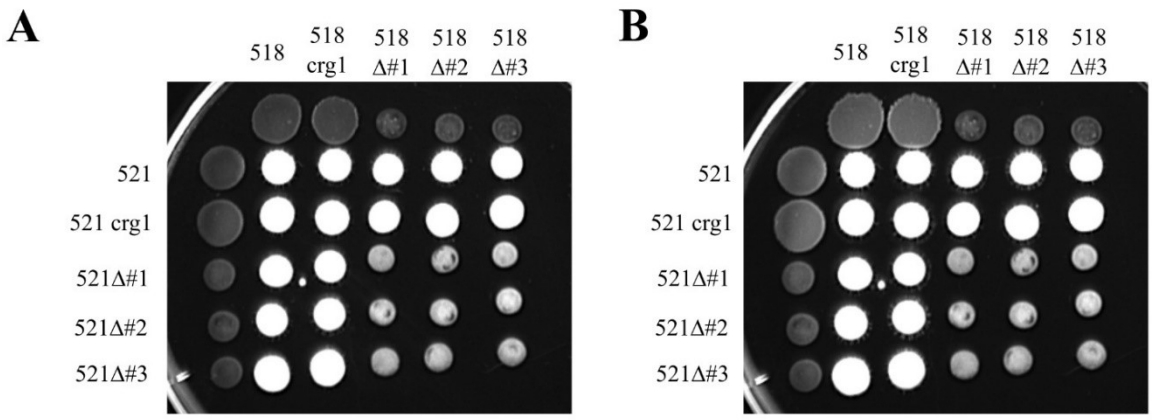

Figure S5.9. Mating assay of *uded1* mutants comparing three days versus five days. All *Ustilago maydis* strains were cultured overnight in DCM containing 1.0% *w/v* L-arabinose and 1 M sorbitol, washed, normalized to an OD_{600} of 1.0, and equal volumes of compatible strains were premixed. The premixed cultures were spotted on PDA containing 1.0% activated charcoal and incubated for (**A**) 3 days and (**B**) 5 days at room temperature. The representative data from three technical replicates of the mating assay is shown. The label abbreviations are: crg1 indicates the crg1:*uded1* mutants and Δ #1–3 indicates the Δ*uded1* crg1:*uded1* mutants.

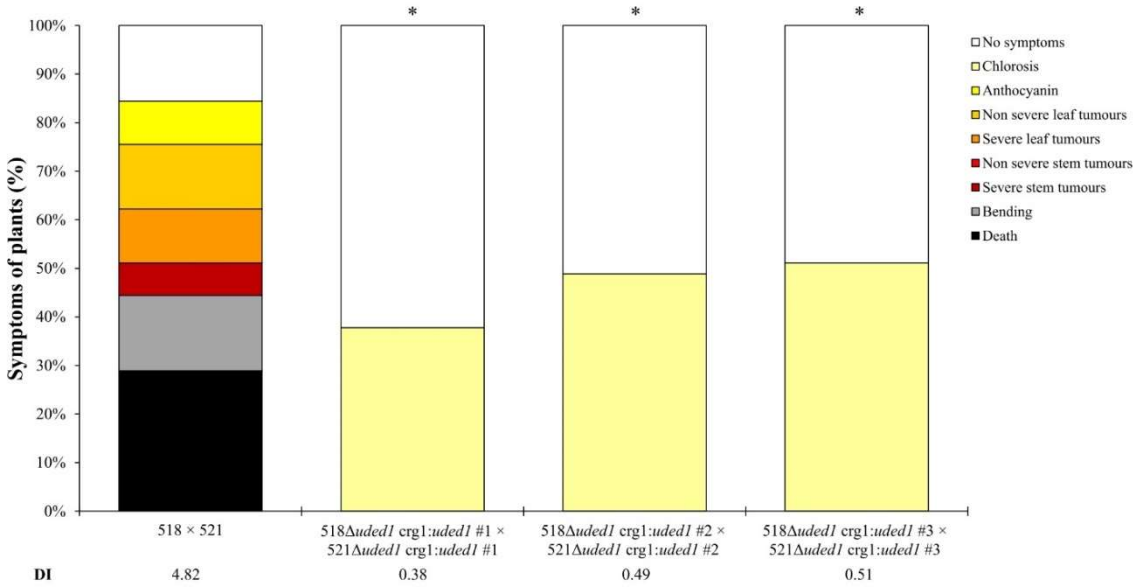

Figure S5.10. Pathogenesis assay of Δ*uded1* crg1:*uded1* mutant strains in maize seedlings. Evaluation of virulence of *Ustilago maydis* 518 × 521 (wild-type) and Δ*uded1* crg1:*uded1* × Δ*uded1* crg1:*uded1* (deletion) infections in *Z. mays*. Bars represent the percentage of plants displaying symptoms at 14 days post inoculation. Colours indicate the scored symptom ranging from mild (chlorosis) to severe symptoms (large stem tumours and plant death) as indicated in the legend. A total of 45 plants per cross were infected and the disease index (DI) is the calculated mean of the disease symptoms. Statistical differences were determined using Kruskal-Wallis test coupled with a Dunn multiple comparison ($p \leq 0.05$). Asterisks indicate a significant difference in virulence of deletion infections relative to wild-type infections (Mann-Whitney U-test, $p \leq 0.05$).

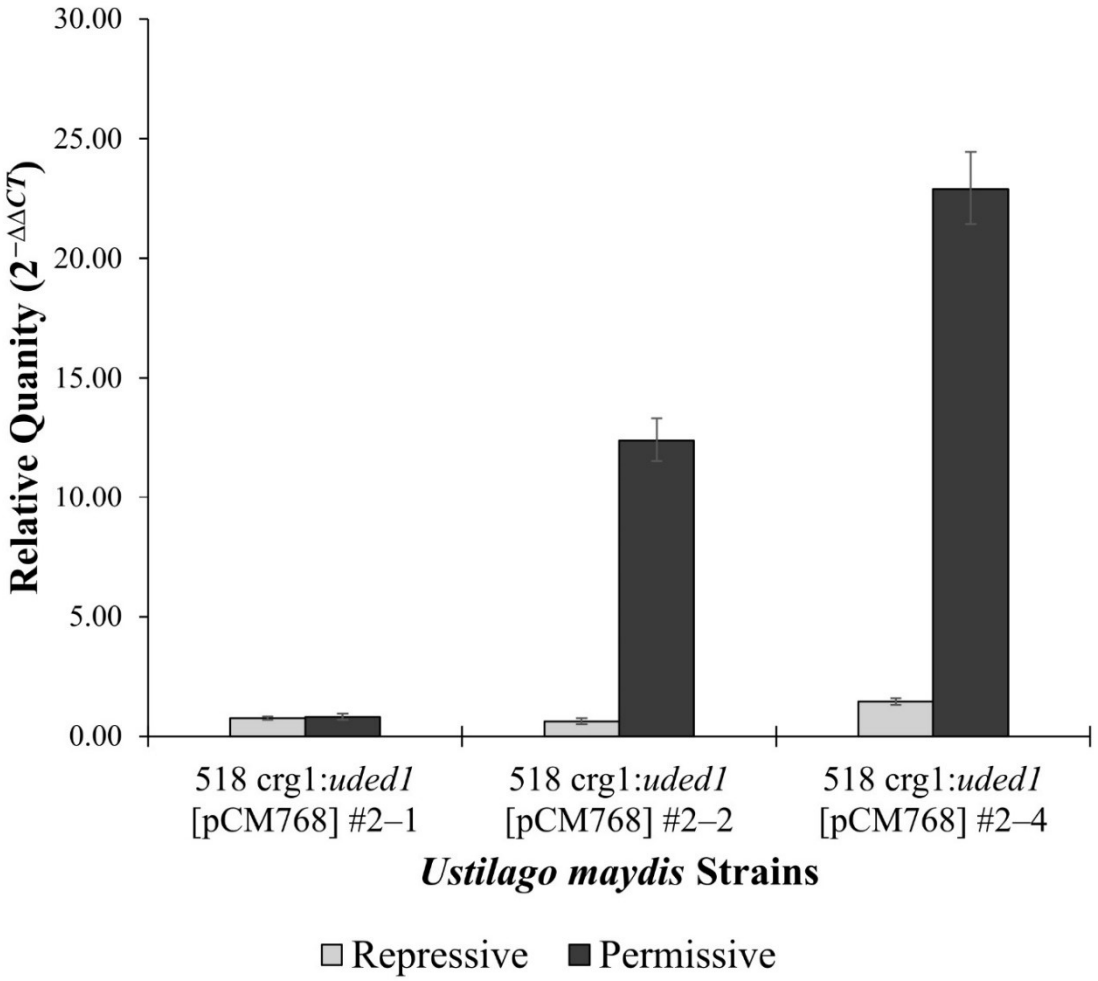

Figure S5.11. RT-qPCR analysis of *uded1* transcript levels in the 518 crg1:*uded1* [pCM768] control samples grown in repressive (YEPS) and permissive (YEPA) conditions. Relative quantities were calculated using the comparative C_T ($2^{-\Delta\Delta CT}$) method, *UMAG_00175* was the endogenous control, and the parent strain (518 crg1:*uded1*) grown in repressive conditions was set as the calibrator. Bars indicate the RQ minimum and RQ maximum values (95% confidence interval, n = 3).

REFERENCES

1. Sussman, A.S.; Douthit, H.A. Dormancy in microbial spores. *Annu. Rev. Plant Physiol.* **1973**, *24*, 311–352, doi:10.1146/annurev.pp.24.060173.001523.

2. Nautiyal, P.; Sivasubramaniam, K.; Dadlani, M. Seed dormancy and regulation of germination. *Seed Sci. Technol.* **2023**, 39–66.

3. McDonald, M.D.; Owusu-Ansah, C.; Ellenbogen, J.B.; Malone, Z.D.; Ricketts, M.P.; Frolking, S.E.; Ernakovich, J.G.; Ibba, M.; Bagby, S.C.; Weissman, J.L. What is microbial dormancy? *Trends Microbiol.* **2024**, *32*, 142–150, doi:10.1016/j.tim.2023.08.006.

4. Banuett, F.; Herskowitz, I. Discrete developmental stages during teliospore formation in the corn smut fungus, *Ustilago maydis*. *Development* **1996**, *122*, 2965–2976.

5. Brefort, T.; Doehlemann, G.; Mendoza-Mendoza, A.; Reissmann, S.; Djamei, A.; Kahmann, R. *Ustilago maydis* as a pathogen. *Annu. Rev. Phytopathol.* **2009**, *47*, 423–445, doi:10.1146/annurev-phyto-080508-081923.

6. Ramberg, J.E.; McLaughlin, D.J. Ultrastructural study of promycelial development and basidiospore initiation in *Ustilago maydis*. *Can. J. Bot.* **1980**, *58*, 1548–1561.

7. Christensen, J.J. *Corn smut caused by Ustilago maydis (Monograph No. 2)*; American Phytopathological Society: 1963.

8. Caltrider, P.G.; Gottlieb, D. Effect of sugars on germination and metabolism of teliospores of *Ustilago maydis*. *Phytopathology* **1966**, *56*, 479–484.

9. Gottlieb, D. The physiology of spore germination in fungi. *Bot. Rev.* **1950**, *16*, 229–257.

10. Griffin, D.H. Spore dormancy and germination. In *Fungal Physiology*; John Wiley & Sons: New York (NY), 1994; Volume 2nd ed, pp. 375–398.

11. Gottlieb, D.; Rao, M.; Shaw, P. Changes in Ribonucleic Acid during the Germination of Teliospores of *Ustilago maydis*. *Phytopathology* **1968**, *58*, 1593–1597.

12. Seshachalam, D. A protein-nucleic acid complex in teliospores of *Ustilago maydis*. *Antonie van Leeuwenhoek* **1974**, *40*, 265–274, doi:10.1007/BF00394384.

13. Donaldson, M.E.; Saville, B.J. *Ustilago maydis* natural antisense transcript expression alters mRNA stability and pathogenesis. *Mol. Microbiol.* **2013**, *89*, 29–51, doi:10.1111/mmi.12254.

14. Ostrowski, L.A.; Saville, B.J. Natural antisense transcripts are linked to the modulation of mitochondrial function and teliospore dormancy in *Ustilago maydis*. *Mol. Microbiol.* **2017**, *103*, 745–763, doi:10.1111/mmi.13587.

15. Bourgeois, C.F.; Mortreux, F.; Auboeuf, D. The multiple functions of RNA helicases as drivers and regulators of gene expression. *Nat. Rev. Mol. Cell Biol.* **2016**, *17*, 426.

16. Jankowsky, E. RNA helicases at work: binding and rearranging. *Trends Biochem. Sci.* **2011**, *36*, 19–29.

17. Linder, P.; Jankowsky, E. From unwinding to clamping—the DEAD box RNA helicase family. *Nat. Rev. Mol. Cell Biol.* **2011**, *12*, 505–516.

18. Gorbalenya, A.E.; Koonin, E.V. Helicases: amino acid sequence comparisons and structure-function relationships. *Curr. Opin. Cell Biol.* **1993**, *3*, 419–429.

19. Singleton, M.R.; Dillingham, M.S.; Wigley, D.B. Structure and mechanism of helicases and nucleic acid translocases. *Annu. Rev. Biochem.* **2007**, *76*, 23–50.

20. Fairman-Williams, M.E.; Guenther, U.-P.; Jankowsky, E. SF1 and SF2 helicases: family matters. *Curr. Opin. Cell Biol.* **2010**, *20*, 313–324.

21. Panepinto, J.; Liu, L.; Ramos, J.; Zhu, X.; Valyi-Nagy, T.; Eksi, S.; Fu, J.; Jaffe, H.A.; Wickes, B.; Williamson, P.R. The DEAD-box RNA helicase Vad1 regulates multiple virulence-associated genes in *Cryptococcus neoformans*. *J. Clin. Investig.* **2005**, *115*, 632–641, doi:10.1172/JCI23048.

22. Ying, S.; Zhang, Z.; Zhang, Y.; Hao, Z.; Chai, R.; Qiu, H.; Wang, Y.; Zhu, X.; Wang, J.; Sun, G.; et al. MoDHX35, a DEAH-Box Protein, Is Required for Appressoria Formation and Full Virulence of the Rice Blast Fungus, *Magnaporthe oryzae*. *Int. J. Mol. Sci.* **2022**, *23*, 9015.

23. Seto, A.M.; Donaldson, M.E.; Saville, B.J. Exploring mechanisms of gene expression control during *Ustilago maydis* teliospore germination. *Can. J. Plant Pathol.* **2025**, *47*, 80–97, doi:10.1080/07060661.2024.2413557.

24. Weaver, P.L.; Sun, C.; Chang, T.-H. Dbp3p, a putative RNA helicase in *Saccharomyces cerevisiae*, is required for efficient pre-rRNA processing predominantly at site A_3. *Mol. Cell. Biol.* **1997**, *17*, 1354–1365.

25. Delaney, J.R.; Ahmed, U.; Chou, A.; Sim, S.; Carr, D.; Murakami, C.J.; Schleit, J.; Sutphin, G.L.; An, E.H.; Castanza, A.; et al. Stress profiling of longevity mutants identifies Afg3 as a mitochondrial determinant of cytoplasmic mRNA translation and aging. *Aging Cell* **2013**, *12*, 156–166, doi:https://doi.org/10.1111/acel.12032.

26. Hilliker, A.; Gao, Z.; Jankowsky, E.; Parker, R. The DEAD-box protein Ded1 modulates translation by the formation and resolution of an eIF4F-mRNA complex. *Mol. Cell* **2011**, *43*, 962–972.

27. Aryanpur, P.P.; Regan, C.A.; Collins, J.M.; Mittelmeier, T.M.; Renner, D.M.; Vergara, A.M.; Brown, N.P.; Bolger, T.A. Gle1 regulates RNA binding of the DEAD-box helicase Ded1 in its complex role in translation initiation. *Mol. Cell. Biol.* **2017**, *37*, e00139–00117.

28. Aryanpur, P.P.; Mittelmeier, T.M.; Bolger, T.A. The RNA Helicase Ded1 Regulates Translation and Granule Formation during Multiple Phases of Cellular Stress Responses. *Mol. Cell. Biol.* **2022**, *42*, e00244-00221, doi:10.1128/MCB.00244-21.

29. Seto, A.M.; Saville, B.J. Annotating the *Ustilago maydis* RNA helicases and predicting roles in pathogenic development [Manuscript in preparation]. **2025**.

30. Kämper, J. A PCR-based system for highly efficient generation of gene replacement mutants in *Ustilago maydis*. *Mol. Genet. Genomics* **2004**, *271*, 103–110, doi:10.1007/s00438-003-0962-8.

31. Kernkamp, M. Genetic and environmental factors affecting growth types of Ustilago zeae. *Phytopathology* **1939**, *29*, 473–484 pp.

32. Gold, S.; Duncan, G.; Barrett, K.; Kronstad, J. cAMP regulates morphogenesis in the fungal pathogen *Ustilago maydis*. *Genes Dev.* **1994**, *8*, 2805–2816, doi:10.1101/gad.8.23.2805.

33. Ruiz-Herrera, J.; León, C.G.; Guevara-Olvera, L.; Cárabez-Trejo, A. Yeast-mycelial dimorphism of haploid and diploid strains of *Ustilago maydis*. *Microbiology (Reading, Engl.)* **1995**, *141*, 695–703, doi:https://doi.org/10.1099/13500872-141-3-695.

34. Klose, J.; De Sá, M.M.; Kronstad, J.W. Lipid-induced filamentous growth in *Ustilago maydis*. *Mol. Microbiol.* **2004**, *52*, 823–835, doi:https://doi.org/10.1111/j.1365-2958.2004.04019.x.

35. Gold, S.E.; Brogdon, S.M.; Mayorga, M.E.; Kronstad, J.W. The *Ustilago maydis* regulatory subunit of a cAMP-dependent protein kinase is required for gall formation in maize. *Plant Cell* **1997**, *9*, 1585–1594, doi:10.1105/tpc.9.9.1585.

36. Raponi, M.; Arndt, G.M. Dominant genetic screen for cofactors that enhance antisense RNA-mediated gene silencing in fission yeast. *Nucleic Acids Res.* **2002**, *30*, 2546–2554, doi:10.1093/nar/30.11.2546.

37. Donaldson, M.E.; Ostrowski, L.A.; Goulet, K.M.; Saville, B.J. Transcriptome analysis of smut fungi reveals widespread intergenic transcription and conserved antisense transcript expression. *BMC Genom.* **2017**, *18*, 340, doi:10.1186/s12864-017-3720-8.

38. Ho, E.C.H.; Donaldson, M.E.; Saville, B.J. Detection of Antisense RNA Transcripts by Strand-Specific RT-PCR. In *RT-PCR Protocols: Second Edition*, King, N., Ed.; Humana Press: Totowa, NJ, 2010; pp. 125–138.

39. Chung, E.; Cho, C.-W.; Yun, B.-H.; Choi, H.-K.; So, H.-A.; Lee, S.-W.; Lee, J.-H. Molecular cloning and characterization of the soybean DEAD-box RNA helicase gene induced by low temperature and high salinity stress. *Gene* **2009**, *443*, 91–99, doi:https://doi.org/10.1016/j.gene.2009.05.005.

40. Kant, P.; Kant, S.; Gordon, M.; Shaked, R.; Barak, S. *STRESS RESPONSE SUPPRESSOR1* and *STRESS RESPONSE SUPPRESSOR2*, Two DEAD-Box RNA Helicases That Attenuate Arabidopsis Responses to Multiple Abiotic Stresses. *Plant Physiol.* **2007**, *145*, 814–830, doi:10.1104/pp.107.099895.

41. Khan, A.; Garbelli, A.; Grossi, S.; Florentin, A.; Batelli, G.; Acuna, T.; Zolla, G.; Kaye, Y.; Paul, L.K.; Zhu, J.-K.; et al. The Arabidopsis STRESS RESPONSE SUPPRESSOR DEAD-box RNA helicases are nucleolar- and chromocenter-localized proteins that undergo stress-mediated relocalization and are involved in epigenetic gene silencing. *Plant J.* **2014**, *79*, 28–43, doi:https://doi.org/10.1111/tpj.12533.

42. Wheeler, M.H. Comparisons of fungal melanin biosynthesis in ascomycetous, imperfect and basidiomycetous fungi. *Trans. Br. Mycol. Soc.* **1983**, *81*, 29–36, doi:https://doi.org/10.1016/S0007-1536(83)80200-9.

43. Piepenbring, M.; Bauer, R.; Oberwinkler, F. Teliospores of smut fungi - general aspects of teliospore walls and sporogenesis. *Protoplasma* **1998**, *204*, 155–169, doi:10.1007/BF01280322.

44. Struhl, K. Nucleotide sequence and transcriptional mapping of the yeast pet56-his3-dedl gene region. *Nucleic Acids Res.* **1985**, *13*, 8587–8601, doi:10.1093/nar/13.23.8587.

45. Bottin, A.; Kämper, J.; Kahmann, R. Isolation of a carbon source-regulated gene from *Ustilago maydis*. *Mol. Gen. Genet.* **1996**, *253*, 342–352, doi:10.1007/PL00008601.

46. Aryanpur, P.P.; Renner, D.M.; Rodela, E.; Mittelmeier, T.M.; Byrd, A.; Bolger, T.A. The DEAD-box RNA helicase Ded1 has a role in the translational response to TORC1 inhibition. *Mol. Biol. Cell* **2019**, *30*, 2171–2184, doi:10.1091/mbc.E18-11-0702.

47. Carey, S.B.; List, H.M.; Siby, A.; Guerra, P.; Bolger, T.A. A synthetic genetic array screen for interactions with the RNA helicase DED1 during cell stress in budding yeast. *G3: Genes Genomes Genet.* **2023**, *13*, doi:10.1093/g3journal/jkac296.

48. Buchan, J.R. mRNP granules. Assembly, function, and connections with disease. *RNA Biol.* **2014**, *11*, 1019–1030, doi:10.4161/15476286.2014.972208.

49. Forbes, K.C.; Humphrey, T.; Enoch, T. Suppressors of Cdc25p Overexpression Identify Two Pathways That Influence the G2/M Checkpoint in Fission Yeast. *Genetics* **1998**, *150*, 1361–1375, doi:10.1093/genetics/150.4.1361.

50. Yoo, B.; Lee, C. Thermoprotective effect of sorbitol on protein during dehydration. *J. Agric. Food Chem.* **1993**, *41*.

51. Loos, H.; Krämer, R.; Sahm, H.; Sprenger, G.A. Sorbitol promotes growth of *Zymomonas mobilis* in environments with high concentrations of sugar: evidence for a physiological function of glucose-fructose oxidoreductase in osmoprotection. *J. Bacteriol.* **1994**, *176*, 7688–7693, doi:doi:10.1128/jb.176.24.7688-7693.1994.

52. Santivarangkna, C.; Kulozik, U.; Kienberger, H.; Foerst, P. Changes in membrane fatty acids of *Lactobacillus helveticus* during vacuum drying with sorbitol. *Lett. Appl. Microbiol.* **2009**, *49*, 516–521, doi:10.1111/j.1472-765X.2009.02703.x.

53. Plante, S.; Moon, K.-M.; Lemieux, P.; Foster, L.J.; Landry, C.R. Breaking spore dormancy in budding yeast transforms the cytoplasm and the solubility of the proteome. *PLOS Biol.* **2023**, *21*, e3002042, doi:10.1371/journal.pbio.3002042.

54. Van Laere, A. Trehalose, reserve and/or stress metabolite? *FEMS Microbiol. Lett.* **1989**, *63*, 201–209, doi:https://doi.org/10.1016/0378-1097(89)90130-4.

55. Van Laere, A.; Fransen, M. Metabolism of germinating teliospores of *Ustilago nuda*. *Arch. Microbiol.* **1989**, *153*, 33–37, doi:10.1007/BF00277537.

56. Caltrider, P.G.; Gottlieb, D. Respiratory activity and enzymes for glucose catabolism in fungus spores. *Phytopathology* **1963**, *53*, 1021–1030.

57. Gottlieb, D.; Caltrider, P.G. Synthesis of enzymes during the germination of fungus spores. *Nature* **1963**, *197*, 916, doi:10.1038/197916a0.

58. Ostrowski, L.A.; Seto, A.M.; Saville, B. Investigating teliospore germination using microrespiration analysis and microdissection. *J. Vis. Exp.* **2018**, e57628, doi:10.3791/57628.

59. Allen, P.J. Metabolic Aspects of Spore Germination in Fungi. *Annu. Rev. Phytopathol.* **1965**, *3*, 313–342, doi:https://doi.org/10.1146/annurev.py.03.090165.001525.

60. Tripathi, R.K.; Gottlieb, D. Sequential biosynthesis of ribonucleic acids during germination of teliospores of *Ustilago maydis*. *Mycologia* **1974**, *66*, 413–421, doi:10.2307/3758485.

61. Van Etten, J.L.; Roker, H.R.; Davies, E. Protein synthesis during fungal spore germination: differential protein synthesis during germination of Botryodiplodia theobromae spores. *J. Bacteriol.* **1972**, *112*, 1029.

62. Edgar, R.C. MUSCLE: multiple sequence alignment with high accuracy and high throughput. *Nucleic Acids Res.* **2004**, *32*, 1792–1797, doi:10.1093/nar/gkh340.

63. Waterhouse, A.M.; Procter, J.B.; Martin, D.M.A.; Clamp, M.; Barton, G.J. Jalview Version 2—a multiple sequence alignment editor and analysis workbench. *Bioinformatics* **2009**, *25*, 1189–1191, doi:10.1093/bioinformatics/btp033.

64. Trifinopoulos, J.; Nguyen, L.-T.; von Haeseler, A.; Minh, B.Q. W-IQ-TREE: a fast online phylogenetic tool for maximum likelihood analysis. *Nucleic Acids Res.* **2016**, *44*, W232–W235, doi:10.1093/nar/gkw256.

65. Brachmann, A.; Konig, J.; Julius, C.; Feldbrugge, M. A reverse genetic approach for generating gene replacement mutants in *Ustilago maydis*. *Mol. Genet. Genomics* **2004**, *272*, 216–226, doi:10.1007/s00438-004-1047-z.

66. Kumar, S.; Stecher, G.; Tamura, K. MEGA7: Molecular Evolutionary Genetics Analysis Version 7.0 for Bigger Datasets. *Mol. Biol. Evol.* **2016**, *33*, 1870–1874, doi:10.1093/molbev/msw054.

67. Wang, J.; Holden, D.W.; Leong, S.A. Gene transfer system for the phytopathogenic fungus *Ustilago maydis*. *Proc. Natl. Acad. Sci. U.S.A.* **1988**, *85*, 865–869, doi:doi:10.1073/pnas.85.3.865.

68. Morrison, E.N.; Donaldson, M.E.; Saville, B.J. Identification and analysis of genes expressed in the *Ustilago maydis* dikaryon: uncovering a novel class of pathogenesis genes. *Can. J. Plant Pathol.* **2012**, *34*, 417–435, doi:10.1080/07060661.2012.697077.

69. Hoffman, C.S.; Winston, F. A ten-minute DNA preparation from yeast efficiently releases autonomous plasmids for transformaion of *Escherichia coli*. *Gene* **1987**, *57*, 267–272, doi:https://doi.org/10.1016/0378-1119(87)90131-4.

70. Basse, C.W.; Stumpferl, S.; Kahmann, R. Characterization of a *Ustilago maydis* gene specifically induced during the biotrophic phase: evidence for negative as well as positive regulation. *Mol. Cell. Biol.* **2000**, *20*, 329–339, doi:10.1128/mcb.20.1.329-339.2000.

71. García-Pedrajas, M.D.; Nadal, M.; Denny, T.; Baeza-Montañez, L.; Paz, Z.; Gold, S.E. DelsGate: A Robust and Rapid Method for Gene Deletion. In *Molecular and Cell Biology Methods for Fungi*, Sharon, A., Ed.; Humana Press: Totowa, NJ, 2010; pp. 55–76.

72. Doyle, C.E.; Kitty Cheung, H.Y.; Spence, K.L.; Saville, B.J. Unh1, an *Ustilago maydis* Ndt80-like protein, controls completion of tumor maturation, teliospore development, and meiosis. *Fungal Genet. Biol.* **2016**, *94*, 54–68, doi:https://doi.org/10.1016/j.fgb.2016.07.006.

73. Sambrook, J.; Russell, D.W. *Molecular cloning: a laboratory manual*; Cold Spring Harbor Laboratory Cold Spring Harbor, NY: 2001.

74. Untergasser, A.; Cutcutache, I.; Koressaar, T.; Ye, J.; Faircloth, B.C.; Remm, M.; Rozen, S.G. Primer3—new capabilities and interfaces. *Nucleic Acids Res.* **2012**, *40*, e115–e115, doi:10.1093/nar/gks596.

75. Kõressaar, T.; Remm, M. Enhancements and modifications of primer design program Primer3. *Bioinformatics* **2007**, *23*, 1289–1291, doi:10.1093/bioinformatics/btm091.

76. Kõressaar, T.; Lepamets, M.; Kaplinski, L.; Raime, K.; Andreson, R.; Remm, M. Primer3_masker: integrating masking of template sequence with primer design software. *Bot. Acta.* **2018**, *34*, 1937–1938, doi:10.1093/bioinformatics/bty036.

77. Donaldson, M.E.; Meng, S.; Gagarinova, A.; Babu, M.; Lambie, S.C.; Swiadek, A.A.; Saville, B.J. Investigating the *Ustilago maydis*/*Zea mays* pathosystem: transcriptional responses and novel functional aspects of a fungal calcineurin regulatory B subunit. *Fungal Genet. Biol.* **2013**, *58–59*, 91–104, doi:10.1016/j.fgb.2013.08.006.

78. Cheung, H.Y.K.; Donaldson, M.E.; Storfie, E.R.M.; Spence, K.L.; Fetsch, J.L.O.; Harrison, M.C.; Saville, B.J. Zfp1, a putative $Zn(II)_2Cys_6$ transcription factor, influences *Ustilago maydis* pathogenesis at multiple stages. *Plant Pathol.* **2021**, *70*, 1626–1639, doi:https://doi.org/10.1111/ppa.13398.

79. Holliday, R. The genetics of *Ustilago maydis*. *Genet. Res. (Camb.)* **1961**, *2*, 204–230, doi:10.1017/S0016672300000719.

80. Kojic, M.; Holloman, W.K. Shuttle vectors for genetic manipulations in *Ustilago maydis*. *Canadian Journal of Microbiology* **2000**, *46*, 333–338, doi:10.1139/w00-002 %M 10779869.

CHAPTER 6

GENERAL DISCUSSION

INTRODUCTION

Fungi survive adverse environmental conditions by forming dormant spores that germinate when conditions are optimal for growth. Fungal spores are also the dispersal agents and are responsible for spreading disease. Understanding the molecular mechanisms during fungal spore dormancy and the switch to germination is important to mitigate disease spread and develop methods for disrupting the disease cycle. The objectives of the research within this thesis were to identify molecular changes and explore how RNA helicases function during the transition from teliospore dormancy to germination. Chapters 2 to 5 are linked through the analysis of transcriptome changes during teliospore germination, defining stages of teliospore germination, and identifying groups of genes of interest. The research objectives were:

1. Identify and define the stages of teliospore germination and molecular transitions and
2. Determine the impact the altered expression of RNA helicases has during the fungal life cycle and their role in the teliospore.

To address the objectives of this thesis, the basidiomycete plant pathogen *Ustilago maydis* was used to study teliospore dormancy and germination. Chapters 2 and 3 address the first research objective by defining the stages of teliospore germination and identifying both physiological and molecular transitions from teliospore dormancy to germination. Both chapters add new findings regarding the stages of teliospore germination originally outlined by Caltrider and Gottlieb (1963) and Ramberg and McLaughlin (1980). The work

in Chapter 3 outlines an updated method for measuring oxygen consumption and details the timing and increase of respiration during the initiation of teliospore germination. In addition, a microdissection method for isolating germinating teliospores at specific stages of germination is introduced. The transcript analysis (Chapter 2) identifies patterns of transcript changes during teliospore germination and groups of genes that may have a role during the exit from dormancy to germination. One group of genes was identified as RNA helicases and these are of interest because of their ability to modulate and bind to RNA. Previous research in the Saville Laboratory identified dsRNAs in the dormant teliospore and hypothesized that these are stored mRNAs. When teliospore germination is initiated, these mRNAs are unwound from their complementary strand or secondary structure to be made available for translation. This provided the basis for investigating RNA helicase in *U. maydis* and addressing the second research objective of this thesis. The number of RNA helicases in *U. maydis* had not been previously established. The goal of Chapter 4 was to identify the RNA helicases in *U. maydis* and hypothesize their roles in the *U. maydis* life cycle by reviewing the transcriptome data from Chapter 2, Donaldson et al. (2017), and Lanver et al. (2018), and the current research in other model organisms. This led to the development of the hypothesis that RNA helicases may function to unwind stored dsRNAs in the teliospore during germination. Two RNA helicases were selected and functionally characterized in *U. maydis* (Chapter 5). This general discussion will highlight the important findings of each chapter, new findings beyond the published work, and directions for future research.

GENE EXPRESSION CONTROL DURING TELIOSPORE GERMINATION

The greatest challenge to studying teliospore germination is the asynchronous nature of teliospore germination. Samples taken from a germination time course contain teliospores in multiple stages of germination. This mixture limits the ability to detect subtle transcript level changes associated with specific germination stages. To combat this challenge, Chapter 2 presents the use of RNA-seq to identify transcript level changes above the background variation created by asynchronous teliospore germination. The RNA-seq analysis identified 1,815 transcripts significantly different at T00 (0 h PIG) compared to the haploid and dikaryon RNA-seq libraries. This analysis led to:

1. Identifying the stages of teliospore germination (Figure 2.3).
2. The identification of 18 patterns of gene transcript level change during teliospore germination (Figure 2.1).
3. Significant GO term overrepresentation for genes present in four patterns of transcript level change (summarized in Table 2.4).
4. Insight into metabolic and molecular changes associated with teliospore germination.
5. A model for gene expression control mechanisms (Figure 2.4).

Dormant teliospores exhibit low metabolic activity and once germination is initiated there is a transition to a state of high metabolic activity and growth. Teliospore germination is characterized by an increase in cell metabolism, changes in gene expression, and the development of a promycelium. One of the key findings in Chapter 2 was linking molecular changes to metabolic changes and promycelium growth observed in Caltrider and Gottlieb (1963) and Ramberg and McLaughlin (1980) respectively. The gene expression changes were related to the visible changes in the teliospore during germination.

Extensive observations of the germination process in the Saville Laboratory and in the research of Caltrider and Gottlieb (1963), Ramberg and McLaughlin (1980), and O'Donnell and McLaughlin (1984) led to the identification of seven stages of teliospore germination (Figure 2.3).

Chapter 2 also provided insight into metabolic and molecular changes associated with teliospore germination. This allowed for the development of a model for gene expression control. The translation and subsequent changes in mRNA levels occur before there are visible signs of germination. For some groups of genes, transcript levels are maintained at a steady state level during germination and others are decreased or increased during germination. These patterns of transcript levels indicate that some events are set during the teliospore formation, primed for germination, or are turned on after germination initiation. An example of the mechanisms of gene expression control, discussed in Chapter 2, is the upregulation and binding of mRNAs as dsRNAs or mRNPs in the dormant teliospore followed by the rapid release and translation of these mRNAs when germination is initiated. This study identified groups of genes and their patterns of expression and linked them to teliospore germination events that have been previously identified. One notable group of genes identified was related to mitochondrial function. These gene transcripts had reduced levels relative to the haploid and dikaryon cell types but remained constant during teliospore germination. The steady state of mRNAs during teliospore germination corresponds to the increase in respiration that occurs as early as 45 minutes PIG. Identifying these genes and their patterns of expression expands the number of genes to be further investigated for their influence on teliospore germination.

MICRORESPIRATION ANALYSIS AND MICRODISSECTION OF GERMINATING TELIOSPORES

Teliospore dormancy is characterized by low metabolic rates, reduced respiration levels, and paused macromolecular biosynthesis. An environmental signal, such as a carbon source, is required to initiate teliospore germination. Germination results in the resumption of macromolecular biosynthesis, increased respiration and metabolism, and morphological changes leading to the development and growth of the promycelium. Chapter 3 outlined two methods for studying teliospore germination. The key contributions from this chapter are:

1. The development of an improved method for measuring cellular respiration during teliospore germination.
2. Confirmation that dormant teliospores exhibit low respiration rates when compared to germinating teliospores.
3. Demonstration, for the first time, that there is an approximately 45 minute delay in oxygen uptake (the first measurable indication of respiration), suggesting that teliospores require time to process germination signals before responding.
4. Development and presentation of a microdissection method for physically isolating germinating teliospores at distinct morphological stages of germination.

Previous methods for measuring cellular respiration relied on a Warburg flask apparatus that measured oxygen levels manometrically (Caltrider & Gottlieb, 1963; Warburg, 1923). Chapter 3 introduces an updated method for measuring oxygen consumption using a Clark-type microrespirometer. This allowed for continuous oxygen

consumption measurements until the available oxygen had been depleted from the chamber. An advantage to this method is that small changes in oxygen consumption during fungal spore germination could be detected. This method detected the approximate start of oxygen consumption (approximately 45 minutes PIG) for the first time.

A microdissection method for isolating specific stages of germination was described in Chapter 3. Various methods for isolating single microorganisms have been described in the past (Choi et al., 1999; Fröhlich & König, 2006; Hildebrand, 1938). I previously attempted to isolate teliospore germination stages of interest using counterflow centrifugal elutriation and filtering germinating teliospores through a nylon membrane of a specific pore size. These methods resulted in an increased percentage of germinating teliospores, however, samples still contained a mixture of teliospores at different germination stages (Seto, 2013). Micromanipulation methods of single microorganisms have improved as higher magnifications and instruments have been developed. These techniques were previously used to isolate single cells for culturing or in single-cell PCR applications (Fröhlich & König, 2006). Using a micromanipulator to isolate single fungal spores has not been established previously. The method I developed utilizes a combination of micromanipulation techniques for bacterial cells (Fröhlich & König, 2006) and *in vitro* fertilization methods for isolating germinating teliospores. I demonstrated that hundreds of common germination stage teliospores could be obtained with this method. These samples could be used for downstream gene expression studies that involve RT-PCR or RNA-seq. Utilizing this microdissection method and the proposed stages of teliospore germination will allow researchers to make hypotheses regarding specific germination stages and not rely on germination time courses to test these hypotheses.

ANNOTATION AND FUNCTIONAL PREDICTIONS OF RNA HELICASES IN *Ustilago maydis*

The transcriptome analysis of gene transcript level changes during teliospore germination in Chapter 2 identified a group of genes called RNA helicases which may function during the exit from teliospore dormancy. The second research objective of this thesis was to determine the involvement of RNA helicases during teliospore dormancy and germination. The number of RNA helicases in *U. maydis* was determined in Chapter 4 by utilizing resources from *Saccharomyces cerevisiae* (Fairman-Williams et al., 2010) and *Homo sapiens* (Bourgeois et al., 2016). The key findings of this review are:

1. Identification of 46 RNA helicases in *Ustilago maydis*.
2. Proposed functions of RNA helicase during *Ustilago maydis* growth, pathogenesis, stress, and teliospore dormancy and germination.

The number of RNA helicases in *U. maydis* had not been previously established. The findings in Chapter 4 identified 46 RNA helicases through reciprocal BLASTp searches and phylogenetic trees for each RNA helicase family were constructed. STRING analysis and transcript patterns of these RNA helicases in *U. maydis* aided in identifying RNA helicases that may contribute to cell growth and pathogenesis. Researchers of RNA helicases in other organisms have demonstrated that dysregulation of RNA helicases can influence stress response or virulence (Panepinto et al., 2005) and contribute to the development of some diseases and cancers in humans (Zhang & Li, 2021). The combined data from the STRING analysis and transcriptome analysis of RNA-seq data from Donaldson et al. (2017), Chapter 2, and Lanver et al. (2018) resulted in identifying several

RNA helicases with possible roles in *U. maydis* growth and pathogenic development. Nine RNA helicases were identified with roles that may contribute to the metabolism, growth, and development of *U. maydis*, four that may contribute to *U. maydis* stress response, eight with predicted roles during *U. maydis* pathogenesis, and 10 RNA helicases with possible roles during teliospore dormancy and germination. The specific functions of these RNA helicases in RNA metabolism vary, however, altering the expression of these RNA helicases can disrupt the coordination of cellular processes.

There are limited studies on the role of RNA helicases in fungal plant pathology. Understanding the broader functions of RNA helicases and their contribution to gene regulation and response to environmental changes will aid in understanding their role in fungal plant pathology. The findings of Chapter 4 allowed for predicting the role that some RNA helicases may have in fungal plant pathology. Characterizing these RNA helicases in fungal plant pathogens may uncover potential avenues for targeting methods to mitigate disease prevention and progression.

CHARACTERIZATION OF *udbp3* AND *uded1* IN *Ustilago maydis* REVEALS LINKS TO STRESS RESPONSE AND TELIOSPORE DORMANCY

The transcriptome analysis in Chapter 2 identified several RNA helicases that potentially function during teliospore dormancy and germination. RNA helicases were found in germination time course transcript patterns 14 and 17. Both patterns contain transcripts upregulated in dormant teliospores. Gene transcript pattern 17 contained five RNA helicases that are upregulated during dormancy, decrease, and remain at a decreased level

during germination. From this group, the orthologs to *S. cerevisiae DBP3* and *DED1* were selected for characterization in *U. maydis*. The key findings of Chapter 5 were:

1. *UMAG_01732* is the *DBP3* ortholog and was named *udbp3*. Deletion strains show increased tolerance to osmotic stress.
2. Deletion of *UMAG_04080*, *uded1*, is detrimental to growth.
3. A hypothesis that upregulation of *uded1* may induce conformational changes to stabilize mRNA, bind to mRNA to form an mRNP to stall translation, or both.
4. Overexpression of *uded1* changes the cells in a way that makes them sensitive to osmotic stress.
5. Fungal spore dormancy is a stress response to protect the fungus from adverse environmental conditions during liberation and dispersal.
6. In response to stress, *udbp3* and *uded1* influence gene expression by interacting with RNA metabolism.

The results of Chapter 5 indicate that *udbp3* is potentially involved in regulating stress-responsive transcription factors or genes. Our results suggest that the absence of *udbp3* increases osmotic stress tolerance induced by NaCl exposure. The upregulation of *udbp3* during teliospore dormancy may suppress stress-related genes as the teliospore possesses other features to protect itself from adverse environmental conditions.

Characterization of *uded1* required the creation of expression (crg1:*uded1*) and deletion (Δ*uded1* crg1:*uded1*) mutants in *U. maydis*. Deletion of *uded1* is detrimental to *U. maydis* growth, indicating that it is an essential protein. These mutants were created by ectopically expressing *uded1* under a carbon-sensitive promoter and then deleting the native *uded1*. A slow growth phenotype and increased *uded1* transcript levels are observed when the

deletion mutant with the ectopically expressed *uded1* is grown in the presence of L-arabinose. The slow growth phenotype is consistent with what is observed in *S. cerevisiae* (Hilliker et al., 2011). Ded1 in *S. cerevisiae* regulates translation, and it was hypothesized that *uded1* had a role in influencing access to mRNAs by interacting with and unwinding dsRNAs when teliospores transition from dormancy to germination. The expression strains (crg1:*uded1*), with ectopic expression of *uded1* and native *uded1*, were used to create mutants that expressed the *ssm1* antisense (*as-ssm1*) transcript from an autonomously replicating vector. These mutants allowed for assessing dsRNA stability when *uded1* expression is altered. The results of Chapter 5 found that *uded1* is involved in slowing growth and interacts with dsRNA. It was proposed that during teliospore dormancy, *uded1* may induce conformational changes to mRNA to stabilize it and/or bind to sense/antisense pairs for storage. Uded1 represses translation, resulting in slow growth. Once germination is initiated, Uded1 promotes translation, and active growth is resumed.

FUTURE DIRECTIONS

The research in Chapters 2–5 focused on two key areas: understanding the molecular transitions from fungal spore dormancy to germination and exploring the role of RNA helicases during this process. Prior to this thesis, previous research identifying the molecular transitions of teliospore germination was hampered by asynchronous teliospore germination. RNA helicases are conserved enzymes, but little was known of their roles in the life cycle of fungal plant pathogens. Considerable research has been done in other eukaryotes, and RNA helicases have been shown to have a role in cellular growth, and metabolism. The insight gained regarding disease progression led to the proposal that

helicases could be targets for screening to identify disease as well as therapeutic targets (Shadrick et al., 2013; Zhang & Li, 2021). The findings in this thesis provided new insights into the molecular transitions during teliospore germination, identified the RNA helicases in *U. maydis*, and characterized two RNA helicases with a function during teliospore dormancy and germination. These new findings have posed new questions and avenues for advancing our understanding of teliospore dormancy and germination, and the role RNA helicases play in the fungal life cycle.

The transitions from dormancy to germination

Teliospore germination can be broken down into seven stages (Figure 2.3). These stages enable researchers to target their research questions to specific stages of germination and reduce the reliance on teliospore germination time courses. Understanding the molecular transitions during specific teliospore germination stages can aid in developing methods to prevent germination from occurring.

Chapter 3 discussed the disadvantages of using germination time courses to study teliospore germination. Future research should utilize microdissection to isolate teliospores at different stages of germination and single-cell RNA-seq to identify the molecular changes during teliospore germination. This will enable researchers to link gene expression changes to the morphological changes in the germinating teliospore.

Germination is an irreversible transition from dormancy and is characterized by increased cellular growth and metabolism (Sussman & Douthit, 1973). Chapter 3 uncovered an approximate 45 minute delay in oxygen consumption after germination was initiated. It was suggested that this delay is required to allow the teliospore to process germination signals before responding. This raises the question of which pathways are

involved in processing these germination signals. A possible area to explore would be environmental sensing during teliospore dormancy. Previous research has shown that a carbon source, such as sucrose, stimulates teliospore germination. (Caltrider & Gottlieb, 1966). Investigating sugar-sensing pathways in the teliospore may uncover regulatory genes involved in sensing and processing environmental carbon sources. Caltrider and Gottlieb (1966) also noted that sucrose may only be required for inducing germination and may not be continuously required as a germination energy source. For example, the teliospore cell wall may contain receptors with an affinity to sucrose, and when sucrose binds to them, it signals germination initiation. This results in a signal transduction within the teliospore to activate cellular metabolism, translation of stored mRNAs, and growth. Nutrient-sensing proteins have been extensively researched in *S. cerevisiae* and can be divided into three types: non-transporting receptors, transceptors, and G-protein-coupled receptors (GPCRs). These proteins are responsible for the activation of downstream signalling pathways (Dijck et al., 2017). Wahl et al. (2010) had identified 19 sugar transporter-like proteins in *U. maydis* where one has been characterized as a hexose transceptor (Schuler et al., 2015) and another as a sucrose receptor (Wahl et al., 2010). The remaining 17 proteins have yet to be characterized and may provide a starting point for identifying a nutrient-sensing protein in the teliospore cell wall. From this list, three are identified as putative sugar transporters, *UMAG_01656*, *UMAG_05602*, and *UMAG_11171* (Wahl et al., 2010). These candidate genes are an ideal starting point and their characterization in *U. maydis* may reveal their affinity for specific sugars and whether they are involved in nutrient-sensing during teliospore dormancy. If any of these genes function

as a sucrose non-transporting receptor or transceptor, then I predict that deletion of that gene would inhibit or decrease teliospore germination.

RNA helicases and teliospore dormancy and germination

Chapter 2 identified RNA helicases as a class of enzymes that may function during teliospore dormancy and germination. Chapter 4 further explored their possible functions during this period of the *U. maydis* life cycle. In Chapter 5, I chose to focus my characterization on RNA helicases that were found in pattern 17. The work presented in Chapter 5 highlights that while RNA helicases have regulatory roles in RNA metabolism, they are also involved in gene expression regulation. In light of this, RNA helicases identified in pattern 14 may also be of interest for their role during teliospore dormancy and germination.

The ortholog to the *S. cerevisiae DBP2*, *UMAG_10095*, would be an interesting RNA helicase to characterize. In *S. cerevisiae* and *H. sapiens*, Dbp2 and DDX5 were both characterized with a conserved role in glucose sensing and promoting glycolysis during growth (Beck et al., 2014; Xing et al., 2017). After teliospores receive the signal to begin germination, glucose is required to initiate the glycolysis pathway for cellular respiration. UMAG_10095 may function to sense the glucose status of the teliospore, and when levels are sufficient, RNA processing and glycolysis are promoted. Creating deletion and overexpression mutants would be a starting point in determining the function of *UMAG_10095* during *U. maydis* growth, pathogenicity, and, more specifically, teliospore dormancy and germination.

Further characterization of udbp3

Chapter 5 explored the importance of *udbp3* in *U. maydis*. The results suggest that *udbp3* negatively regulates osmotic stress response. The increased *udbp3* levels during dormancy would downregulate osmotic stress response genes, and when germination is initiated, the decreased levels of *udbp3* could stimulate the stress-responsive genes. A comprehensive stress response test that included *udbp3* overexpression mutants in the 518 and 521 cell types would help elucidate the role of this RNA helicase during stress response. The overexpression mutants could be created by ectopically expressing *udbp3* under the constitutive *otef* promoter at the *ip* locus. The osmotic stress response of overexpression mutants can be compared to the deletion mutants and wild-type strains. It is predicted that there will be a decrease in osmotic stress tolerance. In *A. thaliana*, overexpression of *str1* resulted in reduced expression of transcription activators that respond to osmotic stress and reduced tolerance to osmotic stress (Kant et al., 2007; Khan et al., 2014). Further characterization of these mutants in *U. maydis* would include identifying osmotic stress response genes and determining their expression when exposed to osmotic stress. Genes of interest are the stress-activated protein kinases such as *HOG1*. In *S. cerevisiae*, osmohomeostasis is achieved through the regulation of the high osmolarity glycerol (HOG) signalling pathway. The core of this pathway contains the MAPK transcription factor Hog1, which is capable of binding to a promotor sequence and increasing the rate of transcription by recruiting other components to achieve this (Bai et al., 2015; Bilsland et al., 2004; Smith et al., 2010). The *S. cerevisiae HOG1* responds to high external osmolarity conditions by activating the HOG pathway to increase the transcription of genes involved in glycerol biosynthesis (Hohmann, 2002; Schüller et al., 1994). In *C. albicans*, *Hog1* regulates genes involved in osmotic and heavy metal stress response (Enjalbert et al., 2005). The *U. maydis*

HOG1 ortholog was identified as *UMAG_02357* (García-Pedrajas et al., 2008; Martínez-Soto & Ruiz-Herrera, 2017) but has not been functionally characterized in *U. maydis*. If altering the expression of *udbp3* regulates osmotic stress response genes, then there will be changes in transcript levels of *UMAG_02357* and/or its downstream targets.

The oxidative stress response assay could be modified and repeated with the *udbp3* deletion and expression mutants. Oxidative stress response was tested with the *udbp3* deletion mutants on solid medium containing 5 mM paraquat. However, this resulted in no growth on the plates after incubation at 28 °C for 3 days (Figure 5.S5). A paper published after I conducted the stress experiments showed that exposure to 2 mM and 5 mM paraquat is lethal to *U. maydis* wild-type cells, and a reduction in growth was observed at 1 mM (Romero-Aguilar et al., 2022). Based on this, the oxidative stress test should be modified by reducing the paraquat concentration to 1 mM and repeating the stress assay for all mutant *udbp3* strains. An additional oxidative stress test could be conducted with hydrogen peroxide (H_2O_2) and may provide further insight into the oxidative stress response of the *udbp3* mutants. Paraquat and H_2O_2 are two different oxidative stress inducers, where paraquat produces superoxide anion radicals, and H_2O_2 is a peroxide stressor. These are two types of reactive oxygen species (ROS) that, when their levels exceed the cell's antioxidant capacity, can cause cellular damage (Buonocore et al., 2010; Fridovich, 1999). It was found that in filamentous fungi, oxidative stress induced by superoxide anion radicals enhanced the expression of the enzyme superoxide dismutase (SOD) and H_2O_2 enhanced the expression of catalase (Angelova et al., 2005). *Ustilago maydis* contains two SOD encoding orthologs, *UMAG_02453* and *UMAG_03085*. The catalase ortholog in *U. maydis* is *UMAG_11067*. Cuamatzi-Flores et al. (2024) showed that overexpression of

UMAG_11067 increases oxidative tolerance to H_2O_2 stress. Null *dbp3* mutants in *S. cerevisiae* have increased tolerance to oxidative stress induced by both paraquat and H_2O_2 (Brown et al., 2006; Delaney et al., 2013). If *udbp3* is a negative regulator of stress-responsive genes and its altered expression influences oxidative stress tolerance, there will be a difference in expression of the stress-responsive genes. In the presence of paraquat, *udbp3* would enhance the expression of *UMAG_02453* and/or *UMAG_03085*. For oxidative stress induced by H_2O_2, *udbp3* would enhance the expression of *UMAG_11067*. This difference in expression would further characterize the role *udbp3* has in regulating stress response based on the type of stressor.

Further characterization of uded1

UMAG_04080 (*uded1*) was identified as the ortholog to *DED1*/*DDX3* in *S. cerevisiae* and *H. sapiens* (Chapter 4). The changes in transcript levels during teliospore dormancy and germination (Chapter 2) identified this gene as an RNA helicase with a role during the transition from dormancy to germination. Functional characterization conducted in Chapter 5 revealed that the altered expression of *uded1* resulted in a slow growth phenotype.

It was found that the Δ*uded1* crg1:*uded1* mutants were unable to infect *Z. mays* seedlings (Figure 5.S8). Insufficient levels of arabinose on the plant surface may contribute to the inability of the mutants to survive long enough to fuse, form a dikaryon, and penetrate the plant surface. L-arabinose is a plant saccharide found in plant cell walls. However, the percentage of L-arabinose content can vary across plant species. The percentage of L-arabinose can be up to 10% of the sugars found in the cell wall of *Arabidopsis thaliana* and *Oryza sativa* (Konishi et al., 2011; Zablackis et al., 1995). In *Zea mays*, the cell wall composition can differ between leaves at different positions on the stalk. It was found that

the percentage of L-arabinose is lower than that of xylose and decreases as the number of leaves on the plant increases (Abedon et al., 2006). To combat this deficiency, future experiments could include adding arabinose to the inoculum before inoculating the seedlings to assess whether this enables *uded1* expression and whether that influences pathogenesis.

I demonstrated that in the presence of sorbitol, normal budding growth is restored in the deletion mutants (Δ*uded1* crg1:*uded1*). Chapter 5 hypothesized that the overexpression of *uded1* in the Δ*uded1* crg1:*uded1* mutants may affect the cellular response to osmotic stress. To further explore this possibility, exposing the Δ*uded1* crg1:*uded1* mutants to osmotic stress conditions in repressive and permissive conditions may help determine its response to osmotic stress. This could be achieved by spotting a serial dilution series of the wild-type, expression (crg1:*uded1*), and deletion (Δ*uded1* crg1:*uded1*) strains on solid medium containing 1 M NaCl and in the presence of glucose (repressive) or arabinose (permissive). The upregulation of *uded1* may function to repress the translation of osmotic stress response genes and it is predicted that reduced tolerance to osmotic stress would be observed in the mutant strains compared to the wild-type.

Several environmental conditions can drive *U. maydis* to switch from budding to filamentous growth. Previous studies have shown that nutrient and nitrogen availability (Banuett & Herskowitz, 1994; Kernkamp, 1939), air exposure (Gold et al., 1994), and acidic pH (Ruiz-Herrera et al., 1995) can drive this switch. Chapter 5 hypothesized that the upregulation of *uded1* in the deletion mutants interferes with the regulation of the MAPK or cAMP pathway causing the switch to mycelial growth. Pathogenic fungi can adapt to changes in ambient pH (Vylkova, 2017). It has been demonstrated that an acidic medium

can induce wild-type *U. maydis* to switch from budding to mycelial growth and that the MAPK and cAMP pathways modulate this transition (Martínez-Espinoza et al., 2004; Ruiz-Herrera et al., 1995). The mycelial growth phenotype in the deletion mutants (Δ*uded1* crg1:*uded1*) is similar to what has been observed in the *uac1* mutants where the mycelial phenotype persists in neutral and acidic pH growth conditions. Budding growth in the *uac1* mutants could be restored with the addition of cAMP to the growth medium (Gold et al., 1994; Martínez-Espinoza et al., 2004). In an acidic environment, wild-type *U. maydis* cells reduce intracellular cAMP levels and switch to mycelial growth. The intracellular cAMP level is low in the *uac1* mutants regardless of the pH of the growth medium (Martínez-Espinoza et al., 2004). If *uded1* is involved in the regulation of the cAMP pathway, the addition of exogenous cAMP would restore normal budding growth. This could be tested as part of the further functional analysis of *uded1*.

Other RNA helicases with possible roles in the Ustilago maydis *life cycle*

Chapter 4 identified 28 RNA helicases with possible roles in the *U. maydis* life cycle. Based on the current research on orthologs to these RNA helicases, I predicted that these RNA helicases would have roles in *U. maydis* growth, metabolism, stress response, pathogenesis, and teliospore dormancy and germination. Future research on the roles RNA helicases have during different parts of the life cycle would give insight into molecular control mechanisms for growth and pathogenesis.

The RNA helicase *MoDHX35* was characterized in *Magnaporthe oryzae* and is involved in appressorium formation (Ying et al., 2022). In Chapter 4, I identified the *U. maydis* ortholog as *UMAG_11913* and hypothesized that if the underlying molecular mechanisms and control of *UMAG_11913* is similar to *MoDHX35*, then the altered

expression of this gene would influence *U. maydis* appressorium formation and pathogenesis. I suggested that *UMAG_11913* deletion strains be created to test this hypothesis, which may indicate a conserved function for this RNA helicase in fungal plant pathogens (Chapter 4). Overexpression mutants could also be created by ectopically expressing *UMAG_11913* under the constitutive *otef* promoter and inserted at the *ip* locus. This would determine if an increased expression of *UMAG_11913* effects *U. maydis* growth and pathogenesis.

Another RNA helicase that future work could focus on is the ortholog of Vad1 in *C. neoformans*. *UMAG_10655* was identified as the *U. maydis* ortholog in Chapter 4 and my investigations revealed that its other orthologs are involved in translation. In *C. neoformans*, Vad1 regulates stress response and the expression of some virulence genes (Panepinto et al., 2005). Chapter 4 hypothesizes that *UMAG_10655* has a role in responding to environmental stressors, changes to the host plant defence system, and/or regulating a subset of genes for successful penetration of the plant. Future work should include creating deletion and expression mutants of *UMAG_10655* to begin characterizing its role in the *U. maydis* life cycle. During pathogenesis, the *UMAG_10655* transcript is co-expressed with genes that are involved in metabolism and cellular activity (Chapter 4). These cellular processes may be affected in *UMAG_10655* mutants. If *UMAG_10655* functions during translation, it may have a role in regulating *U. maydis* virulence factors known as effectors and may affect pathogenesis.

GENERAL CONCLUSIONS

The research in this dissertation was designed to expand our knowledge of the molecular events that occur during teliospore germination. Chapter 2 identified 18 patterns of gene transcript changes during teliospore germination. Through the identification of these patterns and GO enrichment analysis, I identified key molecular changes during teliospore germination, that contribute to the current knowledge of events, and classes of genes that may function during the transition from teliospore dormancy to germination. I also proposed that there are seven stages of teliospore germination based on the combined review of previous research of Caltrider and Gottlieb (1963), Ramberg and McLaughlin (1980), and O'Donnell and McLaughlin (1984), and my personal observations of teliospore germination using light microscopy. Chapter 3 presented an improved method for measuring respiration during teliospore germination. With this improved method, we discovered that metabolic changes begin as early as 45 minutes post-induction of germination, which is well before physical signs of germination are seen. A method that I developed for isolating teliospores at specific stages of germination was also presented in Chapter 3. It utilizes microdissection and *in vitro* fertilization techniques to isolate germinating teliospores at the same stage of germination. This technique allows for increased emphasis to be placed on the changes occurring between stages and opens the door for studying the molecular changes that occur in these transitions. The microdissection technique and the results from Chapter 2 encourage a shift from using time-course-based methods for studying teliospore germination to studying the individual stages of germination instead.

The transition from dormancy to germination requires that teliospores shift from a state of low metabolic and cellular activity to an active state. Previous research indicated

that fungal spores contain components necessary for germination to proceed when triggered by an external signal, sugar in the case of teliospores. One class of components is stored mRNAs in the form of dsRNA or mRNPs. The mRNAs within these complexes are made available for translation once the signal for germination is received. RNA helicases were identified in Chapter 2 as genes that may function to make these stored mRNAs available for translation during teliospore germination. Chapter 4 identified *U. maydis* RNA helicases and utilized transcriptome data from Chapter 2 and Lanver et al. (2018) to determine possible functions during the *U. maydis* life cycle. This review identified RNA helicases with possible functions during *U. maydis* growth, stress response, pathogenesis, and teliospore germination. Chapter 5 focused on the functional characterization of two RNA helicases that were identified in Chapter 2. The research in Chapter 5 indicated that *udbp3* is involved in regulating stress-responsive genes and *uded1* represses translation to slow growth and interacts with dsRNA in response to stress. The development of fungal spores can be viewed as a stress response characterized by changes to the cytoplasm, accumulation of protective compounds, and downregulation of cellular processes (Plante et al., 2023). Disease is spread through the successful dispersal of the fungus. Fungal plant pathogens develop resistant spores to survive environmental conditions during their dispersal. When the fungal spore senses that environmental stressors have been removed, active growth resumes in the form of germination. Understanding the molecular mechanisms that function during the transition from dormancy to germination is crucial to developing methods for mitigating disease spread in fungal plant pathogens. This could be achieved by inhibiting either fungal spore development or germination. Developing methods and technologies to combat fungal plant

pathogens can increase cereal crop production resulting in increased global food availability and security.

REFERENCES

Abedon, B. G., Hatfield, R. D., & Tracy, W. F. (2006, 2006/05/01). Cell Wall Composition in Juvenile and Adult Leaves of Maize (*Zea mays* L.). *Journal of Agricultural and Food Chemistry, 54*(11), 3896–3900. https://doi.org/10.1021/jf052872w

Angelova, M. B., Pashova, S. B., Spasova, B. K., Vassilev, S. V., & Slokoska, L. S. (2005). Oxidative stress response of filamentous fungi induced by hydrogen peroxide and paraquat. *Mycological Research, 109*(2), 150–158. https://doi.org/10.1017/S0953756204001352

Bai, C., Tesker, M., & Engelberg, D. (2015, Jun 15). The yeast Hot1 transcription factor is critical for activating a single target gene, STL1. *Molecular Biology of the Cell, 26*(12), 2357–2374. https://doi.org/10.1091/mbc.E14-12-1626

Banuett, F., & Herskowitz, I. (1994, 1994/09/01/). Morphological Transitions in the Life Cycle of *Ustilago maydis* and Their Genetic Control by the a and b Loci. *Experimental Mycology, 18*(3), 247–266. https://doi.org/https://doi.org/10.1006/emyc.1994.1024

Beck, Z. T., Cloutier, S. C., Schipma, M. J., Petell, C. J., Kit, W., Ma, & Tran, E. J. (2014). Regulation of glucose-dependent gene expression by the RNA helicase Dbp2 in *Saccharomyces cerevisiae*. *Genetics, 198*(3), 1001–1014. https://doi.org/10.1534/genetics.114.170019

Bilsland, E., Molin, C., Swaminathan, S., Ramne, A., & Sunnerhagen, P. (2004, Sep). Rck1 and Rck2 MAPKAP kinases and the HOG pathway are required for oxidative stress resistance. *Molecular Microbiology, 53*(6), 1743–1756. https://doi.org/10.1111/j.1365-2958.2004.04238.x

Bourgeois, C. F., Mortreux, F., & Auboeuf, D. (2016). The multiple functions of RNA helicases as drivers and regulators of gene expression. *Nature Reviews Molecular Cell Biology, 17*(7), 426–438.

Brown, J. A., Sherlock, G., Myers, C. L., Burrows, N. M., Deng, C., Wu, H. I., McCann, K. E., Troyanskaya, O. G., & Brown, J. M. (2006, 2006/01/01). Global analysis of gene function in yeast by quantitative phenotypic profiling. *Molecular Systems Biology, 2*(1), 2006.0001. https://doi.org/https://doi.org/10.1038/msb4100043

Buonocore, G., Perrone, S., & Tataranno, M. L. (2010, 2010/08/01/). Oxygen toxicity: chemistry and biology of reactive oxygen species. *Seminars in Fetal and*

Neonatal Medicine, 15(4), 186–190. https://doi.org/https://doi.org/10.1016/j.siny.2010.04.003

Caltrider, P. G., & Gottlieb, D. (1963). Respiratory activity and enzymes for glucose catabolism in fungus spores. *Phytopathology, 53*(9), 1021–1030.

Caltrider, P. G., & Gottlieb, D. (1966). Effect of sugars on germination and metabolism of teliospores of *Ustilago maydis*. *Phytopathology, 56*(5), 479–484.

Choi, Y.-W., Hyde, K. D., & Ho, W. (1999). Single spore isolation of fungi. *Fungal Diversity, 3*, 29–38.

Cuamatzi-Flores, J., Colón-González, M., Requena-Romo, F., Quiñones-Galeana, S., Cervantes-Chávez, J. A., & Morales, L. (2024, 2024/10/01). Enhanced oxidative stress resistance in *Ustilago maydis* and its implications on the virulence. *International Microbiology, 27*(5), 1501–1511. https://doi.org/10.1007/s10123-024-00489-8

Delaney, J. R., Ahmed, U., Chou, A., Sim, S., Carr, D., Murakami, C. J., Schleit, J., Sutphin, G. L., An, E. H., Castanza, A., Fletcher, M., Higgins, S., Jelic, M., Klum, S., Muller, B., Peng, Z. J., Rai, D., Ros, V., Singh, M., Wende, H. V., Kennedy, B. K., & Kaeberlein, M. (2013). Stress profiling of longevity mutants identifies Afg3 as a mitochondrial determinant of cytoplasmic mRNA translation and aging. *Aging Cell, 12*(1), 156–166. https://doi.org/https://doi.org/10.1111/acel.12032

Dijck, P. V., Brown, N. A., Goldman, G. H., Rutherford, J., Xue, C., & Zeebroeck, G. V. (2017). Nutrient Sensing at the Plasma Membrane of Fungal Cells. *Microbiology Spectrum, 5*(2), 10.1128/microbiolspec.funk-0031-2016. https://doi.org/doi:10.1128/microbiolspec.funk-0031-2016

Donaldson, M. E., Ostrowski, L. A., Goulet, K. M., & Saville, B. J. (2017, May 2). Transcriptome analysis of smut fungi reveals widespread intergenic transcription and conserved antisense transcript expression. *BMC Genomics, 18*(1), 340. https://doi.org/10.1186/s12864-017-3720-8

Enjalbert, B., Smith, D. A., Cornell, M. J., Alam, I., Nicholls, S., Brown, A. J. P., & Quinn, J. (2005, 2006/02/01). Role of the Hog1 Stress-activated Protein Kinase in the Global Transcriptional Response to Stress in the Fungal Pathogen Candida albicans. *Molecular Biology of the Cell, 17*(2), 1018–1032. https://doi.org/10.1091/mbc.e05-06-0501

Fairman-Williams, M. E., Guenther, U.-P., & Jankowsky, E. (2010). SF1 and SF2 helicases: family matters. *Current Opinion in Structural Biology, 20*(3), 313–324.

Fridovich, I. (1999). Fundamental Aspects of Reactive Oxygen Species, or What's the Matter with Oxygen? *Annals of the New York Academy of Sciences, 893*(1), 13–18. https://doi.org/https://doi.org/10.1111/j.1749-6632.1999.tb07814.x

Fröhlich, J., & König, H. (2006). Micromanipulation techniques for the isolation of single microorganisms. In H. König & A. Varma (Eds.), *Intestinal Microorganisms of Termites and Other Invertebrates* (pp. 425–437). Springer.

García-Pedrajas, M. D., Nadal, M., Bölker, M., Gold, S. E., & Perlin, M. H. (2008, 2008/08/01/). Sending mixed signals: Redundancy vs. uniqueness of signaling components in the plant pathogen, *Ustilago maydis*. *Fungal Genetics and Biology, 45*, S22–S30. https://doi.org/https://doi.org/10.1016/j.fgb.2008.04.007

Gold, S., Duncan, G., Barrett, K., & Kronstad, J. (1994, December 1, 1994). cAMP regulates morphogenesis in the fungal pathogen *Ustilago maydis*. *Genes & Development, 8*(23), 2805–2816. https://doi.org/10.1101/gad.8.23.2805

Hildebrand, E. M. (1938, 1938/12/01). Techniques for the isolation of single microorganisms. *The Botanical Review, 4*(12), 627–664. https://doi.org/10.1007/BF02869844

Hilliker, A., Gao, Z., Jankowsky, E., & Parker, R. (2011). The DEAD-box protein Ded1 modulates translation by the formation and resolution of an eIF4F-mRNA complex. *Molecular Cell, 43*(6), 962–972.

Hohmann, S. (2002). Osmotic Stress Signaling and Osmoadaptation in Yeasts. *Microbiology and Molecular Biology Reviews, 66*(2), 300–372. https://doi.org/doi:10.1128/mmbr.66.2.300-372.2002

Kant, P., Kant, S., Gordon, M., Shaked, R., & Barak, S. (2007). *STRESS RESPONSE SUPPRESSOR1* and *STRESS RESPONSE SUPPRESSOR2*, Two DEAD-Box RNA Helicases That Attenuate Arabidopsis Responses to Multiple Abiotic Stresses. *Plant Physiology, 145*(3), 814–830. https://doi.org/10.1104/pp.107.099895

Kernkamp, M. (1939). Genetic and environmental factors affecting growth types of *Ustilago zeae*. *Phytopathology, 29*(6), 473–484 pp.

Khan, A., Garbelli, A., Grossi, S., Florentin, A., Batelli, G., Acuna, T., Zolla, G., Kaye, Y., Paul, L. K., Zhu, J.-K., Maga, G., Grafi, G., & Barak, S. (2014). The Arabidopsis STRESS RESPONSE SUPPRESSOR DEAD-box RNA helicases are nucleolar- and chromocenter-localized proteins that undergo stress-mediated relocalization and are involved in epigenetic gene silencing. *The Plant Journal, 79*(1), 28–43. https://doi.org/https://doi.org/10.1111/tpj.12533

Konishi, T., Aohara, T., Igasaki, T., Hayashi, N., Miyazaki, Y., Takahashi, A., Hirochika, H., Iwai, H., Satoh, S., & Ishii, T. (2011, 2011/11/01/). Down-regulation of UDP-arabinopyranose mutase reduces the proportion of arabinofuranose present in rice cell walls. *Phytochemistry, 72*(16), 1962–1968. https://doi.org/https://doi.org/10.1016/j.phytochem.2011.07.012

Lanver, D., Müller, A. N., Happel, P., Schweizer, G., Haas, F. B., Franitza, M., Pellegrin, C., Reissmann, S., Altmüller, J., & Rensing, S. A. (2018). The biotrophic development of Ustilago maydis studied by RNA-seq analysis. *The Plant Cell, 30*(2), 300–323.

Martínez-Espinoza, A. D., Ruiz-Herrera, J., León-Ramírez, C. G., & Gold, S. E. (2004, 2004/10/01). MAP Kinase and cAMP Signaling Pathways Modulate the pH-Induced Yeast-to-Mycelium Dimorphic Transition in the Corn Smut Fungus *Ustilago maydis*. *Current Microbiology, 49*(4), 274–281. https://doi.org/10.1007/s00284-004-4315-6

Martínez-Soto, D., & Ruiz-Herrera, J. (2017, 2017/10/01/). Functional analysis of the MAPK pathways in fungi. *Revista Iberoamericana de Micología, 34*(4), 192–202. https://doi.org/https://doi.org/10.1016/j.riam.2017.02.006

O'Donnell, K. L., & McLaughlin, D. J. (1984). Ultrastructure of meiosis in *Ustilago maydis*. *Mycologia, 76*(3), 468–485. https://doi.org/10.2307/3793330

Panepinto, J., Liu, L., Ramos, J., Zhu, X., Valyi-Nagy, T., Eksi, S., Fu, J., Jaffe, H. A., Wickes, B., & Williamson, P. R. (2005, 03/01/). The DEAD-box RNA helicase Vad1 regulates multiple virulence-associated genes in *Cryptococcus neoformans*. *Journal of Clinical Investigation, 115*(3), 632–641. https://doi.org/10.1172/JCI23048

Plante, S., Moon, K.-M., Lemieux, P., Foster, L. J., & Landry, C. R. (2023). Breaking spore dormancy in budding yeast transforms the cytoplasm and the solubility of the proteome. *PLOS Biology, 21*(4), e3002042. https://doi.org/10.1371/journal.pbio.3002042

Ramberg, J. E., & McLaughlin, D. J. (1980). Ultrastructural study of promycelial development and basidiospore initiation in *Ustilago maydis*. *Canadian Journal of Botany, 58*(14), 1548–1561.

Romero-Aguilar, L., Vázquez-Meza, H., Guerra-Sánchez, G., Luqueño-Bocardo, O. I., & Pardo, J. P. (2022). The Mitochondrial Alternative Oxidase in *Ustilago maydis* Is Not Involved in Response to Oxidative Stress Induced by Paraquat. *Journal of Fungi, 8*(11), 1221. https://www.mdpi.com/2309-608X/8/11/1221

Ruiz-Herrera, J., León, C. G., Guevara-Olvera, L., & Cárabez-Trejo, A. (1995). Yeast-mycelial dimorphism of haploid and diploid strains of *Ustilago maydis*. *Microbiology, 141*(3), 695–703. https://doi.org/https://doi.org/10.1099/13500872-141-3-695

Schuler, D., Wahl, R., Wippel, K., Vranes, M., Munsterkotter, M., Sauer, N., & Kamper, J. (2015, May). Hxt1, a monosaccharide transporter and sensor required for virulence of the maize pathogen *Ustilago maydis*. *New Phytologist, 206*(3), 1086–1100. https://doi.org/10.1111/nph.13314

Schüller, C., Brewster, J. L., Alexander, M. R., Gustin, M. C., & Ruis, H. (1994). The HOG pathway controls osmotic regulation of transcription via the stress response element (STRE) of the Saccharomyces cerevisiae CTT1 gene. *The EMBO Journal, 13*(18), 4382–4389. https://doi.org/https://doi.org/10.1002/j.1460-2075.1994.tb06758.x

Seto, A. M. (2013). *Analysis of gene transcripts during Ustilago maydis teliospore dormancy and germination* [Master's Thesis, Trent University]. Peterborough, ON.

Shadrick, W. R., Ndjomou, J., Kolli, R., Mukherjee, S., Hanson, A. M., & Frick, D. N. (2013). Discovering New Medicines Targeting Helicases: Challenges and Recent Progress. *Journal of Biomolecular Screening, 18*(7), 761–781. https://doi.org/10.1177/1087057113482586

Smith, D. A., Morgan, B. A., & Quinn, J. (2010, May). Stress signalling to fungal stress-activated protein kinase pathways. *FEMS Microbiology Letters, 306*(1), 1–8. https://doi.org/10.1111/j.1574-6968.2010.01937.x

Sussman, A. S., & Douthit, H. A. (1973). Dormancy in microbial spores. *Annual Review of Plant Physiology, 24*(1), 311–352. https://doi.org/10.1146/annurev.pp.24.060173.001523

Vylkova, S. (2017). Environmental pH modulation by pathogenic fungi as a strategy to conquer the host. *PLOS Pathogens, 13*(2), e1006149. https://doi.org/10.1371/journal.ppat.1006149

Wahl, R., Wippel, K., Goos, S., Kamper, J., & Sauer, N. (2010, Feb 9). A novel high-affinity sucrose transporter is required for virulence of the plant pathogen *Ustilago maydis*. *PLOS Biology, 8*(2), e1000303. https://doi.org/10.1371/journal.pbio.1000303

Warburg, O. (1923). Metabolism of tumors. *Biochemische Zeitschrif, 142*, 317–333.

Xing, Z., Wang, S., & Tran, E. J. (2017). Characterization of the mammalian DEAD-box protein DDX5 reveals functional conservation with *S. cerevisiae* ortholog Dbp2 in transcriptional control and glucose metabolism. *RNA, 23*(7), 1125–1138.

Ying, S., Zhang, Z., Zhang, Y., Hao, Z., Chai, R., Qiu, H., Wang, Y., Zhu, X., Wang, J., Sun, G., & Lin, F. (2022). MoDHX35, a DEAH-Box Protein, Is Required for Appressoria Formation and Full Virulence of the Rice Blast Fungus, *Magnaporthe oryzae*. *International Journal of Molecular Sciences, 23*(16), 9015. https://www.mdpi.com/1422-0067/23/16/9015

Zablackis, E., Huang, J., Muller, B., Darvill, A. G., & Albersheim, P. (1995). Characterization of the Cell-Wall Polysaccharides of *Arabidopsis thaliana* Leaves. *Plant Physiology, 107*(4), 1129–1138. https://doi.org/10.1104/pp.107.4.1129

Zhang, L., & Li, X. (2021). DEAD-Box RNA Helicases in Cell Cycle Control and Clinical Therapy. *Cells, 10*(6), 1540. https://www.mdpi.com/2073-4409/10/6/1540

APPENDIX I

PERMISSION FROM COPYRIGHT HOLDERS

CHAPTER 2: Exploring mechanisms of gene expression control during *Ustilago maydis* teliospore germination
Published in: *Canadian Journal of Plant Pathology* (2025), 47(1): 80–97
doi: 10.1080/07060661.2024.2413557

CHAPTER 3: Investigating Teliospore Germination Using Microrespiration Analysis and Microdissection

Published in: *Journal of Visualized Experiments* (2018) 135(e57628)
doi:10.3791/57628
Video URL: https://www.jove.com/video/57628

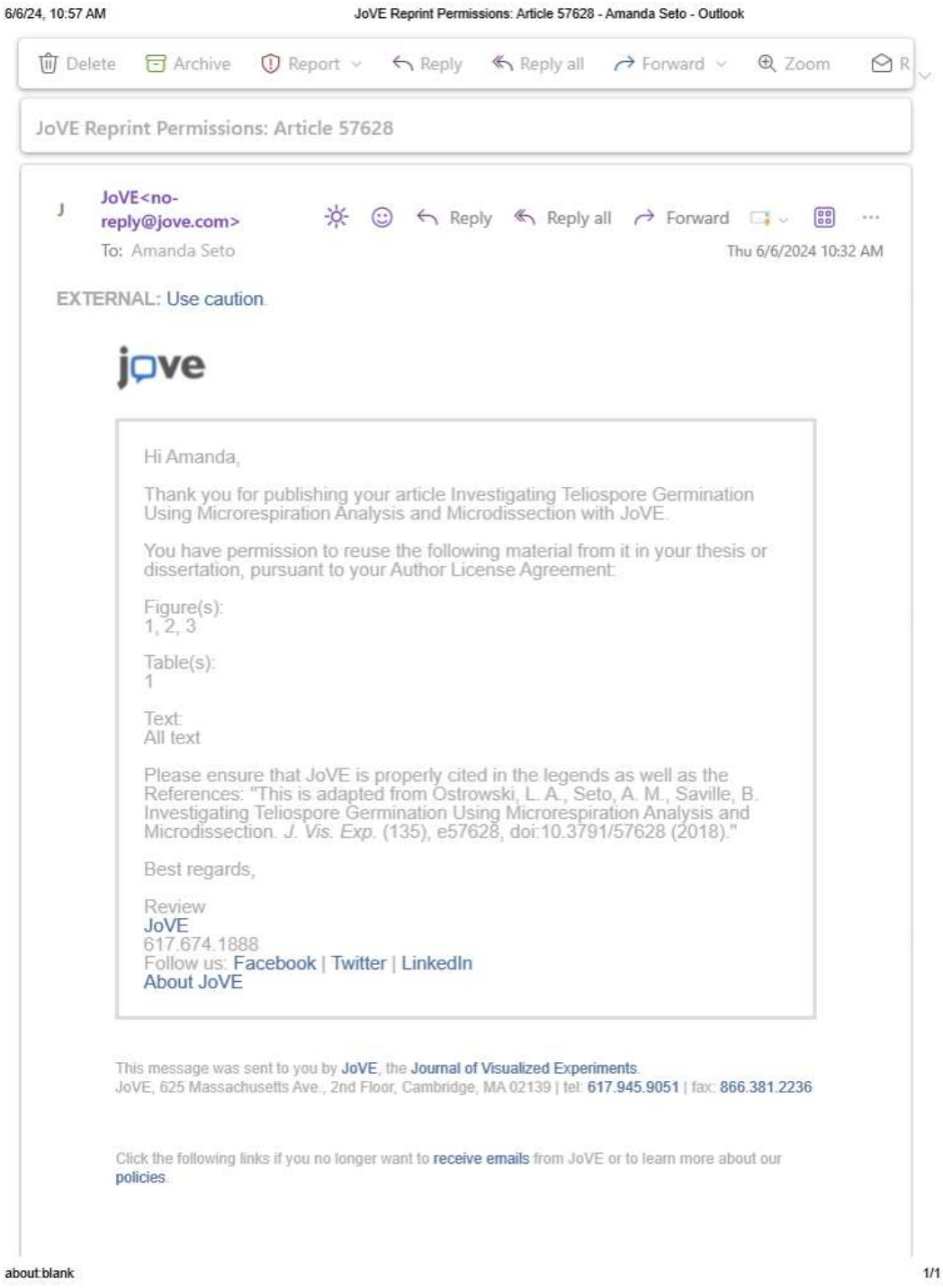

6/6/24, 10:57 AM JoVE Reprint Permissions: Article 57628 - Amanda Seto - Outlook

Delete Archive Report Reply Reply all Forward Zoom R

JoVE Reprint Permissions: Article 57628

J JoVE<no-reply@jove.com>
To: Amanda Seto

Reply Reply all Forward

Thu 6/6/2024 10:32 AM

EXTERNAL: Use caution.

jove

Hi Amanda,

Thank you for publishing your article Investigating Teliospore Germination Using Microrespiration Analysis and Microdissection with JoVE.

You have permission to reuse the following material from it in your thesis or dissertation, pursuant to your Author License Agreement:

Figure(s):
1, 2, 3

Table(s):
1

Text:
All text

Please ensure that JoVE is properly cited in the legends as well as the References: "This is adapted from Ostrowski, L. A., Seto, A. M., Saville, B. Investigating Teliospore Germination Using Microrespiration Analysis and Microdissection. *J. Vis. Exp.* (135), e57628, doi:10.3791/57628 (2018)."

Best regards,

Review
JoVE
617.674.1888
Follow us: Facebook | Twitter | LinkedIn
About JoVE

This message was sent to you by JoVE, the Journal of Visualized Experiments.
JoVE, 625 Massachusetts Ave., 2nd Floor, Cambridge, MA 02139 | tel: 617.945.9051 | fax: 866.381.2236

Click the following links if you no longer want to receive emails from JoVE or to learn more about our policies.

about:blank 1/1

CHAPTER 4: Annotation and functional predictions of RNA helicases in *Ustilago maydis*
Published in: *IMA Fungus* (2025), 16: e151785
doi.org/10.3897/imafungus.16.151785

CHAPTER 5: Characterization of RNA Helicase Genes in *Ustilago maydis* Reveals Links to Stress Response and Teliospore Dormancy
Published in: *International Journal of Molecular Sciences* (2025) 26(6): 2432
doi.org/10.3390/ijms26062432